Determining how chromatin structure is restored after repair of UV damage in *Saccharomyces cerevisiae*

Hamed Aula Hamed

Institute of Cancer and Genetics

School of Medicine

Cardiff University

Thesis submitted to Cardiff University for the degree of Doctor of Philosophy

Ph.D. 2018

DECLARATION

This work has not been submitted in substance for any other degree or award at this or any other university or place of learning, nor is being submitted concurrently in candidature for any degree or other award.

Signed …… (candidate) Date ……

STATEMENT 1

This thesis is being submitted in partial fulfilment of the requirements for the degree of PhD.

Signed …… (candidate) Date ……

STATEMENT 2

This thesis is the result of my own independent work/investigation, except where otherwise stated.

Other sources are acknowledged by explicit references. The views expressed are my own.

Signed …… (candidate) Date ……

STATEMENT 3

I hereby give consent for my thesis, if accepted, to be available for photocopying and for inter-library loan, and for the title and summary to be made available to outside organisations.

Signed …… (candidate) Date ……

STATEMENT 4: PREVIOUSLY APPROVED BAR ON ACCESS

I hereby give consent for my thesis, if accepted, to be available for photocopying and for inter-library loans **after expiry of a bar on access previously approved by the Academic Standards & Quality Committee.**

Signed …… (candidate) Date ……

Acknowledgement

Foremost, I would like to express my sincere gratitude to my supervisor Prof. Simon Reed for giving me the place to study under his supervision and for his continuous, priceless support, advice and guidance throughout the course of my study. I thank his inspiration, patient, enthusiasm and his farseeing attitude. I would never have been able to finish my thesis without the guidance of him. Besides him, I would like to thank my previous supervisor professor Ray waters and my second supervisor Dr Nicholas Kent.

I would also like to send warmest thanks to my sponsor (Ministry of higher education and scientific study of Kurdistan regional government along with my employer from ministry of Agriculture and water resources) for supporting me to finish my study.

My innermost appreciations extend to Dr. Patrick Van Eijk for his precious advice on all aspects of my study, in particular for his valuable information in data analysis during the past three years, without his input, I couldn't continue and finish my study. I would like to thank all the lab members, special thanks to go to my friends Wenbin, Shuvro Prokash and Felix Dobbs. My gratitude also goes to previous lab members Dr. Shirong Yu, Dr Richard Webster, Dr. Mark Bennett, Dr Katie Evans, Dr James Powell for their help and guidance. I must not forget Trish and Marie for their hard working and contribution in the lab.

My gratitude also goes to the head of the PGR Professor Anwen Williams, for her valuable tips and support. I also thank all the staff in the PGR office and the office staff in the International Student Support for their continuous help and advice. I would also like to express my deepest gratitude to my family especially my wife Diman who supported me and motivated me during my study. I would like to thank my parents, brothers and sisters. Finally, I would like to thank all those who helped me especially my colleagues, the academic and administrative staff of Cardiff University.

Summary

Eukaryotic genomic DNA is packaged into chromatin and all aspects of DNA metabolism require chromatin modification to facilitate these processes, including DNA repair. In response to ultra violet (UV) irradiation of cells, the chromatin undergoes structural changes allowing specific factors to gain access to the DNA damage sites to enable the repair of the DNA lesions efficiently. Following repair, these events must be reversed to restore chromatin to its normal undamaged state. The UV light-induced increase in histone H3 acetylation and the subsequent chromatin alteration that is associated with it is important for efficient DNA repair by the nucleotide excision repair (NER) pathway. In wild type cells, the elevated levels of damage-induced histone H3 acetylation is restored to the pre-damage levels following repair of the damage. However, in the absence of effective repair, histone H3 acetylation levels remain constitutively high, and subsequently the chromatin structure stays in an open configuration and does not get restored to its normal undamaged state. In this study, I undertook experiments to determine the mechanism by which the structure of chromatin is restored after the repair of DNA damage in yeast cells exposed to UV-induced DNA damage.

The Rad7/Rad16 containing global genome nucleotide excision repair (GG-NER) complex controls the occupancy of the histone acetyl transferase (HAT) Gcn5 on chromatin, which mediates the level of histone H3 acetylation. Moreover, the activity of histone deacetylaces (HDACs) and HATs are present in an equilibrium status, and any changes in one of them means that the balance of histone acetylation in the cell changes. Here, Chromatin Immunoprecipitation (ChIP) and ChIP-on-chip methods were adapted to study how the above factors bind to chromatin, both before and following UV irradiation in wild-type and specific DNA repair defective cells. My results show that the Rad7/Rad16-containing GG-NER complex, and Gcn5, remain bound to the chromatin in UV irradiated NER defective cells, and as a result, this keeps histone H3 acetylation status continuously high. My results also showed that, immediately following UV irradiation when histone H3 acetylation levels are increased, the histone deacetylases (Rpd3 and Hda1) levels decrease. Importantly, in wild type cells, where repair has taken place, restoration of histone H3 acetylation levels and HDAC occupancy to pre-damaged levels was observed. I showed that these changes are dependent upon active DNA repair.

In conclusion, my results provide evidence that the GG-NER complex and HDACs are contributing to the regulation of UV-induced histone H3 acetylation levels in order to

control the chromatin structure following DNA damage. This suggests that these factors have a role in the access and restore phases of the ARR model.

Abbreviations

6-4PP	Pyrimidine (6–4) pyrimidone photoproduct
7-DHC	7-dehydrocholesterol
8-oxo-dG	8-oxo-7,8-dihydro-2'-deoxyguanosine
AP-1	activating protein 1
AP site	Apurinic / Apyrimidinic
FAS	apoptosis stimulating fragment
ARR	Access, repair, restore
ATR	Ataxia-telangiectasia mutated and Rad3-related
ATRIP	ATR-interacting protein
ATM	Ataxia telangiectasia mutated
BER	Base excision repair
BS	Binding site
CDK1	Cyclin-dependent kinase 2
ChIP	Chromatin immunoprecipitation
Chip	DNA microarrays
Chk1	Checkpoint kinase 1
Chk2	Checkpoint kinase 2
CPD	Cyclobutane pyramedine dimer
CS	Cockayne's Syndrome
DBD	DNA binding domain
DBS	DNA binding site
DDB1	Damaged DNA-binding1 (protein)
DDR	DNA damage response
DIP	DNA immunoprecipitation
DMA	Dimethyl adipimidate dihydrochloride
DMSO	Dimethly sulfoxide
DNA	Deoxyribonucleic Acid
DNA-PK	DNA- protein kinase
DSB	Double strand break
dsDNA	Doubled stranded DNA
EDTA	Ethylenediamine tetraacetic acid
FAD	Fas-associated protein
GG-NER	Global genome NER
H2AX	Histone 2 variant H2A.X
H3K9/K14	Histone H3 acetylation at lysine 9 and 14
HAT	Histone acetyl transferase

Hda1	Histone deacetylase 1
HDAC	Histone deacetylase
HDACi	Histone deacetylase inhibitors
HR	Homologous recombination
ICL	Interstrand crosslink
IN	Input microarray samples (whole DNA of the cell)
IP	Immuno-precipitated DNA (interested DNA)
IR	Ionising radiation
LM-PCR	Ligation-mediated polymerase chain reaction
LP-BER	long patch repair
MAPK 1	Mitogen-activated protein kinase 1
MDC1	Mediator of DNA damage checkpoint protein 1
MMR	Mismatch repair
MKP1	MAPK phosphatase 1
MRN	Mre11-Rad50-Nbs1/Nibrin complex
MRX	Mre11/Rad50/Xrs2 in yeast
NER	Nucleotide excision repair
NHEJ	Non-homologous end joining
NTS	Non-transcribed strand
ORF	Open reading frame
O6MeG	O6-methylguanine
PCD	Programmed cell death
PCNA	Proliferating nuclear antigen
PCR	Polymerase chain reaction
PCR	Polymerase chain reaction
PIKKs	phosphoinositide 3-kinase-related kinases
qPCR	quantitative PCR
RNAPII	RNA polymerase II
RNF111	Ring Finger Protein 111
ROS	Reactive oxygen species
PR	Photoreactivation
RPA	Replication protein A
SD	Standard deviation
SDS	Sodium dodecyl sulphate

ssDNA	Single stranded DNA
SP-BER	Short patch repair
TC-NER	Transcription coupled NER
TES	Transcription end site
TF	Transcription factor
TFIIH	Transcription factor II Human
TNF	Tumour necrosis factor
TS	Transcribed strand
TSS	Transcription start site
WCE	Whole cell extract
WT	Wild type
UV	Ultra-violet light irradiation
YPD	Yeast Extract Peptone Dextrose media
γH2AX	gamma-phosphorylated histone H2AX

Content

Chapter one

1. Deoxyribonucleic acid: the master molecule for life

Generally, in the eukaryotic cell the nucleus is considered as the control centre for life, since it contains the genetic material (the cell's program for life), which is encoded in the macromolecule deoxyribonucleic acid (DNA). DNA carries all the information required for the downstream cellular process, involving the growth and functions of all organisms, except certain viruses. It has all the instructions necessary for creating the various cellular components, such as ribonucleic acid (RNA) and proteins. The functional unit that holds this information, and exists as a sequence of DNA, is known as the gene.

In its B-form, DNA exists as a right-handed helix consisting of two complementary strands, running in anti-parallel, held together via hydrogen bonds between its bases, which gives it a double helical structure. It has two grooves (major and minor) and one complete turn of the helix measures 3.4 nm and contains ~10 base pairs. It is considered as the genetic blueprint that holds and transfers genetic information from parents to their off-spring. It is of utmost importance for the all living organisms to preserve their genomic stability in order to function properly. DNA has three main components: Nitrogen bases (A, C, G and T), a pentose sugar and a phosphate backbone. The Nitrogen bases are paired complementarily, adenine is paired to thymine and guanine complementary to cytosine (Avery et al., 1944), and they form a long polymer via hydrogen bond. Figure 1.1 demonstrate some important features of DNA.

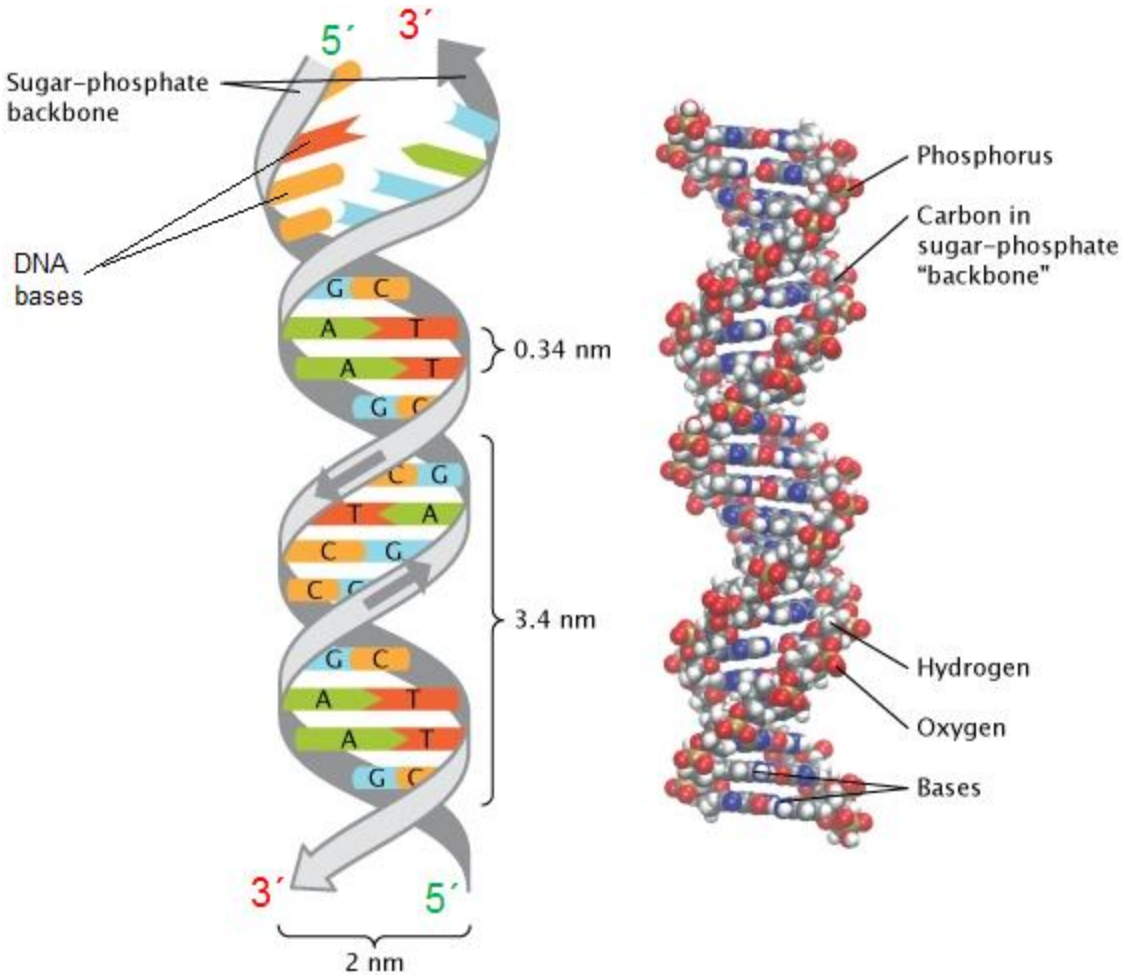

Figure 1.1. The structure of DNA. The simplified illustration of DNA, which is shown at the left, demonstrates some important properties of DNA. The grey ribbons, which represent the sugar-phosphate backbone, have arrows that run in opposite directions to indicate that the two strands of the helix are arranged in an anti-parallel manner. The upper end of one strand is labeled five prime (5'), and the lower end of the same strand is labeled three prime (3'). The upper end of the opposite strand is labeled 3', and the lower end of the same strand is labeled 5'. As a result, the 5' end of one strand matches up with the 3' end of the other strand on each end of the double helix. The two strands are held together by the pairing of complementary nucleotide bases on opposite DNA strands. The nucleotide bases are shown as differently colored rectangles that fit together like a puzzle piece where they meet in the middle. The nucleotide guanine (G, shown in blue) binds with the nucleotide cytosine (C, shown in orange). The nucleotide adenine (A, shown in green) binds with the nucleotide thymine (T, shown in red). The base pairs between the two strands look like the rungs of a ladder. The distance between two base pairs, or "rungs," is 0.34 nanometers. The length of one turn of the double-helix is ~3.4 nanometers. The width of the DNA molecule is two nanometers.In the space-filling molecular model on the right, gold spheres represent phosphorus atoms, grey spheres represent carbon atoms, white spheres represent hydrogen atoms, red spheres represent oxygen atoms, and blue spheres represent nitrogen atoms. The DNA molecules sugar-phosphate backbone is made up of gold-coloured phosphorus atoms, grey carbon atoms, white hydrogen atoms, and red oxygen atoms. The bases, which contain Hydrogen, Oxygen, Nitrogen, and Carbon, connect the two sugar-phosphate backbone chains (Pray, 2008).

1.1 DNA damage

Initially, it was reasoned that the molecule responsible for encoding the genetic information of the cell was likely to be a highly stable one, since the genetic information must be maintained and transferred accurately and with high fidelity from one generation to the next. However, following the identification of the molecule of hereditary, it quickly became apparent that the DNA structure is in fact quite chemically reactive molecule, and it is susceptible to changes within its structure caused by both internal and external cellular effects. DNA is continuously under attack from exposure to both endogenous and exogenous DNA damaging agents.

The endogenous agents originate from hydrolytic and oxidative reactions of H_2O and reactive oxygen that are prevalent in living cells. The environmental agents on the other hand are either physical or chemical factors that are mostly created outside of the cells. Damage of the DNA can occur in any of the DNA components, from which it is comprised: bases, sugars, and the phospho-diester backbone (Albert, 2002).

Normal cellular metabolism generates DNA damaging agents that can present changes in the DNA bases, like alkylation and oxidation, or sites of base loss. On the other hand, exogenous agents, such as environmental chemicals or UV and ionising radiation (IR) from the cosmos, initiate various kind of lesions in the DNA strand, if unrepaired successfully, may lead to cancer. Exposure to UV irradiation (UVB and UVC) can have a direct effect, UV photons from UVB and UVC are absorbed by DNA, leading to photochemical reactions and generating photolesions like production of CPDs and 6-4 PP. However, UVA is not absorbed by DNA as efficiently as UVB and UVC, instead it has an indirect effect on the DNA through excitation of cellular photosensitisers, which leads to the production of reactive oxygen species (ROS) (Mouret et al., 2010). ROS are major endogenous DNA damaging agents produced during normal cellular metabolism, like intrinsic mitochondrial oxidative metabolism, but exogenous sources such as exposure to UVA can generate ROS as well (Maynard et al., 2009). For example 8-oxo-7,8-dihydro-2'-deoxyguanosine (8-oxodG) generated indirectly by ROS (de Gruijl et al., 2001). In addition to that, protein cross-links and DNA strand breaks are also induced by solar radiation (Ichihashi et al., 2003).
Inside the cell, spontaneous DNA damages are generated as a result of the reaction of DNA with oxygen and water. Spontaneous cytosine alteration to uracil by deamination results in G·C to A·T mutations. Deamination of adenine and guanine also occurs but at a lower rate than the previous one (Friedberg *et al*., 2005).

During normal aerobic metabolism, ROS are produced and these form one of the major sources of endogenous DNA damage. These agents can oxidize reactive moieties within DNA and as a result generate a lesion in the DNA. Through its potential for introducing genetic mutations, DNA damage counts as a leading cause for the initiation of cancer, neurological diseases and aging.

The ROS either removes hydrogen atoms from the deoxyribose sugar, or can add double bonds within certain of the DNA bases, causing oxidised forms of the base residues, base losses and single-strand breaks (Bjelland and Seeberg, 2003). DNA modification can also be generated by incorrect base insertion during DNA replication that may result in the introduction of base mismatches.

While several DNA polymerases can synthesize DNA with high precision, yet DNA replication is not entirely an error-free process, and the errors occur still at a frequency of around 10^6 - 10^7 (Kunkel and Bebenek, 2000). This rate increased during imbalanced dNTP pool production when specific proteins are deficient (Watt et al., 2016). Watt and his colleagues revealed that increased mismatch formation and reduced error correction across the genome are caused by imbalanced dNTP pools (increased dCTP and dTTP pools) in yeast (Watt et al., 2016).

1.1.1 Spontaneous DNA damage.

During cell division, replication of DNA must be performed with a high degree of accuracy to sustain the genetic information. To achieve that, the complementary base pairing of the DNA strands must be performed precisely in an error-free manner (Alberts et al., 2002). DNA replication enzymes (DNA polymerase) have a powerful proof-reading mechanism which removes miss-paired nucleotides via its 3´ - 5´ endonuclease activity. With the help of this mechanism the rate of errors decreases to one error per 10^5 to 10^6 bases (Keohavong and Thilly, 1989), this rate further decreases via Accessory proteins to 10^{-7} then it is decrease even more through the post-replicational mismatch repair – an important DNA repair mechanism. This hierarchical system gives rise to an error rate of around one base per 10^{10} nucleotides in newly replicated DNA – a remarkable way of ensuring the stability of the genome between the generations.

1.1.2 Spontaneous chemical alteration

Due to continuous reaction of DNA with both oxygen and water, multiple “spontaneous” DNA lesions are forming. Depurination, depyrimidination, deamination, base modification are all common DNA changes happening naturally over time (Friedberg,

2005). There are some other chemical changes that occur spontaneously. They are generated due to thermodynamic degradation pathways and the by-products from the normal metabolic processes, which in turn generate free radicals such as peroxides, OH and reactive oxygen species. Base modifications are perhaps the most common type of endogenous DNA damage, accounting for thousands of lesions per cell per day (Lindahl, 1993).

1.1.2.1 Deamination of bases

As shown in figure 1.2, this involves a spontaneous loss of exocyclic amino groups (Kuraoka, 2008) from guanine, adenine, 5-methylcytosine and cytosine DNA bases, which give rise to novel chemical bases called xanthine, hypoxanthine, thymine and uracil respectively (Friedberg, 2005),

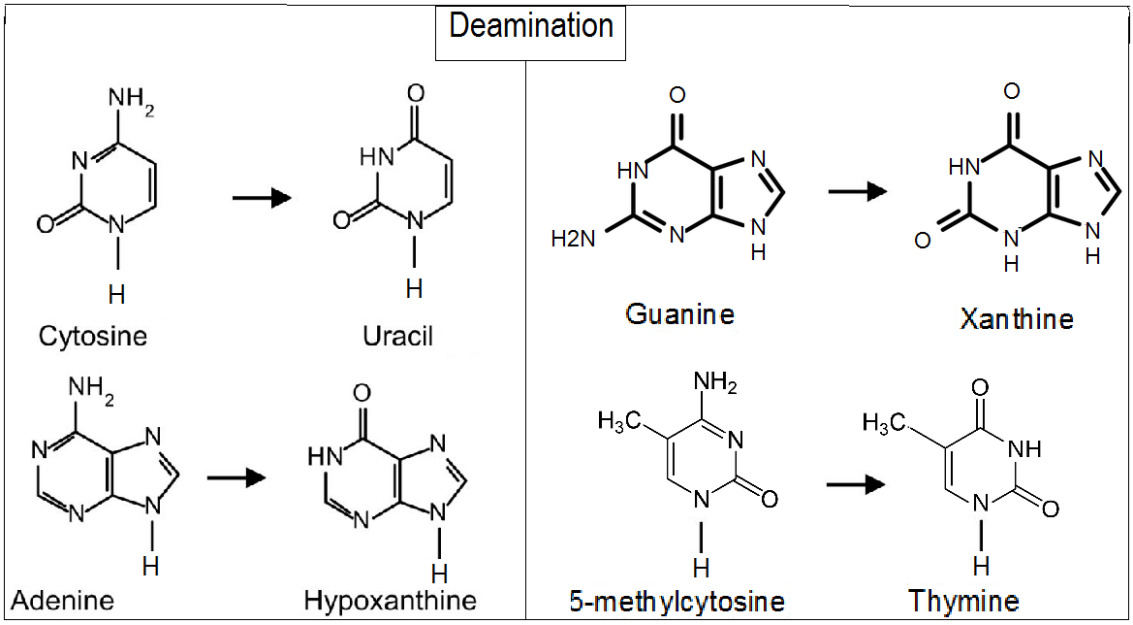

Figure 1.2 Products formed from the deamination of bases in DNA. .adapted and reproduced from (Friedberg, 2005)**.**

1.1.2.2 Depurination and Depyrimidination of DNA

Pyrimidines and purines can be lost as a result of spontaneous hydrolyses of N-glycosyl bond and formation of abasic sites (the sugar-phosphate chain remains intact). For instance around 5000 purine bases (adenine and guanine) are lost in a single human cell every day, and 100 pyrimidines per cell are lost daily (Alberts, 2002). These abasic sites occur at acidic, neutral and alkali conditions. Adenine hydrolysis is 1.5 times slower than Guanine in neutral and acidic pH, while hydrolysis is faster in alkaline

pH. BER is the predominant DNA repair pathway to repair these kinds of damages. If left unrepaired these sites of base loss can give rise to mutation following DNA replication.

1.1.2.3 Oxidative DNA Damage

ROS are considered a chief source of spontaneous damage to all macromolecules in the living cell including nucleic acids (Friedberg, 2005). ROS are the causative agent of oxidative DNA damage which is produced as a result of normal metabolic by-products as well as due to exposure to different natural and synthetic agents (Friedberg, 2005). Our atmosphere is enclosed by oxygen, it was estimated that single human inhalation generates a billion free radicals (Friedberg, 2001). Oxygen has a paradoxical property, in one face it is vital for respiration and energy production, but it also participates in several diseases. Oxygen-based reactive species known as free radicals (Butnariu, 2012; Davies, 2016; Jones and Radi, 2014; Kuksal et al., 2017). A variety of sources (both from outside the cell and inside the cell) donate oxygen radicals. Nevertheless, oxygen (when it is in a radical form) is the most notorious one since it alter lipids, proteins, and DNA and trigger a number of human diseases (Friedberg, 2005). Cell respiration co-products are singlet oxygen peroxide radicals (·O2) hydrogen peroxide (H2O2) and hydroxyl radicals (·OH). They can induce single chain breakage due to their ability to modify DNA bases such as thymine ethylene glycol, hydroxymethyl uracil and other base modified forms.

1.1.2.4 Unusual DNA structures

There are a number of DNA sequences, which are intrinsically challenging for the replication machinery. For example secondary DNA structures are produced due to repeats of trinucleotide (hairpins, triplexes, etc). These structures cause blockage or slippage of replication fork progression or promote replication slippage (Zeman and Cimprich, 2014). GC-rich DNA formed in G-quadruplexes, secondary structures are also considered to induce DNA lesions. In response to DNA damage, repair and recombination several types of DNA structures are formed which are processed via specific nucleases. For example, DNA hairpins formed during V(D)J recombination, DNA transposition, palindrome extrusion, and some types of DSBs.

In order to repair DNA hairpins, they have to be removed and/or opened by specialized nucleases. They are produced in a variety of ways, programmed hairpin formation resulting from V(D)J recombination are the most well characterized ones (Roth et al, 1992). Hairpin structures capping DNA ends are also formed at inverted repeat

sequences and in some instances, as intermediates during DNA repair (Lobachev et al, 2007). Prior to ligation, these ends must be processed properly otherwise DSB will be generated (Lobachev et al, 2007). Hairpin removal is achieved via two mechanisms. The first step involves the Mre11/Rad50/Xrs2 in yeast (MRX) and Mre11/Rad50/Nbs complex in humans (MRN), which is well characterized for its essential role in processing double strand breaks (DSB) during repair (Huang & Dynan, 2002). The second specialized nuclease, which deals with DNA hairpins is artemis (SNM1C). Its mainly exclusive to repair in the non-homologous end-joining (NHEJ) DSB repair pathway following V(D)J recombination.

1.1.3 Physical DNA damage

1.1.3.1 Radiation damage to DNA

The two major forms of radiation that cause DNA damage are: solar-generated ultraviolet (UV) radiation and ionizing radiation generated from the wider cosmos. These physical agents can induce DNA damage both directly and indirectly. DNA can absorb radiation energy from the radiation sources, or it be affected indirectly by other molecules (e.g. H_2O) in its surrounding environment, which absorb radiation energy to generate highly reactive free radicals that can interact with and modify DNA.

1.1.3.1.1 Ionizing radiation

1.1.3.1.1.1 Base Changes

Base changes occur via oxidation of DNA strands by OH-free radicals which produce peroxide and base-rings. Both pyrimidines and purines are affected, however purines seem to be more stable than pyrimidines (Friedberg, 2005).

1.1.3.1.1.2 Deoxyribose changes

Deoxyribose decomposition and DNA strand breaks formed due to the reaction of carbon atom and hydrogen atom on the hydroxyl of deoxyribose with OH- (Friedberg, 2005).

1.1.3.1.1.3 DNA strand breakage

Serious biological DNA strand breakage arises due to Ionizing radiation and the dose and the quality of the radiation in question governs the severity of the breakage. The

backbone of the DNA is very sensitive to radiation and thus breaks can occur easily. DSBs are typically more complex to repair than single strand breaks (Szumiel, 2008).

1.1.3.1.1.4 DNA cross-links.

DNA-DNA strands cross-links (inter-and intra-strand cross-links) and DNA-protein cross-links are generated as a result of IR. Radiation to generate cross-linking to DNA strand, nevertheless, there are also protein-DNA crosslinks as well (Cecchini et al., 2005). Genetic information is disrupted on both DNA strands by DNA interstrand crosslinks (ICL) and they are among the most toxic forms of DNA damage, causing potent blocks to DNA replication and transcription which lead to toxic and mutagenic effects (Wood, 2010)

Bifunctional alkylating agents introduce ICLs into DNA which covalently bind to the bases of the complementary DNA strands joining them together. These structures inhibit the transcription and replication of DNA, making ICLs toxic to the cell (Scharer, 2005). Various chemicals can generate an ICL including: cisplatin, nitrogen mustard, mitomycin C, psoralen, carmustin, and malondialdehyde (Lawley & Phillips, 1996). A Major DNA distortion is generated due to cisplatin's reaction with guanine in GC sequences (Tomasz et al, 1987). A minor distortion is formed on the DNA duplex as a result of direct reaction of nitrogen mustards with guanine residues at GNC sequences on opposite strand (Guainazzi et al, 2010). DNA intercalating agents such as psoralen form crosslinks upon UV activation at AT sequences which also cause slight DNA distortion (Guainazzi et al, 2010). Widening (slight) of the minor groove (at GC sequences) occurs as a result of mitomycin C reaction with guanine residues in the opposite complimentary strands of the groove (Stern, 2007). Carmustine generates crosslinking across a G-C base pair with very little DNA perturbation (Jamieson & Lippard, 1999).

To maintain genomic integrity and prevent cell death, a particular repair mechanism is in operation to repair ICLs. While this is not fully uncovered, it initiates with damage recognition followed by incision of the DNA, and the formation of the single strand break (SSB) (Wood, 2010), due to the action of endonucleases that nick the DNA flanking the lesion.

Most of the repair factors implicated in ICL repair are also involved in other DNA repair mechanisms such as nucleotide excision repair (NER), translesional synthesis TLS and homologous recombination (HR). Nevertheless, there are other proteins which are solely dedicated to the ICL repair system (McHugh et al, 2000). It begins by damage recognition via Rad4/Rad23 (XPC/RAD23B in humans) which belongs to nucleotide

excision repair proteins. Subsequently, Incision of the DNA lesion on either side of the damage of the DNA strand by Rad2 (on the 3' end) and by Rad1/Rad10 (on 5' end) of the same strand (Wood, 2010). Then the strand that contain the nick is flipped out and the opposite strand is used as a template for various translesional polymerases such as Polζ, Polη, or Pol κ which are able to read through the damage-containing ICL (McPherson et al, 2004). Similar nicking reactions then occur on the opposite strand, completely removing the sequence containing the ICL. Polymerases will fill in the gap and the ligases seal the nick.

DSB may generate when DNA polymerase come across these nicks during cellular replication or repair (Yamanaka et al, 2010). This broken end invades the newly repaired DNA utilizing homologous recombination machinery, restarting the replication fork (Hinz, 2010). During replication-independent ICL repair, double strand breaks are not generated and homologous recombination is not required (Hinz, 2010).

1.1.3.1.2 UV radiation

Ultraviolet (UV) light is an electromagnetic radiation whose wavelength lies between that of visible light and X-rays in the electromagnetic spectrum. It is divided into three different ranges of wavelengths: ultraviolet A (UVA, 320–400 nm), ultraviolet B (UVB, 280–320 nm) and ultraviolet C (UVC, 200–280 nm) (Anna et al., 2007; Slominski and Pawelek, 1998). UVC is considered as the most harmful radiation, however; it does not reach to the Earth's surface as most if not all of it is absorbed via the stratospheric ozone layer, although exposure to UVC might happen through manmade sources, like germicidal lamps. Around 95 % of UVA and 5 % of UVB reach the earth's surface and this has important biological consequences for the skin and eyes of humans. The extent of UV rays reaching the earth's surface depends on a number of factors like the time of day, and the time of year; its intensity is strongest during summer and at early afternoon. Latitude and altitude might play a role in the UVR level; UVR intensity increases at places close to the equator and at higher altitudes. Moreover, clouds, fog and haze and other weather conditions can reduce the UVR level. Furthermore, up to 90-95% of UVR can be reflected by snow, sand and water surfaces (Narayanan et al., 2010).

Exposure to any kind of UV irradiation develops distinctive biological outcomes and has both positive and negative effects for human (Lucas and Ponsonby, 2006; Tuorkey, 2015). For example, UVB reacts with the skin's 7-dehydrocholesterol (7-DHC) which leads to the production of vitamin D and this is the most common beneficial effect of UV radiation (UVR). Moreover, endorphin hormone is generated as a result of UV

exposure which ameliorates wellbeing and mood. Artificial UV radiation is used to treat some skin diseases, such as psoriasis, vitiligo, atopic dermatitis and localised scleroderma. Another positive effect of UVR plays a beneficial role in the blood pressure reduction via its positive effect on the production of nitric oxide (NO). Nevertheless, overexposure even to UVA and UVB may induce erythema, skin cancer, sunburn, aging and cell death. UVC is the main risk and threat to the genomic DNA as it has a strong absorption near the range of UVC wavelength (265 nm) (Ravanat et al., 2001). UVC irradiation has a direct effect on the DNA and produces cyclobutane pyrimidine dimers (CPDs) and 6-4 photoproducts (6-4 PPs) DNA lesions (figure 1.3).

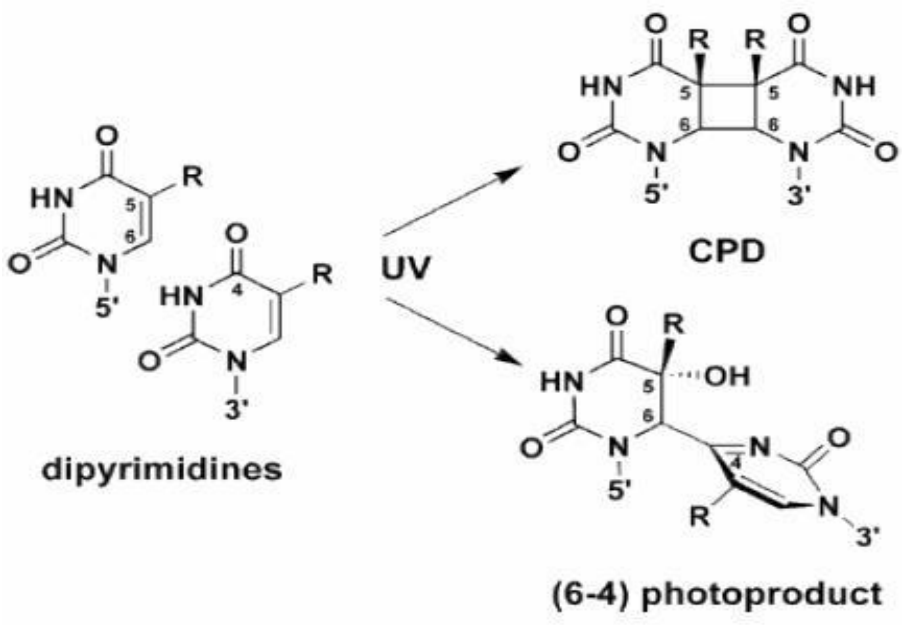

Figure 1.3 Absorption of UV light can result in two main lesions between adjacent pyrimidines. These are cyclobutane pyrimidine dimers (CPD) which predominantly form between two thymines by the formation of a four-membered ring by the saturation of the double bonds between C5 and C6 of two adjacent pyrimidines. Also (6-4) photoproducts are formed between the 5‟ C4 position and the 3‟ C6 position of two adjacent pyrimidines, most frequently T-C sites (Li et al., 2006).

Generally, pyrimidine dimer sites are the main locations for UV-lesion formations and a cluster of them (neighbouring) are a hotspot platform for both the formation of DNA damage and for UV-induced mutations (Brash et al., 1985; Zavala et al., 2014). PolydT has a great effect on the density and the distribution of CPD formation. For instance, more than 73% of Alu-linked CPD hotspots are connected with the repeated polydTs. In other words the presence of polyDT tracts serve as hotspots for CPD formation(Zavala et al., 2014). The orientation of the DNA on the histone core surface influence CPD formation as well (Gale et al., 1987), they form at 10-fold higher levels when the phosphate backbone faces away from the histone surface (Zavala et al.,

2014). There may be other factors affecting the distribution and formation of the CPD that most probably are related to the chromatin structure.

DNA absorbs UV photons and photochemical reactions occur that eventually produce pyrimidine dimers and 6-4 PPs. These two forms of DNA damage are the source of mutation in sunlight-exposed skin cancer, and they constitute 95 % of all DNA photo-lesions (Jen et al., 1997). The predominant form of DNA lesions induced by UV is the CPD, which has high levels of cytotoxicity. The formation of the cyclobutane ring between the 5 and 6 carbon atoms of the two adjacent pyrimidine leads to the formation of a four-membered ring structure of CPD lesions (Friedberg, 2005). Thymine-thymine (T-T) are the most prevalent photoproducts among the other forms of CPDs, however cytosine-cytosine (C-C) and cytosine-thymine (C-T) dimers also form (Friedberg, 2005). As a result of UV exposure, various diastereoisomers of CPDs may form when two pyrimidines sit adjacent to each other, depending on the configuration of the pyrimidine base moieties. These configurations of diastereoisomers may be in one of the following forms cis-syn, trans-syn, trans-anti and cis-anti forms (Douki, 2013) see figure 1.4 and 1.5.

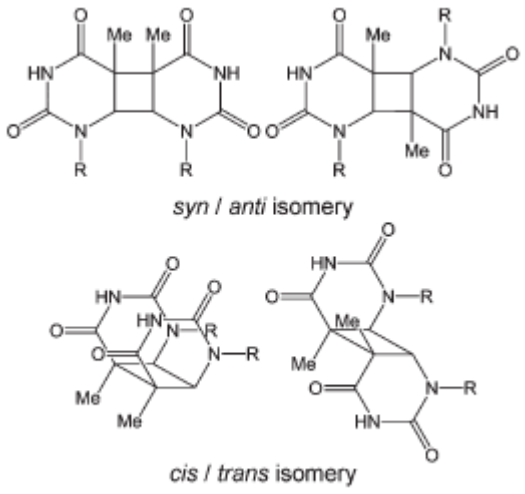

Figure 1.4 The two stereoisomeries for CPDs. A syn/anti stereoisomery reflects the parallel or antiparallel orientation of the bases (upper panel) while a cis/trans stereoisomery corresponds to the relative position of the two pyrimidines with respect to the cyclobutane ring (lower panel). The figure shows thymine CPD (R = H in bases or 2-deoxyribose in nucleosides and DNA). The cis and trans isomers presented are syn derivatives but the equivalent anti isomers are also formed (Douki, 2013).

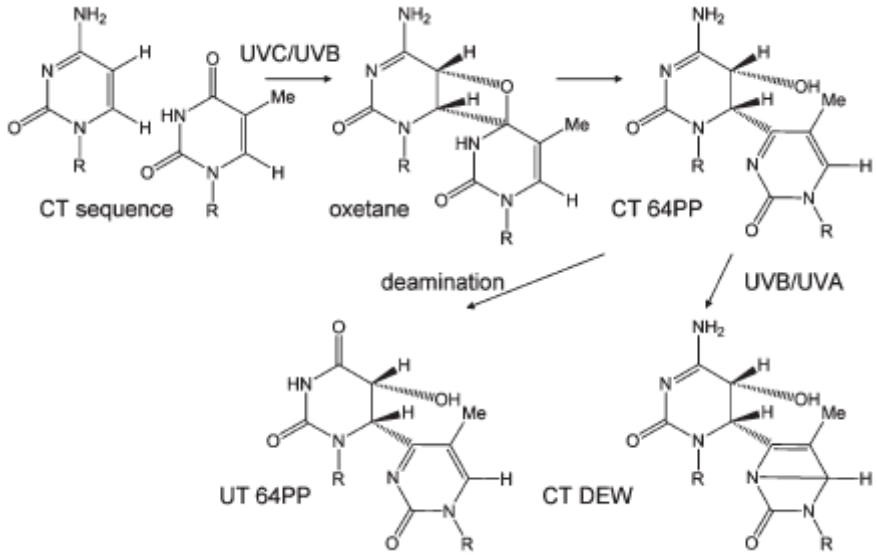

Figure 1.5 Formation and fate of CT 64PP (R = H for bases or 2-deoxyribose in nucleoside and DNA). Photoinduced [2 + 2] cycloaddition leads to a transient oxetane that rearranges into 64PP. This photoproduct can then deaminate into its uracil derivative UT 64PP or undergo a secondary photoinduced intramolecular cycloaddition leading to CT DEW. The represented stereochemistry is that found in dinucleoside monophosphates and DNA (Douki, 2013).

1.1.3.1.2.1 The effects of UV-induced DNA lesions on DNA structure

CPD's and 6-4 PP's induce structural helical distortions in the DNA molecule. In eukaryotic cells, DNA damage response pathways respond to this distortion, via cell cycle arrest at distinct phases of the cycle, either to promote DNA repair which is crucial for survival of the cell, or undergo apoptosis when the burden of the genetic damage is too great (Harper and Elledge, 2007; Huen and Chen, 2010). Sensors of the DNA damage response are elicited and they recognise these structural distortions in DNA. A sequence of events involving sensing, signalling, and repair and/or bypass of DNA damage occur. After a series of phosphorylation events involving activation of downstream proteins in the transducer cascades, the lesion will eventually be fixed by a suitable repair mechanism (NER for repairing CPDs) or eliminated through the programmed death of the cell via a mechanism called apoptosis.

1.1.4. Chemically induced DNA damage

DNA molecules respond to some chemical agents directly such as alkylating compounds.

1.1.4.1 Alkylation of the bases

Alkylating agents add Alkyl groups to the N- or O- atoms of pyrimidines or purines like in alkylations of N^3 of adenine and N^7 of guanine. During replication and following O6

guanine alkylation, hydrogen will no longer bond with cytosine but instead it will make a bond with thymine which is a strong mutagenesis form (Shrivastav et al., 2010).

1.1.4.2. Base shedding

Apurinic sites are formed as a result of base loss because following alkylation the guanine's glycosidic bond becomes less stable.

1.1.4.3 Strand breakage

This type of breakage arises as a result of alkylation of phosphodiester bonds of DNA and form unstable phosphatetriesters which can introduce breaks on the DNA.

1.1.4.4 Cross-links

Either one site or two sites of DNA become cross-linked by alkylating agents such as monofunctional or bifunctional alkylating agent, respectively. This will generate cross-links between DNA strands and/or DNA and proteins (Siddik, 2005).

1.1.4.5 Base analogs

DNA damage can be induced by many kind of synthetic base analogs and oppose the action of the anti-cancer drugs such as 5-bromouracil, 5-fluorouracil, because of their ability to affect the normal function of the replicative polymerases. These analogs are taken up by cells and they can replace the normal base during DNA replication, as their structure is similar to that of the normal base. 5-bromouracil resembles thymine, pairing with adenine when in the keto form, and pairing with guanine when in its enolic form. As a result of that, a guanine-cytosine pair may alter to a thymine adenine pair (Rizki and Rizki, 1969).

1.2 The DNA damage response

DNA damage is unavoidable, thousands of DNA damage occur daily in our cells. It is anticipated that approximately 10,000 to 20,000 lesions or events produced on the DNA strand each day in a single human cell due to a broad spectrum of damaging agents (Lindahl, 1993). Spontaneous loss of thousands of purine residues occur every day (Nakamura et al., 1998), methylation of adenine residues happens thousands of times daily through intracellular metabolite of S-adenosylmethionine (Rydberg & Lindahl, 1982). Furthermore, DNA replication itself is also an error-prone process. Aging and other diseases and disorders are connected to insufficient response to DNA lesions or linked to defects in DNA repair factors (Kastan and Bartek, 2004; Setlow and Carrier, 1964).

Genomic instability is an established landmark of cancer and defective DNA repair is a major contributor to its cause. DNA repair pathways are integrated within a system-wide process known as the DNA Damage Response (DDR). Since DNA acts as the molecular blueprint for life, it is not as other macromolecules in the cell. To retain its function, damaged DNA must be repaired, because it cannot be simply turned-over as it is for other molecules. Therefore, a sophisticated DNA-damage response (DDR) has evolved in cells, which comprises DNA repair and damage signalling processes that regulate other cellular functions. The DDR has special sensors designed for that purpose and detects DNA-damage signals, which ultimately determine the physiological response of the cell to DNA damage (Jackson and Bartek, 2009; Lazzaro et al., 2009).

During their lifetime, cells react to various extrinsic and intrinsic stresses and stimuli to maintain genomic information intact, stay alive, reproduce and avoid tumourigenesis. The DNA damage response (DDR) plays a central role in buffering and counter acting the harmful effects of the damaging agents. It brings together and coordinates several pathways accurately, such as the regulation of cell cycle (e.g cell cycle checkpoint activation) DNA repair, regulation of transcription including DDR genes or cells with un-repairable genomes via apoptosis (programmed cell death) see Figure 1.6 However if cell death pathways have been deactivated genomic instability will arise (Halazonetis et al., 2008).

Cells may experience replication stress due to the continuous attack by a broad spectrum of the DNA damaging agents and the cells effort to replicate the genome accurately. This stress may cause diseases and other genomic instabilities (Zeman and Cimprich, 2014).

In eukaryotic cells, the cellular response to DNA damage is regulated and coordinated by the DDR signalling pathway. Like classic signal transduction pathways, the DDR uses signal sensors, transducers, and effectors (Zhou and Elledge 2000). DNA damage sensing is accomplished by the ataxia telangiectasia mutated (ATM) and ataxia telangiectasia mutated and Rad3 related (ATR) kinases (DNA-PK) (Maréchal and Zou, 2013). In order for the cell to retain its genomic stability, cells have evolved elegant mechanisms to respond to DNA damage. The network comprises a number of orchestrated cellular pathways which involve DNA replication, DNA repair, cell cycle progression and transcription regulation (Maréchal and Zou, 2013). The ATM and ATR kinases coordinate the DNA damage response (DDR) with the signaling pathway in response to DNA damage (Maréchal and Zou, 2013) (see figure 1.6 and 1.7) .
DNA damage and DNA replication stress activate both ATM and ATR, yet each has discrete DNA damage specificities. Nevertheless, they often work together to signal DNA damage and control downstream processes (Maréchal and Zou, 2013).

DNA damage evokes the following four mechanisms: DNA repair, DNA damage checkpoints, transcriptional response and apoptosis (see figure 1.6). The DNA damage checkpoints utilise sensor proteins to recognise the damage, such as ATM, ATR, the Rad17-RFC complex, and the 9-1-1 complex, and uses checkpoint kinase 1 (Chk1) and checkpoint kinase 2 (Chk2) Ser/Thr kinases and Cdc25 phosphatases to start signal transduction cascades. The tumour suppressor gene (p53) induces cyclin-dependent kinases inhibitor p21 to arrest the progression of cell cycle and hence inhibits the transition of G1 to S (the G1/S checkpoint), DNA replication (the intra-S checkpoint), or G2 to mitosis (the G2/M checkpoint).

DDR Signalling

Detection of the DNA lesions takes place quickly via a DDR signalling mechanism. Then, the signals are transduced to other proteins to arrest the progression of the cell cycle, thus allowing the repair mechanisms to exert their action to repair and fix the damage (Sancar et al., 2004; Zhou and Elledge, 2000). Sensor proteins detect DNA damage, or replication stress, and downstream DDR kinase proteins are activated (Sancar et al., 2004; Zhang et al., 2012).

1.2.1 Cell cycle arrest

The cell cycle is a series of stepwise events that ends up with two identical daughter cells following replication of cellular DNA into two identical copies, a process that is imperative in organismal development and homeostasis (Morgan, 2007). Components of the cyclin-dependent kinase proteins (CDK) firmly control and coordinate the cell cycle progression.

The recurring activation and inactivation of cyclin-dependent kinase (CDK) complexes controls the cell cycle progression. Ser/Thr protein kinases are the two CDK proteins, and their kinase activities are controlled by cyclin proteins (Hydbring et al., 2016; Malumbres, 2014). Throughout the cell cycle, CDK levels remain stable, but the levels of their partners (cyclins) change throughout the entire period of cell division (due to an equilibrium achieved by gene expression and protein degradation). When the cyclin concentration is high, it combines with Cdk and therefore the latter becomes active and *vice versa*. Cell cycle progression depends on the appropriate regulation of different CDK/cyclin complexes, since these complexes are responsible to start S-phase, and to go from G1 and proceed to G2 and trigger mitosis. These pathways are preserved in yeast, humans and other organisms (Nurse, 2000). The kinase activity of the CDKs is also tightly controlled by the binding of inhibitors and phosphorylation events. Uni-directionality and quality control mechanisms regulate DNA replication to ensure the maintenance of genetic integrity (never under or over replicating the DNA), this activity is performed by degradation of cell cycle regulators (by proteolysis) (Morgan, 2007). Several diseases, cancers in particular, may arise from misregulation of the timing of cell cycle initiation and progression (when to inter the cell cycle , and when not to enter the cell cycle) enter the cell cycle program) (Massagué, 2004). Cyclins and cyclin-dependent kinases (CDKs) are the two important factors participating in cell cycle regulation and they possess regulatory and catalytic functions. Around 9 cyclins (Cln1-3 and Clb1-6) and CDK1 (Cdc28), exist in yeast (Hartwell, 1991). At specific stages of the cell cycle they form a heterodimer complex and the catalytical subunit (Cdc28) of the complex is active only when in a complex with a cyclin (Evans et al., 1983). Transcription of a growing number of genes (~800 genes) in yeast, is regulated by cell cycle (Spellman et al., 1998). In 2007 Matsuoka and his colleagues found more than 900 phosphorylation sites containing a consensus ATM and ATR phosphorylation motif in 700 proteins that are inducibly phosphorylated following exposure to IR (Eliopoulos et al., 2016; Matsuoka et al., 2007; Ribezzo et al., 2016), which emphasises the importance of this pathway in many cellular processes.

In the eukaryotic organism, the cell cycle is separated into interphase (Gap phase 1, S phase, Gap phase 2) and divisional Mitosis stage. Gap phases 1 and 2 are responsible for cell growth and its expansion. However, replication of genetic material (DNA) is handled in S phase, while M phase is responsible during the separation of sister chromosomes (Tyson and Novak, 2008).

Exposure of eukaryotic cells to DNA-damaging agents triggers an immediate response that involves arrest of the cell cycle. These vital responses are momentary, dynamically structured and are highly valuable to the organism (Nyberg et al., 2002; Zhou and Elledge, 2000). In this way it provides sufficient time to the cell to repair the damage and prevent detrimental consequences that may arise if left unrepaired. However, if the damage is too high then the alternative mechanism will be triggered to eradicate the cell and this achieved through programmed cell death (cell suicide).

1.2.1.1 Checkpoints of the cell cycle

A complex network of cell cycle checkpoint pathways has evolved in eukaryotic cells. The order and timing of cell cycle transition is regulated and controlled by the cell cycle checkpoint pathways to guarantee the completion of specific cellular events before the initiation of the next one (Nyberg et al., 2002; Osborn et al., 2002; Weinert and Hartwell, 1988; Zhou and Elledge, 2000). ATM and ATR are the two central regulatory protein kinases, which are both related to the serine-threonine kinase family that has a phosphatidylinositol 3-kinase domain within its c-terminal catalytic motif (Abraham, 2001; Shiloh and Kastan, 2001). These kinases are able to phosphorylate a broad range of protein substrates (Kim et al., 1999), however, each of them deal with a distinct class of DNA lesions. The DSB is mainly sensed by ATM, whereas, ATR is engaged with the response to UV lesions and during DNA replication.

The cell cycle checkpoints are participating in more cellular processes than initially thought. Its function was thought to be confined to cell cycle arrest in response to DNA damage (Hartwell and Weinert, 1989). Nevertheless, extensive study in this field found that the checkpoints play a range of regulatory roles in a variety of processes in the cell (Sherr, 2004). For instance, they are contributing to transcription regulation of the genes that are involving in the DDR (Foiani et al., 2000; Sancar et al., 2004), in telomere length maintenance and chromatin structure (Nakamura et al., 2002), protein recruitment to the site of the DNA damage (Nakamura et al., 2002; Zhou and Elledge, 2000), attachment of the kinetochore to microtubule spindles (Cleveland et al., 2003), in cytoskeleton arrangement (Harrison et al., 2001) and in programmed cell death

(apoptosis) activation when the damage remains unrepaired (Manfredi, 2003; Roos and Kaina, 2013; Roos et al., 2016).

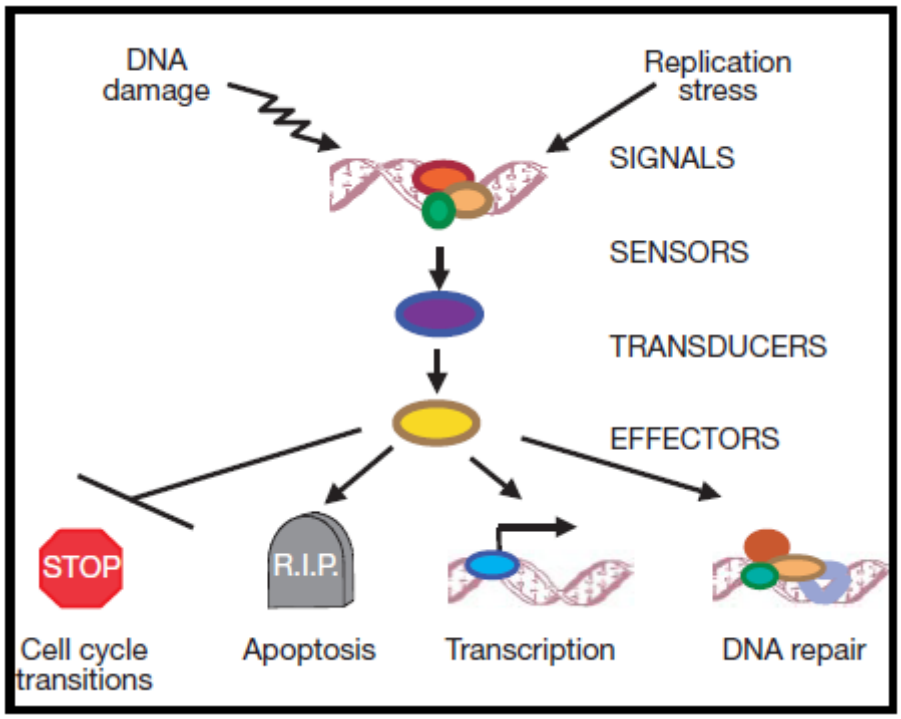

Figure 1.6 The general outline of DNA damage response signal transduction pathway. Arrowheads represent activating events and perpendicular ends represent inhibitory events. Cell-cycle arrest is depicted with a stop sign, apoptosis with a tombstone. The DNA helix with an arrow represents damage-induced transcription, while the DNA helix with several oval-shaped subunits represents damage-induced repair. For the purpose of simplicity, the network of interacting pathways are depicted as a linear pathway consisting of signals, sensors, transducers and effectors. (Zhou and Elledge, 2000).

In mammalian cells, ATM and DNA-PK (DNA protein kinase), which identify DSBs (double strand breaks) is the key signalling protein kinases. However, single stranded DNA induces the ATR signalling kinase (Sancar et al., 2004). Under normal conditions, ATM exists as a homodimer. However, a conformational change in the ATM protein occurs due to the induction of a DNA DSB, and thus serine 1981 is auto phophorylated by the Cdk5 kinase (the serine/threonine kinase Cdk5 has been shown to phosphorylate ATM on Ser794, a modification that precedes and is required for the activating autophosphorylation of ATM on Ser1981), which causes homodimer dissociation (Bakkenist and Kastan, 2003) and formation of a monomer ATM. In this form, it can phophorylate a range of substrates. The intermolecular autophosphorylation event that happens extremely rapidly and extensively due to conformational changes in ATM does not require the binding of the ATM dimer to sites of DNA damage. However, the ATM dimer can sense alterations in higher-order

chromatin structure (away from the DNA damage site) (Bakkenist and Kastan, 2003). DNA damage activates ATM and ATR, however, the ATM and MRN (MRE11, Rad50-NBS1) complex senses DSBs (Eliopoulos et al., 2016; Kastan and Bartek, 2004; Ribezzo et al., 2016), ssDNA is detected by ATR with its regulator ATRIP (ATR-interacting protein). The sensing of damage is achieved by the processing structural changes in DNA (DSB or ssDNA) at halted replication forks. As a result, various downstream substrate proteins become phosphorylated by both (ATM and ATR) kinases. This will trigger a signalling cascade that includes many common substrates including (Chk1) and (Chk2) which in turn initiates a secondary wave of phosphorylation events to amplify the signal. ATM and ATR phosphorylate more than 700 proteins at 900 regulated phosphorylation sites in response to DNA damage (Eliopoulos et al., 2016; Matsuoka et al., 2007; Ribezzo et al., 2016) (see figure 1.7).

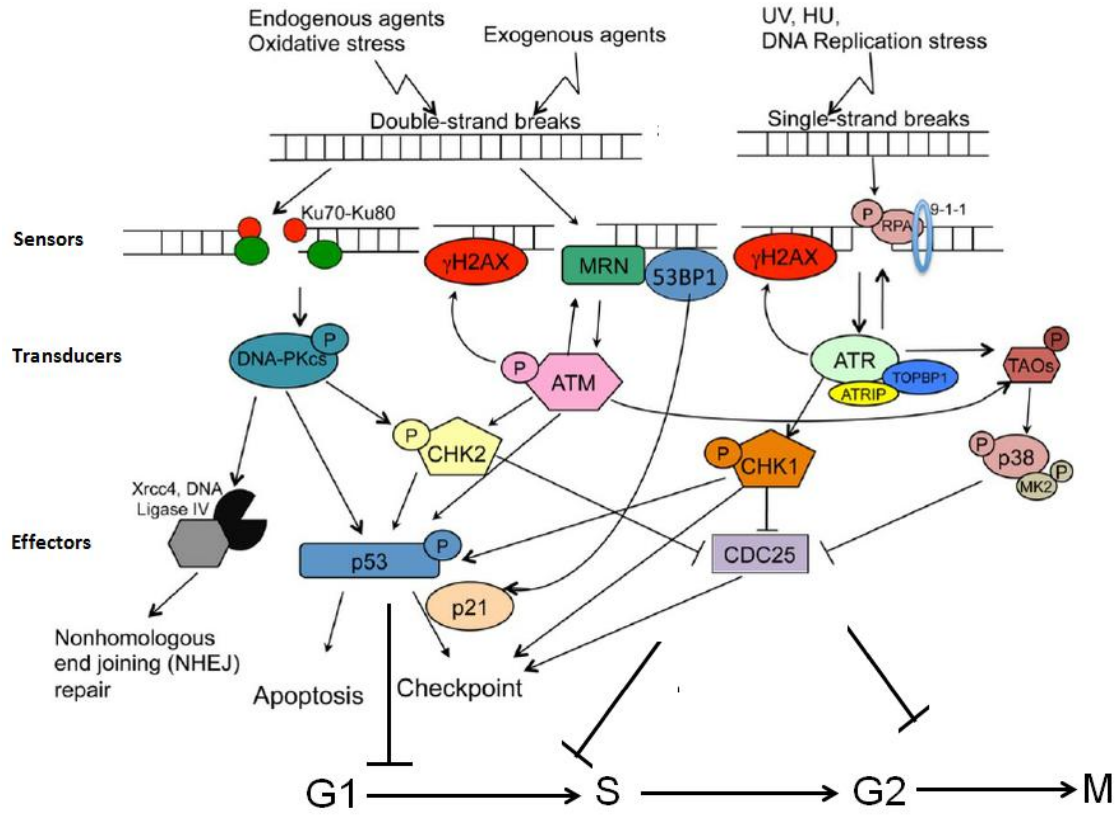

Figure 1. 7 DNA damage-induced cell cycle checkpoint network. Schematic representation of ATM, ATR and DNA-PK signaling pathways. DNA-PK responds to DNA double-strand breaks and regulates nonhomologous end joining (NHEJ). The DNA ends are captured by the KU heterodimer. Ku regulatory proteins recruit DNA-PK to double-strand breaks; two DNA-PKcs molecules in concert tether DNA ends together and recruit the DNA Ligase IV–XRCC4 complex to rejoin broken DNA ends. ATM responds to DNA double-strand breaks; phosphorylates H2AX and NBS1, which localize to sites of DNA damage, where upon the MRN complexes form. ATM activation regulates cell-cycle checkpoints through the phosphorylation of CHK2 and p53. ATR is activated in response to single-stranded DNA (ssDNA). Activation of ATR requires TopBP1. ATR is recruited to RPA-coated ssDNA by its binding partner ATRIP. ATR regulates the cell-cycle through activation of CHK1. Both ATM and ATR are required to activate the p38MAPK/MK2 effector kinase complex downstream of TAO kinases in response to DNA damage. The three effector kinases, CHK1, CHK2, and MK2 are directly responsible for inhibitory phosphorylation on members of the Cdc25 family. Arrows indicate the flow of the respective DDR pathways. Reproduced from (Xiaofei and Kowalik, 2014).

1.2.2 Apoptosis

1.2.2.1 Programmed Cell Death (apoptosis)

Programmed cell death (PCD) is the cell's capability to trigger molecular programs that when activated can cause the cell to destroy itself. This pathway is evolutionarily conserved, and it is crucial for the appropriate development of all multicellular organisms. In other words apoptosis is an organised destruction of a cell, characterised by shrinking of the cytoplasmic membrane, cell diminution, chromatin condensation, and rapid engulfment of the residual material by adjacent cells, prior to DNA fragmentation In this process, there is no inflammatory process as is seen with

necrosis. it is a genetically regulated form of cell death, which plays important roles in embryogenesis, ageing, and in several diseases (Renehan et al., 2001). Apoptosis is complex network pathways that combine to control genomic integrity, cell proliferation and survival and involves the cell-cycle checkpoints, DNA repair and recombination pathways. Alteration in the regulation of apoptosis has major consequences on genomic stability. It is a protective pathway to eradicate unrepaired DNA damaged following UV irradiation. If the lesions are not repaired via repair processes or not eliminated by apoptosis, this will generate mutations which may eventually lead to carcinogenesis. Figure 1.8 shows the main pathways leading to apoptosis after UV irradiation in mammalian cells.

DNA photoproducts, primarily cyclobutane pyrimidine dimers (CPDs) and 6-4 pyrimidine-pyrimidone photoproducts (6-4PPs) generated following UV irradiation that severely impairs DNA metabolism, terminating in the induction of cell death by apoptosis. The toxic effects of both CPDs and (6-4)PPs signals for apoptosis due of the presence of the high levels of unrepaired DNA lesions. These damages induces apoptosis signals as DSBs generate at the stalled replication forks sites (Christmann et al., 2007; Ljungman and Zhang, 1996; Roos and Kaina, 2013; Roos et al., 2016) and replication blockage at the replication fork sites generate initial photoproducts, then converted to DSBs via collapse of replication forks during replication of unrepaired DNA (Batista et al., 2006; Roos et al., 2016). The DSBs induce apoptosis and inhibit S phase progression diminishes the apoptotic response.

Apoptosis via UV-induced reactive oxygen species (ROS)

ROS causes release of cytochrome c into the cytoplasm as result of the ROS damaging action on the mitochondrial inner membrane, which results in a loss of membrane potential (Farber, 1994; Roos and Kaina, 2013). The cytochrome C causes caspase 9 activation, and this activates caspase 3, this eventually leads to cell death (Roos and Kaina, 2013)

DNA damage-independent apoptosis induced by UV light

Tumor necrosis factor (TNF) receptor super-family, has a family termed ‘‘death receptors’’ which includes a variety of related molecules consisting of similar cysteine-rich extra-cellular domains and a homologous cytoplasmic sequence termed ‘‘death domain have (TRAIL) receptors CD95 (FAS/APO-1) and other receptors. Once these bind with their natural ligands, forming receptor clusters can activate death domains (Gaur and Aggarwal, 2003). Caspase-8/FLICE recruited and activated following

recruitment of Fas-associated protein (FADD) to this activated death domain, which cleaves and activates caspase-3 and its downstream proteins, and finally cell death by apoptosis (Chinnaiyan et al., 1996).

Apoptosis by phosphoinositide 3-kinase-related kinases (PIKKs)

Cellular response to genotoxic stress takes place following the early signals provided by processing of the DNA lesions, which involves a cascade of events. Hence the DDR pathways are activated and using their specialised proteins from sensors, to transducers, eventually ending with effectors for the processing of the DNA damage.

DNA-PK (DNA-dependent protein kinase), ATM and ATR are three of the PIKK proteins involved in the DNA damage response. Downstream target p53 is one of the most important factors of ATR after DNA damage. This target protein regulates numerous proteins that control cell death by apoptosis after being activated by ATR-dependent phosphorylation. JNK induced activation is required for mitochondrial cytochrome C release (Tournier et al., 2000).

Signal transduction via mitogen-activated protein kinases

DNA lesions can inhibit the transcription of MAPK phosphatase 1 (MKP1), by which JNK phosphorylation and activating protein 1 (AP-1) activity is increased that drives FASL and the extrinsic apoptosis pathway (Roos and Kaina, 2013), these events lead to activation of caspase-8, then caspase-3 and ends with apoptosis cell death. The JNK also can directly lead to apoptosis.

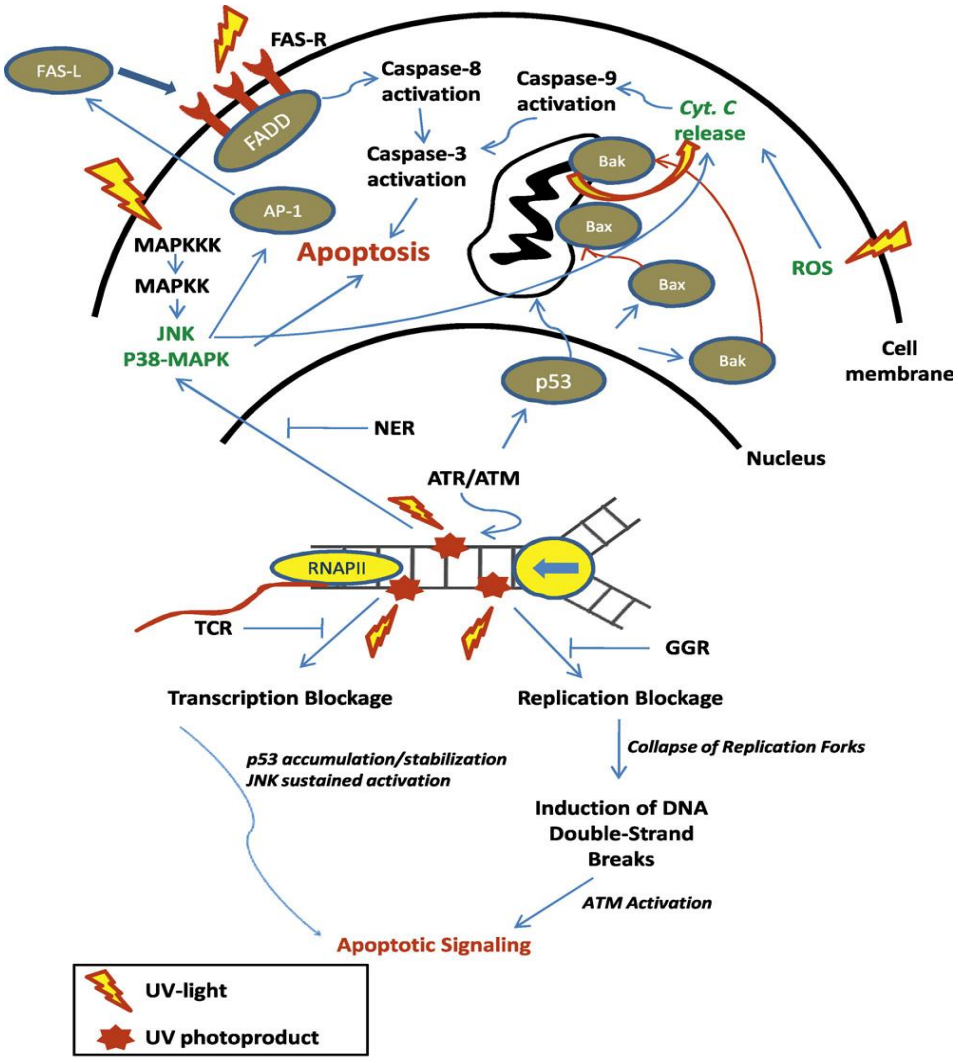

Figure 1.8 Summary of the main cellular responses after UV irradiation. UV light targets several different molecules within the cell, leading to cell death by apoptosis. DNA is the main target of UV irradiation, culminating in the formation of photoproducts (CPDs and (6-4)PPs) that represent a blockage to replication and transcription machineries. Interference with DNA metabolism pathways has been shown to be a major factor contributing to UV-apoptosis induction, either through activation of key proteins such as p53, or through formation of DNA DSBs, that will ultimately lead to cell death. UV light (mainly UVA and UVB) is also able to directly activate membrane death receptors and MAPKs that may trigger apoptosis independently of DNA damage. Generation of ROS by UVA is also responsible for the toxic effects of UV irradiation in mammalian cells (Batista et al., 2009)

Apoptosis triggered by O6-methylguanine

O6-methylguanine (O6MeG) is an important killing lesion for all these compounds that have the ability to methylate DNA, such as environmental carcinogens and endogenous metabolic products together with the paradoxically cancer targeting therapies (methylating agents) (Bartsch and Montesano, 1984; DeMarini, 2004; Jagerstad and Skog, 2005).

MGMT enzyme repairs the O6MeG in a single step by deleting the methyl group from guanine and transferring it to an internal cystein residue (Cys145). This causes MGMT inactivation and restores guanine in the DNA. However, to be able to initiate apoptosis O6MeG lesion requires DNA mismatch repair (MMR) since the lesion is too small to do it directly (Pepponi et al., 2003). MMR enzyme complex inserts wrong base again and again with failure attempts to remove the thymine. DSB formed as a result of the faulty repair in the subsequent cell cycle produced from blocked replication at secondary DNA lesions (Ochs and Kaina, 2000). Another way is that the O6MeG lesions can directly signal from the mispairs of the MMR-O6MeG–thymine complex to apoptosis since the ATR and Chk1 are activated by MMMR complex (Yoshioka et al., 2006). P53 activated by O6MeG lesions (DSB), which in turn triggers the apoptosis stimulating fragment (FAS), also termed (CD95 or APO-1) of the death-receptor pathway

1.2.3 Transcription arrest

DNA damage triggers the DDR which is a signal transduction pathway. In response to DNA damage, several cellular processes are changed and this includes the altered regulation of transcription of the genes. In general, DNA damage causes the down regulation of the bulk transcription of the genes, while a small subset that are engaged in promoting genome stability, including NER genes, are upregulated (Friedberg et al, 2005)

RNA polymerase II transcribes DNA efficiently. However, when there are obstructions, for example, due to UV-induced DNA lesions the RNA pol II is blocked from further elongation, which causes disturbed cellular homeostasis and results in a generalized transcriptional arrest. Nevertheless, there are certain specialised genes; such as those involved in DNA repair or those that promote DNA repair (e.g. certain chromatin modifiers) that are up regulated. For instance, transcription of certain NER genes are increased in response to UV irradiation and their RNA synthesis levels increase over a period of time until repair has finished.

Despite the different DNA repair processes that remove many types of DNA lesions, replication and transcription machineries frequently encounter unrepaired lesions that disturb replication fork progression and transcription elongation or may even cause stalling.

Following successful repair of DNA damage, the levels of normal RNA synthesis will recover to pre-damaged levels. However, in TC-NER defective cells such as those found in Cockayne's syndrome (CS) patients this recovery of RNA synthesis does not

happen. CS is a rare heritable autosomal recessive disorder manifested by sensitivity to sun light, but not cancer predisposition. However, the failure to recover RNA pol II synthesis after DNA damage results in severe physical abnormalities including a delay in development, abnormal gait, ataxia, deafness, cold in the extremities, cataracts, leukodystrophy and many more features severe symptoms (Hanawalt and Spivak, 2008).

1.2.4 DNA repair mechanisms

Genomic instability is an established hallmark of cancer and defective DNA repair is a major contributor to its cause. DNA repair pathways are integrated within a system-wide process known as the DDR. Since it acts as a genetic blueprint for all living organisms, unlike other cellular macromolecules, damaged DNA cannot be simply turned-over and replaced, and exclusively it depends on repair to its structure to retain its function. Therefore, a sophisticated DDR has evolved in cells, which comprises DNA repair and damage signalling processes. To counteract the deleterious effect of DNA damage, cells have acquired specialized DNA repair systems. Due to the diversity of the damaging agents and their consequences for the stability of the genome, the DNA repair systems can be subdivided into a number of repair mechanisms and pathways.

DNA repair is one of the most important functions that are undertaken by organisms. Studies into DNA damage, DNA repair and other related fields have confirmed the importance of this process. A large number of enzymes are specifically dedicated for DNA repair. For example, just in nucleotide excision repair (NER) more than thirty proteins are involved to accurately detect, remove and repair the lesion. This shows that, cells invest significant energy and resources to ensure as much damage as possible has been rectified and genomic integrity is maintained.

The importance of each mechanism is evaluated clearly through the diseases that occur when any of their repair factors are defective. A study conducted by Doll and Peto in 1981, showed that about 80–90 % of human cancers might be due to unrepaired DNA (Doll and Peto 1981) {Doll, 1981, The causes of cancer: quantitative estimates of avoidable risks of cancer in the United States today}. Furthermore, inherited defects in DNA repair genes cause severely elevated levels of cancer predisposition (Menck, 2014). For example, *Xeroderma pigmentosum*, (DiGiovanna, 2012; Kraemer, 2007) which is characterized by excessive sensitivity to ultra violet radiation that comes from the sun, is a well-known disease caused by defects in any

one of many genes involved in the NER pathway.

Although, the evolutionary process depends on genetic variation to drive the formation of new species or for adaptation to an environment, in general the stability of the genome is a fundamental requirement for life. The repair mechanisms in general operate in an extremely accurate and efficient way such that they remove and repair adducts in the right time at the right place within the genome. Based on their mode of action, DNA repair mechanisms employ various strategies from as simple as damage bypass, and DNA damage reversal (photolyase repair), to very complex processes like excision repair (BER, MMR and NER), recombinant repair (HR) and non homologous end joining (NHEJ) that involve a number of steps and many enzymatic reactions.

1.2.4.1 Photoreactivation:

In the middle of the last century (1949), Albert Kelner reported that treating UV damaged bacterial cells (*Streptomyces griseus*) with visible light can restore their ability to survive, and he called the process photoreactivation (Friedberg, 2015). This mechanism is distinctive from all the DNA repair systems known, in that it collects energy from light to repair the DNA lesion (Zhao et al., 1997). It neither needs a template strand nor involves nucleotide removal. It presents in prokaryotes and eukaryotes (yeast and blue-green alga) and it recovers UV-damaged DNA to its undamaged state by exposing damaged cells to visible light. In 1958 Dr. Stan Rupert calls the protein mediating this light dependent DNA repair reaction DNA photolyase. In 1978 Aziz Sancar and Rupert purified the enzyme from *E. coli*, and then he explained the molecular mechanism of this process (Sancar and Rupert, 1978). Generally, Photolyase enzyme is a flavo-protein that contains two chromophores (reduced flavin adenine dinucleotide and a Folate group) that act as the catalytic factors. First, the lesion (thymine dimer) is detected by photolyase enzyme. Then, the enzyme absorbs the light at 300 to 500 nm. Consequently, the FADH co-factor is excited and transfers the electron to the thymine dimer. Finally, in this way the dimer is cleaved and the DNA molecule returned to its normal pre-damaged state without altering other adjacent nucleotides in the DNA. It is important to mention that, the enzyme itself doesn't need the light to bind to the lesion, however, to repair the lesion it uses the energy source from light and can only operate in a light dependent manner (Kim et al., 1991).

There are two photolyases, CPD photolyase that reverse CPDs and 6-4 photolyase that restore 6-4 pyrimidine-pyrimidone photo-products (6-4PP). Unlike CPD photolyase, which is more common and found present in bacteria, fungi and plants, 6-4 photolyase is not found in *E. coli* and *S. cerevisiae* (Thoma, 1999). However, it can be found in

some higher eukaryotes like *D. melanogaster* (Todo et al., 1996) and *X. laevis* (Todo et al., 1997). This mechanism is not present in human and other placental animals; instead, they rely on NER to remove thymine dimers.

1.2.4.2 Base excision repair:

This mechanism of DNA repair is present in both prokaryotes and eukaryotes and it is a highly conserved mechanism from bacteria to humans, which indicates the importance of this repair pathway. It is probably one of the most commonly used machineries in nature (Friedberg, 2005). It repairs a wide range of endogenous DNA damage such as oxidation, alkylation, deamination, depurination (Memisoglu and Samson, 2000; Robertson et al., 2009; Wallace, 2014) and single strand breaks (SSBs) (Wallace, 2014).

For the first time, Tomas Lindahl described this mechanism about 43 years ago. He reported that uracil-specific N-glycosylase enzyme in *E. coli* could detect and remove free uracil, which was produced by deamination of cytosine (Lindahl, 1974). Altered DNA bases are removed by DNA glycosylases; through splitting the N-glycosyl bond between the base and the sugar and as a result an abasic site is formed which is rectified by the combined action of AP endonuclease, a DNA polymerase, and a DNA ligase (Lindahl, et al, 1997).

As shown in figure 1.9 the core machinery of BER consists of four proteins; a DNA glycosylase, an AP endonuclease or AP DNA lyase, a DNA polymerase, and a DNA ligase (Robertson, et al, 2009). Firstly, the DNA glycosylase recognizes the damaged base of the DNA and cleaves the bond between the base and deoxyribose sugar. Then, the damaged base is excised and an apurinic/apyrmidinic site (AP site) is formed. The DNA backbone adjacent to the AP site is cut, either 5' to the AP site by AP endonuclease or 3' to the AP site by AP lyase activity (Seeberg et al., 1995). The remaining deoxyribose phosphate residue is removed by a phosphodiesterase. Then, DNA polymerase initiates repair synthesis and fills the gap and the strand is sealed by DNA ligase (Krokan et al., 1997; Robertson et al., 2009; Sakumi and Sekiguchi, 1990).

A simplified version of BER for AP sites can be described as follows: (a) enzymatic incision of the AP site; (b) excision of the cleaved AP site at the single-strand break; (c) repair DNA synthesis; (d) ligation of the nick in DNA (Sung and Demple, 2006). Based on the length of the repair patches in mammalian cells, two pathways of BER have been described: short patch repair (SP-BER) which removes/replaces only one lesion and constitutes 80-90% of all BER and long patch repair (LP-BER) through which two

or more bases are removed/replaced (Fortini and Dogliotti, 2007; Friedberg, 2005). Figure 1.9 illustrate both BER pathways.

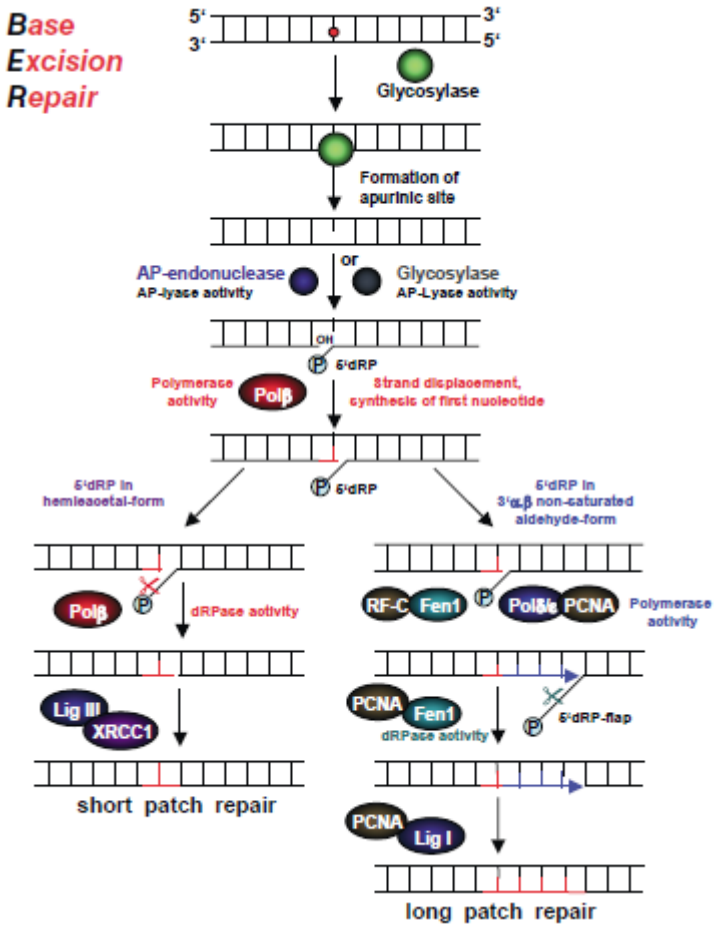

Fig. 1.9 Schematic representation of base excision repair (BER) mechanism. BER consists of two main pathways, short patch repair(left) and long patch repair (right). The first step of BER involves recognition, base removal and incision. The choice between short-patch BER or long-patch BER depends on the state of the 5' deoxyribose phosphate (5'dRP) terminus. In the final step ligation is performed (Christmann et al. 2003).

1.2.4.3 Mismatch Repair (MMR)

The MMR repair mechanism plays a crucial role in maintaining genomic integrity and it is a highly conserved system present in both prokaryotes and eukaryotes. Mismatches can arise due to incorrect incorporation of nucleotides by errors of DNA replication. In addition to that, MMR also repairs insertion/deletion loops (IDLs) produced as a result of polymerase slippage when DNA replication meets repetitive DNA sequences (Friedberg, 2005; Modrich, 1991, 1994).

In bacteria (*E. coli*) this system, also called methyl-directed pathway, as the newly synthesized strands are un-methylated unlike the parent strand that are methylated

(figure 1.10 A). In this way, the transient un-methylated form of nascent DNA identifies the newly formed DNA strand enabling correct strand responsible for the mismatch to be identified (Modrich 1991). The repair of the mismatched pairing is started by recognition of the DNA mismatch by MutS protein that has a DNA-ATPase activity (Haber and Walker, 1991). MutS then recruit MutL and forms a complex, which is activated by binding to the MutH. Then, with helicase assistance, MutH introduces an incision at a GATC site on the un-methylated DNA strand near the mismatch. Then the mismatch and the strand covering the nick is excised by an exonuclease and a new DNA strand is created by a DNA polymerase (Modrich, 1991; 1994; Friedberg et al., 2005).

In Eukaryotes, the system uses okazaki fragment (instead of methylation mechanism) as an indicator which is called nick-directed MMR (figure 1.10 B). In this system a strand discontinuity, rather than methylation, serves as a signal to direct MMR onto a specific strand. During DNA synthesis (replication), discontinuities can (DNA breaks) exist as a3' end or termini of the okazaki fragments. The discontinuation of the DNA strand can act as a signal for nick-directed MMR machinery to direct its activity onto the nascent DNA strand (Kunkel and Erie, 2005). Generally, all eukaryotes and most prokaryotes (those that do not have MutH) use this mechanism. This pathway of nick-directed MMR is very similar in both organisms (prokaryotes and eukaryotes) apart from MutS and MutL factors. In prokaryotes, these two proteins work in a homodimer forms, just like methyl-directed MMR, nevertheless, they work heterodimers in eukaryotes. The endonuclease activity motif in the C-terminal of MutL (when MutH does not exist as in some bacteria or MutH-less bacteria) is used in methyl-directed MMR. The molecular mechanism for nick-directed MMR is conserved between eukaryotes and MutH-less bacteria because same domain is found in MutL-related proteins in eukaryotes (Fukui et al., 2008). In eukaryotes, MSH which is a MutS homologues, work in a heterodimer forms (but MutS is homodimers in bacteria), attach to the DNA and recognize mismatches on the newly synthesised strand. Then eukaryotic MutS recruit MLH or PMS (post-meiotic segregation) which are MutL homologues form a MSH-MLH/PMS complex. This complex is then moves from the mismatch, away from the existing break, and a nick is produced by the MLH1 endonuclease. Thus, the mismatch is bracketed by an incision in the nascent DNA strand on either side. Then, EXOI exonuclease takes out the error-containing strand (Dzantiev et al., 2004; Genschel et al., 2002), and the resulting gap is filled by DNA polymerase and sealed by DNA ligase.

Most of the other features described such as helicase, incision, excision and re-synthesis of new DNA strand are shared by other eukaryotes because the mechanism is highly conserved (Groothuizen, 2016).

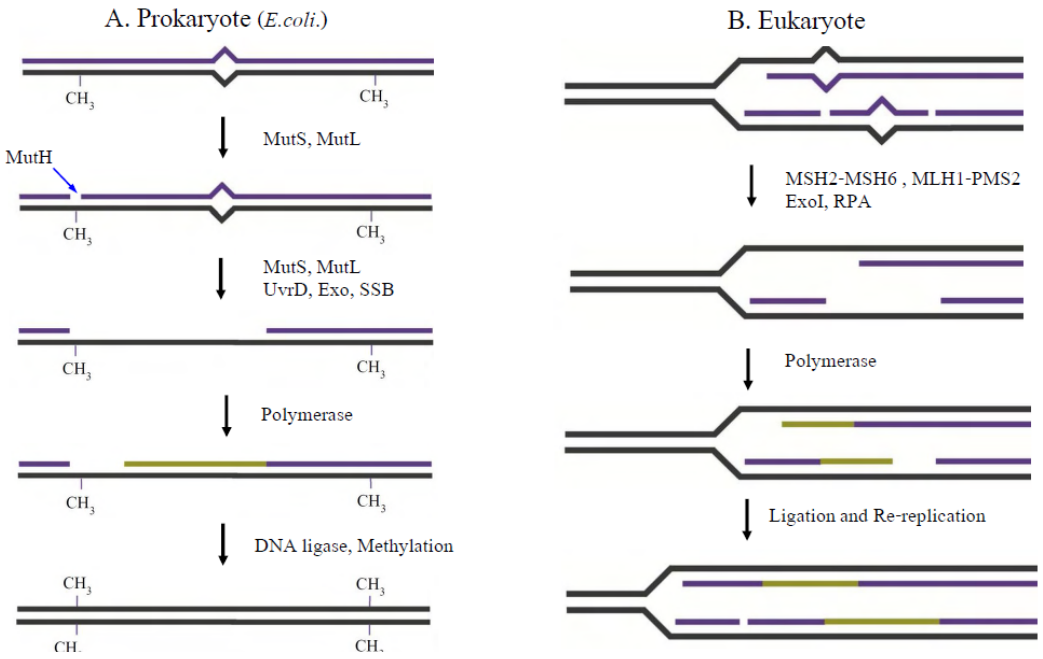

Figure 1. 10 DNA Mismatch Repair in Prokaryote and Eukaryote Systems. A. Prokaryote MMR (gram negative enteric bacteria E.coli). MutS recognizes the mismatch and MutS and MutL together activate the MutH endonuclease. MutH introduces a strand scission on the unmethylated strand of a nearby hemi-methylated GATC site (-CH3). The newly replicated strand is transiently unmethylated following replication ultimately providing strand discrimination for MMR. The strand scission serves as an entry site for the UvrD helicase and one of four exonucleases that unwind and degrade the daughter strand to just past the mismatch. E.coli SSB protects the template single strand DNA until the replication machinery reengages to synthesize the complementary strand. The remaining strand scission is sealed by DNA ligase, completing the MMR process. **B.** Eukaryote MMR (and prokaryote MMR other than gram negative enteric bacteria). Mismatched nucleotides are primarily recognized by MSH2-MSH6. MSH2-MSH6, MLH1-PMS2 (Pms1 in S.cerevisae) and EXOI degrade the mismatched strand, starting at scissions on the newly synthesized strand. The single-stranded DNA binding heterotrimer RPA protects the ssDNA gap, while the replication machinery rengages to synthesize the complementary strand. Remaining strand scissions are sealed by DNA ligase (Hanne, et al, 2013).

1.2.4.4 Double-Strand Break Repair (DSB)

DSBs are highly toxic DNA lesions that can cause genetic instability and genome rearrangements. These damages may develop from the effect of endogenous agents, these agents blocks DNA polymerase at DNA replication forks. DNA DSBs are also produced following exposure to exogenous agents like ionizing radiation. Cells and

organisms operate two main mechanisms named homologous recombination and non-homologous end joining (NHEJ) (Friedberg, 2005) to rectify DSBs effectively.

1.2.4.4.1 Homologous recombination (HR)

Homologous Recombination (HR) is one of the two main pathways for the repair of DSBs. It is mainly limited to late S and G2 stages of the cell cycle, it uses the complementary undamaged strand of the sister chromatid as a template to repair the DSB-damaged strand, it is very accurate and error-free mechanism (Bohgaki et al., 2010). Nevertheless, the Single Strand Annealing (SSA) subpathway is not so accurate and genomic loss may occur (San Filippo et al., 2008; Krejci et al., 2012). Mechanistically, HR is consist of the following steps: (1) nucleolytic resection of the DNA DSB ends; (2) nucleoprotein filament formation; (3) homology search and strand invasion; (4) DNA repair synthesis; and (5) resolution of recombination intermediates via different sub-pathways

Following DSB formation, HR initiate and DNA ends are first processed to generate 3' ssDNA overhangs. The Mre11- RAD50-NBS1 (MRN) binds to DSB at either sites and different repair factors are then activated and recruited by the MRN like ATM and nucleases. Then, RPA binds to ssDNA and Rad51 forms DNA/protein filament. On the other hand, BRCA1, BRCA2 and Rad52 complex interact with Rad51. At this point the complex search and find unbroken copy of the damaged DNA on the sister chromatin lead to heteroduplex or displacement loop (Dloop) formation. Then the D-loop changes to a Holliday junction (HJ) which is then resolved to a recombinant product by endonucleases and finally ligation by DNA ligase

This is induced by the unidirectional 5'->'3 removal of the DNA that is close to the DSB. As a result, the 3' single-stranded DNA ends produced may displace the homologous sequence of the original strand, and this may occur at sister chromatids, the homologous chromosome or same chromosome, due to the invasion of abnormal DNA ends to the homologous sequence and the formation of a hetero-duplex (Friedberg, 2005). Using the donor duplex as a template, the 3' end of the invading strand is extended by DNA synthesis. In the synthesis dependent strand annealing (SDSA) model, the invading strand is displaced by unwinding of the D-loop (via BLM helicase) and annealed with the other 3' single stranded tail which is also exposed by resection, allowing DNA synthesis to complete repair (figure 1.11). In the absence of the factors leading to SDSA, Mus81 cleaves the D-loop intermediates and creates crossovers, or the D-loops might grow to a double Holliday junction (dHJ) intermediate that can be

dissolved by BLM (Sgs1) or cleaved by a HJ resolvase, which may produce either crossover or non-crossover (figure 1.11).

As a result of ssDNA invasion an intermediate structure known as a Holliday junction is formed when DNA is synthesized from the 3'-end of the invading strand by DNA polymerase and subsequent DNA ligase. This structure is removed by resolvase enzymes in one of three ways; by 'dissolution' carried out by the BLM-TopIII complex, by symmetrical cleavage by GEN1/Yen1 or Slx1/Slx4, or by asymmetric cleavage by the structure-specific endonuclease Mus81/Eme1 (Mimitou and Symington, 2009). This mechanism is performed in an error free fashion because it uses an undamaged sister chromatid as a template. The main steps and pathways of this mechanism are displayed in (figure 1.11).

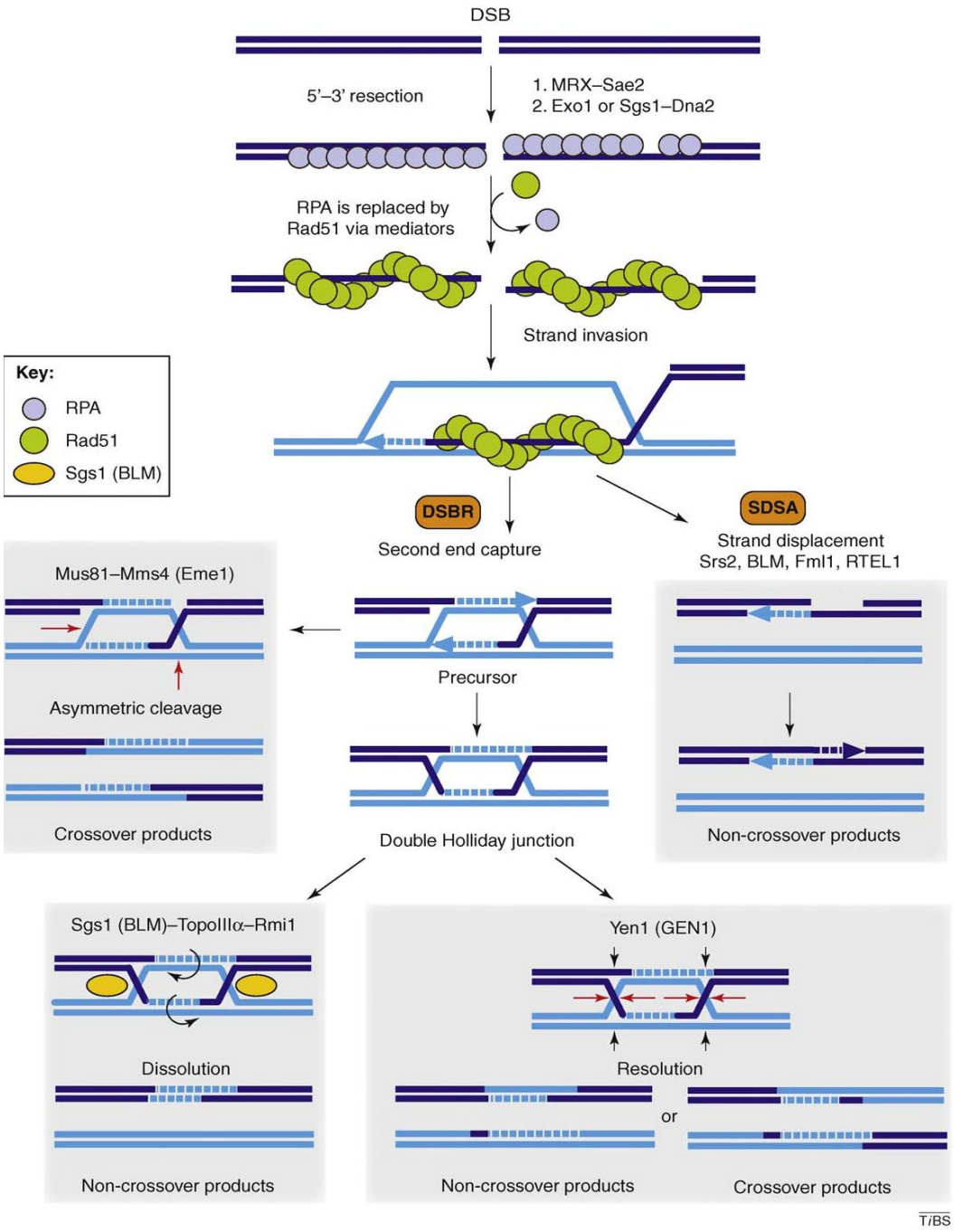

Figure 1.11 Models and outcomes of the homologous recombination pathway. 30–50 nucleotides resection of the broken ends creates 30 nucleotides ssDNA tails that are rapidly coated by RPA (light blue). RPA is replaced by Rad51 (green) to form the nucleoprotein filament, which can initiate pairing and strand invasion with the homologous duplex DNA. The 30 end of the invading strand is extended by DNA synthesis using the donor duplex as a template. In the SDSA model, the invading strand is displaced and pairs with the other 30 single stranded tail, allowing DNA synthesis to complete repair of the break. In the DSBR model, second end capture forms an early strand exchange intermediate. Processing of this precursor by Mus81–Mms4 (Eme1) generates crossover products, and ligation of this precursor creates a dHJ. Dissolution of the dHJ (via Sgs1 [BLM]–TopoIIIa-Rmi1) gives rise to non-crossover products, whereas resolution (via Yen1 [GEN1]) can lead to either crossover or non-crossover products (Mimitou and Symington, 2009).

1.2.4.4.1.1 Repair of DSBs in chromatin.

DNA DSB repair must occur within the context of the natural cellular DNA structure in cells: chromatin. Among the major factors influencing DNA organization are specific histone and non-histone proteins that form chromatin. The overall chromatin structure regulates DNA damage responses since chromatin status can impede DNA damage site access by repair proteins. During the process of DNA DSB repair, several chromatin alterations are required to sense damage and facilitate accessibility of the repair machinery. The DNA DSB response is also facilitated by hierarchical signalling networks that orchestrate chromatin structural changes that may coordinate cell-cycle checkpoints involving multiple enzymatic activities to repair broken DNA ends. During DNA damage sensing and repair, histones undergo posttranslational modifications (PTMs) including phosphorylation, acetylation, methylation and ubiquitylation. Such histone modifications are thought to represent a histone code that directs the recruitment of proteins involved in DNA damage sensing and repair processes. Considerable progress has been made in understanding the histone modifications that mediate DSB repair and an overview of these can be found in the following review (Hunt et al., 2013).

1.2.4.4.2 Non-Homologous End-Joining (NHEJ)

NHEJ involves the direct re-joining of the broken DNA ends and it does not rely on strand exchange or the existence of extensive homologous DNA sequences (Friedberg, 2005). NHEJ is normally error-prone and involves elimination of DSBs by direct ligation of the broken ends (Lieber, 2010). It is a predominant mechanism in mammalian cells as it operates throughout the cell cycle, in contrast to HR, which is only active during late S and G2 phase (Lieber, 2010). The fact that the mammalian genome is so vast and repetitive that it becomes challenging to find a suitable substrate or template to allow rejoining by HR. This may explain why this system is so important in mammalian cells and not in yeast, which has a genome 300 times smaller than in humans. The molecular mechanism of NHEJ is facilitated by a reasonably small number of critical factors that are consecutively driven to the sites of the lesion. These factors are XRCC4, DNA ligase IV, Ku70/80 heterodimer and the DNA dependent protein kinase catalytic subunit (Weterings and van Gent, 2004). The primary step in the NHEJ pathway can be seen in (figure 1.12) which involves recognition and binding of the Ku70/Ku80 heterodimer (Ku) to the exposed strand termini and recruits the DNA-

dependent protein kinase catalytic subunit (DNA-PKcs), generating the DNA-PK complex (Boulton and Jackson, 1998). Then, other complexes are recruited to the area, including RAD50, and MRE11, which assist in forming a bridge that keep the ends close to one another. Finally, XRCC4 and DNA ligase IV complex re-join the DNA ends (Weterings and van Gent, 2004).

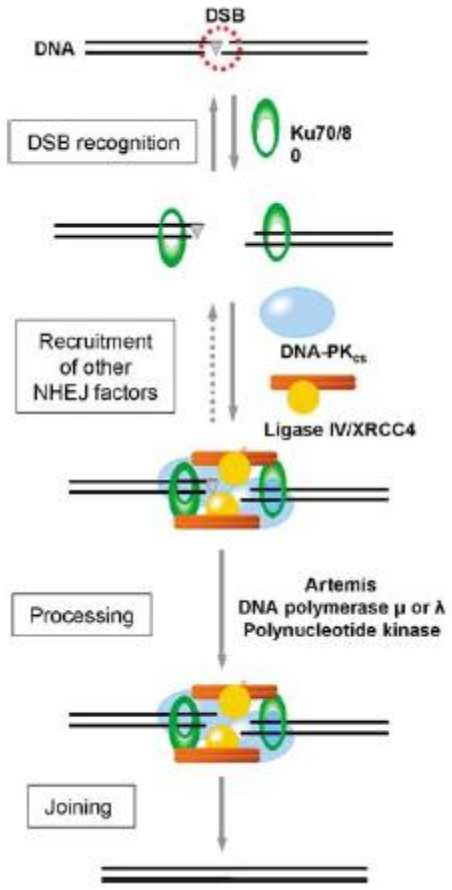

Figure 1.12 Non-homologous end-joining model. After double-strand break formation, the Ku70/80 heterodimer binds to the DNA ends and attracts DNA-PK_{cs}. This activates the DNA-PK kinase activity, which leads to autophosphorylation, which enables the subsequent processing and ligation steps. The small triangle symbolizes a DNA end that needs processing before ligation (van Gent, 2007)

1.3 Nucleotide excision repair (NER)

1.3.1 An over view of NER

Most repair pathways have a set of factors specific for detection of a particular lesion, or class of lesions, to recognize any of a bewildering number of potential DNA lesions in an ocean of normal DNA conformations. However, Nucleotide excision repair (NER) is the exception, it can recognize and repair a wide spectrum of structurally unrelated DNA lesions, yet only utilising a limited number of enzymes (Gillet and Scharer, 2006; Marteijn et al., 2015).This system is a highly conserved mechanism between prokaryotes and eukaryotes; it was shaped and evolved in an environment of high levels of radiation (Friedberg, 2005). NER is highly flexible and versatile multistep DNA repair mechanism that can detect and remove a wide variety of bulky DNA adducts including base losses and modifications, strand breaks, and other DNA changes. The UV induced CPDs and 6-4 PPs are among the most prevalent lesions that NER acts on (Friedberg, 2001; Schärer, 2013; Marteijn et al., 2015). In addition to the above lesions, NER also repairs DNA intrastrand crosslinks, bulky chemical adducts and several forms of oxidative damage and those that change the chemical structure of the DNA helix (Friedberg, 2005; Schärer, 2013; Marteijn et al., 2015). If these lesions are not repaired (either due to high level of damage or due to defective repair pathways), they can accumulate, then either will be eliminated by apoptosis or become mutagenic and/or cytotoxic. At the cellular level, genomic instability, apoptosis, or senescence may arise, if the damage remains undetected or left unrepaired. This can greatly affect the aging and developmental processes. At the organism level, genetic instability can predispose the organism to immunodeficiency, neurological disorders, and cancer (Tatum and Li, 2011).

Defective NER in humans causes Xeroderma pigmentosum (XP), a rare heritable autosomal recessive disease, characterized by excessive sensitivity to ultraviolet radiation from the sun and it is also characterized by about a 2,000- fold increased risk of skin cancer. This disease clearly demonstrates the important role of NER in humans. Seven genes of the NER pathway can be defective and result in XP, and many other genes also contribute to efficient NER (Van Steeg, and Kraemer, 1999; Friedberg et al., 2001; Kraemer et al 2007; Melis, et al., 2008). Defects in NER genes is also associated with Cockayne syndrome (CS) and trichothiodystrophy (TTD) without having a tendency to develop to a skin cancer, however, they can develop neurological disorders. These symptoms are generally ascribed to a defect in transcription-coupled NER (TC-NER) and mild transcriptional defects (Schärer, 2013).

While NER mechanism has similarities to BER (both excise the damage containing DNA and uses the undamaged complementary strand to resynthesise and repair the DNA),nevertheless, the NER pathway is much more complex, especially in eukaryotes since it repairs a wider range of DNA damages and more proteins are involved in this pathway. In other words NER primarily removes bulky DNA adducts (helix-distorting) produced by chemicals or UV radiation, while BER corrects non-helix-distorting lesions generated by ionizing radiation or cellular metabolic events**.** It is estimated that about 30 core polypeptides are involved in NER to successfully remove damage from naked DNA *in vitro* (Friedberg, 2001; Prakash and Prakash, 2000). In chromatin, NER is much more complex because NER has to gain access to the damage in the chromatin (discussed later in this chapter). The core mechanism of NER consists of the following five sequential steps (Figure 1.13)

1. Recognition of DNA damage: The NER process initiates with the detection of DNA helix distortion. **2. Open complex formation:** Two directional helicases unwind DNA in opposite direction to isolate the DNA and the damaged region. **3. Dual incisions:** incision of the damaged DNA on either side of the lesion by two junction specific endonucleases. **4. Excision of damage:** the damage-containing oligonucleotide (around 25-30 nucleotides in length) is excised from the helix. **5. Repair and ligation:** the remaining gap is filled during repair synthesis (figure 1.13). The undamaged strand is used as a template to synthesise nascent DNA and the nick is sealed by DNA ligase. The process is highly accurate and considered to be error-free.

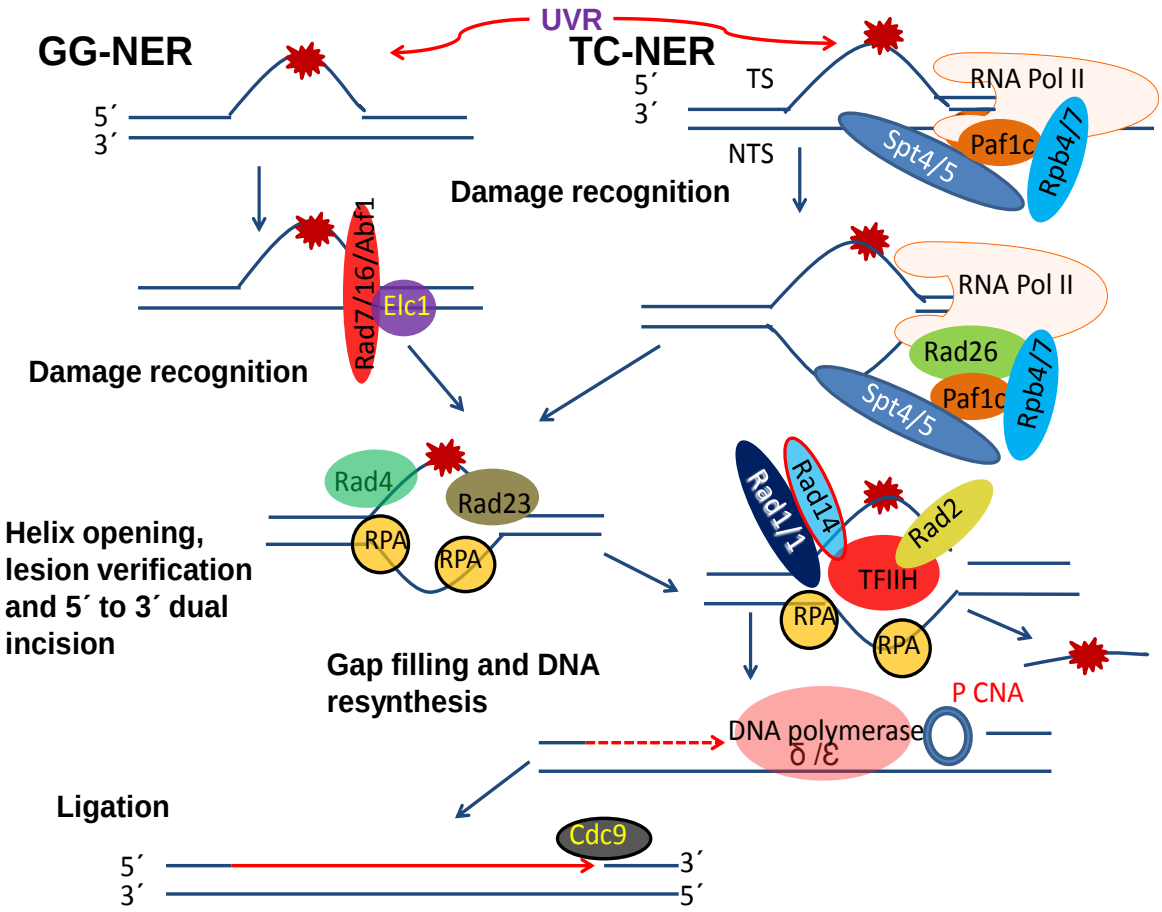

Figure 1.13 Nucleotide excision repair (NER) mechanism. There are two routes for the repair of DNA photolesions: global genome repair (GG-NER) and transcription coupled repair (TC-NER). In first route, the damaged sites are recognised by the complex protein Rad7/Rad16/Abf1 factor and Rad4-R23. In the second route, TC-NER is initiated by the arrest of RNA polymerase II at a lesion on the transcribed DNA strands. Following recognition, the DNA lesions are opened by activation of transcription factor IIH (TFIIH), and then replication protein A binds the single-stranded DNA. The damage is cleaved on both the 3' and 5' sites, which releases the damaged oligonucleotide. Gap filling proceeds by DNA polymerase δ/Ɛ, using the opposite DNA strand as a template. Finally, the new synthesised DNA is ligated by DNA ligase. Reproduced and adapted from (Li, 2012).

NER is classified into two sub-pathways global genomic repair (GG-NER) which removes DNA damage in non-transcribing DNA throughout the genome (in both transcriptionally active or inactive genes) and transcription coupled repair (TC-NER) which removes DNA lesions only from transcribed strand of actively transcribing genes. Apart from the first step of damage recognition other steps are common in both sub-pathways (Friedberg et al., 2005) which ends with DNA synthesis and ligation.

1.3.2. NER in yeast

Researchers have used *Saccharomyces cerevisiae* as a model organism in the DNA repair research field, because NER is highly conserved amongst eukaryotes. It doesn't have ethical and experimental limitations, it is a genetically tractable organism due to short life cycle (in yeast cell cycle takes 90 min to 120 min compared to an average of 24 h in human cells), and it possesses NER genes that are comparable to those in human cells (for example, Rad1-Rad10 in yeast with XPF-ERCC1 in human, Rad2 in yeast with XPG in human, Rad4 in yeast with XPC in human, Rad23 in yeast with HRad23B etc.). In addition, yeast cells can be rapidly created that contain a spectrum of mutations, including genes with functions in NER and chromatin modification (Botstein and Fink, 2011; Friedberg, et al, 2005; Conconi, 2008; Waters et al., 2012) .

NER in yeast as well as in human has two sub-pathways; global genome repair (GG-NER) and transcription coupled repair (TC-NER). Apart from the first step of damage recognition, other steps are common to both sub-pathways (Friedberg et al., 2005). The recognition step in GG-NER depends on the translocase activity of the ATPase domain of the Rad16 factor within the GG-NER Rad7/Rad16 complex. However in TC-NER, this step is achieved by the elongating RNA polymerase II during gene transcription, which stalls when it encounters DNA lesions (see figure 1.14).

Following recognition, the Rad4-Rad23 complex (XPC-HRAD23B) binds with the DNA damage. Then the transcription Factor II H (TFIIH) Rad3 and Rad25 (XPD and XPB ib human, respectively) is recruited, which unwinds the DNA strand in opposite directions of the DNA lesion forming a bubble structure at and around the site of the damage. This process is performed by two directional helicases, Rad 3 helicase (XPDin human) unwinds DNA in a 5´ to 3´only and Rad25 helicase (in human is XPB) only unwind DNA in 3´ to 5´ direction (Prakash and Prakash, 2000). Thus, they can differentiate the damaged DNA strand from the un-damaged strand (Prakash and Prakash, 2000), as stated above, this leads to the formation of a bubble structure; a region of unpaired DNA at the damage site. After that, Rad14 (XPA in human) and RPA will stabilise and protect the ssDNA from degradation. Then, two junction specific endonucleases, Rad2 (XPG in human) which cuts only at the 3' side and Rad1-Rad10 (XPF-ERCC1 in human) cuts only at the 5' side, will incise the DNA from either side of the lesion (Friedberg, 2005). Then, the damage-containing oligonucleotide (around 25-30 nucleotides) is removed (Huang et al., 1992; Prakash and Prakash, 2000)). Finally, using the intact complementary ssDNA as a template and with the assistance of proliferating cell nuclear antigen (PCNA), DNA polymerase delta/epsilon (Pol δ Pol ε)

will resynthesise the DNA (Friedberg, 2005), and the remaining nick is sealed via DNA ligase. Figure 1.13 or 1.14 illustrates the core steps of this pathway. The NER process is highly conserved between yeast and humans and there are orthologs of all the NER core reaction proteins, in both organisms (Krasikova et al., 2013).

1.3.2.1 GG-NER in yeast

Initiation of DNA repair during GG-NER in yeast involves the Rad7 and Rad16 proteins, which are part of a heterotrimeric complex with a protein called Abf1 ((Reed et al., 1999; Yu et al., 2016). Both the known activities of the Rad16 component of the GG-NER complex (i.e. ATPAse function and the RING E3 ubiquitin ligase function) as well as Abf1 are all essential to facilitate the repair of the DNA lesion (Yu et al, 2016). Rad16 is a member of the SWI/SNF superfamily of ATP-dependent DNA translocases. It produces supercoiling into the DNA through its DNA translocase activity associated with its ATPase domains. This is necessary for the excision of damaged bases during GG-NER (Yu et al. 2004). This activity pauses when DNA lesions are encountered, and this is thought to facilitate the recruitment of other factors that have a role in efficient repair. Rad16 also has a RING domain and forms an ubiquitin E3 ligase that also involves the Cul3 and Elc1 proteins (Gillette et al., 2006; Yu et al., 2016). In response to UV irradiation, Elc1 exerts two different activities regarding its ubiquitin ligase function. Firstly, it regulates cellular Rad4 (XPC in human) levels when it is a component part of a ubiquitin ligase (E3) that also contains Rad7 and Rad16 (Gillette et al. 2006; Ramsey et al. 2004), and secondly, it can also phosphorylate and degrade RNA pol II when it is a component part of a different ubiquitin ligase complex, that also contains Ela1, Cul3, and Roc1 (Ribar, Prakash, and Prakash 2006, 2007). There are some important functional similarities between the Rad7/Rad16 GG-NER factors in yeast, and the DDB1-DDB2 complex found in human cells, but no obvious structural homologies exist (Reed, 2005). GG-NER activity is lost in both human and yeast cells when these factors are mutated. Moreover, the human and yeast complexes both have affinity to physically bind to DNA lesions. Importantly, Rad7/Rad16 form a component of the cullin-based E3 ubiquitin ligase with the substrate for ubiquitination being Rad4 in the case of yeast. DNA-damage binding complex DDB1-DDB2) also form components of a cullin-based E3 ligase, which ubiquitinates the human substrate XPC. XPC is the human homologue of the yeast Rad4 NER gene. In yeast both TC-NER and GG-NER requires Rad4 in yeast (Prakash and Prakash 2000). Frome this stage

forward the remaining steps of the pathway are identical to those outlined above see (figure 1.13 and 1.14) and text in section 1.3.2, page 40).

1.3.3 NER in humans

As stated above, the NER pathway and sub-pathways in yeast and human cells are evolutionarily conserved; and the common core reaction of NER in human is similar to that in yeast and other eukaryotic organisms. It consists of two pathways with the same core NER steps as in yeast. The genes and proteins involved in these steps are also present in humans, with great structural and functional similarities. The importance of this pathway is manifested when any of the several NER genes are defective. Many other genes are also involved in promoting efficient NER. Defective NER in humans causes Xeroderma Pigmentosum (XP), a rare heritable autosomal recessive disease, characterized by excessive sensitivity to ultraviolet radiation from the sun and it is also characterized by about a 2000 fold increased risk of skin cancer. A wide spectrum of bulky DNA lesions are removed by NER including UV-induced CPDs. Likewise in yeas, NER is performed by two sub-pathways: transcription-coupled repair (TC-NER, see figure 1.15 and its legend on page 45 for a brief description of the mechanism of this sub-pathway in human) as well as global genome repair (GG-NER).These initial stages of NER are subsequently followed by the coordinated actions of other NER-associated factors. Immediately after the recognition step, downstream NER factors including transcription factor II human (TFIIH) comprising XPB (Rad25 in yeast) and XPD (Rad3 in yeast) factors, are recruited by XPC (Sugasawa, 2010) to unwind the DNA . Then, the DNA becomes exposed and the damaged DNA site is loaded by XPA Rad14 in yeast), whereas the undamaged DNA is bound by RPA, which promotes XPG to cut at 3' side and ERCC1-XPF to cleave at 5' side (Prakash and Prakash, 2000).as discussed above after recognition all the steps are the same in both human and yeast (see above section 1.3,2, page 40) and see figure 1.13 and 1.14.

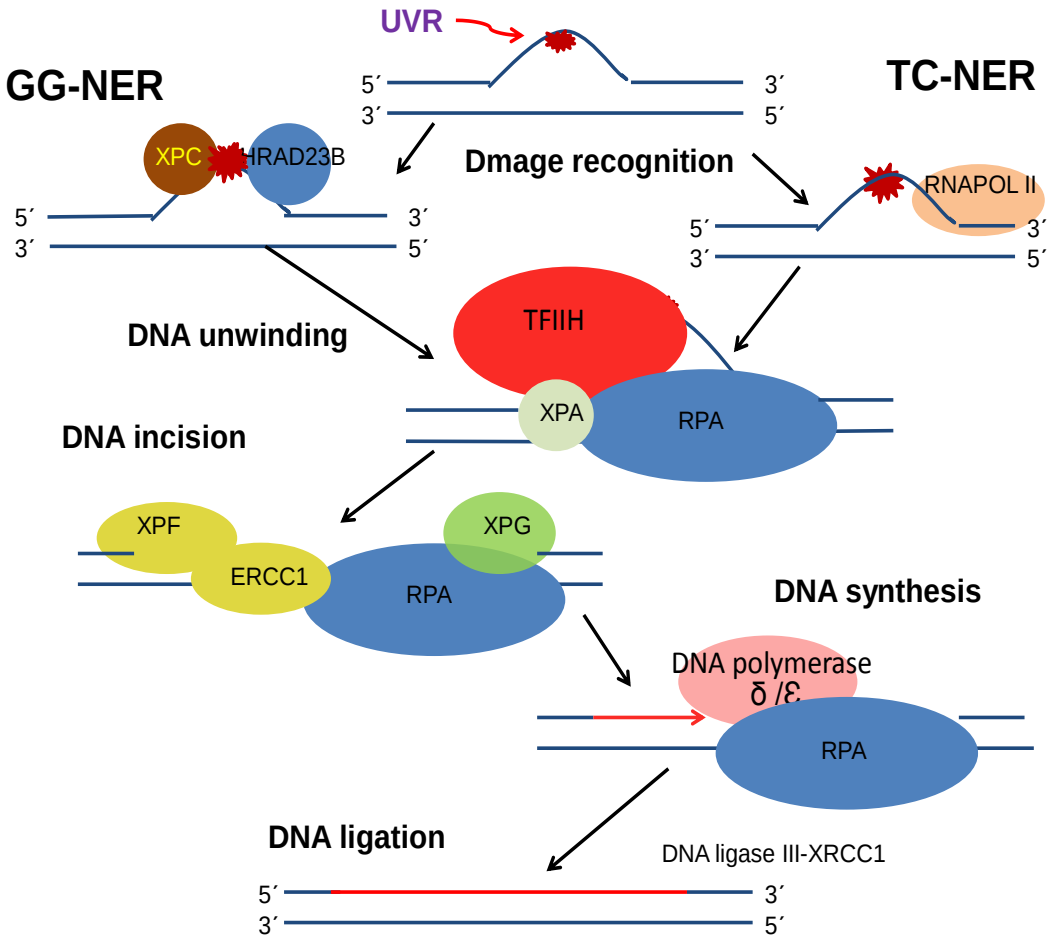

Figure 1.14 Nucleotide excision repair (NER) mechanism. There are two routes for the repair of DNA photolesions: global genome repair (GG-NER) and transcription coupled repair (TC-NER). In first route, the damaged sites are recognised by the complex protein XPC-hHR23B. In the second route, TC-NER is initiated by the arrest of RNA polymerase II at a lesion on the transcribed DNA strands. Following recognition, the DNA lesions are opened by activation of transcription factor IIH (TFIIH), and then replication protein A binds the single-stranded DNA. The damage is cleaved on both the 3' and 5' sites, which releases the damaged oligonucleotide. Gap filling proceeds by DNA replication factors such as replication factor C (RF-C) and DNA polymerase δ/or ε, using the opposite DNA strand as a template. Finally, the new synthesised DNA is ligated by DNA ligase. This figure was reproduced from (van Steeg and Kraemer, 1999, Friedberg, 2001).

1.3.3.1 GG-NER in humans

In this pathway both DNA strands (TS and NTS) in active and inactive genes are repaired throughout the entire genome. It has (DDB) and XPC, Rad23B and centrin 2 (centrosomal protein) sensors that form a heterotrimeric complex and form a complex that acts as a sensor of "DNA damage" and scans over the genome and can identify helix distortions. While, DNA helix distortion can be detected by the XPC-Rad23B complex, however, some UV-induced damages can be recognised by DDB1 and DDB2 as well (Le May et al., 2010). It is believed that centrin 2 augments XPC recognition

ability. Following detection several other proteins are recruited to the damaged area for verification.

This pathway repairs a wide spectrum of different DNA adducts and crosslinks generated by carcinogenic agents, UV irradiation from the sun light or by-products from normal cellular metabolism and hence retains genetic and epigenetic integrity. Xeroderma Pigmentosum group C (XPC) locate the lesion and other complex subunits are then recruited which ends with DNA damage excision. In this pathway, two ubiquitin ligases (cullin-type CRL4DDB2 and sumo-targeted RNF111) regulate the XPC function by their ubiquitination system that promotes GG-NER reactions and subsequently secure the XPC-DNA damage interaction (Natarajan and Takeda, 2017). Both of the CRL4DDB2 or RNF111, are essential for efficient UV induced DNA excision repair (Natarajan and Takeda, 2017). Following UV irradiation, XPC is recruited and ubiquinated by CUL4 E3 ligase complex and this boosts its sensitivity to identify and bind the distorted DNA and this in turn recruits more NER factors to the site of damage. The cullin 4A of the E3 complex serves as a scaffold, an E2-binding subunit (RBX1/ROC1 or RBX2) on one side, adaptor subunit DDB1 is located on the other side with DDB2/XPE. In this way they can detect tiny DNA distortions. Following lesion detection, the E3 ligase is neddylated and activated by the CUL4 and E3 ligase it then recruits XPC complex to the DNA damaged site.

XPC binding affinity increases due to its ubiquitination by UBCH5 as E2ates to associate with RAD23 which is bound to XPC to prevent degradation by ubiquitin-mediated proteasome and bind to the undamaged DNA strand (Sugasawa, 2010). Then, XPC recruits downstream NER factors including transcription factor II human (TFIIH) comprising XPB and XPD factors. So UV-DDB not only recognizes UV-induced lesions but also provide XPC substrate to trigger NER (Sugasawa, 2010). Degradation of the DDB2 and CUL4A is initiated since its affinity to DNA is diminished due to self-ubiquitination. Hence, from the whole complex, only XPC remains at the site of the lesion which has increasing affinity for the DNA lesion, and at the same time as reduces its own level, and thus the recognition and verification of the damage is achieved. After this point both GG and TC-NER converge, and follow a common pathway see section 1.3.2 in page 40 and section 1.3.3 and also Figure 1.14 and 1.15.

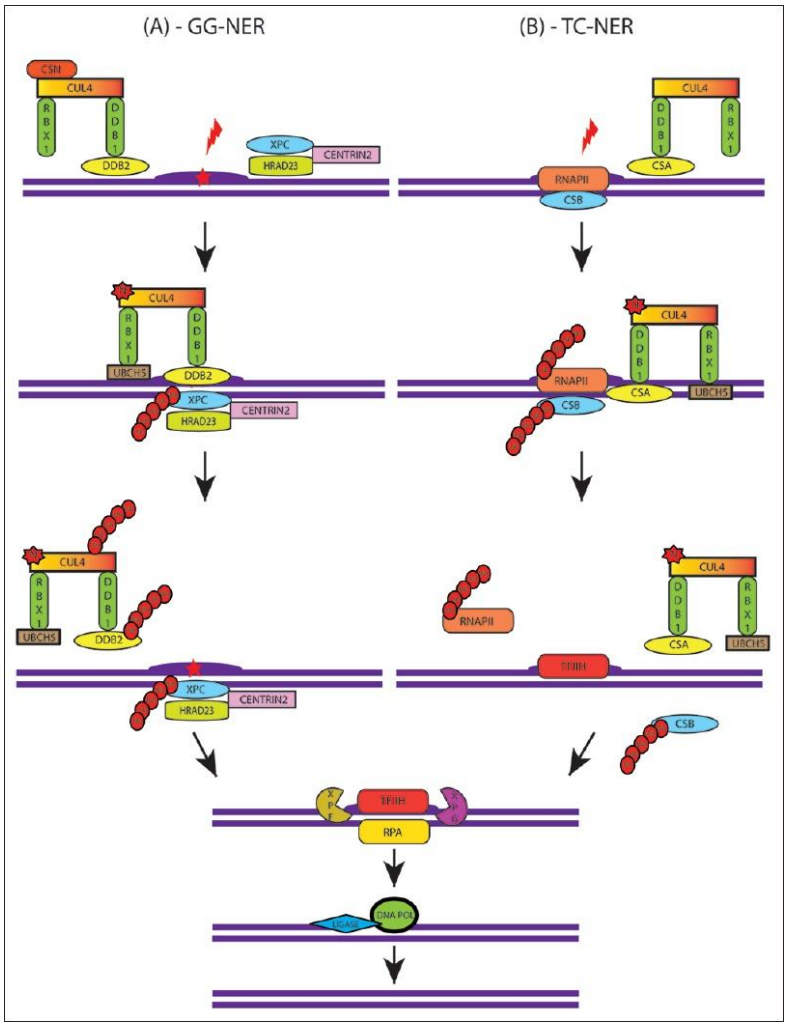

Figure 1.15 illustrates the early stages of DNA damage recognition by GG-NER and TC-NER of the NER sub-pathways.(A) During DNA damage, CUL4 E3 ligase complex recruits and ubiquitinates xeroderma pigmentosum Group C and increases its sensitivity to recognize and bind the distorted DNA. Xeroderma pigmentosum Group C recruits further nucleotide excision repair core repair components to complete the repair of global genome-nucleotide excision repair. (B) In transcription coupled-nucleotide excision repair, RNA polymerase II recognizes the distorted DNA and recruits Cockayne syndrome Type B. Cockayne syndrome Type B then recruits CUL4 E3 ligase and core nucleotide excision repair proteins and also ubiquitinates Cockayne syndrome Type B. Ubiquitinated Cockayne syndrome Type B detaches from the distorted DNA which otherwise acts as physical block for the repair process and transcription (Natarajan and Takeda, 2017).

1.3.4 NER in chromatin

In eukaryotic cells NER occurs in the chromatin context, which can act as a barrier for NER factors to access and remove the DNA lesions, and also poses a challenge in restoring the chromatin structure after repair is complete (Polo and Almouzni, 2006). Chromatin is the resulting structure created when

DNA is packaged in eukaryotic cells. In human cells it enables the two metres of DNA

to be compacted and organised into chromosomes. The DNA is wound around nucleosomes, which are composed of histone proteins. A nucleosome is an octamer that consists of a tetramer of H3 and H4 flanked by two H2A-H2B dimers. It has about 147bp of DNA wound around it, and linker regions of varying DNA length separates the nucleosomes. The chromatin aggregates and condenses further via histone H1 (Dinant et al., 2012; Linger and Tyler, 2007; Luger et al., 1997) (Figure1.16). Folding and stacking nucleosome on each other acts as a physical barrier for various cellular processes involving DNA transactions, since DNA becomes 'hidden' and cannot be accessed by various factors acting on the DNA template. Therefore, chromatin disruption becomes a necessary step for local modulation of DNA during transcription, replication and DNA repair. NER factors must gain access to the DNA damage through disruption of chromatin via histone modifications and remodelling of chromatin. After repair the chromatin must be restored to its pre-damaged state and the central question here is: what is the mechanism that restores chromatin to its pre-damaged state following repair.

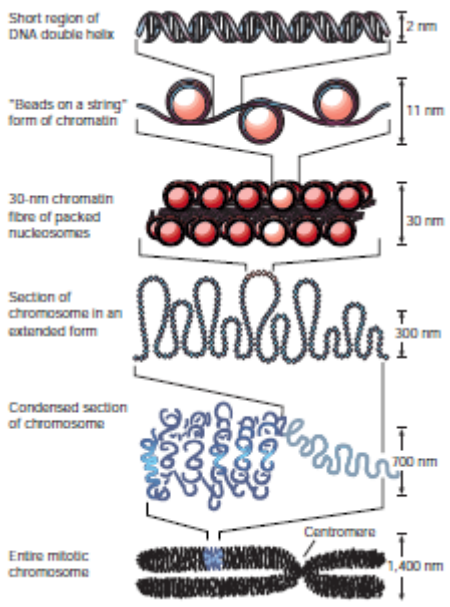

Figure: 1.16 The organization of DNA within the chromatin structure. The lowest level of organization is the nucleosome, in which two superhelical turns of DNA (a total of 165 base pairs) are wound around the outside of a histone octamer. Nucleosomes are connected to one another by short stretches of linker DNA. At the next level of organization the string of nucleosomes is folded into a fibre about 30 nm in diameter, and these fibres are then further folded into higher-order structures. At levels of structure beyond the nucleosome the details of folding are still uncertain (Felsenfeld and Groudine, 2003). https://www.nature.com/articles/nature01411/figures/1

At present our knowledge of how NER operates in chromatin is in its early stages, but recent advances are providing important insights into this process. The Access-Repair-Restore (ARR) model was established as a paradigm for understanding the removal of DNA damage from chromatin (Smerdon, 1991). According to this model chromatin rearrangement occurs to promote the access of repair factors to the site of the damaged DNA. This event promotes both the recognition of lesions in chromatin and their removal during repair. Following repair, the chromatin is reassembled to restore it to its original pre-damaged state. Importantly, chromatin also plays an active role in genome stability, ensuring efficient DNA repair takes place just in the right place at the right time in the genome (Smerdon, 1991). During DNA repair three main processes control chromatin structure: sliding of nucleosomes (promoted by chromatin remodellers), histone eviction/exchange (canonical histones or histone variants controlled by histone chaperones, e.g. CAF-1 and HIRA) and disruption of higher order chromatin structure (Histone modifications such as acetylation), such as unfolding of chromatin fibres (Polo, 2015). Each of these processes is driven by the combined activities of the following four regulatory factors: ATP-dependent chromatin remodellers, histone chaperones, histone modifiers, and histone variants (Peterson and Almouzni, 2013).

It became obvious from the studies conducted by Ramanathan and Smerdon (Ramanathan and Smerdon, 1986, 1989) and also by Smerdon and Thoma (Smerdon and Thoma, 1990; Wellinger and Thoma, 1997) that damaged DNA in the context of chromatin cannot be repaired by *in vitro* NER core factors and that some other factor promotes efficient NER in chromatin (House et al., 2014). Ramanathan and Smerdon revealed that histone H3 acetylation has an important role in NER (Ramanathan and Smerdon, 1986, 1989). Smerdon and Thoma indicated that DNA lesions located within nucleosomes were repaired much slower than the damage residing between nucleosomes (linker DNA). These studies revealed that NER in eukaryotic organisms must occur in the context of chromatin and that repair and modification of chromatin are closely connected.

Previously researchers have determined that during transcription there is dynamic coordination between chromatin remodelers and histone modifications (Cairns et al., 1996; Carey et al., 2006). Transcriptional activators attract HATs and other chromatin remodeling complex factors on to the chromatin to assist chromatin unfolding and transcription process (Yudkovsky et al., 1999). Investigations by Duan and Smerdon on a reconstituted nucleosome of H3 acetylated histone, showed that a RSC (which is a

complex with the capacity to remodel the structure of chromatin, termed RSC) which is a well-known abundant chromatin remodeler complex (with a DNA-dependent ATPase activity stimulated by both free and nucleosomal DNA and a capacity to perturb nucleosome structure), has a critical role in erasing UV-induced DNA damages. They determined that acetylated histone H3K14 in association with RSC can change the unfolding dynamics of the nucleosome and repair the damage-induced DNA lesions of the nucleosomal DNA effectively. However, such events do not occur with H3K14 acetylation alone (without RSC) (Duan and Smerdon, 2014).

Histone acetyltransferases (HAT) enzymes transfer acetyl groups from acetyl CO-A to specific lysine residues at histone tails (Lee and Workman, 2007). As a result of the altered chemistry of the histone the close association between DNA and the histones is reduced. Many DNA processes including gene transcription (Kurdistani et al., 2004; Pokholok et al., 2005) are aided by the acetylation of histones, which leads to the increased access of specific regulatory proteins to DNA.

Reed and his colleagues have demonstrated that Histone H3 hyperacetylation of induced DNA damage is driven by Rad7/Rad16 GG-NER complex. As stated above, the yeast GG-NER pathway requires both Rad7 and Rad16 proteins (Friedberg, 2005; Reed et al., 1998; Verhage et al., 1994). These two proteins form a complex and are crucial for lesion removal from non-transcribed DNA and the non-transcribed strand (NTS) of transcriptionally active genes (Reed et al., 1999; Reed et al., 1998; Verhage et al., 1996). Similarly, both Rad7 and Rad16 components are required for efficient excision events (Reed et al., 1998). In 1999, Reed purified a third component of this complex from yeast; the ARS binding factor 1 (Abf1), which is now known to be required for GG-NER. Abf1 is a DNA-binding protein that localises to numerous genomic locations such as certain origins of DNA replication, in addition to the silencing loci associated with *HML* and *HMR* loci (Diffley and Stillman, 1989). The GG-NER complex can be found bound at Abf1 binding sites (ABS) at gene promoters in the absence of DNA damage (Yu et al., 2009). In response to UV exposure, the Rad7-Rad16 complex dissociates from Abf1 and is redistributed away from these promoter-bound positions. Abf1, on the other hand, remains bound at these sites (Figure 1.17). It was suggested that this mechanism primes the chromatin for UV-induced chromatin remodeling and redistribution of the Rad7-Rad16 GG-NER complex necessary for efficient repair (Yu et al., 2016; Yu et al., 2009). The UV-induced Rad7 and Rad16 redistribution occurs predominantly into ORFs and intergenic non-transcribed regions upstream of gene promoters (Yu et al., 2016).

Rad16 has two essential functional domains: a RING domain bounded by two ATPase domains (Guzder et al., 1998). It is a member of the SWI/SNF family of chromatin remodelers that have a DNA translocase activity that can produce superhelical torsion in linear DNA fragments via this activity (Havas et al., 2000). Although Rad16 has the ability to generate torsion during scanning on the DNA strand via its ATPase domain and has the potential to drive chromatin remodeling necessary for efficient DNA repair, through its ring domain unlike some SWI/SNF super family complexes, it is unable to slide nucleosomes (Yu et al., 2009). This feature may help prevent spurious, unregulated gene expression during DNA repair as a result of nucleosome sliding which is a known mechanism of chromatin remodeling that is associated with gene activation (Yu et al., 2004). Mutating either of the known domains of Rad16 alone leads to moderate sensitivity to UV irradiation and reduced repair. However, inactivating both domains by site-directed mutagenesis produces a UV sensitivity phenotype similar to a complete deletion of *RAD16* (Ramsey et al., 2004; Yu et al., 2011). Rad16 occupancy was observed at Abf1 binding sites in wild type cells and is lost in the ATPase/RING double mutant cells. This means that both functional domains are needed for proper distribution of Rad16 (Yu et al., 2016), before and after UV irradiation. Interestingly, the unique separation of function point-mutations in the E3 ligase and ATPase domains allowed for the mechanism of Rad16 chromatin binding to be resolved in great detail. In the absence of ATPase activity, Rad16 occupies the chromatin at and around the Abf1 binding sites as seen in wild type cells. However, in response to UV irradiation there is no active redistribution of Rad16 into more distal regions of the genome. On the contrary, when the E3 ligase is inactivated the normal wild type enrichment of Rad16 is lost at the promoter regions upstream of genes and the distribution of the protein loses its structure in the absence of UV exposure. In response to UV irradiation, however, redistribution of Rad16 can be observed as a minor enrichment into the coding area and loss from promoter regions due to the activity of the ATPase domains (Yu et al., 2016). This indicates that, establishing and maintaining Rad16 occupancy on the chromatin at the Abf1 binding sites before UV irradiation is dependent on its E3 ligase activity and not on the ATPase activity. Yet, the latter activity is indispensable for damage induced Rad16 redistribution (Yu et al., 2016)

.Reed's lab has contributed to advancing and understanding the access repair restore (ARR) model for GG-NER, especially the first two phases (access and repair). Under unchallenged conditions, Figure 1.17 below and 4.1 in page 101 illustrates the model whereby Rad7-Rad16 regulates the chromatin occupancy of the HAT Gcn5. In response to DNA damage the Rad7/Rad16 GG-NER complex dissociates away from

Abf1 and recruits Gcn5 on to the chromatin leading to the increased chromatin occupancy of Gcn5 and consequently increased levels of histone H3 acetylation. These events promote chromatin remodelling necessary for effective NER by making the chromatin more accessible. This mechanism was uncovered by restriction enzyme digest assay that demonstrated that increased chromatin accessibility at positions downstream of Abf1 binding relied on all GG-NER factors, including Gcn5 and histone H3 acetylation (Yu et al. 2005; Yu et al. 2011). In *RAD16* deleted cells, increased Gcn5 occupancy and UV-induced H3 acetylation does not occur. This means that in response to UV, the Rad7-Rad16 GG-NER complex controls both increased Gcn5 occupancy and H3 acetylation (Yu et al., 2011). When both Rad16 and Gcn5 are absent, H3 acetylation is reduced both before and following UV irradiation (Yu et al., 2011). Furthermore, we reported that Rad16 controls UV-dependent histone H3 acetylation throughout the genome (Teng et al., 2008). Importantly, all of these changes to protein chromatin occupancy and chromatin structure are restored to their pre-damaged state (i.e. Rad7-Rad16, Gcn5 and histone H3 acetylation).

In studying the restoration phase of chromatin remodelling after DNA repair, it became apparent that UV-induced increased levels of histone H3 acetylation remain constitutively high (see chapter 4 section one Figure 4.2A, page:101) in repair defective strains such as *RAD4* and *RAD14* deleted cells (Yu et al. 2005). This indicated that, while the UV-induced increase of histone H3 acetylation level is dependent on the GG-NER complex of proteins, it occurs independently of the Rad4 and Rad14 genes that are essential for the repair of UV induced DNA damage. Therefore, damage-induced histone H3 acetylation does not depend on the removal of DNA damage by the NER process itself. On the other hand, histone H3 deacetylation and chromatin remodelling after DNA repair is entirely dependent on completion of the NER reaction as these events do not take place in Rad4 and Rad14 deleted repair deficient cells (Yu et al., 2016; Yu et al., 2011; Yu et al., 2005). This indicates that efficient removal of DNA damage is a vital step for late stage chromatin remodelling during GG-NER. This can be achieved either by direct reversal of the histone modification or by exchange of the modified histone (see Figure 4.2, page 101).

Enzymes known as histone deacetylaces (HDACs) are involving in chromatin restoration in yeast when they recruited (HDACs) on to chromatin to erase acetyl mark (Beckouët et al., 2016; House et al., 2014). HDACs are involved in removing acetyl groups from histone tails during several cellular processes such as during gene activation and their activities are in equilibrium with the activity of HATs (Ekwall, 2005;

Kurdistani et al., 2002). Any changes in this balance will change the acetylation levels found on the histones.

Furthermore, during NER histone covalent modifications take place, in which histone acetylation/deacetylation is one of the most essential chromatin remodelling processes. This process of the histone acetylation/deacetylation at the histone tails including H3 is regulated by HATs and HDACs, influencing gene activation or inactivation, respectively (Wilner Martínez-López, 2013). Moreover, during the early stages of the repair process, mammalian HDACs are recruited to a DSB site which indicate a direct involvement of HDACs in this pathway (House et al., 2014). There is also evidence of H3K56 deacetylation by HDAC1 and HDAC2 during micro-irradiation-induced DSB (House et al., 2014). Deacetylation of H3K56 takes place during replication and repair of nucleosome assembly (Chen et al., 2008; House et al., 2014).

Knowing all the above facts about histone modifications, which are needed for chromatin alteration to promote efficient repair, extra modifications are also needed to reset the chromatin state immediately following successful repair. These are coupled to what we described earlier of the ARR model and the fact of lingering of histone H3 acetylation in a hyperacetylated state. Hence, we hypothesised that HDACs are involved in histone H3 deacetylation to revert chromatin to its pre-damage state following GG-NER. Therefore, I set out experiments to define the mechanism by which damage-induced acetylation in chromatin is restored to its undamaged state. The level of histone H3 acetylation in wild type and different HDAC mutants can be examined both before and after UV irradiation.

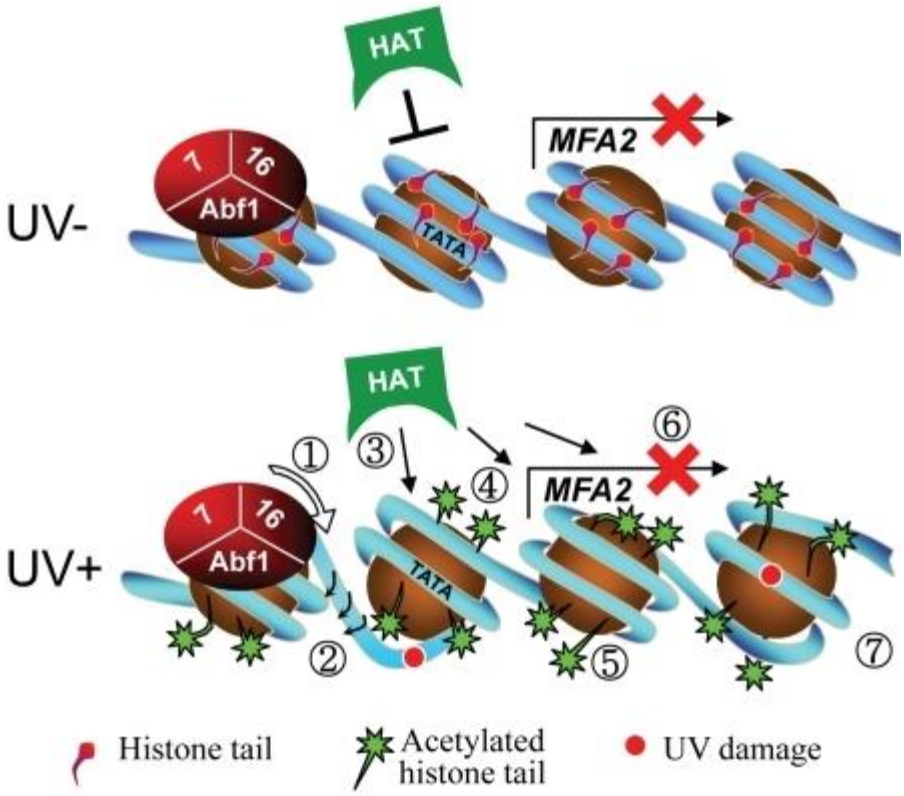

Figure 1.17 Model for UV-induced chromatin remodelling during GG-NER. Upper panel: In the absence of UV, basal levels of histone acetyl transferase occupancy are detected on the chromatin of the MFA2 promoter. The absence of histone acetyl transferase occupancy is marked by the presence of an inhibitory link. Consequently, histone H3 tails remain unacetylated and chromatin remains repressed. Lower Panel: Following UV the DNA translocase (1) and E3 ligase (2) activities of Rad16 in the GG-NER complex promote increased histone acetyl transferase occupancy on chromatin as indicated by the presence of arrows (3) and histone H3 acetylation (4) that drives chromatin remodelling as shown by a more open chromatin structure around the nucleosomes (5). Failure of the GG- NER complex to slide nucleosomes may prevent transcription factor binding explaining the continued repression of MFA2 transcription (6) despite chromatin remodelling. GG-NER dependent chromatin remodelling promotes efficient lesion removal (7) (Yu et al, 2011). Rad7/16

1.4. Aim of my study

Genomic DNA in eukaryotic organisms is organised and packaged into chromatin, which may act as a physical barrier for DNA binding proteins to interact with the DNA. Hence, any operation that uses DNA as a template, such as during DNA replication, transcription and DNA repair, chromatin requires certain rearrangements in order to successfully accomplish this task. In the context of genome stability, these changes to the chromatin structure have been framed and explained by the introduction of the Access-Repair-Restore (ARR) model, which provides a paradigm for the study of chromatin dynamics in response to DNA damage. Much of the current focus of research in to DNA repair mechanisms involves different aspects of understanding how genome stability is maintained in the context of chromatin. Progress is being made in each of the various DNA pathways, with notable advances in the area of double strand break repair. The Reed laboratory has conducted research into understanding how chromatin is remodelled during NER, and in particular GG-NER for many years. A complex of proteins containing the SWI/SNF chromatin remodelling factor Rad16 was purified and biochemically characterised and shown to be essential for the remodelling of chromatin to permit repair of UV-induced lesions; a major source of DNA damage repaired by the NER pathway. Reed's group has shown that following UV irradiation, this complex of proteins that is referred to as the GG-NER complex, modifies the UV-induced acetylation status of lysine 9 and lysine 14 of histone H3. This in turn changes the chromatin structure and these changes are necessary for repair of UV induced damage in chromatin. How nucleosome remodelling affects the ability of DNA damage recognition factors to access the damaged DNA in chromatin to permit DNA repair at the right time at the right place in the genome is a current major focus of research in the laboratory. However, the focus of my study is a different, but related one. As described above, it has been shown that in response to UV irradiation, histone H3 acetylation levels increase and promote the formation of a more open chromatin structure necessary for efficient DNA repair. However, these changes to the histones and the nucleosome structures they regulate, must return to the normal, undamaged state following DNA repair. In this study, I aim to investigate the mechanisms involved in restoring these changes to the chromatin that return it to its pre-damaged state. This will involve conducting experiments designed to determine the factors that control the restoration of UV-induced histone acetylation following removal of DNA damage during GG-NER.

Chapter 2

2. Materials and methods

In this Chapter, all the methods that were used regularly in the lab was explained including storage and growing conditions of *S. cerevisiae* yeast strains with all the techniques used regularly like UV treatment, DNA extraction, chromatin preparation and its sonication, quantitative real-time PCR (qPCR) and immuno-slot-blot experiment. A detailed chromatin immunoprecipitation on chip (ChIP-on-chip) technique was described in chapter 5 in addition to describing the main points here in this chapter as well.

2.1 Yeast Strains

Strains	**Genotype**	**Source**
Wildtype	MATα, *his3Δ1, leu2Δ0, met15Δ0, ura3Δ0*	Euroscarf
*hda1*Δ*α*	MAT*α*, *his3Δ1, leu2Δ0, met15Δ0, ura3Δ0, HDA1::kanMX4*	Euroscarf
*rpd3*Δ*a*	MATa, *his3Δ1, leu2Δ0, met15Δ0, ura3Δ0, RPD3::kanMX4*	Euroscarf
*rpd3*Δ*α*	MATα, *his3Δ1, leu2Δ0, ura3Δ0, RPD3:: kanMX4*	Euroscarf
*hos1*Δ*α*	MATα, *his3Δ1, leu2Δ0, lys2Δ0, ura3Δ0, hos1::kanMX4*	Euroscarf
*hos2*Δ*α*	MATα, *his3Δ1, leu2Δ0, lys2Δ0, ura3Δ0, hos2::kanMX4*	Euroscarf
Wildtype	MATα, *GCN5-18myc, his3Δ1, leu2Δ0, met15Δ0, ura3Δ0*	Dr S. Yu
rad7Δ	MATα, *GCN5-18myc, rad7Δ, his3Δ 1, leu2Δ0, met15Δ 0, ura3Δ0*	Dr S. Yu
rad14Δ	MATα, *GCN5-18myc, rad14Δ, leu2Δ0, met15Δ0, ura3Δ0*	This study
Wildtype	MATα, *RAD7-18myc, his3Δ1, leu2Δ0, met15Δ0, ura3Δ0*	Dr S. Yu
rad14Δ	MATα, *RAD7-18myc, rad14Δ, leu2Δ0, met15Δ0, ura3Δ0*	This study
Wildtype	MATα, *RAD16-18myc, his3Δ1, leu2Δ0, met15Δ0, ura3Δ0*	Dr S. Yu
rad14Δ	MATα, *RAD16-18myc, rad14Δ, leu2Δ0, met15Δ0, ura3Δ0*	This study
Wildtype	MATα, *HDA1-18myc, his3Δ1, leu2Δ0, met15Δ0, ura3Δ0*	This study
rad14Δ	MATα, *HDA1-18myc, rad14Δ, leu2Δ0, met15Δ0, ura3Δ0*	This study
Wildtype	MATα, *RPD3-18myc, his3Δ1, leu2Δ0, met15Δ0, ura3Δ0*	This study
rad14Δ	MATα, *RPD3-18myc rad14Δ, leu2Δ0, met15Δ0, ura3Δ0*	This study

Note: All the strains used in this study are BY4742 orthologue haploid yeast strains

2.2 Storage and growth conditions

During the whole study, all the equipment, glassware and growth media were disinfected by autoclaving and sterilisation before use for each experiment and all manipulations were executed in sterile environment where appropriate.

Yeast strains were grown in Yeast Extract Peptone Dextrose (YPD) broth, YPD-agar plates (1% (w/v) BactoYeast extract, 2% (w/v) BactoPeptone; 2% (w/v) Dextrose and 2% (w/v) agar) or in synthetic drop out media (minimal media (MM)) and incubated at a 30°C incubator (shaking at 200 rpm for liquid cultures) see appendix I page 162. For the long-term storage of yeast strains, cells were grown to log-phase in YPD and suspended in a 30% (v/v) glycerol solution and stored at -80°C. For short-term storage strains were streaked on YPD-agar plates and kept at 30°C (LEEC compact incubator) for 3 days to grow and stored at 4°C. To obtain a pre-culture, a single isolated colony was picked and inoculated into 10 mL of YPD and incubated at 30°C in a shaking incubator to grow overnight. The culture reaches stationary phase overnight and is then stored at 4°C for future use. For each experiment to prepare chromatin, 100 mL of cell culture was used per repair time point (for some experiments 200 mL of culture per repair time point was used as in the case of HDACs). To achieve this, a pre-determined volume of the stock stored at 4°C was inoculated into YPD media. The cells were then harvested when the density reached 2 $x10^7$ cells/mL during which the cells are in the exponential growth phase.

2.3 Analysis of UV sensitivity - Cell survival

In order to analyse UV sensitivity, the targeted yeast strains (WT and different HDAC mutants), was exposed to UV-C light 254nm from a previously calibrated germicidal VL-21G mineralight lamp (UV products, San Gabriel, CA, USA) at a fluence of 10 J/m^2/ to induce 6-4PP and CPD lesions. This technique was used to test and compare the survival rates between different strains, comparing wild type and different HDAC mutants. The detailed process was as follows:

1) YPD agar plates were prepared and labelled beforehand. A density of 2-4 $x10^7$ cells/mL was obtained from an overnight cell culture of 10 mL. Samples were then diluted using a serial dilution to a concentration of 2 cells/µL (2,000 cells/mL) to accommodate the strain and UV dose used. For example, samples were diluted 10 to 100-fold and were exposed to higher UV doses (20,000 cells per plate were used for

UV doses above 80 J/m^2). However, those hit with lower dose were diluted up to 10000 folds (no UV and up to 30 J/m2 doses a total of 200 cells per plate were used and for 40 to 80 J/m^2 doses a total of 2000 cells per plate were used). This was done to achieve on average ~200 colonies for adequate quantification. High UV-dose causes more cell death and requires a high cell density to allow quantification.

2) After final dilution, the samples were all mixed by vortexing, after which 100 µL of cell suspension was applied onto the agar plates. The cell suspension was spread onto the plates using glass beads (diameter 3mm). Plates were prepared in triplicate for all the experiments.

3) The 254nm UV-C lamp was switched on and calibrated prior to irradiation. The plates were placed centrally under the UV lamp one by one and treated at a dose rate of 10J/m^2s. Typically, doses of 0, 20, 40, 80,120 and 160J/m^2 were applied but for the very sensitive strains used here lower doses 0, 2, 6, 8, 10, 20 J/m^2.

4) Plates were incubated at 28ºC for 3 days in the dark to prevent photoreactivation repair. The number of colonies was calculated on every plate and UV sensitivity was determined via survival curves.

5- The percentage of surviving cells was calculated using the average number of colonies recovered on the un-irradiated plates (grown colonies on Un-irradiated plates were calculated as 100% survival). Each replicate was summed to get the average of 3 replicate of one single experiment. Then the average (mean) of three independent experiments was calculated and finally the standard deviation was applied to calculate the deviation from the mean. Standard deviation (SD) is a measure of variation from the mean of the samples that have been investigated, that was calculated using a standard formula in Microsoft excel package.

Below is the formula of the SD to calculate the data manually

$$s_x = \sqrt{\frac{\sum \left(x_i - \bar{x}\right)^2}{n-1}}$$

X = is the average of 3 replicate of one experiment

X bar = mean of 3 independent experiment

N = number of experiments

S = standard deviation (SD)

$\sum$ = summation

See appendix III, page 172-176 as an example, all the analysis for UV survival, CPD repair and ChIP qPCR are calculated this way. (See raw data in the appendices III and IV)

2.4 UV drop tests

Logarithmically growing cells were subjected to 10-fold serial dilution, with dilutions ranging from 1 x 10^{-3} to 1 x10^{-5} in 1xPBS (see appendix I page 164). 1 µL of each of the 5 dilutions was then spotted onto YPD plates. The strains used were either wild type or different mutant strains were all plated on YPD agar plates. The cells, were then exposed to same doses of UV irradiation (one sample plate from each strain were kept un-irradiated as a control). Finally, the plates were incubated for 3-4 days at 28 to 30˚C.

2.5 UV Irradiation of yeast cells

When cells reach a desired density during exponential phase, they were harvested, counted, centrifuged and re-suspended in chilled PBS (4°C) and standardised to 2x10^7 cells/mL prior to chromatin extraction. Yeast cells were aliquoted in a 50 mL petridish (14cm Pyrex dish, the depth of cell suspension was approximately 0.32cm). An un-irradiated sample was kept in chilled PBS on ice. Then, the cells were exposed to the desired dose of UV-C irradiation (typically 100 J/m^2) at 254nm from a germicidal lamp to induce DNA damage. The irradiated cells were re-suspended in YPD and allowed to repair in the dark (to avoid photoreactivation repair) for different times at 28 - 30°C. Then, using a Beckman Avanti J-25 centrifuge, JA-10 or JA-20 rotors and Beckman

polypropylene tubes (500 mL) were used for centrifugation for 5 min at 5000 rpm at 4°C.

The entire UV irradiation workflow is as follows:

1) An overnight culture of yeast strains, was grown to density of 2-4 $x10^7$ cells/mL. Cells were collected by centrifugation at 4000 to 5000 rpm for 5 min at 4°C the following day.

2) The cells were re-suspended in pre-chilled PBS and diluted or concentrated to a density of $2x10^7$ cells/mL. The cells were then vortexed to obtain a homogenous cell suspension.

3) For each strain used in this study, an Un-irradiated (U) sample was reserved prior UV irradiation. For each experiment, depending on the repair time points a desired volume is prepared such that the number of cells for each repair sample is constant.

4) 50 mL aliquots of cell suspension were placed in a 14cm Pyrex dish, with a depth of cell suspension of approximately 0.32 cm. The UV-C lamp (UVP Inc., CA, USA) VL-21G lamp (Vilber Lourmat, France) was calibrated and the cells were irradiated at a dose of 10 J/m^2s for 10 seconds. To ensure that all the cells receive a constant dose of UV irradiation during UV exposure, the dish was gently shaken laterally 20 times. Immediately following irradiation, the cells were kept in a sterile flask in the dark on ice. This procedure was repeated for the remainder of the cell suspensions.

5) Depending on the experimental design, immediately after UV irradiation a sample was taken for zero repair time (0).

6) The irradiated cells were pelleted by centrifugation at 5000 rpm for 5 min and re-suspended in the same volume of YPD. The irradiated cells were then incubated at 30°C in a shaking incubator to allow repair to take place for each repair time (15, 30, 60, 120, 180 min) during these time points the cells are still in the arrested phase.

7) After the repair time the yeast cells in all samples were pelleted at 5000 rpm for 5 min at 4°C and re-suspended in 40 mL of pre-chilled PBS then transferred into a 50ml conical tubes (Falcon™, Fisher Scientific, Loughborough, UK) and kept in the dark on ice.

2.6 Extraction of Yeast DNA

Approximately $1x10^{10}$ cells/sample are required to yield ~300-500 µg of genomic DNA from yeast cells. DNA extraction from yeast is initiated by zymolyase treatment to create spheroplasts. These are then lysed in lysis buffer contain sodium dodecyl sulphate (SDS). The DNA is then extracted by phenol/chloroform and precipitated using ethanol, after removing both RNA and protein by RNase A and Pronase (Sigma-Aldrich Company Ltd, Gillingham, UK), respectively. See appendix I page 165

1) Cells from step 6, section 2.5 were centrifuged at 5000 rpm for 5 min and washed with 5 mL Sorbitol-TE solution (0.9M sorbitol, 0.1M Tris-HCL, pH 8.0, 0.1M EDTA) and pelleted again See appendix I page 164.

2) Cells then centrifuged and re-suspended in 5ml of Sorbitol with the addition of 1mg/ml zymolyase 20T and 0.28M β-mercaptoethanol (Sigma-Aldrich Company Ltd, Gillingham, UK). Cells were then incubated at 37ºC in a shaking incubator for 1 h or at 4°C overnight. Using a light microscope, the spheroplast formation can be checked.

3) Next, the spheroplasts were pelleted at 2000 rpm for 5 min and re-suspended in 5 mL of lysis buffer/PBS 1:1(v/v) solution (see appendix I. page 164). RNA was then removed by adding 300 µL of RNase A (10 mg/mL in TE buffer, incubated at 95ºC for 10 min, Sigma). Each sample was mixed and incubated at 37°C for 1 h with intermittent shaking. Next, 200 µL Pronase (20 mg/mL in TE buffer) was added to each sample and incubated at 37ºC for 1 h and then at 65ºC for 1 h, with intermittent shaking.

4) DNA was extracted by adding an identical volume of phenol/chloroform 1:1 (v/v). The tubes were vortexed vigorously to obtain a uniform emulsion. Centrifugation at 10000 rpm for 10 min separates the aqueous and organic layer of which the upper phase was transferred to a new tube (care was taken to not transfer any cell debris or protein precipitant from the interphase).

5) To avoid any protein or other contamination a second round of extraction was carried out by phenol/chloroform. Finally, a third extraction was performed now using chloroform/isoamyl alcohol (24:1). The complete deproteinisation was confirmed by monitoring the presence of protein precipitate at the interphase. When this achieved, the aqueous phase was transferred to a new tube.

6) To precipitate DNA, two volumes of chilled 100% ethanol were added to every sample. The solution was inverted gentle to mix and stored at -20ºC overnight.

7) DNA was pelleted by centrifugation at 10000 rpm for 15 min at 4ºC. The pellets were then air dried and dissolved in 1 mL TE. The DNA, was precipitated again by adding 1 mL of chilled isopropanol. The DNA pellet is now visible to the naked eye in solution after inverting the tubes gently several times. The precipitated DNA was transferred to a new 1.5 mL tube containing 500 µL TE.

8) Finally, DNA was qualified and quantified by non-denaturing agarose gel electrophoresis and a NanoDrop 1000 Spectrophotometer (Thermo Scientific, Hempstead, UK) respectively. Finally, the DNA was stored either at 4ºC or -20ºC for later use.

2.7 Immuno-slot Assay

For the identification of UV-induced CPDs, DNA needs to be extracted as explained in the previous section (2.6, page 58). The presence of DNA adducts was assessed from DNA samples using a Bio-Dot SF Microfiltration device and antibody detection, using the following protocol:

1) A double layer of Bio-DOT SF (Bio-Rad) paper was placed on the equipment and covered by a layer of pre-soaked (in 0.4M NaOH for 2 min) Gene Screen Plus Hybridisation transfer membrane.

2) The lid was firmly secured and the outlet was attached to a VacuGene pump (Pharmacia Biotech, UK). A 60 mbar pressure was applied.

3) 200 ng DNA solution in 200 µL (200ng DNA in 1X TE buffer and NaOH at a final concentration of 0.4M) was pipetted into each slot. Then 200 µL NaOH was applied to each well and aspirated again to the membrane.

4) The membrane was removed from the equipment and placed in 3% non-fat milk powder/1x TBST solution for 2 h at room temperature to block any non specific binding.

5) To detect UV damage (CPDs), the membrane was soaked in 3% (w/v) milk powder/1x TBST solution, with the addition of 2 µL CPD antibody (Kamiya Biomedical Company, Seattle Anti-Thymine Dimer Clone KTM53) in a shallow tray. Then, the membrane was submerged for 2 h at room temperature on a shaking platform with mild agitation.

6) The membrane was immersed in 10 mL 3% milk/1x TBST with the addition of 5 µL alkaline-phosphatase linked Goat anti-rat IgG secondary antibody (Sigma-Aldrich A8439) (1:10,000) at room temperature for 1 h.

7) The membrane was washed 3 times using 1x TBST for a total of 10 min each wash. After adding secondary antibody, the blot was incubated at room temperature for 1 h. Finally, the membrane was washed 3 more times using TBST.

8) The membrane can now be exposed to 2 mL of Enhanced Chemo-Fluorescence (ECF) solution (GE Healthcare) at room temperature for 2 min. The Typhoon TRIO Variable Mode imager (Amersham Biosciences) was used to capture the fluorescence emission and the resulting image were quantified using ImageJ software version 1.47 (http://imagej.nih.gov/ij/).

2.8 Yeast transformation

Transformation is commonly used for introducing plasmid DNA and linear DNA fragments for recombination-induced transformation of yeast strains. The protocol consists of the following basic steps:

1. Target DNA for transformation was obtained from a plasmid. Disruption constructs containing a selection marker flanked by genomic DNA targeting the gene of interest was amplified by PCR and purified.

2. Yeast cells were grown overnight in a shaking incubator at 30°C. Next day, the cells were counted and re-inoculated in 50 mL fresh YPD (appendix 1, page 162) to a density of 5×10^6 cells/mL. Growth was monitored by tracking cell count. After two divisions (~3-4 h) the cell density is about $2.0x10^6$ cells/mL which takes 2-4 h. At this stage the cells are ready to take up foreign DNA.

2. To harvest, the cells were spun at room temperature for 5 min in an Eppendorf tube at 1000 rpm. The cells were collected and washed with 25 mL of sterilised ddH_2O and pelleted.

3. The pellet was re-suspended in 1 mL of 100 mM lithium acetate solution (LiAc) (1.02g LiAc + water to 100ml, filter sterile.) and transferred to 1.5 mL tube. Next, the cells were centrifuged at maximum speed for 15 to 30 seconds and re-suspended in 500 µL 100 mM LiAc ($2x10^9$ cells/mL).

4. Next, the cells were vortexed to obtain a homogenised suspension. Then, 50 µL samples were transferred to a new tube, pelleted, after which the supernatant was removed with pipette. After that, the transformation reagents were added to the pellet of competent cells in order.

240 µL poly-ethylene-glycol (PEG 50% w/v) (50g PEG_{3350} + 50ml H_20 autoclave at 121^oC for 15 min)

36 µL 1 M LiAc (10.2g LiAc + water to 100ml. sterile filter).

10 µL SS-DNA (10 mg/mL)

10 µL PCR

64 µL sterile H_2O

360 µL total

Prior to adding the transformation reagents, a single stranded DNA (carrier DNA) (Dilute stock of sheared salmon sperm DNA to 2mg/ml in sterile water. Boil for 10 minutes. Chill rapidly to make single stranded DNA. Store at -20^oC for future use) thaw it on ice.

5. The cells were mixed vigorously by vortexing for 1 minute and subjected to heat shock for 40 min at 42°C. The suspension was spun down at 6000 to 8000 rpm and the supernatant was discarded by pipetting. After that, 500 µL of YPD was added and incubated at 30°C for 30-60 min in the Thermomixer and pelleted again.

6. The pelleted cells were dissolved in 100 µL of ddH_2O. Plates of selective media were prepared and labelled beforehand. Finally 20 µL of the cell suspension was plated on selective media. Similarly, 1:10 and 1:100 diluted cells suspension were put on plate as well. The cells then were plated in triplicate and incubated at 30°C for 3 days.Successful DNA transformation was confirmed by colony PCR and/or by western blot for protein expression (as in Myc tagging to both Rpd3 and Hda1).

2.9 Colony PCR

In order to examine the precise size of specific sequence of exogenous DNA that incorporated by HR into *S. cerevisiae* strains, Colony PCR was employed The recovered colonies on the selective media were numbered as a reference and subjected to colony PCR by inoculating a part of the colony into 15 µL of 20mM NaOH in a PCR tube. The tubes were vortexed and put in the heating block at 95°C for 15 min to lyse the cells releasing the cell content (DNA). The cell lysate was then vortexed and spun at 4000g for 2 min and 0.5 to 1µL of supernatant was used for PCR.

B. PCR reactions were mixed by vortex, spun down and run on a PCR machine as following conditions:

1. 95.0ºC for 4:00 min

2. 94.0ºC for 0:40 min

3. 55.0ºC for 0:50 min

4. 72.0ºC for 1:00 min

5. Go to 2. +3 sec/cycle x30 times

6. 72.0ºC for 10:00 min

7. End

C. For each sample 7µL of the PCR mix was loaded onto a 1% (w/v) agarose TAE gel with a ladder to check for production of the correct product.

2.10 Whole Cell Protein Extracts - TCA extracts

To prepare whole cell protein extracts, yeast cells are treated with a strong acid and boiled in a standard electrophoresis loading buffer which is both efficient and easy to perform. This method can be applied to any yeast strains, molecular weight of the target protein and growth conditions.

Yeast cells were grown until lag phase (OD_{595} = 5), then centrifuged and re-suspended in 200 µL of 20% (w/v) trichloro acetic acid (TCA). Then, 200 µL of Glass beads were added. Using vortex, the cells were mixed for 15 to 30 seconds. Then, a hot needle was used to generate a hole in the tube. The samples were centrifuged and transferred into a new Eppendorf tube. The samples were centrifuged again at 13000 rpm for 5 min and the supernatant removed. The extracts were re-suspended in 1x TCA sample buffer (see below) and boiled for 5 min. To separate the soluble protein fraction the extracts were spun for 1 minute at 13000 rpm before use. The supernatant was loaded on a gel.

1x TCA Sample Buffer:

1 volume	4x SDS sample buffer
1 volume	1 M Tris, pH 8
2 volume	dH_2O
2.5%	β-mercaptoethanol

4x SDS Sample Buffer

250 mM	Tris-base, pH6.8
20%	Glycerol
0.004 g/mL (w/v)	Bromphenol blue
0.08 g/mL (w/v)	SDS

2.10.1 SDS-Polyacrylamide gel electrophoresis

Using 4 - 20% gradient Bolt® Bis-Tris Plus gels (Invitrogen™, Life Technologies Ltd., Paisley, UK), the denaturated lysate from the last step of the previous section 2.10 on page 62 were loaded in order onto a gel, with the first lane being loaded with 5 µL of Novex® Sharp pre-stained standard (Novex™, Life Technologies Ltd., Paisley, UK) separately. Then, the gel was run at 150V for about 15 mins with a Bio-Rad PowerPac 300 (Bio-Rad laboratories Ltd., Hertfordshire, UK). The gel then separated from the cassette after disconnecting the plastic cassette and before moving it was immersed (the gel) in plenty of dH_2O.

2.10.2 Western blot, probing and detection

Protein transfer to the PVDF membrane from the gel was performed via an iBlot® 2 Dry blotting system (Invitrogen™, Life Technologies Ltd., Paisley, UK). The gel was placed on the PVDF membrane provided in the iBlot® 2 transfer stack (Invitrogen™, Life Technologies Ltd., Paisley, UK) on its face and a filter paper soaked in dH_2O was placed on it. All the bubbles were eliminated using a roller, then to complete the transfer stack, the remaining cathode stack and sponge was placed on top. Then,

based on the proteins' molecular weight, the blotting system was run according to the manufacturers' protocol (Invitrogen™, Life Technologies Ltd., Paisley, UK).

Once the transfer has completed, the PVDF membrane is removed from the stack and rinsed in dH_2O. Using an iBind™ Western gadget (Invitrogen™, Life Technologies Ltd., Paisley, UK), membrane probing was conducted.

1) The iBind solution was prepared by mixing 23.7 mL of dH_2O with 300 µL of 300x additive (Novex™, Life Technologies Ltd., Paisley, UK) and 6 mL of the 5x iBind™ buffer (Novex™, Life Technologies Ltd., Paisley, UK).

2) Then, primary antibody and secondary antibody were prepared (diluted) separately in a separate tube. To do so, 2 mL of the iBind solution was mixed with an optimised concentration of primary antibody in one tube and secondary antibody in a second tube separate from primary antibody tube.

3) For membrane probing, an iBind™ card (Novex™, Life Technologies Ltd., Paisley, UK) was placed in the iBind™ Western device (Novex™, Life Technologies Ltd., Paisley, UK) and soaked with 5 mL of the working iBind solution.

4) Then, approximately 1 mL of the working iBind solution was covered on the center of the card and the PVDF membrane placed on top, with the protein side facing down. After closing the iBind device, the antibody solutions were added to the wells of the cassette in order as described in the manufacturers' instructions (Life Technologies Ltd., Paisley, UK). The blot was run by lateral flow at room temperature for 2 to 3 h.

5) Once blotting has finished, the PVDF membrane was separated from the iBind Western device and immediately placed in dH_2O (as the PVDF membranes dry quickly). Then, the membrane was placed in 1 mL of SuperSignal™ West Dura Extended Duration Substrate (Thermo Scientific, Hempstead, UK) containing a 1:1 mixture of luminol enhancer and stable peroxide buffer and then incubated for 5 mins. Using Labworks software v4.6 (Labworks Inc., Costa Mesa, USA) connected to a BioSpectrum 610 Imaging System with an OptiChemi 610 camera (UVP Inc., Upland, USA), the chemiluminescent signals from the blot were detected.

2.10.3 Membrane stripping

To re-use the blot, the PVDF membrane is stripped in 10 mL of Restore™ PLUS Western Stripping buffer (Thermo Scientific, Hempstead, UK) at room temperature for 15 mins. Next the blot is washed with dH_2O as described earlier. The stripping

efficiency is checked using SuperSignal™ West Dura Extended Duration Substrate (Thermo Scientific, Hempstead, UK).

2.11 Yeast chromatin preparation

When cells reach a desired density (2×10^7 cell/mL), exponential phase, they were harvested, measured, centrifuged and re-suspended in chilled PBS (4°C) and standardized to $2x10^7$ cells/mL. Prior to the chromatin extraction, yeast cells were aliquoted in 50 mL petridish. An un-irradiated sample was always kept in chilled PBS at 4°C that was not irradiated with any UV. Then, the cells were exposed to a desired dose of UV irradiation (usually 100 J/m^2) at 254 nm from germicidal lamp to induce DNA damage. The irradiated cells were re-suspended in YPD and allowed to repair in the dark (to avoid photoreactivation repair) for different times at 28 - 30°C. Then, using a Beckman Avanti J-25 centrifuge, JA-10 or JA-20 rotors and Beckman polypropylene tubes (500 mL), all the samples were gathered (various repair times) by centrifugation at 4°C.

The entire process of chromatin extraction is as following::

Steps from 1 to 6 are exactly the same as in section 2.5 of this chapter (page 56).

7) Following re-suspending the cells in YPD as in un-irradiated samples zero points and also after each repair points, a cross-linking agent (usually 3 mL of 37.5% formaldehyde (Sigma-Aldrich Company Ltd, Gillingham, UK)) in the cell/YPD media to a final 1% (v/v) were added to cross-link the proteins with the DNA in some cases when the targeted protein not directly bind to DNA at first dimethyl adipimidate dihydrochloride 97% (DMA) (Sigma-Aldrich Company Ltd. The Old Brickyard NEW ROAD, GILLINGHAM Dorse, UK) 10 mL of 10mM DMA (freshly prepared in chilled PBS containing 0.25% dimethyl sulfoxide (DMSO)) was used to cross-link protein to protein. Then formaldehyde used to cross-link protein to DNA. Samples were incubated at room temperature on a shaking platform for between 10 min to 45 min dependent on the targeted protein. In case of Rd3 and Hda1 which have been used in this study, prior adding formaldehyde I added 10 mL of 10mM DMA (freshly prepared in chilled PBS) to cross link either Rpd3 or Hda1 and incubated on shaking platform for 11 h at RT. To stop the cross-linking 5.5 mL of 2.5 M glycine was added and incubated at room temperature on a shaking platform for 5 min

8) All samples were collected by centrifugation at 5000 rpm for 5 min and washed in 40 mL PBS and re- suspended again in 40 mL PBS, then the cells were kept in dark on ice.

9) Cells were transferred to a 2 mL micro-centrifuge tube using 1 mL of FA/SDS buffer (see appendix I, page 165) after being centrifuged at 5000 rpm for 5 min. The cells were pelleted at 12000 rpm for 10 min at 4°C the pellet was then re-suspended in 500 to 750 µL FA/SDS (+ PMSF (stock is 200mM and final concentration in the sample is 1mM)).

10) The cells were lysed mechanically by bead beating by adding 0.25 to 0.5 mL of glass beads to each sample. The cells were vortexed 5 min at 4°C for four times for with 3 min interval on ice to prevent warming of the protein

11) The beads were separated from chromatin by creating a hole in the 2 mL micro-centrifuge tube with a hot 25 gauges needle, after which the tubes were placed in a 15 mL Falcon tube.

12) The lysate was centrifuged at 2000 rpm for 2 min to collect the lysate in the 15 mL Falcon tube. Next, 500 µL of FA/SAS buffer (+PMSF) was added to the glass beads and subjected to a further centrifugation at 2000 rpm for another 2 min to wash the beads.

13) The cell lysate was transferred to a 2 mL micro-centrifuge tube and centrifuged at 15000 rpm for 10-20 min at 4°C. This way any soluble proteins that were not cross-linked to the DNA were removed.

14) Following centrifugation, the pellet was re-suspended again in 900 µL FA/SDS and to a total volume of 1000 µL with the pellet. The 1000 µL lysate was then divided equally into two tubes for sonication.

2.11.1 Sonication

15) Utilising a Bioruptor (Diagenode, Ougrée, Belgium), chromatin was subjected to fragmentation. Sonication was performed using the High setting at 4°C, for 30 seconds ON followed by 30 seconds OFF. The programme started with 4 to 20 cycles depending on desired fragment size of the chromatin.

16) After fragmentation, the lysate was centrifuged at 4000 rpm for 10 min. The supernatant was transferred to a 1.5 mL micro-centrifuge tube and centrifuged for 15-20 min at 15000 rpm in a microfuge.

17) Finally the supernatant was transferred to a fresh 1.5 mL micro-centrifuge tube. Before chromatin was snap-frozen, 50 µL was kept to prepare input samples. The chromatin was then snap frozen with liquid nitrogen and stored at -80°C for the later use.

2.11.2 Input preparation

To prepare input (IN) samples, 50 µL of chromatin and 50 µL of TE buffer were mixed and 25 µL of 5x pronase buffer was added. Next, 6.25 µL of pronase enzyme was added and incubated in a water-bath at 65°C overnight. Finally, 1 µL of RNase was added and incubated at 37°C for 1 h. After the incubation, the DNA was purified using the PureLink® PCR purification kit (Invitrogen™, Life Technologies Ltd., Paisley, UK) following manufacturer's instructions and eluted into 50 µL elution buffer. One to 2 µL of input samples were loaded and run on a 1.5% agarose gel and subjected to electrophoresis to check quality and the average size of fragmented DNA. Finally, the DNA quantity was measured via NanoDrop. A representative gel of appropriately sheared DNA is shown in the appendix III figure 1 page 176).

2.12 DNA gel electrophoresis

To check the quality and relative quantity of the DNA, DNA electrophoresis in agarose gel was prepared as in table 2.1. The DNA required to be checked was mixed with 6× Blue Gel Loading Dye and loaded into wells at the cathode end of a gel. Using a BioSpectrum 610 Imaging System the image is then assessed for its quality under UV light (UVP Inc., Upland, USA).

Table (2.1) Recipes for DNA Agarose gel electrophoresis

Buffer	Ingredients and methods
50×Tris/acetate/EDTA buffer (TAE) (pH 8.0)	242.2 g Tris base (1 M) and 18.6 g EDTA (50 mM) complete to 1000 mL of dH_2O. To adjust buffer pH to 8.0 acetic acid added. Stored at room temperature.
1 × TAE buffer	20 mL of 50 × TAE buffer (pH 8.0) was used and mixed with 980 mL of dH_2O. Stored at RT
1% to 2 % (w/v) agarose gel	1 or 2 g agarose powder was mixed to 100 mL of 1 × TAE buffer, to get homogenised solution the mixture was boiled for 2-5 min. 2-3 µL of 2 µg/mL of Ethidium Bromide (EtBr) was added. Gel cassette was used to cast it.

2.13 Chromatin Immunoprecipitation (ChIP).

Chromatin was subjected to immunoprecipitation using magnetic Dynabeads (Invitrogen™, Life Technologies Ltd., Paisley, UK) and specific antibodies raised against the protein of interest (2 to 2.5 µL Anti-acetyl-Histone H3 (rabbit polyclonal))(#06-599, Millipore) antibody (anti-H3 K9K14 antibody to target H3K9/K14 acetylation or 2 mL of Mouse monoclonal [9E10] to c-Myc - ChIP Grade (AB32) (Abcam, Cambridge, UK) to target myc-tagged proteins (Gcn5, Rad7, Rad16, Rpd3 and Hda1). The selected antibody was incubated with magnetic Dynabeads (Dynabead selection depend on the antibody being used which is protein IgG) (Dynabeads® M-280 Sheep anti-Rabbit IgG used with anti-acetyl-histone H3 and Dynabeads™ Pan Mouse IgG Used with anti myc antibody) to precipitate the targeted protein bound to DNA fragments. Both IP and input (see section 2.11.2) samples were incubated at 65°C to reverse the cross-link, treated with pronase and RNase. Finally, the DNA was purified using the PureLink® PCR purification kit (Invitrogen™, Life Technologies Ltd., Paisley, UK).

For every ChIP 50 µL of Dynabeads was transferred to a 1.5 mL tube (maximum 500 µL for 10 samples in one tube). Anti-acetyl-Histone H3 (rabbit polyclonal) was used with Sheep anti-Rabbit IgG dynabeads likewise mouse anti-Myc monoclonal antibody is added to Pan Mouse IgG,dynabeads® (Invitrogen™, Life Technologies Ltd., Paisley, UK). Then, the tubes were placed on a DynaMag™-2 Magnet rack (Fisher Scientific, Loughborough, UK) (cat. No. 12321D) to separate the beads from the solution. Next,

the beads were washed 3 times with 500 µL fresh PBS-BSA (0.1%). After washings, the Dynabeads were re-suspended in 50 µL PBS-BSA (0.1%) per sample. Following this, 2-4 µg of specific antibody was added per sample and incubated for 20 to 30 min at 1300 rpm at 30°C.

After incubation of antibody and dynabeads, the samples were washed 3 more times with 500 µL PBS-BSA (0.1%). Samples were re-suspended in 50 µL of PBS-BSA (0.1%) per sample. For each sample 100 to 200 µL of chromatin is added to 50 µL of beads plus 30 µL 10x PBS-BSA (10 mg/mL) and the volume is adjusted to 300 µL with 1x PBS. This mixture is then incubated in a Thermomixer® comfort (Fisher Scientific, Loughborough, UK) at 21°C for 3 h at 1300 rpm. Then, the samples were washed once with 500 µL FA/SDS buffer (appendix I, page 165) and twice with 500 µL to 1 mL FA/SDS + NaCl buffer (appendix I, page 165), followed by washing with 500 µL LiCl buffer (See appendix I page 166) and 500 µL 1x TE. Finally, 125 µL of pronase buffer was added to each sample and incubated in an Thermomixer® comfort for 20 to 30 min at 65°C, at 900 rpm to elute the DNA. The supernatant was transferred to a new tube and 6.25 µL of pronase was added and incubated at 65°C overnight in a water-bath.

Lastly, as for input samples, 1 µL of RNase was added and incubated for 30 min to 1 h at 37°C. DNA purification was applied after the incubation, using the PureLink® PCR purification kit (Invitrogen™, Life Technologies Ltd., Paisley, UK) PCR purification kit (as per manufacturer's instructions) and eluted with 50 µL elution buffer. IP and input samples were used for downstream applications such as qRT-PCR and ChIP-on-chip experiments.

Note: To determine the amount of antibody for any new experiments, an antibody titration was performed to determine the optimal immunoprecipitation conditions (see figure 4 appendix III page 177 and appendix IV, figure 5, page 192).

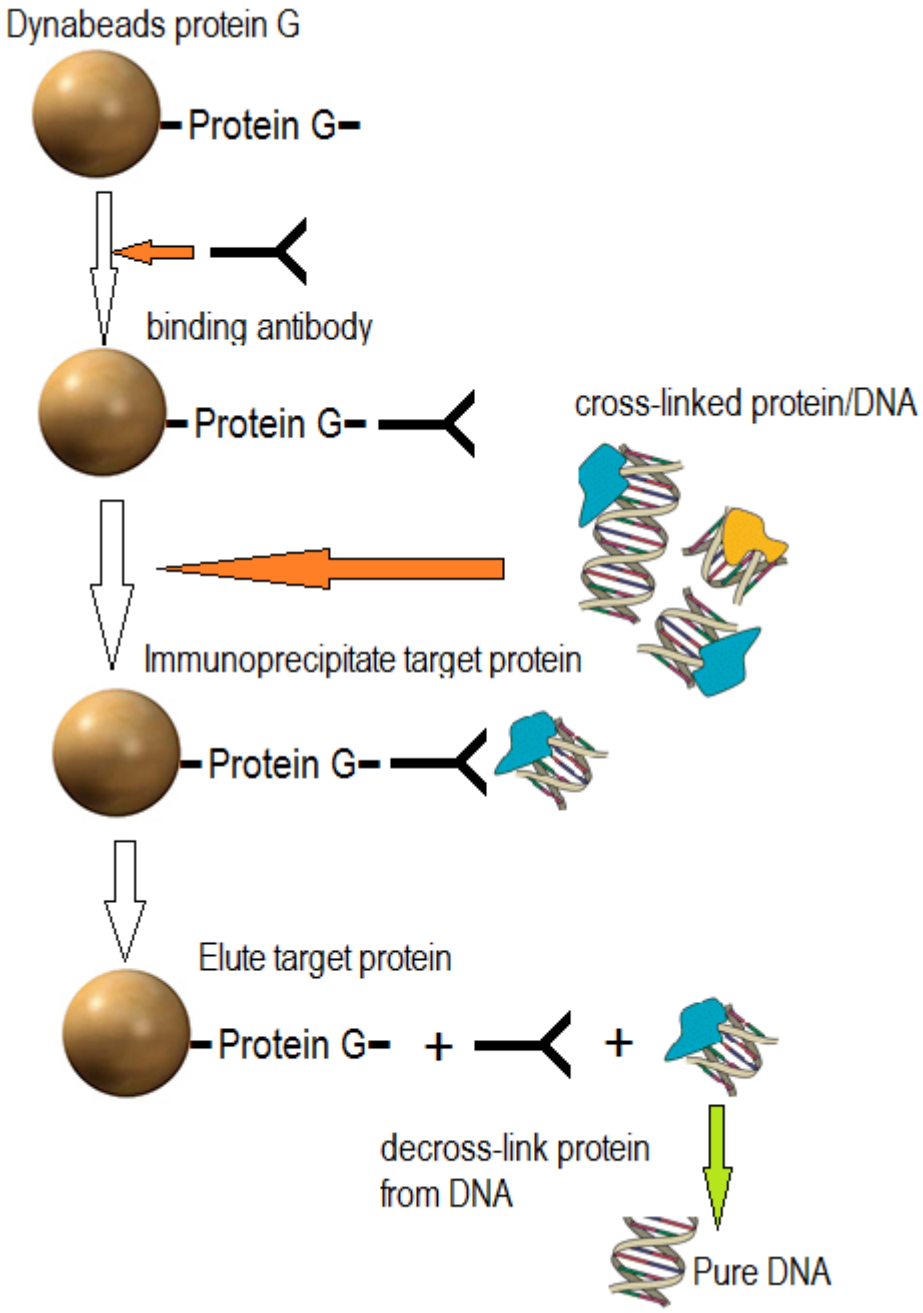

Figure 2.1 Principle of immunoprecipitation of antigen using Dynabeads® Protein G. first, the dynabeads were washed and incubated with the antibody specific for targeted protein. Then the sonicated chromatin (DNA/protein) was added, finally after a number stringent washes the targeted DNA/protein was eluted before being decrosslinked. The DNA is then used for different downstream application.

2.14 Quantification of DNA by qPCR

Real-time or quantitative polymerase chain reaction (qPCR) was utilised to determine enrichment of immunoprecipitated chromatin-bound protein over the input sample using Universal SYBR® Green Supermix (Bio-Rad laboratories Ltd., Hertfordshire, UK) with the designed primer sets that are specific for a gene of interest. To examine the

level of enrichment for any given protein or histone modification over the background, ChIP-qPCR is routinely performed for validation before it will be applied onto the microarray. Ten-fold dilutions of the IP and IN samples were prepared in ddH_2O (appropriate dilution of the IP and IN samples were made in ddH_2O for IN samples the dilution ranged between 100x dilution for IP from 5x to 10x fold dilution). Standard samples can be prepared from any sample with known concentration (i.e. IN samples). Here, 2 µL of IN sample was added to 98 µL ddH_2O to generate a 100x to 100,000 fold dilution series. Furthermore, a non-template control (NTC) is included that contains no template DNA using ddH_2O instead. Following preparation, 10 µL from each sample (NTC, standard, IN and IP) was added to Hard-Shell® 96-well semi-skirted PCR plate in triplicate including the standards (Bio-Rad laboratories Ltd., Hertfordshire, UK). Sample runs were performed on a CFX Connect™ Real-Time PCR detection system (Bio-Rad laboratories Ltd., Hertfordshire, UK) following the cycling protocol documented by the manufacturer. Using CFX Manager™ Software v3.1, the data was then analysed, sample wells within triplicates shows greater than 0.5 Ct variation were then removed and not included in the calculation. The presence of non-specific amplicons was tested by examining the melt curves.

Each qPCR well	**Amount (µL)**
2x iQ SYBR Green Supermix (Biorad)	5 µL
Primer 1 (100µM)	0.1 µL
Primer 2 (100µM)	0.1 µL
IN sample DNA to be quantified	5 µL (1000X to 1000000X) dilution
Total	10 µL

The following conditions were applied during qPCR run:

1. 95ºC for 3 min
2. 95ºC for 0:15 min
3. 55ºC for 0:20 min
4. 55ºC for 0:10 min - followed by optical image
5. Go to 2. x45 times
6. 95ºC for 1:00 min
7. 55ºC for 0:30 min
8. Melt curve from 55ºC

2.15 ChIP-on-chip

Since the DNA obtained from ChIP is generally too low to be detected and microarray analysis requires at least 1.5 µg, ChIP samples were amplified using two-step PCR. Using a similar microarray analysis protocol to that developed in 2010 by Teng et al. To prepare DNA from ChIP samples for microarray detection (Teng et al., 2010) the DNA is first treated with the PreCR repair kit (New England Biolabs) to remove UV-induced damage from the DNA. CPD lesions are induced following UV irradiation which may stall the DNA polymerases needed to amplify the genomic DNA. Some lesions may still remain even after repair time points (1h, 2h, 3h) if this vital step was not carried out. Therefore this step of *in vitro* repair was to ensure that no lesions would inhibit the LM-PCR required to amplify all the DNA fragments. In addition to CPD repair, this kit also repair other lesions on the DNA such as nicks; abasic sites; oxidised guanine; oxidised pyrimidines; deanimated cytosines and blocked 3‟ ends. Following lesion removal, the genomic DNA is then amplified by ligation mediated PCR (LM-PCR). Then, the amplified DNA was labelled by Cy3 and Cy5 dyes and later on applied to microarrays.

The detailed process is explained in the following paragraphs.

2.15.1 Yeast cell growing, UV-irradiation, Chromatin, IN and IP preparation

A single colony was grown overnight to stationary phase and used as a pre-culture. Then a known amount of yeast cells were inoculated in to 600 mL of YPD (200 mL per repair time and for untreated samples) and grown overnight incubated at 30°C in a shaking incubator. The next day, the cell density should be around 2-4 x 10^7 cells/mL for the cells to be harvested. Cells are pelleted by centrifugation and resuspended in chilled PBS to a cell density of 2 x 10^7 cells/mL. Before UV irradiation 200 mL from each strain was kept as untreated sample. Cells were aliquoted in 50 mL batches, exposed to 100J/m^2 of UV light at 254 nm. Then, the cells pelleted and re-suspended in 400 mL YPD for one-hour and three-hour repair times and incubated at 30°C in a shaking incubator. Following completion at each repair time, crosslinking agents were added. Here we added two cross-linkers, firstly 20 mL of 10 mM of DMA is added to 200 mL cell suspension and incubated at RT for 11 h on shaking platform in the dark, this ensures proteins-to-protein cross-linking. After washing the samples, a second cross-link was added to cross-link the proteins to DNA by adding 6 mL of 37.5% formaldehyde to 200 mL YPD and placed on shaking incubator at room temperature for 45 min. Then, 11 mL of 2.5M glycine was added to 200 mL cell suspension and placed on a shaking platform for 5 min at RT to stop crosslinking at RT. Cells then were then pelleted at 5 000 rpm (Beckman Avanti J-25 centrifuge) for 5 min and re-suspended in

40 ml pre chilled PBS. The cells were harvested once again for 5 min at 5000 rpm, before the cells were washed again and transported to a 2 mL micro-centrifuge tube in FA/SDS buffer. Then, 750 µL of FA/SDS lysis buffer (+PMSF) and 250 µL of glass beads were vortexed in the cold room (4ºC) for 4 times for 9 min with 3 min intervals between each time. After pelleting the cells were re-suspended in 900 µL of lysis buffer (+PMSF) to obtain 1 mL lysate. The 1 mL lysate is then divided over two 2 mL tubes for sonication via a Bioruptor Sonicator (Diagenode) on High settings for 30 seconds on and off for 30 seconds at 4ºC for 20 to 24 cycles. Input (IN) (see 2.11.2 on page 67) and IP (2.13 page 68) were prepared, purified and used in downstream applications such as qRT-PCR and microarray (see appendix III, IV for all CHiP qPCR raw data, statistical analysis).

2.15.2 LM-PCR and DNA labeling

DNA obtained from ChIP is not sufficient for downstream applications; the amount is too little to be used in a microarray experiment. At least 1.5 µg of yeast genomic DNA is needed before starting DNA labelling. Amplification of the DNA IP is therefore required before labelling and hybridisation to the microarray because. Following the ChIP, two samples per experiment, IP and input, are processed in parallel. The DNA was first repaired with pre-CR repair kit (New England Biolabs). The pre-CR step is required to repair the CPD lesions, which will stall the DNA polymerases if not repaired and hence amplifying the whole genomic DNA is not achieved. Some but not all the lesions will be repaired after one-h or even three-h repair time in the YPD. Thus this *in vitro* repair step is required to ensure that there are no lesions left in the DNA before amplification by LM-PCR. This step is essential to allow amplification of the DNA fragments. The preCR kit is used to repair 1 µL of input sample diluted in 40 µL ddH_2O and 40 µL of IP sample, by incubated the DNA with a 10 µL mixture of the preCR repair reagent following manufacturer's instructions. Next, the DNA was purified using the PureLink® PCR purification kit (Invitrogen™, Life Technologies Ltd., Paisley, UK) following the manufacturer's instructions) and eluted in 50 µL elution buffer and kept on ice.

Then, to blunt end the DNA fragments, T4 DNA polymerase (New England Biolabs) was added. Briefly, a 70 µL mix comprising 11 µL NEB buffer 2 (included with the T4 DNA polymerase), 0.5 µL BSA (10 mg/mL), 1 µL dNTPs (10 mM), 0.2 µL T4 DNA polymerase (New England Biolabs, catalogue # MO203S) and 57.8 µL of ddH_2O were added to 50 µL of IP or input DNA on ice. The samples were mixed with pipetting and incubated in a water bath for 20 min at 12ºC, which is the optimal temperature at which

the T4 DNA polymerase endonuclease function is active, while its polymerase activity is not. Following this incubation, 11 µL of NaAc (3 M, pH 5.2) and 0.5 µL Glycogen (20 mg/mL) was added to each sample to help precipitate the DNA using phenol/chloroform extraction. To this end, 120 µL phenol/chloroform (v/v) was added to each sample, which was vortexed vigorously until the solution appears milky. This was followed by a 5 min centrifugation at 15000 rpm in a microfuge at room temperature. The upper phase of the phenol/chloroform extraction was then removed carefully and transferred to a fresh 1.5 mL micro-centrifuge tube and the DNA was precipitated with 130 µL cold ethanol for one hour at -20ºC. After that, to pellet the DNA, the samples were centrifuged at 15000 rpm at 4ºC for 15 min. Since the DNA pellets are invisible to the naked eye, great care was taken at this stage; therefore the supernatant was carefully removed with pipetting. The pellet was washed with 500 µL of 75% ethanol and pelleted again with centrifugation for 5 more min, finally, the DNA was resuspended in 25 µL of ddH_2O.

Following this step, 25 µL of the ligation master mixture containing linker DNA (13 µL of ddH_2O, 5 µL DNA ligase buffer, 6.7 µL linker hybrid and 0.5 µL T4 DNA ligase (New England Biolabs)) was added to each sample to reach a total volume of 50 µL of DNA and ligation mixture. The samples were then left at 16ºC overnight. At this step the linker hybrid fragments will be ligated to the DNA fragments. By using one set of primers the amplification of all sampled DNA fragments is ensured.

Next day these following reagents were added to the ligation mixture as follows: 6 µL of NaAc (3 M) and 130 µL of chilled ethanol. This precipitation mixture can be stored at -20°C for one hour or -80°C for 20 min to precipitate the DNA (during this and the next stage of centrifugation and pelleting, care should be taken to not disturb the pellet as it is too small to be seen by eye). Next, the samples were pelleted at 15000 rpm for 15 min at 4ºC, and then washed again with 75% chilled ethanol (500µL) and centrifuged and finally re-suspended in 25 µL ddH_2O.

Ligation-mediated PCR (LM PCR) was performed (first round amplification) of all of the DNA fragments for amplification using one set of primers (oligo JW102) (during ligation a common linker hybrid DNA was ligated to the ends of the DNA fragments, this allows amplification of all fragments to occur using a single set of primers) . For the first round DNA amplification two master mixes (A and B) were prepared beforehand as follows:

PCR mixture A for one sample

Reagent	**Amount in µL**
5x Q5 Reaction Buffer	8 Ml
dNTP (10mM)	1.25 µL
Oligo 102 (40µM)	1.25 µL
ddH_2O	4.5 µL
Total	15 µL

PCR mixture B for one sample

Reagents	**Amount in µL**
ddH_2O	7.5
5x Q5 Reaction Buffer	2
Q5 High-Fidelity DNA polymerase	0.5 (1 unit)
Total	10

Sequence for linker hybrid DNA:-

oligo JW102 5'- GCGGTGACCCGGGAGATCTGAATTC - 3'

oligo JW103 5'- GAATTCAGATC - 3'

After adding 25 µL of ddH_2O to the DNA pellet, 15 µL of mixture A was added, mixed and then heated to 60ºC on the pre-heated PCR blocks for 2 min. After 2 min the PCR machine is paused to add 10µL of mixture B while the sample temperature was 60°C. (this is to give the time for polymerase to repair the nick that may remain following ligation and blunt ending of the DNA). Finally, the programme was resumed. The PCR programme was run according to the following conditions.

PCR conditions:

1. 60.0°C for 4:00 min

2. 72.0°C for 3:00 min

3. 98.0°C for 1:00 min

4. 98.0°C for 0.10 min

4. 60.0°C for 0.30 min

5. 72.0°C for 0.40 min

6. Go to 4. 14 times

7. 72.0°C for 5:00 min

8. End

Following amplification, the PCR product was either subjected to purification by a PCR purification kit and 0.5µL to 1µL was used for second round amplification, or the PCR product was diluted by adding 450 µL of ddH_2O and 5 µL of it was used for a second round amplification. Second round of amplification is utilised to ensure sufficient quantities of DNA were produced for labelling.

PCR mixture for 2nd round PCR for one sample

Reagents	**Amount in µL**
5x Q5 Reaction Buffer	10
dNTP (10mM)	1.25
Oligo 102 (40µM)	1.25
Q5 High-Fidelity DNA polymerase	0.5 (1 unit)
ddH2O	36.5 or 32
Total	49 or 45

The second round of DNA amplification was performed either by adding 0.5 µL purified DNA to 49 µL of PCR master mix 2 or 5 µL of diluted PCR product to 45 µL of PCR mixture 2 utilising the following PCR conditions:

1. 98.0°C for 1:00 min

2. 60.0°C for 0:10 min

3. 72.0°C for 0:40 min

4. Go to 2. 23 times

5. 72.0°C for 5:00 min

6. End

The final PCR product is now 50 µL. This product is either precipitated by NaAc and ethanol or purified by PCR purification kit and quantified using a Nanodrop (ND-1000 Thermofisher Scientific). Next, after purification 1.5 µg to 2 µg in ~12 µL of ddH_2O was used for DNA labelling.

In my entire ChIP-on-chip work, the Bioprime® Total Genomic Labeling system (Invitrogen™, Life Technologies Ltd., Paisley, UK) was utilised. Routinely, the input samples are labelled with Alexa Fluor® 3 (Cy3), while the IP samples were labelled with Alexa Fluor® 5 (Cy5). In brief, a volume of 10.5 µL of DNA in ddH_2O was placed in a 0.5 mL PCR tube before the addition of 2.5 µL of 5 mM EDTA and 15 µL of either

Alexa Fluor® 3 2 x reaction mix or Alexa Fluor® 5, 2 x reaction mix. The contents of the tubes were mixed and incubated in the dark at 95ºC for 5 min. Immediately after this incubation the PCR tubes were placed on ice for an additional 5 min. Whilst remaining on ice, 2 µL of highly concentration Exo-Klenow fragment (40 units/µL) was added to each tube (total volume in PCR tubes is 30 µL). The PCR tubes were subjected to a 2 h incubation in the dark at 37ºC. The labelled DNA was purified using the PureLink® PCR purification kit (Invitrogen™, Life Technologies Ltd., Paisley, UK) and eluted in 51.5 µL of elution buffer (provided in the labelling kits). From this 1.5 µL was used on the NanoDrop spectrophotometer to measure the labelling efficiency. The 50 µL of labelled IP and input DNA were combined and precipitated with the addition of 12 µL of NaAc (3 M), 5 µL of Polyacrylamide (2.5 µg/mL) and 290 µL of chilled ethanol at -20ºC overnight. The following day the DNA was pelleted with centrifugation at 15000 rpm for 15 min at 4ºC. washed once with 75% ethanol and re- suspended in 39 µL of ddH_2O. Linear polyacrylamide can precipitate small amount of DNA (picogram amounts of DNA) fragments larger than 20 base pairs while it doesn't precipitate shorter fragments and free nucleotides. This property makes it ideal for separating reaction products from unincorporated nucleotides and oligonucleotide primers. It also improve the recovery of nucleic acids during alcohol precipitation of restriction fragments, PCR products and decrease the storage time at lower degrees.

2.15.3 DNA Hybridization to microarray slides

To prepare for hybridisation the following agents were added to the labelled DNA in order: 5 µL of Human Cot-1 DNA (1 mg/mL) (Life Technologies Ltd., Paisley, UK), 11 µL of 10x aCGH Blocking Agent (10 x) (Agilent Technologies Ltd., Cheshire, UK) and 55 µL of 2 x HI-RPM Hybridisation Buffer (Agilent Technologies Ltd., Cheshire, UK). Then the mixture was incubated for 3 min at 95ºC and then instantly moved to 37ºC for 30 min. Before loading samples on to the array, a matching gasket slide is placed on top of a SureHyb Microarray Hybridisation Steel Chamber (Agilent Technologies Ltd., Cheshire, UK). Then 110 µL of the samples was applied slowly on to the center of each array (4X44 K), finally placing in a rotating hybridisation oven (Agilent Technologies Ltd., Cheshire, UK) to hybridise the sampled DNA with the printed oligonucleotides on the slide for 24 h at 65ºC at 20rpm.

2.15.4 Washing and scanning of the microarrays

For the washing steps Washing buffer 1 (300 ml of 20 x SSPE, 250 µL of 20% Sarcosine and 700 mL of H20) was used after hybridisation for 5 min (care should be taken to minimize any damage that may occur during handling the slides). Then, this

was followed by a 5 min wash in Washing buffer 2 (3 mL of 20 x SSPE and 997 mL of ddH_2O), it is important to ensure that the slides were dried completely. Then, the Agilent microarray scanner (G2505B, Agilent Technologies) was used to scan the microarray slides and the features were then extracted from the TIFF file of the microarrays image. The Agilent Feature extraction software (version 10.7.3.1) and the protocol ChIP_1007_Sep09 were used to analyse the image achieved earlier. This software enables us to compare and determine the relative IP to input fluorescence values for each probe (or features) on the array which denotes a particular part of the yeast genome. Data were exported as a tab delimited text file and the following column titles: „Row", „Col", „ProbeUID", „ControlType", „ProbeName", „GeneName", „SystematicName", „Description", „rBGSubSignal" and „gBGSubSignal" were extracted from the text files. „gBGSubSignal" represents the quantification of Cy3 labelled DNA hybridisation, which is referred to as the „Green channel" or G. „rBGSubSignal" represents the quantification of Cy5 labelled DNA hybridisation, which is referred to as the „Red channel" or R and corresponding data were imported into R. The $\log_2$ ratio of the signals from IP and input for each probe (IP/input) was determined and value represents the relative enrichment of the target protein or histone modification at each probe position.

Chapter Three

3. Investigating the role of HDACs and histone deacetylation in the response to UV-induced DNA damage

3.1 Introduction

In eukaryotic cells, genetic material is stored in the nucleus as a protein-DNA complex. Chromatin is the resulting structure created by the association of DNA with histones and other non-histone proteins like DNA binding factors. Structurally, the basic subunit of chromatin is the nucleosome consisting of 2 turns of DNA wrapped around it. The nucleosome itself is an octamer that consists of two copies of each histone protein; making up a tetramer of H3 and H4 flanked by two H2A-H2B dimers (Luger et al., 1997). Each of these highly conserved proteins has about 147bp of DNA wound around it. . Linker DNA which is free from nucleosome connects each two nucleosomes. At the point where linker DNA reaches the nucleosome there is a linker histone. Linker histones, such as histone H1, can aggregate the chromatin further and condense it to be packaged as chromosomes inside the nucleus of the cell (Luger et al., 1997). The nucleosome is the primary determinant of DNA accessibility in many cellular processes, including DNA repair.

Nucleotide excision repair (NER) is the main pathway employed by cells to remove various classes of structurally unrelated DNA lesions introduced by different damaging agents that distort the normal structure of the DNA double helix (Friedberg, 2005). More than 30 proteins are required to remove lesions from the DNA (Friedberg, 2005; Prakash and Prakash, 2000; Tatum and Li., 2011). There are two sub-pathways of NER, transcription coupled NER (TC-NER) and global genome NER (GG-NER), which only have a difference during lesion recognition and each have a specific set of proteins, however, following damage identification, they converge and follow the sequential core repair reaction steps and (Gillet and Scharer, 2006; Hanawalt, 2002).

As in other cellular DNA metabolic processes like replication and transcription, factors that regulate these processes need to remodel the chromatin to promote access to the damaged DNA. This helps the detection of DNA damages in chromatin. NER follows similar rules when operating on a DNA template that is embedded within chromatin. NER factors must gain access to the DNA to remove the lesion efficiently. High level of coordination is required between the DNA repair machinery and chromatin dynamics, to maintain both genetic and epigenetic information (Smerdon, 1991). Following repair,

the chromatin must be re-assembled to return it to its normal undamaged state. It is important to appreciate the role of chromatin in maintaining stability of the genome, as its presence should not just be considered as an absolute barrier for repair factors. Chromatin plays an active role in genome stability, warranting that effective DNA repair occurs in the right place at the right time in the genome (Smerdon, 1991; Friedberg et al., 2005). Although little is known about how NER is primed and functions in response to DNA damage in chromatin, extensive work has been done in order to study the important biochemical reactions of the core NER pathways (Friedberg et al., 1995). Recent progress has revealed how chromatin is set up for repair of damaged DNA and the organisation and structure to the repair reaction in chromatin are beginning to emerge (Yu et al., 2016). However, how chromatin is restored to its pre-damaged states is still a topic of active research.

Previous studies have made important insights into how NER works in the context of chromatin (Adam and Polo, 2012; Green and Almouzni, 2002; Groth et al., 2007; Polo and Almouzni, 2015). For example, *in vivo* observations in mammalian cells made by Smerdon and Lieberman in 1978, showed that nuclease accessibility (staphylococcal nuclease) of DNA is modulated during UV-induced DNA synthesis. They confirmed for the first time that chromatin rearrangements occur during NER (Smerdon and Lieberman, 1978). Later studies led to the establishment of an Access-Repair-Restore (ARR) model initially proposed by Smerdon in 1991 (Green and Almouzni, 2002; Polo and Almouzni, 2015; Smerdon, 1991). This model has served as a useful framework to better understand how chromatin can act as a molecular scaffold for DNA repair.

During DNA repair three principal mechanisms control chromatin structure: Nucleosome sliding, eviction/exchange of nucleosome or part of it (canonical histones or histone variants), and disruption of higher order chromatin structure e.g. unfolding of chromatin fibres (Polo, 2015). Each of these events is driven by the possible joined actions of the following four regulatory factors: ATP-dependent chromatin remodelers, histone chaperones, histone modifiers, and histone variants (Peterson and Almouzni, 2013). As stated above, because eukaryotic DNA is packaged in chromatin, any cellular transactions involving DNA are likely to require the modulation of chromatin structure.

Modification of histones by acetylation is one of the most widely studied areas and histone acetylation is involved in many cellular processes like, replication, transcription, histone deposition and DNA repair (Bannister and Kouzarides, 2011; Kouzarides, 2000, 2007). Histone acetylation is not a permanent mark but rather is a dynamic

reversible process in which histone acetyltransferase (HAT) enzymes transfer acetyl group from acetyl COA to some lysine residues in the N-terminal tails of histone proteins. Generally, histone acetylation is linked to transcription (euchromatin) with some exceptions at certain residues (Wang et al., 2002). In contrast, there is another set of enzymes that exhibit the opposite activity to HATs, called histone deacetylases (HDACs). Both sets of enzymes are linked to cellular processes including transcriptional activation or repression, replication and DNA repair (Kurdistani and Grunstein, 2003). HDACs and HATs are present in an equilibrium status and play vital roles in remodelling of the chromatin structure in eukaryotes. Hence, any changes of this balance affect the proper cellular functions.

Histone acetylation levels increase when cells and organisms are exposed to ultraviolet radiation. This reduces the association between histones and the DNA around it. As a result chromatin structure becomes more permissive to allow the access of repair specific proteins and other related complexes to UV-induced DNA lesion sites and provide adequate time for damage detection, removal and repair completely and effectively. Lys9 and lys14 (K9/K14) on histone H3 are the important locations for acetylation (Bjerling et al., 2002; Vogelauer et al., 2000) as well as K5, K8, K12 and K16 on histone H4 (Bjerling et al., 2002; Vogelauer et al., 2000). This indicates that restoration of histone H3 acetylation following UV damage is dependent on efficient removal of DNA damage by NER.

3.1.1 Rpd3

In yeast Rpd3, a class I HDAC, is present in two sub-complexes Rpd3L (1.2 MDa) and Rpd3S (0.6 MDa (Carrozza et al., 2005; Keogh et al., 2005; Yang and Seto, 2008; Yeheskely-Hayon et al., 2013). Rpd3L is responsible for promoter deacetylation of targeted genes (Carrozza et al., 2005; Kadosh and Struhl, 1997), However, Rpd3S is recruited to the coding area (Carrozza et al., 2005; Keogh et al., 2005).

Rpd3 primarily plays a role in deacetylation of histones H3 and H4 (Kurdistani and Grunstein, 2003; Rundlett et al., 1996), besides to deacetylation of both H2A at lysine 7 and H2B at lysine 11 and 16 (Suka et al., 2001)**.** On a global scale, Rpd3 also deacetylate wider regions of chromatin in a process named global deacetylation (Alejandro-Osorio et al., 2009; Kurdistani et al., 2002; Robyr et al., 2002).

This HDAC also has a role in re-joining the homologous ends of chromosomes during NHEJ repair pathway of DSB by Rpd3/Sin3 complex (Jazayeri et al., 2004) that have the ability to bind directly at non promoter sites (Kurdistani and Grunstein, 2003;

Kurdistani et al., 2002). Induced DSB DNA damaging agents recruit human HDAC1 and 2 to the damage site rapidly in response to damage and they promote hypoacetylation of histone H3 lys56 (H3K56).

There is significant functional interplay between HDAC and HATs that has an effect on gene regulation, as for instance the antagonistic function of Gcn5-dependent histone H3 acetylation and Rpd3-dependent histone H4 deacetylation on a single promoter (IME2) transcription (Burgess et al., 1999) and genetic interaction between Gcn5, Esa1 and Rpd3 (Lin et al., 2008).

3.1.2 Hda1

Hda1, is a class I HDAC in yeast, which specifically deacetylates histones H3 and H2B (Robyr et al., 2002; Wu et al., 2001). Like Rpd3, Hda1 also functions to deacetylate histones both on a global and local scale (Robyr et al., 2002). Hda1 removes acetyl groups from subtelomeric domains of chromosomes (10–25 kb away from the telomeres).

Most of the deacetylations on the targeted promoters are performed either by Hda1 or Rpd3, however there is some degree of redundancy between each of them globally (Robyr et al, 2002).

The most important feature that needs careful consideration in relation to this current study, is the antagonistic functions of Hda1 and Gcn5. These two proteins oppose each other for recruitment to the same promoter. It has been found that Hda1 with Tup1 can partially block the promoter space and form a repressor complex, likewise targeted by Gcn5 binding and binding of this complex is exacerbated by GCN5 deletion (Islam et al., 2011).

In all of the examples provided above, it became apparent that chromatin behaves in a highly dynamic way. It defined a common method by which histone acetylation status is rapidly restored to its normal level, upon inactivation or removal of the regulator in response to developmental or environmental signals including DNA damaging agents.

Based on the properties of HATs and HDACs (Kurdistani et al, 2002; Robeyr et al 2002; Ekwall 2005), and previous work done by my colleagues, either at the MFA2 locus or other locations of the genome, suggests a possible role for HDACs in restoring UV-induced histone H3 hyperacetylation levels to pre UV levels after DNA repair.

3.1.3 Hos1, hos2 and Hos3

The Hos (HDA One Similar) HDACs, which includes Hos1, Hos2 and Hos3, deacetylate ribosomal DNA, (Robyr et al., 2002). Deacetylation of Hos1 is necessary for secure transmission of chromosomes (Beckouët et al., 2010). Hos1 plays a crucial role during anaphase in dissociation of NScc1's from Smc3 by deacetylating Smc3 (Beckouët et al., 2016).

While UV induced histone H3 hyper acetylation is dependent on Rad7 and Rad16 GG-NER proteins in yeast, it occurs independently of Rad4 and Rad14 proteins. Single mutants in these latter two genes are completely defective in the removal of DNA damage by NER (Yu Y et al., 2005; Waters *et al.*, 2012). This indicated that whilst damage-induced histone H3 acetylation is dependent on the Rad7 and Rad16 GG-NER factors, it does not depend on the removal of DNA damage by the NER process itself. Significantly, the return to pre-UV histone H3 acetylation levels observed in wild type cells was absent in cells defective in NER such as Rad4 or Rad14 mutants (Yu Y et al., 2005).
In the present study, I aim to determine the mechanism involved in restoring the chromatin structure following the removal of UV-induced DNA damage by the NER pathway.

I tested the hypothesis that HDACs are involved in removing the acetyl groups from the histone tails of UV-induced histone H3 hyper acetylation, and that they also contribute to the restoration of the chromatin structure to its pre-damaged state after lesion removal. Wild type and different HDAC mutants were used to measure the effect of HDAC mutants on UV survival, CPD repair, both pre and post UV, applying genetic approaches. Using a specific anti-H3K9K14 antibody, the H3 acetylation levels was measured at lysine 9 and 14 (H3K9/K14) both before and after UV in the above strains through chromatin immunoprecipitation and standard qPCR. By analysing the results, we hoped to obtain a clear indication of whether they have a role or not. If we identified any significant biological differences, then this could indicate a role for HDACs in the restoration of chromatin during the post repair process. Not seeing any meaningful variations might indicate that they are either not involved in the repair process, or that the approaches used here are not sensitive enough to detect their contribution or that there may be redundancy in the cells. In this case, then alternative scenarios were conducted to tackle this biological question.

As previously stated, increased levels of histone H3 acetylation following exposure of

cells to UV damage causes modifications to histone tail and makes chromatin more accessible and amenable to DNA repair. For the chromatin to be restored to its undamaged structural configuration, this acetylation should be returned to its normal level. There are several possible mechanisms by which DNA damage-induced H3 acetylation levels might be restored to normal. Since HDACs participate in a lot of cellular process as described earlier, it is possible that they are also involved in returning damage induced histone H3 hyperacetylation to its undamaged state. Therefore, I decided to design experiments to tackle the question whether or not HDACs contribute to the restoration of chromatin structure by deactylating the UV-induced histone H3 hyperacetylation after repair.

3.2 Materials and methods

materials and methods was discussed throughout the chapter 2 on page 53

3.3. Results

3.3.1 Examining a possible role for HDACs in repair and survival of UV-induced DNA damage

3.3.1.1 UV survival experiment to examine the effect of deleting different HDACs on DNA damage sensitivity:

UV survival experiments are a straightforward assay to determine whether or not a yeast mutant strain deleted for a gene of interest is UV sensitive. This is achieved by calculating what number of cells within a population has the ability to survive exposure to any given dose of UV irradiation. After a period of time (typically 2 to 4 days), the number of colonies on solid media can be counted to quantify UV survival. Here, this method was applied to determine whether HDACs play a role in DNA repair, by examining the effect of HDAC mutants on UV survival. Lower levels of UV survival can be an indicative of the role of a gene in the DNA damage response. Therefore, wild type and HDAC mutant cells (lacking one of the yeast HDAC genes *RPD3, HDA1, HOS1* and *HOS2*) were treated with different doses of UV radiation. After treatment, cells are allowed to grow on YPD plates at 30°C for 2-3 days. Finally, the survival percentage of these mutants can be calculated and compared with the wild type strain after counting the recovered colonies (see appendix- III, page 172-173).

The cells were grown overnight in liquid media and harvested at the density of 2×10^7 cell/mL. Serial 10-fold dilutions were prepared from each culture in such a way that the

last dilution contains ~200 cells /100µL. Before pipetting the diluted cells were mixed by vortexing. One hundred µL of cell suspension was pipetted onto YPD agar plates in triplicate such that ~200 colonies were expected to grow on the un-irradiated plates. The cell suspension was spread evenly across the surface of the plates. Next, these plates were exposed to various doses of UV light. Following irradiation, the plates were incubated at 28-30°C in the dark for 48 to 72 hours to avoid photo-reactivation. By this time any surviving cells will produce a colony. Counting these allows us to calculate the percentage of surviving cells using the average number of colonies on the un-irradiated plates as 100%. To compare the sensitivity of each strain relative to wild type, we plotted a survival curve (see Figure 3.1). The results shown here represent the average from at least three independent biological repeats. Taken together, these results demonstrate that individual deletion of the non-essential HDACs tested does not have a significant impact UV survival. With the Rpd3 deleted strain in alpha cells actually showing a very small increase in UV survival compared to wild type cells, but only at very high doses. (For raw data, average, mean of survival and standard deviation see appendix-III, page 172-173 and also materials and methods in chapter 2 section 2.3, page 54-56).

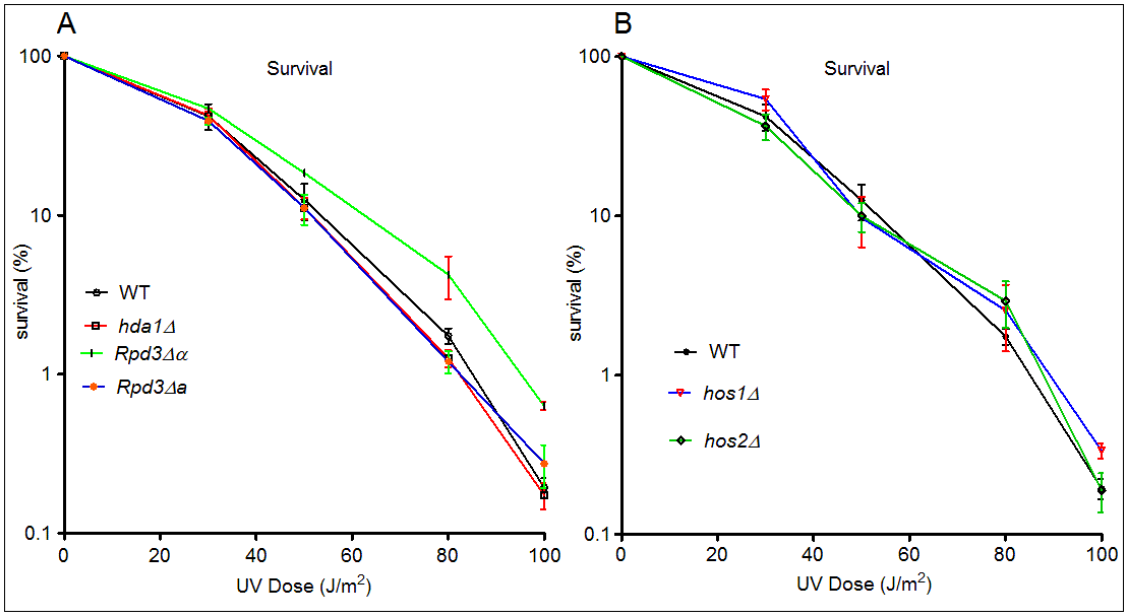

Figure 3:1 UV survival assay of wild-type (BY4742) and HDAC mutant strains (BY4742). A. WT, *rpd3*Δ, *rpd3* Δ , *hda1* Δ strains. B WT, hos1Δ , and *hos2* Δ strains. Strains were grown to exponential phase in YPD, re-suspended in 1X PBS to a density of $2x10^7$ cells/mL and UV irradiated or mock-treated. The cells were treated with a range of UV (254 nm) doses and plated on YPD plates. Colonies were counted after three days growth at 28-30°C and the percent survival calculated compared to the un-irradiated sample. Survival curves are the mean of at least three independent experiments and the error bars represent standard deviation (SD) of the mean see raw data, mean, and SD in the appendix III page 172-173 and also Materials and methods in chapter 2 section 2.3 for the same purpose and also for the purpose of the process of calculating and analysing the SD.

3.3.1.2 Examining the effect of HDAC mutants on the global rate of CPD repair

UV survival of yeast cells relies on the coordinated action of the DNA damage response, which includes DNA damage signalling, regulation of gene expression and DNA repair. Under the conditions tested, no significant effect of deleting HDACs on UV survival was observed. Therefore, DNA slot-blot assay was employed to investigate DNA repair directly by measuring CPD removal (if HDACs have a role before, during or after repair, then the differences could be seen between WT and HDAC mutants by conducting this assay). Immuno-slot-blot (ISB) is a basic variation on the western blot technique. Genomic DNA samples are directly applied to a membrane and probed with antibodies that detect DNA lesions (i.e. CPDs or 6-4-PPs). This technique was used in this study to measure the incidence and rate of CPD removal in wild type cells and two HDAC mutants (*hda1Δ* and *hos1Δ*), for more detail see chapter 2, section 2.7, page 59.

To demonstrate precisely the effect of HDAC mutants on the incidence and repair of UV-induced CPDs, the immuno-slot-blot assay with anti-CPD (Anti-Thymine Dimer Clone (KTM53)) antibodies was utilised. Thus, wild type and both *hda1Δ* and *hos1Δ* yeast cells were grown overnight to exponential phase. Sufficient numbers of cells were harvested by centrifugation to yield 300-500µg of genomic DNA after purification. The cells were re-suspended in pre-chilled PBS and adjusted to $2X10^7$ cells/mL. Cells were exposed to UV light (254 nm) in 50 mL aliquots to induce DNA damage prior to the DNA extraction. Untreated samples were always treated in parallel as a negative control for the detailed process see chapter two section 2.7, page 59. Using specific antibody (anti CPD antibody) and secondary antibody the damage is detected via a film. The intensity of the band is proportional to the amount of antibody bound to the damage. The DNA damage detection is then analysed using Image Quant software for quantification. The percentage of remaining CPDs at different time points after UV irradiation is a measure for repair. Both the wild type and HDAC mutant strains display similar repair rates. Figure 3.2 A and B show the immune-slot blot assay of the wild type *hda1Δ* and *hos1Δ* strains. The quantifications of these results are shown in Figure 3.3 which represents the average of three biologically independent experiments (only 2 repeats for Hos1 green line). These results are consistent with the UV survival test and both experiments show the same result. This demonstrates that DNA damage induction and repair are slightly slower in both mutants than in wild type.

.

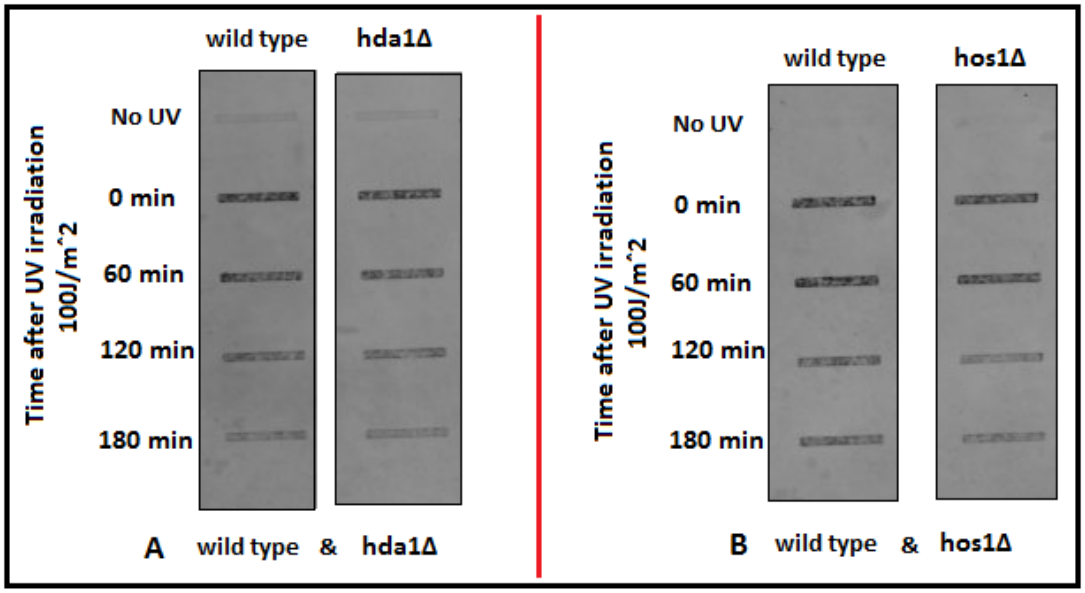

Figure 3:2 Immuno-slot-blot of UV-induced DNA damage induction and repair in wild type and HDAC deleted cells using Anti-Thymine Dimer Clone KTM53). (A) Immuno-slot-blot of damage-induced CPD in wild type and *hda1Δ* (B) Immuno-slot-blot of damage-induced CPD in wild type and *hos1Δ* cells. Shown here is a slot blot representative of 3 biological repeats of wild type and *both hda1Δ hos1Δ* cells. UV-induced CPDs are detected by a CPD-specific primary antibody. Remaining CPDs are detected directly after exposure to UV irradiation (0 min) up to 180 minute recovery period**.**

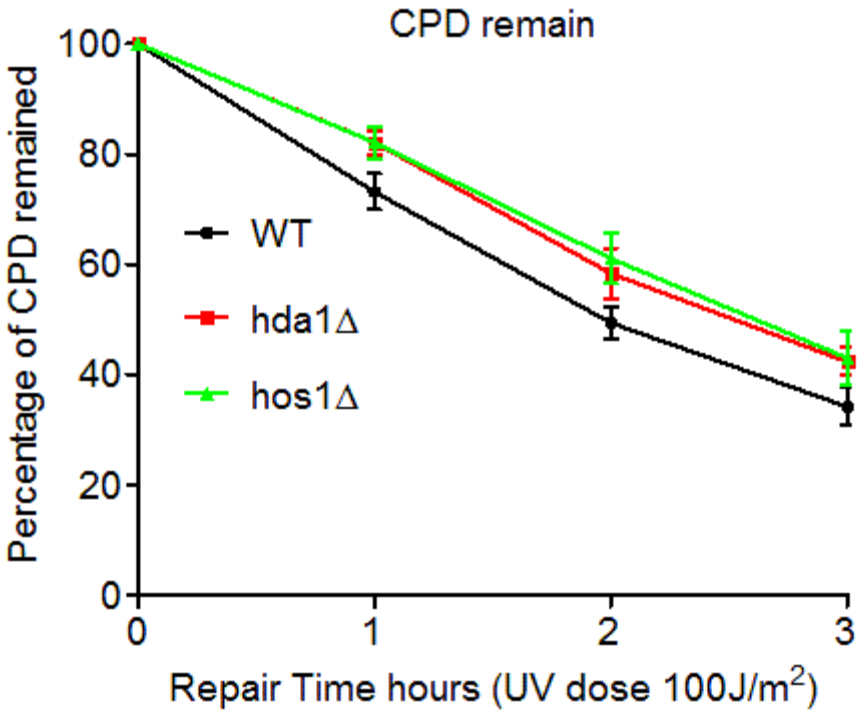

Figure 3.3 Quantification from Immuno-slot-blot assays of UV-induced DNA damage of wild type versus *hda1Δ* and *hos1Δ* . The Typhoon TRIO Imager is used to scan the image and the ImageQuant software was used to display and quantify the ISB bands. The figure shows the changes in the CPD lesions in each strain. The results are a mean of 7, 3 and 2 biological repeats for WT, Hda1 and Hos1, respectively and the error bars represent standard deviation (see appendix III, page 173-174

3.3.1.3. Cell cycle arrest following UV irradiation.

In UV-induced survival experiments, cells irradiated with (100J/m^2), will arrest during the cell cycle. Following 3-4 hour of repair time, the cells go back again into the cycle, following recovery of RNA synthesis, which is an important process in the response to DNA damage. Therefore, the experiments were conducted within this time frame, since the irradiated cells are still in the arrested phase when DNA repair is active. This ensures that any changes in DNA damage levels reflect changes specifically due to DNA repair. Following UV exposure at this dose, typically around 20% of cells will die. However, the surviving cells will return to the cycle again after repair of the damage.

3.3.2 UV-induced Histone H3 K14 acetylation levels of wild type and *hda1Δ* and *hos1Δ* mutant cells

As mentioned previously, histone H3 acetylation at the *MFA2* locus increases in response to UV irradiation and is reduced to pre-damage levels after completion of the repair reaction (Yu et al., 2005). We were able to establish this because histone H3 K14 acetylation remains high in repair deficient cells such as *RAD4* and *RAD14* mutants. In order to extend on this finding we examined H3 acetylation status in wild type and HDAC mutant cells to determine whether they have a role in controlling the level of UV-induced histone H3 acetylation at this locus. To do this, cells were prepared for UV treatment. For each strain tested, an un-irradiated control aliquot was stored separately. The cells were treated with 100 J/m^2, after which they were incubated at 30°C at different repair time points according to the experimental design. Following formaldehyde cross-linking, chromatin was prepared as described in chapter two section 2.11, page 65.

DNA was fragmented by sonication and input samples were prepared for quality control (see appendix-III figure 1, page 176). The chromatin was used for ChIP after adding H3K9/K14 antibody. Finally, qPCR was applied to measure the acetylation status at *MFA2* to measure the enrichment of histone H3 acetylation. Figure 3.4 shows the relative histone H3 acetylation at the *MFA2* locus in wild type and two HDAC mutants (*hda1Δ* and *hos1Δ*), Three independent biological experiments were conducted to take the average and the error bars representing standard deviation (SD) (appendix-III, page 175-176).

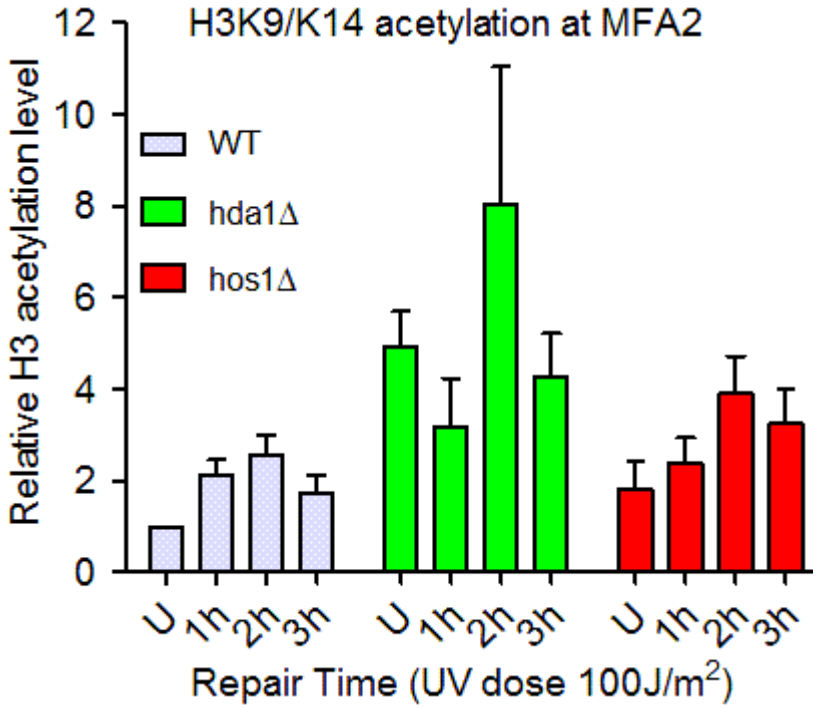

Figure 3.4: Relative levels of Histone H3 acetylation in wild type (gray bars), *hda1Δ* (green bards) and *hos1Δ* (red bars) before and after UV irradiation (100 J/m2) at the MFA2 region. ChIP assay of H3 acetylation at K9/14 was performed, as described in (chapter 2), with anti H3K9/K14 antibody. Cells were either untreated or irradiated with 100 J/m^2 and incubated at the indicated time points to allow for repair to take place. Acetylation level represent as the fold-changes relative to un-irradiated cells. The results reported are the average from at least 3 biological repeats and the error bars represent standard deviation (appendix-III, page 176-177).

In line with previous findings, we observe the UV-induced increase of H3 K9/K14 acetylation at *MFA2* 1 and 2 h after UV irradiation (Figure 3.4). Similarly, after 3 h, when most repair has taken place, acetylation levels are reduced. Interestingly, basal levels of histone H3 acetylation are increased in the absence of Hda1 (Figure 3.4, green bars) and to a lesser extend in Hos1 deleted cells (figure 3.4 red bars). This indicates that the activity of Hda1 is required to maintain wild type levels of H3 K9/K14 acetylation at this genomic locus. However, UV-induced up regulation can still be observed after 2 h of repair and indeed deacetylation can also be detected after DNA repair is completed. A similar pattern can be discerned for the *hos1Δ* mutant strain (red bars). See appendix-III, page 176-177 for raw data and statistical analysis.

3.4 Discussion

In this chapter, I describe my attempt at identifying a role for a subset of HDACs in DNA repair of UV damage in yeast. As we mentioned earlier in chapter 1 section (1.3.4 on page 44-51)., histone H3 acetylation increases in response to UV irradiation, while completion of the repair reaction reduces the HAT occupancy at these genomic locations and acetylation levels return to normal levels (Yu et al., 2005, Teng et al., 2002, Yu et al 2011' Yu et al., 2016). In this chapter I aim to examine the effect of deacetylases on the UV survival and DNA repair process. In order to determine this, three different assays was employed that would assist in finding out whether or not these factors were having a discrete role in restoring histone H3 acetylation to pre-damage levels. In the first experiment the UV survival assay was conducted. This is a powerful method that measures the UV resistance of cells after exposure to a given dose of UV radiation. It is an end point assay that is useful to identify genes that are involved in the DNA repair process (Verhage et al., 1994). Our results demonstrate that the HDAC mutants tested are not hypersensitive to UV irradiation. This means that these genes do not significantly affect UV survival. It is known that HDACs have considerable redundancy in other processes like the regulation of gene expression. It is therefore possible that deleting a single HDAC has a minimal effect on DNA metabolism due to the presence of residual HDAC activity of other factors, a phenomenon referred to as redundancy. Simultaneous deletion of multiple HDAC-coding genes, could help us to investigate this in more detail, but double and triple HDAC mutant strains have severe growth defects in yeast (un-publish observations, this lab).

Since the UV survival assay is an end-point assay, it is possible that HDACs are involved in the early repair reaction that is completed after about 3 h without impacting overall survival. However, because of the nature of the assay, and the caveats mentioned above (relating to the period during which colonies form) it might be that there is a small effect on repair, which could be masked. Therefore, I initiated the slot blot assay, which directly measures CPD removal from the entire genome of the cells as a population. The slot blot assay is a simple method employed to measure the level of the remaining CPDs in the genome within a few h after UV radiation. This will reveal what may be masked in the preceding assay, and directly examines the repair process. As the results showed, there is no significant difference between wild type and both of the HDAC mutants (*hda1Δ*, *hos1 Δ*) tested, indicating no apparent role for HDACs in CPD removal.

Finally, I aimed to examine the acetylation status of histone H3 at the single *MFA2* locus in the gneome. We know a considerable amount about this location in response

to UV damage, as described in chapter 1 (section 1.3.4, page 44-51). Similarly, the results presented here reveal no significant difference in H3 acetylation between wild type and HDAC mutant cells. Taken together, these three experimental approaches are consistent with each other, in indicating that there is no effect on DNA repair outcome, UV survival or H3 acetylation in the absence of the HDACs Hda1 and Hos1. Based on the above investigations we conclude that there is no evidence that HDACs play a role in the NER pathway (see the next section (3.5) below). However, we realize that this absence of evidence may be due to considerable genetic redundancy in the pathways investigated. Technical issues regarding the viability of the double mutant strains meant that we were unable to address this possibility further.

3.5. Main conclusion in this chapter

In this chapter experiments were conducted in an effort to determine the mechanism by which the UV-induced histone H3 acetylation levels are restored to the normal pre-damaged levels to reassemble the chromatin structure after the repair of the DNA damage.

In summary, the results showed the following:

1. There is no significant difference in UV sensitivity, CPD repair and histone H3 acetylation levels between wild-type and the various HDAC mutants examined. These results could suggest that HDACs are not involved in the mechanism of resetting the chromatin structure in response to UV damage. However, since there are multiple copies of HDACs present in the cell, each playing slightly different roles in removing acetyl groups from histones, there is the very real possibility that redundancy of function compensates for the loss of any individual HDAC.

2. To overcome this problem, double mutant or triple mutant HDAC strains can be constructed and the same experiments repeated. However, the cells of mutants defective in multiple HDACs are very difficult to grow. Such cells are sick, since deletion of multiple HDACs affects other cellular pathways).

3. Alternative methods were considered in order to address the problems identified above. For example HDAC inhibitors may be used in wild type cells to prevent histone deacetylation following damage-induced H3 hyper acetylation. In this case, histone H3 acetylation levels may remain constitutively high, and it will be possible to measure how this affects Gcn5 and Rad7/Rad16 occupancy in the genome. An alternative

approach is to measure histone H3 acetylation levels genome wide in the different HDAC mutants and to compare these results against each other, and against CPD repair rates, Gcn5 occupancy and the occupancy of other GG-NER factors. This approach may be further refined by examing directly HDAC occupancy in the genome in order to overcome the problems of redundancy. These ideas will be examined in the following chapters

Chapter Four

4. Investigating the role of repair factors in restoring chromatin following repair of UV lesions

4.1 Introduction

According to the results presented in chapter three, no evidence was found for HDACs having a role in DNA repair or UV survival in response to UV irradiation. However, it is well known that chromatin needs to be restored to its undamaged state after DNA repair. Therefore, I describe here the experiments I undertook to define the mechanism by which chromatin is reassembled following repair of UV-induced DNA damage.

Studies have determined that there is crosstalk between chromatin remodelers and histone modifications during transcription regulation (Cairns et al., 1996; Carey et al., 2006). HATs and chromatin remodeling complexes are typically recruited to chromatin by transcriptional activators (Yudkovsky et al., 1999). In 2014 Duan and Smerdon reconstituted an acetylated histone H3-containing nucleosome *in vitro* on DNA with a strong positioning sequence (Duan and Smerdon 2014). They noticed that H3K14 acetylation alone did not alter nucleosome unfolding dynamics, neither did it affect UV damage repair. Conversely, when the chromatin remodeler RSC was added to the reaction, H3K14 acetylation was able to promote removal of UV-induced DNA lesions and facilitate repair of nucleosomal DNA through stabilizing the binding of RSC to the nucleosome substrate (Duan and Smerdon 2014). Moreover, Ramanathan and Smerdon in 1986 and 1989 found the correlation between acetylation and repair. These findings demonstrated the connection between histone acetylation in UV-induced DNA damage and implied an important role for acetylation in facilitating NER (Ramanathan and Smerdon, 1986, 1989). These studies have led to the formulation of the access repair restore (ARR) model (Smerdon, 1991) (see Figure 4.1, page 98).

Reed's lab has provided significant insight to this model in order to understand the mechanism of each stage. I have explained in detail the roles the Rad7/Rad16 GG-NER have in assisting efficient GG-NER repair and how these events of early access are regulated in the context of chromatin. I have also described the structure and functions of their domains and their response to UV exposure at single genomic loci as well as over the entire genome (Yu et al., 2016; Yu et al., 2011; Yu et al., 2005). Reed and his colleagues have found that these factors are in a complex with Abf1 at Abf1 BS and that after UV irradiation they detached away from abf1 and recruit Gcn5 on to the chromatin. This is explains how chromatin set up initiated following UV-induced H3

acetylation at lysine 9 and 14 in the genome. Previously, researchers in the reed's lab showed that this hyperacetylation are dependent on the HAT Gcn5 and Rad7/Rad16 GG-NER factor and this have a role in inefficient repair (Yu et al., 2016; Yu et al., 2011; Yu et al., 2005). The role of these factors is independent of transcription and they are involve in repair without disturbing transcription of genes that are not necessary to be transcribed (Yu et al., 2016; Yu et al., 2011; Yu et al., 2005).

Following successful lesion removal and repair of the DNA damage these events of induced UV hyper acetylation and the chromatin alteration together with the GG-NER factors (Rad7/Rad16 and Gcn5 HAT) are reversed to preserve genetic and epigenetic integrity of the organism and ensure the transmission of the intact genetic information to the offspring's. However, in repair deficient cells like *RAD4* and *RAD14* mutant strains, elevated levels UV-induced histone H3 acetylation remains consecutively high and the chromatin persist in an open configuration (figure 4.2A & B) and that implies that chromatin is not restored to its pre undamaged state (Yu et al. 2005). This means that during GG-NER efficient lesion removal is necessary for the alteration of chromatin in later stages. This demonstrated that, the events required for preparing the chromatin for the access phase are dependent on the Gcn5 and GG-NER complex factors, but independent on the repair factors themselves. For this reason, UV-induced hyperacetylation of histone H3 does not rely on the lesion removal by the NER process itself. On the other hand, deacetylation and reversing of elevated levels of histone H3 acetylation and chromatin structure following repair is entirely dependent upon the effective repair. In Rad4 and Rad14 deleted cells, H3 acetylation remains continually high and the chromatin stays open. In order to understand the mechanism behind the reduction of the elevated levels of H3 acetylation, a number of experiments were designed involving the investigation of GG-NER factors as well as Rpd3 and Hda1 factor to unravel their possible role in this task.

Firstly, as we explained above, the Rad7/Rad16 GG-NER complex controls histone H3 acetylation through GCN5 chromatin occupancy in response to UV induced DNA damage. So in wild type cells the GG-NER first responds to the UV and drives GCN5 rapidly to occupy the chromatin for a short period of time and this leads to induction of histone H3 acetylation driving chromatin alteration (Yu et al., 2016; Yu et al., 2011). In the normal wild type cells these events all reversed to normal undamaged state within their normal time scale (less than one h for Rad7/Rad16 and Gcn5 and 2 to 3 h for H3 acetylation) (Yu et al., 2016; Yu et al., 2011). In Rad14 deleted cells histone H3 acetylation remains high for a long period of time (Waters et al., 2012; Yu et al., 2016;

Yu et al., 2005) (following UV exposure to the cells at 100J/m2, the cell cycle arrest for 3 to 4 hours, after this period it returns into the cycle again (explained in chapter three, page 90)). One possibility that could explain this observation is that, in repair defective mutants such as Rad14 it might be the case that, Rad7/Rad16 factors (driving machine of Gcn5) or GCN5 occupancy remains at a high level on the chromatin. Thus, maintaining high levels of histone H3 acetylation irrespective of the presence or absence of any mechanisms involved in H3 acetylation reduction and this means H3 acetylation remains constantly at high levels subsequently promoting an open chromatin structure and this means restoration not occurred. This will be achieved by examining chromatin occupancy at MFA2 locus for each of the factors Gcn5, Rad7 and Rad16 in the RAD14 deleted strains as well as wild type cells both before and after UV irradiation. To do so an isogenic Rad14 deletion in each of the above myc tagged strains will be constructed. By examining Gcn5 occupancy on the chromatin, it will turn out whether it remains on the chromatin or not. If not occupy the chromatin for longer period in these deleted cells, then other alternatives will also be investigated. However, if they do remain on the chromatin, then it may infer that Gcn5 is responsible for continuous H3 hyperacetylation due to constant acetyl COA addition on to the H3 histone tails. On the other hand, if it turns out that Gcn5 have a role in this event, then the same experiment will also be done inspecting the factors (which is Rad7/Rad16) driving Gcn5 to occupy the chromatin and thus keeping H3 acetylation status high.

Secondly, there are also HDAC factors participating in a number of DNA metabolic process as described in the introduction of chapter 3 and in section 5 of general introduction. These proteins have an antagonistic function to what HATs have. Hence it is of utmost importance to investigate their roles in a more direct way and it is likely that HDACs come during GG-NER and reverse reaction and restore the chromatin back to normal. I will examine direct reversal of the elevated levels of damage-induced histone H3 acetylation at K9/14, by histone deacetylation. To do this experiment, the chromatin occupancy of Rpd3 and Hda1 will be investigated before and after UV irradiation both in wild type and Rad14 mutants. In addition, genome-wide UV-induced HDAC histone H3 acetylation levels will be explored to determine the relationship between these two events.

Relative acetylation status of histone H3 (using highly specific chip grade antibody) will be measured before and following UV irradiation in wild type and different of HDAC mutants, including hda1 and rpd3 to determine their involvement in restoring H3 acetylation levels after repair genome-wide. If HDACs involve in restoration then the

UV-induced increased levels of the histone H3 acetylation will remain high in HDAC mutants as it was observed in Rad4 and Rad14 deleted strains. Moreover, UV-induced HDAC occupancy will also be examined both at the local and global scale to examine HDAC involvement in a more direct way and to establish the details of histone H3 acetylation and deacetylation during the early and late phases of GG-NER. To this end, ChIP-qPCR experiments will be performed to determine whether the HDACs are being recruited to the chromatin during the time H3 acetylation levels decrease after repair has taken place. To examine the involvement HDACs in chromatin remodelling after repair, then, these experiments will be repeated in NER deficient Rad14 deleted cells both locally and genome-wide. These observations will help to shed light on the mechanisms involved in histone H3 deacetylation and chromatin remodelling during the unfolding as well as refolding phase of GG-NER. To do the above experiments the required strains will be construct and myc tagged and then anti-myc antibody will be used to pull down the targeted Rpd3 or Hda1 factors. The results will give a lot of insight of how these events takes place and will give a better understanding on how chromatin is restored after repair. To establish the details of histone H3 acetylation and deacteylation during the early and late phases of GG-NER.

Thirdly, the role of histone exchange will be investigated in GG-NER during the restoration step. Evidence shows that during the restoration phase of GG-NER the damage-induced exchange of histone H3-H4, is feasible to take place (Luijsterburg et al., 2012). The idea is, instead of removing of the acetyl mark from the tail after DNA repair, it might be the case that the acetylated histone is ejected from the chromatin. The nucleosome itself or some part of the nucleosome including histone H3 may be evicted and then a new unmodified histone is incorporated into the chromatin. Such a mechanism of histone eviction is known to exist and can be catalysed by chromatin assembly factor (CAF-1) sequentially (Adam and Polo, 2012; Polo et al., 2006). The histone chaperone CAF-1, encoded by the yeast CAC1-3 genes, is involved in histone H3-H4 deposition linked to both replication and DNA repair synthesis during late GG-NER that may restore the chromatin structure (Polo, 2015). New histones are deposited at the site of DNA damage by CAF-1. This possibility can be studied initially by examining histone H3 lysine 56 acetylation statuses. Acetylation of lysine 56 on histone H3 is indicative of newly incorporated histones into chromatin (Masumoto et al., 2005). The result can be confirmed by using an independent method such as a classical pulse chase experiment or SNAP-tag-based pulse chase imaging (Adam and Polo, 2012) which is based on differential labeling with a probe that labels newly synthesised histones.

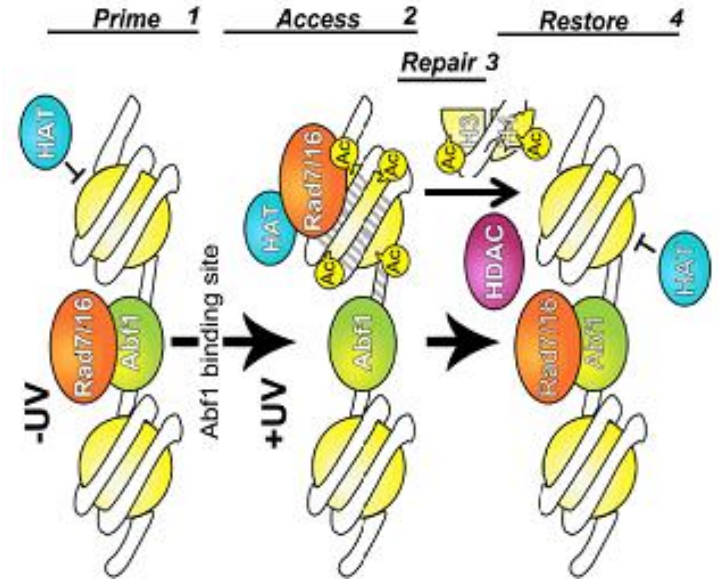

Figure 4.1: Model depicting the phases of ARR for Abf1-Rad7-Rad16 controlled histone H3 acetylation & possible mechanism for restoring chromatin structure to pre-UV state. Left pane: Before UV irradiation, the GG-NER complex is located at Abf1 binding sites predominantly in the promoter regions of genes. Middle panel: In response to UV irradiation, the GG-NER complex dissociates from the Abf1 component at Abf1 binding sites. Concomitantly, the HAT Gcn5 is recruited onto the chromatin with its increased levels and distribution dependent on the Rad7-Rad16 GG-NER complex. Consequently, histone H3 acetylation level is increased. This mechanism drives the chromatin remodelling necessary for the efficient repair of UV damage. Following repair, there are various mechanisms that may contribute in the restoration of the chromatin into pre-damaged state (including HDACs). Right panel: restoration of chromatin into normal undamaged configuration.

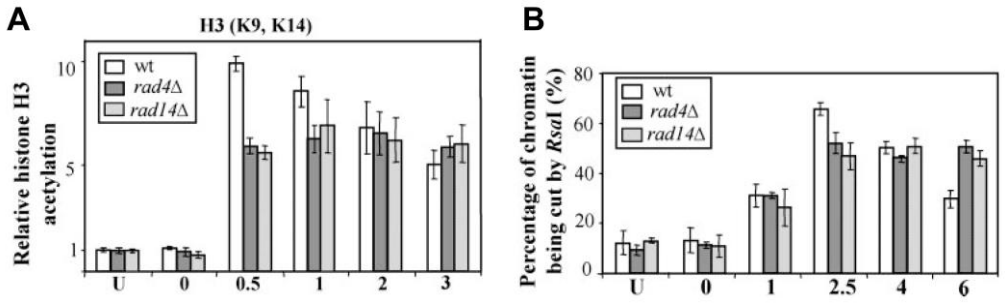

Figure 4.2 Histone H3 acetylation and accessibility of chromatin at the repressed *MFA2* promoter in the *rad4* and *rad14* mutants. (*A*) Histone H3 acetylation (K9 and K14) in response to 100 and 150 J/m^2 UV irradiation. The histone H3 acetylation level is presented as the fold increase relative to that before UV irradiation (U). The remaining samples are from UV-treated cells after repair from 0–3 h. (*B*) Accessibility of DNA in chromatin to RsaI in response to 400 J/m^2 UV irradiation. The accessibility of DNA in chromatin is represented by the percentage of chromatin sensitive to RsaI at the *MFA2* promoter. DNA digested by both HaeIII and RsaI; lane U, chromatin sample with no UV; lanes 0–6, chromatin samples from cells receiving 400 J/m^2 UV irradiation after various repair times in hours (Yu et al, 2005). This result was reproduced in this current study (examining H3K9/K14 acetylation) in WT, *RAD7* deleted and *RAD14* deleted cells (see figures Figure 4.6 on page 102 and also appendix IV, figure 9 on page 194).

4.2 Materials and methods

For detail see chapter 2 on page 53

4.3 Results

4.3.1 Strain construction of NER deficient cells

In order to investigate the chromatin occupancy of various repair factors (Gcn5, Rad7 and Rad16) during the early and later phases of GG-NER, I needed to generate strains with epitope tagged forms of these factors in both wild type and repair deficient genetic backgrounds. For this Lithium Acetate (LiAc) was used for transformation of yeast cells; a powerful technique for generating genetic modifications or deletions of gene of interest to investigate the effect of that gene on cellular processes (Gietz and Schiestl, 1991, 2007; Gietz and Woods, 2002; Ito et al., 1983; Liu et al., 2017) including DNA repair. Using this approach I deleted the *RAD14* gene in three strains containing epitope tagged versions of Gcn5, Rad7 and Rad16 (see table 2.1, page 53). Similarly, I constructed Rpd3 and Hda1 Myc tagged strains in wild type and repair deficient *rad14Δ* backgrounds using the same approach. The resulting strains will be used to examine the chromatin occupancy of each of these factors before and after UV irradiation at multiple time points during and after repair. For primers, see both appendix II, page 167-171 (for primers), colony PCR and UV drop test samples are in the appendix-IV, page 190 and for raw data of CHiPqPCR see appendix-IV, page 178-190)

RAD14 in the epitope tagged Gcn5, Rad7 and Rad16 strains was successfully deleted. Large 70-mer PCR primers were used to generate disruption constructs with 5' homology to the genomic sequence of the Rad14 gene (see Figure 4.3). The 3´ ends of the primers annealing to the sequence of the selectable *HIS3* marker gene residing on plasmid pRS313 and was used for amplification. The amplified DNA was transformed directly into yeast, and homologous recombinants that carry the selection marker were identified. Then, by using a set of internal selection marker primers, the deletion of the target gene can be confirmed by single colony PCR of successful transformants.

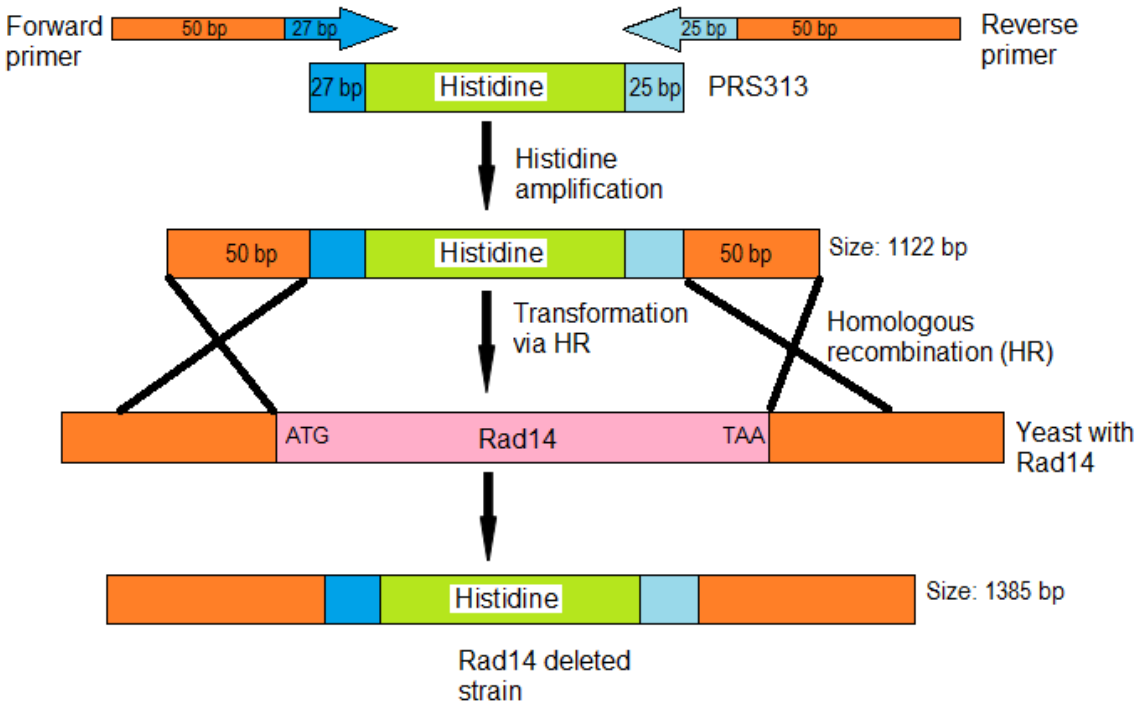

Figure 4.3 Complete deletion of *RAD14* gene in wild type yeast BY4742 strains tagged with either *GCN5* or *RAD7* or *RAD16* but lacking Histidine and replacing it with Histidine marker, which present in PRS313 plasmid by homologues recombination, through using LiAc/SS Carrier DNA/PEG Method. This method was also used successfully for deleting *RAD14* gene in *RPD3* and *HDA1* myc tagged strains. See appendix II, page 167-171 for primers, amplicon size and more.

4.3.2 Confirmation of *RAD14* deletion by single colony PCR & UV survival

A set of primers was designed to confirm whether the gene of interest (*RAD14*) was deleted from each strain. To do this, a single colony from transformants of each strain on the histidine drop out plates were labelled, numbered and selected for colony PCR. The scPCR of Rad7-Myc, Rad-Myc and Gcn5-Myc transformed cells returned positive clones deleted for *RAD14* (see Figure 4.4, lanes 4,5 and 6 for Rad7, Rad16 and Gcn5 myc respectively). The predicted amplicon size is base pairs (1385 bp)... all strains scored at least one successful recombinants with the scPCR producing the expected amplicon indicating that *RAD14* was deleted successfully in those strains as well. Primers used for strain transformation, sequence of RAD14 and Histidine as well as colony PCR can be seen in appendix-II page 167-170.

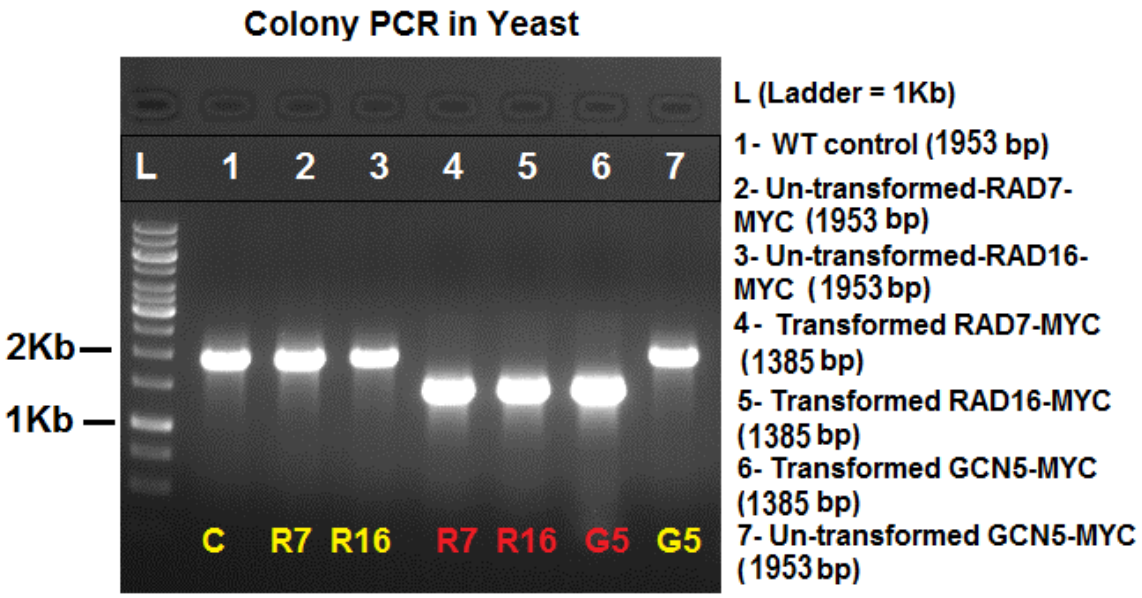

Figure 4.4 Single colony PCR results demonstrating successful integration of the *RAD14::HIS3* disruption construct. Strains containing Gcn5-Myc, Rad7-Myc and Rad16-Myc were transformed with *RAD14::HIS3* and successful recombination assessed using scPCR. Primers were designed for the detection of *RAD14* deletion. Deletion is confirmed in lane 4, 5 and 6 for WT-Gcn5-Myc, Rad7-Myc, Rad16-Myc and Gcn5-Myc, respectively. Rad7-Myc, Rad16-Myc and Gcn5-Myc in lanes 2, 3 and 7, are not transformed correctly and lane 1 is negative control of WT strain. Ladder is a 1Kb ladder. See appendix II, page 167-170, for primers and the sequence of both RAD14 and Histidine.

To compare the sensitivity of the newly constructed strains relative to wild type cells, a UV survival assay was performed and plotted the resulting survival curve. The results are shown in Figure 4.5 and the strains showed the expected phenotype. The result were taken from two independent biological repeats and show that *rad14Δ* mutant cells are extremely UV sensitive compared to both wild type (resistant) and *rad7Δ* strains (moderately sensitive).

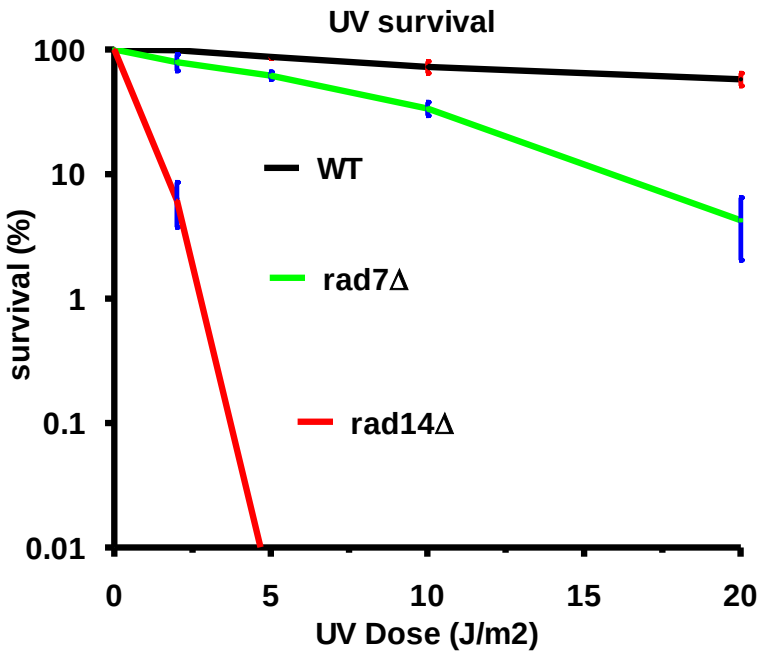

Figure 4.5 The UV sensitivity of wild type, rad7*Δ* and *rad14Δ* strains. All strains were grown to log-phase, re-suspended in 1x PBS to a density of 2 x 10^7 cells/mL. Before exposing the cell suspension to UV irradiation a sample from each strain was kept un-irradiated for control and comparison. Next, the cells were treated with a range of UV (254 nm) doses and plated on YPD plates. Colonies were counted after three days growth at 28-30 °C and the percentage of survival were calculated and compared to the un-irradiated sample. My result for UV sensitivity of constructed RAD14 deletion is the similar as Verhage result {Verhage et al 1996b}

4.3.3 UV-induced histone H3 hyperacetylation observed in response to UV irradiation in NER defective cells.

We previously showed that GG-NER specific Rad7/Rad16 factors and Gcn5 are required for acetylation of histone H3 after UV irradiation, and this process is necessary for efficient GG-NER (Teng et al, 2007; Yu et al, 2011). The UV-induced hyperacetylation is subsequently reverted to its pre-damaged state (Teng et al, 2002). However, damage induced histone H3 acetylation remains high when NER is deficient as in *RAD4* an *RAD14* deleted cells (Yu et al, 2005). To confirm these results in the newly constructed *RAD14* deleted strain, the Gcn5-myc-*rad14*Δ strain was compared to the WT-Gcn5-myc and Gcn5-myc-*rad7*Δ strains by subjecting them to ChIP-qPCR experiments measuring histone H3 acetylation at *MFA2*. Figure 4.6 shows that there is a basal level of H3 acetylation in all strains before exposure of the cells to UV irradiation. After UV irradiation, there is an initial increase in H3 acetylation (white bar 1h), which gradually reduces over time in wild type cells (white bars 2h and 3h). Histone H3 acetylation is not induced after UV irradiation in *RAD7* deleted cells (green bars 1h, 2h and 3h) confirming previous results. On the other hand, histone H3 acetylation status in *rad14*Δ cells does increase after UV irradiation (red bars).

Importantly, in the absence of NER activity, the level of histone H3 acetylation is not reduced as seen in wild type cells (2h and 3h). Histone H3 acetylation levels also examined in newly constructed Rad14 deleted cells versus WT (in these strains Rad16 were myc tagged), see appendix IV figure 9, page 194). Collectively, these results confirm our previous observation at *MFA2,*(Yu et al, 2005; Yu et al, 2011) confirming that these novel strains show similar histone H3 acetylation patterns and are suitable for further examination of chromatin remodelling and repair factor recruitment during GG-NER.

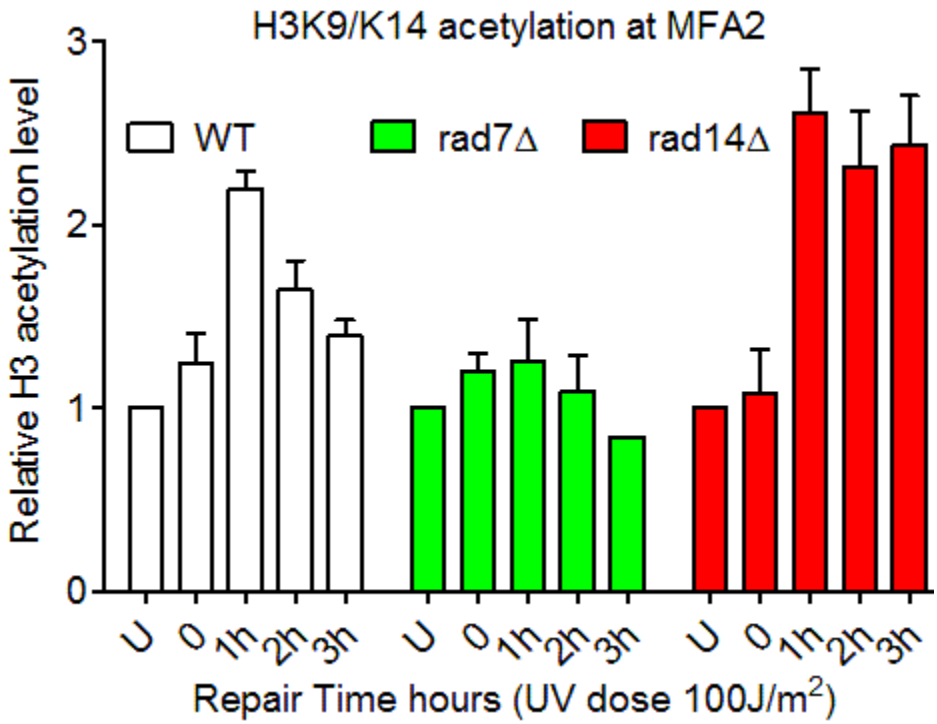

Figure: 4.6 ChIP analysis of the H3 acetylation at the *MFA2* promoter without UV or after UV (100J/m2). Cells were either un-irradiated or received 100 J/m^2 of UV and then the chromatin prepared either immediately 0 h or allowed to repair in YPD in dark for 1 h or 2 h. White bars represent WT-*GCN5-Myc*, green bars are rad7*Δ-GCN5-Myc* and red bars for rad14*Δ-GCN5-Myc* Acetylation level is shown as a fold change relative to its untreated. Data are the average of at least three independent biological repeats and the error bars represent standard deviation (SD) of the mean (see appendix IV, page 178-179, for the raw data, average and SD)..

4.3.4 Gcn5 chromatin occupancy promotes histone H3 acetylation in a UV-dependent manner in *RAD14* defective cells

My colleagues have observed that the UV-induced levels of histone H3 acetylation remain high when NER is defective (Yu et al., 2005). We know that Gcn5 controls the

UV-induced histone H3 acetylation and has a role in the distribution of both H3 acetylation at K9/K14 and on the distribution of the repair rates throughout the genome (Yu et al., 2016). These observations suggest that chromatin retention of Gcn5 maintains high levels of histone H3 acetylation in repair deficient cells. In order to study this possibility, Gcn5 occupancy on the chromatin was examined both before and following UV irradiation using the strains generated here. ChIP-qPCR experiments were employed to determine whether Gcn5 is retained at the chromatin, in turn sustaining histone H3 hyperacetylation. To do this, yeast strains (WT-*GCN5-Myc*, *rad7*Δ-*GCN5-Myc* and *rad14*Δ-*GCN5-Myc*) were grown, UV treated and their chromatin preparation were conducted as reported previously in chapter two, sections (2.11 and 2.13). ChIP was performed to enrich for chromatin associated Gcn5-Myc and qPCR targeted the *MFA2* locus that is well characterised. The results of the ChIP-qPCR experiments are presented in Figure 4.6. The data show that after UV, a rapid increase in the occupancy of Gcn5 was observed on the chromatin (white bar 1 h). This increase is followed by a rapid loss of Gcn5 occupancy 2 to 3 h after UV irradiation in wild type cells (white bar 2h and 3h). These changes are not detected in *rad7*Δ cells, where Gcn5 occupancy did not change in response to UV (brown bars) confirming previous results (Yu et al., 2005). On the other hand, in *rad14*Δ cells, increased occupancy of Gcn5 was observed on the chromatin (blue bar 1h), but instead of returning to its pre-damaged state as was the case in wild type cells, Gcn5 chromatin occupancy remains high (blue bars 2h and 3h). Therefore, Gcn5 is retained at the chromatin due to failure of the repair reaction to complete. This may explain why histone H3 acetylation at K9/K14 remains constitutively high in cells defective in NER. These results are in line with the work that was done in our lab previously (Yu et al, 2005; Yu et al, 20011). (see page 171 in appendix-II for qPCR primers and page 178-179 in appendix-IV for qPCR raw data).

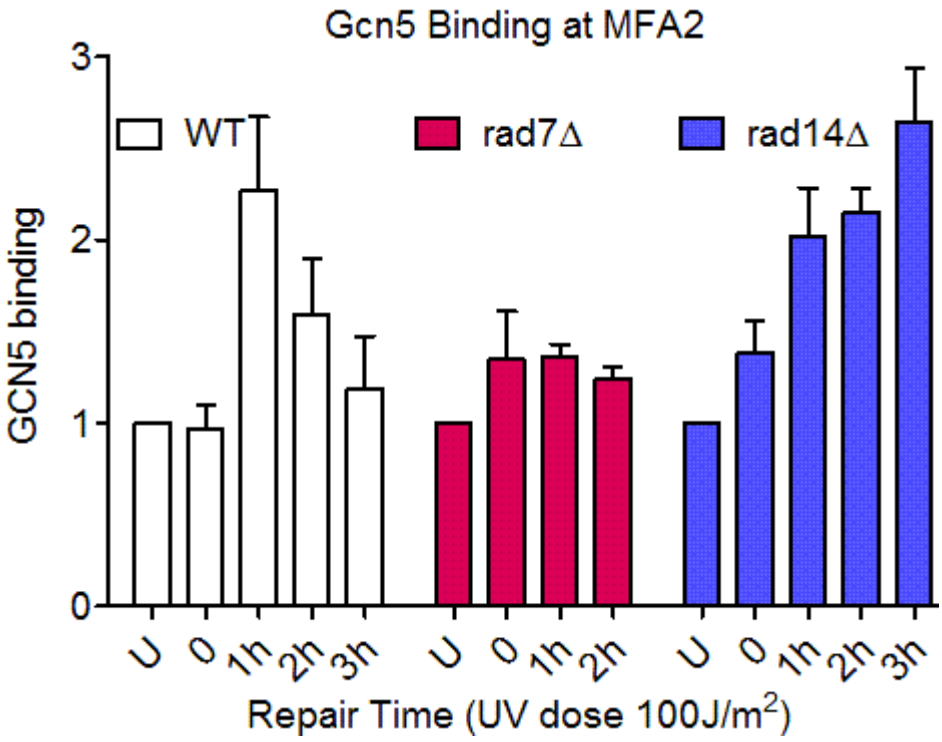

Figure: 4.7 The Gcn5 occupancy on the chromatin of the repressed *MFA2* locus of wild type, *rad7*Δ & *rad14*Δ strains. Cells were either untreated or received 100 J/m^2 UV and then incubated at various repair times in YPD. The Gcn5 binding is shown as a fold change relative to its untreated sample. ChIP analysis of the occupancy of Gcn5 was performed with anti-Myc. Data are the average of three independent experiments and the error bars represent standard deviations (SD) of the means. see appendix IV, page 179-181.

4.3.5 Rad7 and Rad16 control damage-induced histone H3 hyperacetylation by recruiting and maintaining Gcn5 on to the chromatin in the absence of functional NER.

Previously, Reeds lab showed that Gcn5 occupancy on the chromatin relies on the GG-NER factors Rad7/Rad16 (Yu et al, 2011). Furthermore, Yu and her colleagues have shown that genome-wide DNA repair rates were altered in pattern when UV-induced chromatin remodelling is not functional (Yu et al., 2016). Reed has also demonstrated that the GG-NER complex is bound at the ABF1 binding sites (ABS) that are located at many hundreds of consensus sequences throughout the genome (Reed et al, 1998). In wild type cells, in the absence of UV, the factors remain bound to the ABS and form a complex with Abf1. However, in response to UV-induced DNA damage the GG-NER complex dissociates from Abf1 and redistributes away from these binding sites (Waters et al., 2012; Yu et al., 2016; Yu et al., 2011). I have shown in the previous section (4.3.4, page 103) that following UV, Gcn5 remains associated with the chromatin in a Rad7-dependent manner. These observations have led us to speculate

that in the absence of functional NER, the GG-NER complex may remain bound to the chromatin, which promotes the constitutive recruitment and occupancy of Gcn5 on to the chromatin. This in turn ensures the persistent high levels of the damage-induced increase of histone H3 acetylation. To examine GG-NER complex occupancy on the chromatin in response to UV, the same experimental procedures was followed as described in (section 4.3.4 on page 103-105) using WT-*Rad7-Myc* and *rad14*Δ-*Rad7-Myc*, as well as in WT-*Rad16-Myc* and *rad14*Δ-*Rad16-Myc* strains.

ChIP-qPCR measurements of Rad7 and Rad16 binding at the *MFA2* locus indicate that there is an immediate increase in the occupancy of both Rad7 (light grey zero) and Rad16 (dark grey zero) in wild type cells (Figure 4.8). Nevertheless, this increase is rapidly followed by a reduction in its occupancy within 60 min repair time following UV exposure (light and dark grey 30 and 60 min). On the other hand, in a *rad14Δ* strain while there is an initial increase in Rad7 as well as Rad16 occupancy (red bars zero), the reduction of this occupancy is not observed (red bars 30 and 60 min). Collectively, these results indicate that the constitutive Gcn5 chromatin occupancy and high acetylation levels observed in repair deficient cells are consistent with the retention of Rad7 and Rad16 at the chromatin (Figure: 4.8 A and B and also see figure 4.7, page 105).

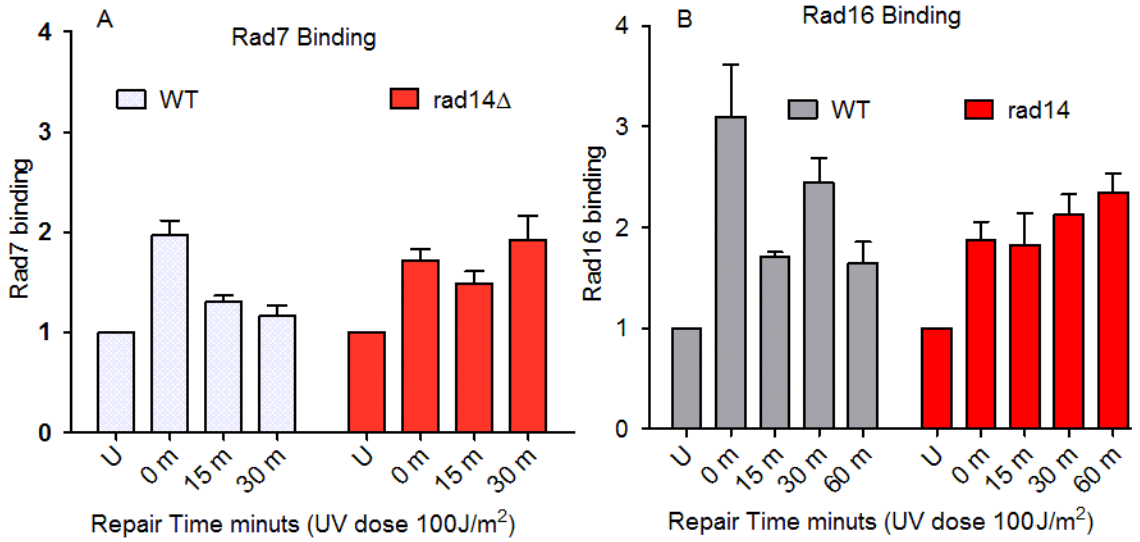

Figure: 4.8. A. Rad7 occupancy levels and **B.** Rad16 occupancy levels in wild type and rad14 deleted Myc tagged cells at repressed MFA2 promoter loci Cells either treated with UV (100J/m2) or without UV. ChIP with anti-myc antibody was performed; Rad16 binding is presented as the fold change relative to untreated cells. Data are the average of at least three independent biological repeats and the error bars represent SD, see appendix IV, page 182-184.

4.3.6 Investigating the role of HDACs in chromatin remodelling by deacetylating histone H3 after repair of UV-induced DNA damage

4.3.6.1 Strain construction

Wild-type Myc-tagged *HDA1* and *RPD3* strains were constructed by tagging with 18 copies of myc epitope using (RY7446 = p3747) plasmid (a kind gift from Richard A Young) as a template to make PCR products containing the Myc and a *URA3* selectable marker flanked by homologous regions to recombine at the 3′ end of *HDA1* and *RPD3,* respectively. *URA3* expression supports the growth of successfully transformed cells. Then by using another set of primers and a conventional PCR, the transformations were confirmed. Expression of the epitope-tagged protein was also confirmed by Western blotting using an anti-Myc antibody. From the transformed, Hda1- and Rpd3 myc-tagged strains, next *RAD14* was deleted in these two new strains in exactly the same process as in section 4.3.1., on page 99 and also appendix II for primers used in the transformation

To confirm that each target gene was tagged with Myc epitope correctly, colonies on the plate were numbered and a colony PCR was performed as described earlier in this chapter and in chapter 2 materials and methods. Results of the transformation for both tagging of Myc epitope to Rpd3 and Hda1 and for the deletion of RAD14 gene after tagging (see page 171 in appendix-II for primers used and page 190-193 in appendix-IV figure 1, 2, 3 and 4 for confirmation).

4.3.6.2 Expression of myc-tagged HDACs Hda1 and Rpd3 as determined by western blot

After colony PCR two positive clones from both Rpd3 and Hda1 were selected for western blot detection of myc-tagged protein to confirm that the Myc epitope-tagged protein is correctly expressed in case of both *RPD3* and *HDA1* genes.

A strain expressing myc-tagged Rad16 was included in the analysis as a positive control, while whole cell extract from strains that contain no myc-tagged gene were included as a negative control. Whole cell extracts were prepared for Rad16-Myc, Hda1-Myc and Rpd3-Myc containing strains using TCA (see methods, section 2.10, page 62). After SDS-PAGE and protein transfer to a PVDF membrane, myc-tagged proteins were probed with myc-specific antibodies and detected by chemiluminesence. The correct expression of myc-tagged Hda1 (lane 5 and 6) and Rpd3 (lane 3 and 4) is presented in Figure 4.9A.

Having established the correct phenotype (see appendix- 108, figure2, page 190) and expression of tagged Hda1 and Rpd3, we next performed a titration among non-transformed strains and those 4 transformed strains to select one with higher binding levels. Chromatin immunoprecepitation was performed or two clones of each strains as detail in chapter 2 section 2.13, page 68) and a fixed amount of anti-myc antibody was added to all of the samples. The results show that all the transformed strains were show a much greater binding levels compared to non-transformed strain figure 4.9B. Nevertheless, clone number 17 from Rpd3 and clone number 1 from Hda1 shows the highest level of binding comparing to the clone number 16 of Rpd3 and clone number 20 of Hda1, respectively figure 4.9B (see appendix-IV, figures 1-8 page 190-193),.

The constructed new strains have been fully characterised for this study. Two important experiments were conducted to examine the effect of tagging the myc protein in both strains (Rpd3 and Hda1) which are expression and UV survival. The results showed that the protein is expressed with a full length expression (figure 4.9A) and the tagged protein in the new strains is fully functional because there is no effect on repair after tagging and the tagged strains are recovered after UV (see appendix IV, figure 2, page 190) The next sections describe the further investigation of HDAC chromatin occupancy before and after UV irradiation to find out whether they are involved in UV-induced chromatin remodelling during GG-NER.

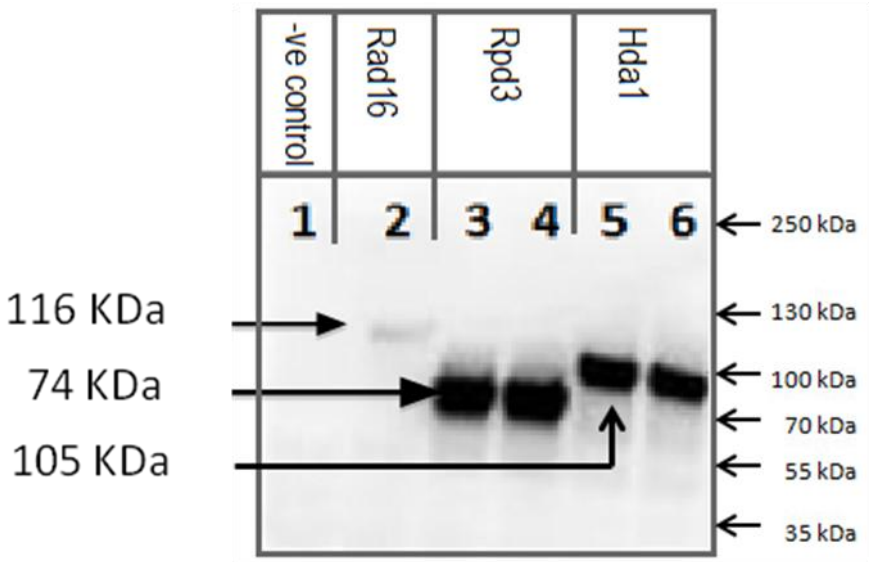

Figure 4.9A Western blot analysis of novel yeast strains containing myc-tagged Hda1 and Rpd3. Wild type cells containing no epitope-tagged proteins are used as a negative control in lane 1, Lane 2 represents a positive control of Rad16-Myc. Transformed cells containing Rpd3-myc clone 16, and clone 17 were run in lanes 3 and 4, while transformed cells containing Hda1-myc clone1 and clone 20 are loaded into lanes 5 and 6. Myc was detected using mouse mAb.

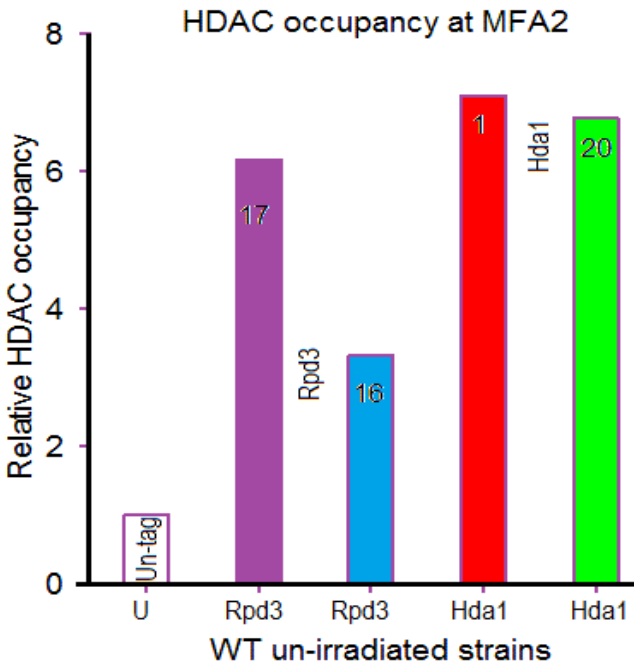

Figure 4.9B Enrichment of untagged (untransformed not coloured) and two transformed clones from Rpd3 (clone 17 and 16 coloured red) and two transformed clones from Hda1 (clone 1 and 20 coloured green) using ChIP qPCR and Myc antibody**.**

4.3.7 Hda1 and Rpd3 occupancy on chromatin after repair of DNA damage at the promoter region of *MFA2, HML* and *RAD23*.

The activity of Histone acetyltransferases (HATs) and Histone deacetylases (HDACs) exists in a dynamic steady state - any change in the activity of these two enzymes has a great effect on many cellular processes including NER. HDACs play a critical role in the maintenance of genome stability. Rpd3 primarily erases acetyl groups from histones H3 and H4 (Kurdistani and Grunstein, 2003; Rundlett et al., 1996). This active process of deacetylation by HDACs is well known in several DNA-based processes including repair of DSBs. It has been established that UV-induced histone H3 hyperacetylation of chromatin is essential for efficient NER (Teng et al, 2002, Yu et al, 2005). I previously showed that Gcn5 and the GG-NER containing Rad7/Rad16 complex remains associated with the chromatin. This demonstrates that the factors controlling H3 acetylation in response to DNA damage can continuously promote histone tail acetylation, thereby keeping acetylation levels high. We therefore considered whether HDACs might have a role in reversing this acetylation, restoring chromatin to its pre-damaged state. In order to perform this, ChIP-qPCR experiments was undertaken to measure the chromatin occupancy of each HDAC before UV and after UV irradiation at varying point during and after DNA repair. Cells were grown , chromatin was prepared as described in chapter 2 (section 2.11, page 65) and the ChIP-qPCR experiment was performed as described previously. Interestingly,

quantifying the qPCR data reveals that, in wild type cells, basal levels of Rpd3 and Hda1 occupancy at the three genetic loci examined are reduced 1 h after UV irradiation, as shown in Figure 4.10 (A and C, respectively). This occurs concurrently with the increased occupancy of the HAT Gcn5 in wild type cells (see Figure 4.7, page 105) and is consistent with the increased levels of histone H3 acetylation observed in wild type cells after UV damage (Figure 4.2 page 98 and figure 4.6 , page 102 and figure 4.11A red lines in page 112). At later time points after UV irradiation, HDAC occupancy increases close to normal levels before DNA damage induction (Figure 4.10A and C 3h). This occurs concurrently with the reduction of the histone H3 acetylation toward normal levels (see Figure 4.2 page 98, 4.6 page 103, and Figure 4.11A black lines, see page 112). Taken together, HDAC chromatin occupancy follows a pattern mirroring that of HAT occupancy in response to UV irradiation. These observations provide a novel example of how the equilibrium between HAT and HDAC occupancy can control histone acetylation, in this instance, in response to UV-induced DNA damage. We propose that recruitment of Gcn5 and dissociation of the HDACs Hda1 and Rpd3 together control the UV-induced histone H3 acetylation described previously (Yu et al., 2016; Yu et al., 2011; Yu et al., 2005).

In an attempt to confirm that active repair is required for the above described recruitment of HDACs after repair (i.e. 3 h post UV irradiation), the above experiments were repeated in repair defective cells (Figure 4.10B for Rpd3 binding and figure 4.10D for Hda1 binding levels). While it is possible to observe an initial reduction of both Rpd3 and Hda1 chromatin occupancy (1h) following UV exposure, their recruitment after DNA repair to pre-damage levels is absent or delayed in *rad14Δ* mutant cells. Instead, further reduction can be observed (Figure 4:10B and D 3h post UV) (see raw data for all strains at 3 different loci is in appendix-IV, page 185-190). Both Rpd3 and Hda1 are also investigated at three other genomic locations in Rad14 deleted cells, a single qPCR-ChIP data for each locus in both Rpd3 and Hda1 are presented in (appendix-IV, figures 6-8, page 192-193). In summary, the data presented here help explain the hyper acetylated state of chromatin in repair defective cells due to the constitutive chromatin retention of Gcn5 and concomitant reduced levels of HDACs. Therefore, active repair is required for HDAC recruitment to chromatin during the restoration phase of GG-NER to facilitate histone H3 deacetylation.

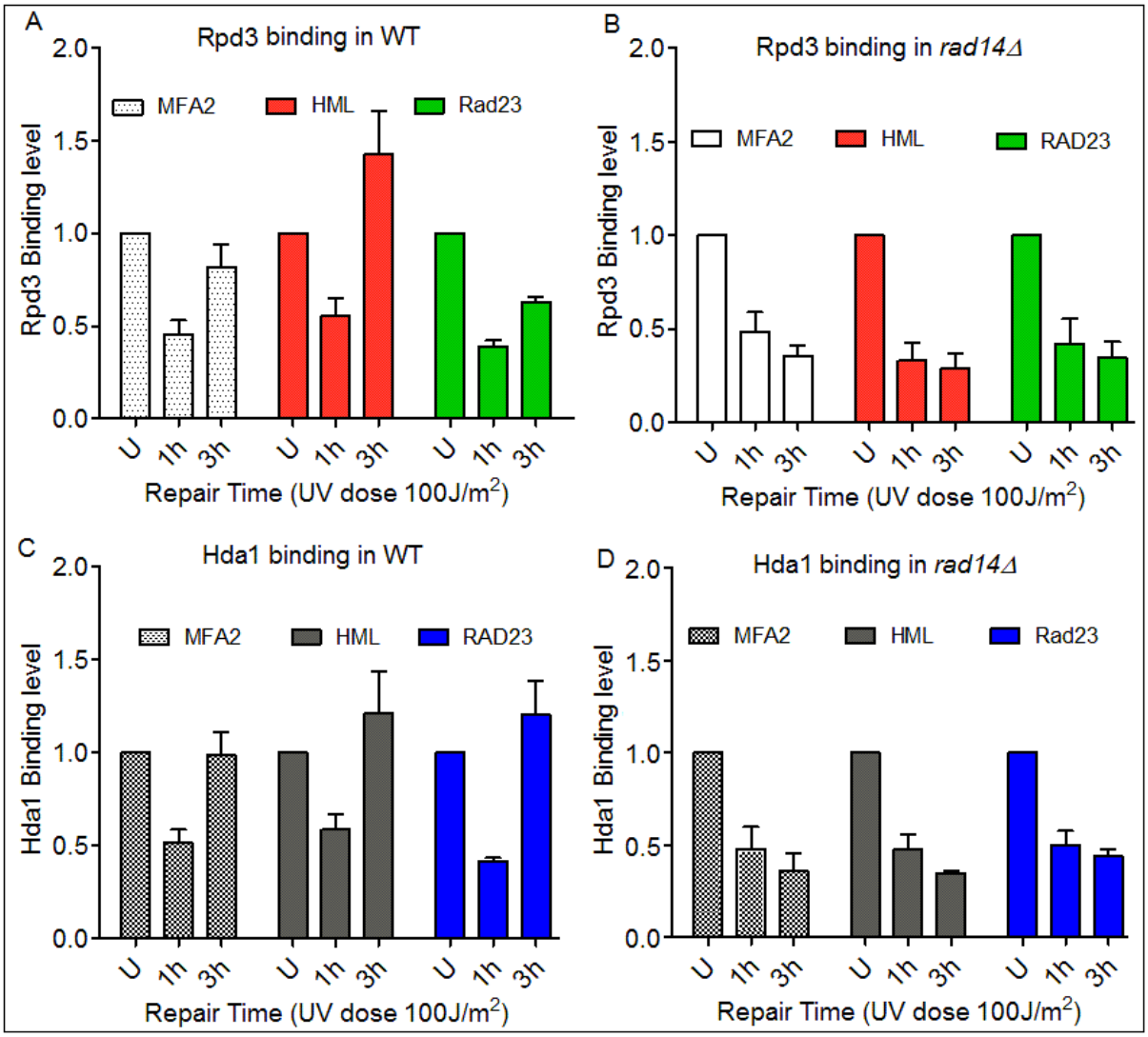

Figure: 4.10 A-D HDAC occupancy (Hda1 and Rpd3) at *MFA2*, Rad23 and *HML I* in response to UV. ChIP with anti-myc antibody was performed in wild type (Hda1 and Rpd3 myc tagged and their Rad14Δ counter) cells at MFA2, Rad23 and HML I loci. In wild type (A and C), it is observed that following UV there is a loss of the occupancy of both Rpd3 and Hda1 and returning of the occupancy is detected again within 3 h repair time. However, in the Rad14 deleted cells, although the levels of Rpd3 and Hda1 has dropped as were observed in wild type, yet, the returning of their occupancy to pre-UV is absent figure: 4.10B and D 3h. The HDAC binding is presented as the fold change relative to untreated cells. Data are the average of at least three repeats (Rpd3 and Hda1 binding at HML and Rad23 in Rad14 deleted samples are only two repeat)**. The error bars represent SD, See appendix IV, page 185-190, for raw data and statistical analysis).**

4.3.8 Antagonistic relationship between HDACs and histone H3K9/K14 acetylation in response to UV exposure at *MFA2* locus.

I have explained that HAT and HDACs have a reciprocal function in the cell and that they are involved in many cellular processes. Here in figure 4.11A and 4.11B both H3K9K14 acetylation and HDAC occupancy were plotted using ChIP qPCR data from a single locus at the *MFA2* gene in wild type and RAD14 deleted cells, both before and after UV irradiation. In wild type cells, prior to UV exposure there is a background level of signal for each histone H3K9/K14 and for HDACs occupancy (each normalised against its own un-irradiated samples). One hour following UV, while there is an increase in the acetylation levels of H3K9/K14, the HDAC levels diminished to its lowest level. However, during later times after DNA damage (three hour following UV exposure), the H3K9/K14 acetylation levels reduced, and at the same time the levels of the HDACs goes up again (Figure 4.11 A). Importantly, in the repair defective strains such as RAD14 mutant cells, although we observe the first part of increased H3K9/K14 and decreased HDAC levels of the response to UV irradiation as we noticed in wild type cells, the return of HDACs occupancy and histone H3 acetylation (reduction of the former and the elevation of the latter) to their previous levels are no longer observed (figure 4.11B).

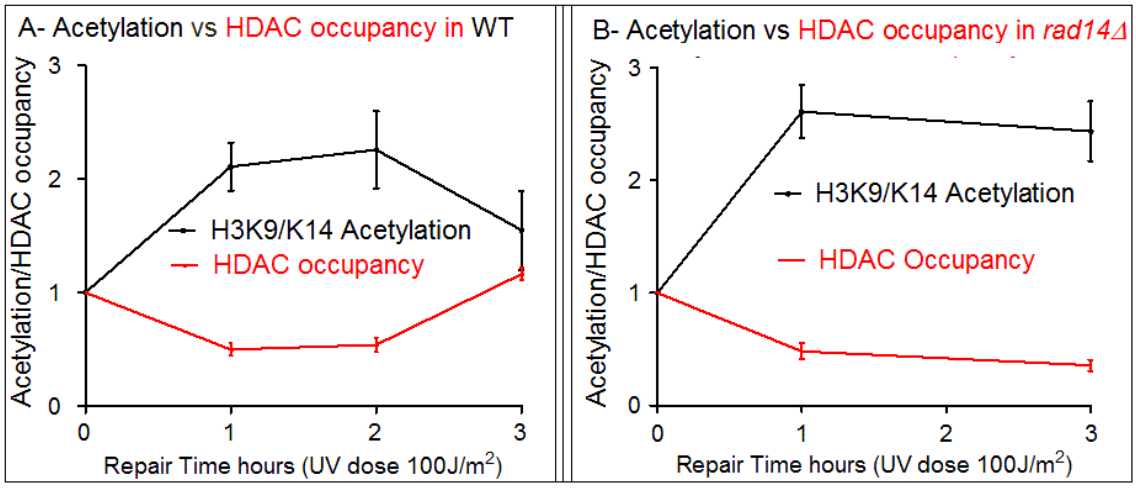

Figure 4.11: Opposing UV-induced association between HDACs and H3K9/K14 acetylation at *MFA2* in wild type and rad14. (A) Their (HDAC=red line and H3K9/K14=black line) relation before UV (No UV), and after multiple time points following UV irradiation (1 h, 2 h and 3 h) in wild type cells. **(B)** Same as **(A)** but in *RAD14* mutant cells.

4.4 Discussion

As proposed by the access repair restore (ARR) model, chromatin must be disassembled to facilitate DNA repair factors with access to the damaged DNA. Following repair, to maintain important genetic and epigenetic integrity, the structure of the chromatin must be reassembled in the wake of DNA repair. A lot of work has been done on the first two phases of the ARR model and several proteins were found that have roles in the access as well as the repair phases (Reed et al., 1999, Teng et al., 2002, Yu et al., 2011; 2016). It is the restoration phase that remained largely unrevealed and work in this area is in its infancy.

In this study, I tried to widen our current understanding on the role that each of the repair factors (Rad7 and Rad16) and the accessory chromatin remodelers (Gcn5, Rpd3 and Hda1), play in the chromatin restoration process after UV-induced DNA damage in yeast. We've shown previously, that the HAT Gcn5 and the Rad7-Rad16 (GG-NER) proteins are essential for UV-induced histone H3 hyperacetylation to facilitate chromatin remodelling at *MFA2*, a process that is necessary for effective NER in that region of the genome. Recently, Reed's lab has found that Gcn5 plays an important role in repair events at a genome-wide scale as well (Yu et al., 2016).

In order to study the relationship between chromatin occupancy and recruitment of the GG-NER factors and chromatin remodelling factors, epitope-tagged strains were required to perform ChIP-qPCR. The strain construction was performed as described in this chapter (section 4.3, page 99 and section 4.3.6.1, page 107), and resulted in the successful deletion of *RAD14* from strains with myc-tagged repair factors. Initially, previous results of UV-induced histone H3 acetylation were reproduced in these novel strains to confirm that this phenotype is unaltered by the introduced genetic modifications. In wild type cells, the levels of H3K9/K14 acetylation increased in response to UV irradiation, while they return to nearly pre-damage levels at later time points. Nevertheless, in strains with defective repair such as a *RAD14* mutant as well as *RAD4* deleted cells, the increased levels of damage-induced histone H3 acetylation are not depleted at later time points due to failure of these cells to finish repair.

Next, each of the mentioned repair and remodelling factors was examined in wild type and *RAD14* deleted cells both before and after UV irradiation at a few locations on the genome, especially at the well characterised *MFA2* locus. Basal levels of Gcn5 are present at *MFA2* before UV exposure. However, following UV irradiation, an abrupt increase in the occupancy of Gcn5 on the chromatin is observed. This is in line with the UV-dependent histone H3 hyperacetylation observed in wild type cells (Yu et al., 2016;

Yu et al., 2011; Yu et al., 2005). The induced increase of Gcn5 occupancy is lost 1 h after UV irradiation in wild type cells and returns to pre-damaged levels. On the other hand, failure to complete the repair reaction in *RAD14* deleted cells results in the retention of high levels of Gcn5 on the chromatin in response to UV irradiation. These results explain the constitutive histone H3 hyperacetylation observed in repair defective cells. Moverover, this may indicate that, when repair is defective, the mechanism involved in decreasing elevated levels of histone H3 acetylation is not sufficient to counteract the persistent Gcn5 activity or that this activity is not recruited to the chromatin at all. Consequently, in repair deficient cells chromatin can't be restored to its normal state as observed in wild type cells and will remain in an open conformation. This has important implication for mutagenesis and genotoxicity of chemotherapeutic drugs (Since some drugs affect the epigenetic status, acetylation in particular, and can change the structure of the chromatin and thus the damage levels is potentially increased as the chromatin is already open. There open status of chromatin, generates DNA:RNA structure (R-loops) due to transcription-replication collisions which can induced DSBs and ultimately lead to the cancer and neurologic diseases).

Chromatin retention of Gcn5 appears to be the main cause of constitutive histone H3 hyperacetylation in repair deficient cells after DNA damage induction. We hypothesised that one underlying cause could be the chromatin retention of the GG-NER factors tethered to damaged DNA-bound intermediate complexes unable to complete repair. Therefore, the Rad7 and Rad16 GG-NER factors were investigated before and after UV irradiation in wild type and *RAD14* deleted cells. As shown previously, in response to UV irradiation, a sharp increase in the Rad7 and Rad16 occupancy can be observed, followed by reduced occupancy at 15 to 30 min after UV irradiation (Yu et al., 2016). However, as predicted, the repair factors remain bound to the chromatin in the absence of active repair. This indicates that GG-NER factors are trapped at repair intermediates that fail to excise UV-induced lesions. The presence of Rad7 and Rad16 at the chromatin for prolonged periods of time, results in continuous retention or recruitment of Gcn5, in turn maintaining the hyper acetylated status of the chromatin. This is in agreement with previous observations and demonstrates that dissociation of the GG-NER complex at later phases of the repair reaction is required for restoration to take place, returning the chromatin structure to its original conformation.

Having established that active repair is required to remove the GG-NER complex and associated HAT Gcn5 from the chromatin to reduce histone H3 hyperacetylation, the question remains what activity is required for the deacetylation. To address this question, initially the possible role of different HDACs in UV survival and CPD removal

were examined through genetic approaches (see chapter 3, page section 3.3, page 85). Unfortunately, due to some caveats such as redundancy between various HDACs and the nature of the approach conducted, their involvement couldn't be confirmed. Because of these facts their contribution during repair process could not be ruled out directly. Hence, the two major classes of HDACs were investigated through ChIP-qPCR to measure their chromatin occupancy in relation to GG-NER at different genomic loci both before and following UV exposure at different repair times. To do so, two strains were constructed by epitope tagging either Rpd3 or Hda1. Before UV irradiation, a basal level of both Rpd3 and Hda1 can be observed on the chromatin. This demonstrates for the first time, the presence of both HATs and HDACs in the context of repair, maintaining the acetylation status of chromatin. This may indicate that in addition to HATs like Gcn5, there are also HDACs that have a role in setting up the chromatin during the access phase of the ARR model. Similar to Gcn5 chromatin occupancy, HDAC occupancy at chromatin prior to DNA damage induction does not depend on the core repair reaction as it is readily detectable in *RAD14* deleted cells. In response to UV exposure, the occupancy of both Rpd3 and Hda1 is lost at all the loci examined. These results show that when GG-NER factors, Gcn5 occupancy and histone H3 acetylation levels increase in response to UV, HDAC occupancy is reduced. Importantly, this process does not depend on active repair as it can still be observed in repair deficient cells. Repeating these experiments in GG-NER defective cells would reveal to what extend chromatin occupancy of these HDACs is controlled by this pathway. Regardless, these data demonstrate that UV-induced histone H3 acetylation is controlled by the synergistic effect of attracting HAT remodelers on to the chromatin and releasing HDACs.

Strikingly, during later stages after UV irradiation when restoration takes place, HDAC chromatin occupancy recovers gradually to near pre UV-damage levels during a three-h period. Importantly, this process is entirely dependent on active repair as this is not observed in *RAD14* deleted cells. The recruitment of HDAC after repair is concomitant with the reduction in Gcn5 and histone H3 acetylation levels at the chromatin. This demonstrates that HDACs contribute to the restoration phase of the ARR model by deacetylating histone H3 after the repair reaction is completed. This will eventually lead to compaction and remodelling of the chromatin. How the chromatin is remodelled at the level of the nucleosome during this process is a topic for future study.

Taken together, my results clearly show the inverse relationship between HATs and HDACs in the context of GG-NER. These are all consistent with what was found so far in this current study. My results indicate that Rpd3 and Hda1 are involved in this repair

pathway and may have a role in setting up chromatin at the access phase as well as in restoring chromatin to its status that exists prior to DNA damage induction by UV irradiation. My results have expanded our understanding on how the last phase of ARR model might be working. The current study describes the mechanism of histone acetylation at individual genetic loci. Although it provides a good understanding on how these factors work on the chromatin and how they relate and affect each other *in vivo*, it does not provide a genome-wide view of the process. In order to obtain a thorough understanding of the role that each of the above examined repair factors and remodellers have, I next aim to investigate this process in more detail by examining this process on a genome-wide scale using ChIP-chip. In the next and final chapter, chromatin occupancy of Rpd3, Hda1, Gcn5 and the GG-NER complex will be investigated throughout the genome.

In this chapter, experiments were conducted to determine the role of Gcn5 and the Rad7/Rad16 GG-NER complex in restoring the levels of UV-induced histone H3 acetylation, following the repair of damage from the genome..

In summary the results showed the following:

1- Following UV exposure

In wild-type cells there is an immediate increase in the chromatin occupancy of Gcn5 at specific locations in the genome, and this rapid increase in the level of histone acetylation is reversed and restored to steady state levels very rapidly in repair proficient cells. In GG-NER defective Rad7 deleted cells, Gcn5 occupancy does not change in response to UV damage. In cells completely defective in NER such as Rad14 deleted cells, although there is UV-induced increase of the Gcn5 occupancy on the chromatin at specific genomic positions, remarkably, it was found that these levels remain constitutively high in cells that cannot repair UV damage in their genomes.

2- The Rad7/Rad16 GG-NER complex redistributes away from its initial genomic locations at Abf1 binding sites in response to UV damage. In WT cells, the GG-NER complex returns to its normal chromatin occupancy following DNA repair. However, in Rad14 deleted cells it remains bound at its UV-induced location. As a result of this in repair defective Rad14 deleted cells, the histone acetyl transferase Gcn5 is retained on the chromatin and constitutively high levels of histone H3 acetylation are observed at the genomic locations of GG-NER Rad7/Rad16 complex retention.

3- Prior to UV exposure, basal levels of HDACs (Rpd3 and Hda1) can be detected on the chromatin, in the vicinity of GG-NER complex occupancy.

4- In response to UV damage in wild type cells, the occupancy of HDACs is lost rapidly and at one hour after UV irradiation, reaches the lowest level. This point corresponds with the peak increased level of Gcn5 occupancy, and increased H3 acetylation levels at these genomic locations.

5- Following 3 hours of repair in wild type cells, HDAC returns to its previous occupancy, and the levels of H3 acetylation decreased to steady state levels. The combined affect of HDAC loss of occupancy and recruitment of HAT Gcn5 together controls histone H3 acetylation levels in a GG-NER dependent fashion.

6- Restoration of chromatin structure depends on an active repair. These results broadened our understanding on how the restoration phase of ARR model functions.

Chapter Five

5. Genome-wide investigation of HDACs (Rpd3 and Hda1) occupancy in response to UV-induced DNA damage

5.1 Introduction

Over the last two decades, the development of high-throughput analytical tools, such as microarray technologies, made the rapid analysis of thousands of protein-interacting events feasible and has led to the fast progression of this field. During its infancy DNA microarrays only contained 378 probes, but the resolution of DNA microarrays has improved greatly and expanded significantly up to 2.1 million probes on a single array. A variety of features have been successfully mapped for their localisation throughout the entire genome, including protein-DNA and protein-chromatin interactions using ChIP-on-chip (Venters et al., 2011). This method was also used to map histones and histone modifications (Pokholok et al., 2005) and to detect DNA damage (Teng et al., 2011). Microarray technology has been proven to be very important in discovering new genome-wide mechanisms in yeast and other organism. This approach can be developed and extended to any protein or histone modification. The key factor is the availability of a good ChIP-grade antibody and/or epitope tags and a suitable cross-linker for capturing protein-chromatin complexes. The widespread availability of epitope tagged proteins (including those already present in our lab as well as those I generated for this study) and the wide variety of commercially available ChIP-grade antibodies, coupled with the presence of genome-wide datasets, provides a platform for correlative studies.

DNA microarray studies revealed that HDACs are required for transcriptional activation and repression in *Saccharomyces cerevisiae*. HATs and HDACs act in an opposite fashion and maintain the acetylation states of chromatin at an equilibrium. When HATs increase the acetylation levels, HDACs can counteract that and vice versa (Kurdistani and Grunstein, 2003). A Microarray study on histone acetylation in HDAC mutants revealed increased acetylation levels in the intergenic zones of those strains (Robyr et al., 2002). It appeared that the two main HDACs that are active on various gene promoters throughout the genome are Rpd3 and Hda1.

Chromatin responds to environmental agents (UV irradiation) in a highly dynamic way. Histone acetylation can be altered by the activity of HATs and HDACs to alter chromatin structure in response to external stimuli. Regardless of the changes to

chromatin, mechanisms are put in place that restores the alterations back to the basal equilibrium state to maintain genome stability and normal gene expression patterns.

It is well-established that chromatin modifications are required for efficient transcription. The analogy with DNA repair mechanisms lead to the proposal of the Access Repair Restore model that serves as a useful frame of reference for studying chromatin remodelling during DNA repair. Indeed, histone H3K9/K14 acetylation was shown to increase in response to UV irradiation both at a single gene and at a genome-wide level (Yu et al., 2016).

Therefore, I proposed that, since HDACs function antagonistically to HATs, there should be a role for HDACs in reducing the UV-induced histone H3 hyperacetylation during the restoration phase posed by the ARR model. Hence the two chief HDAC factors (Rpd3 and Hda1) were selected to be investigated globally before and after UV in wild type strains (it was planned to examine most of the HDAC mutants. However, due to the time lime only two of them have been dealt with).

Previously, Teng and his colleagues in the Reed's lab has developed the original work from studying only a single gene (*MFA2* as a model), to a genome-wide scale with the aid of this technology. They created a genome-wide high-resolution analysis of UV-induced histone H3 acetylation (Evans, PhD thesis 2011), CPD induction and repair by utilising the microarray techniques (Waters et al., 2012, Teng et al., 2011). Similarly, the molecular mechanism of the recruitment of Abf1, Rad7, Rad16 and Gcn5 has been derived from the analysis of genome-wide chromatin occupancy changes of these factors (Yu et al., 2016).

In Chapter 4, the role of the Gcn5, and the GG-NER factors Rad7 and Rad16, in the access phase of the ARR model during NER to control UV-induced histone H3 acetylation levels in wild type cells was confirmed. Establishing this work allowed me to further document the role HDAC factors (Rpd3 and Hda1) play in the repair process during the later restoration phase. These events were examined at a single genetic locus located at the *MFA2* gene. Based on these results I wanted to determine whether chromatin occupancy of Rpd3 and Hda1 responds to UV irradiation and is linked to repair activity throughout the genome. To do this, genome-wide approach was employed such as ChIP-on-chip technique that has been widely used in Reed's lab. Rpd3 and Hda1 Myc (their phenotype has been checked, see appendix IV, figure 2, page 190 tagged strains were used as described previously, to investigate the role of HDACs in the NER process genome-wide. A lot of studies have been done to try and

understand the access phase of the ARR model, nevertheless, less is known about how these changes that facilitate chromatin remodelling, are reversed to return the chromatin to its pre-damaged state. The question is do Rpd3 and/or Hda1 contribute to repair by returning chromatin to its pre-UV state. In this chapter, my previous findings will be expanded to involve the entire genome. By finishing these experiments, it will give a good indication of whether or not Rpd3 and Hda1 have a role in remodelling chromatin and its restoration.

In this current study, the ChIP-on-chip approach has been undertaken to investigate the genome-wide chromatin occupancy of Rpd3 and Hda1. This ChIP-on-chip technology is carried out by chromatin immunoprecipitation of a protein of interest. Here the same genome-wide method used by Kurdistani and his colleagues was utilised to study genome-wide binding of Rpd3 and Hda1, but now in relation to UV irradiation and GG-NER. To successfully capture HDAC complexes on chromatin, a two-step cross-linking method was used. At first a protein-protein crosslinking agent (DMA in this case) is used, since Rpd3 is present in a complex with a number of subunits and doesn't bind directly to DNA. Due to the presence of this large protein complex the proximity of Rpd3 to the DNA is too great to be able to crosslink the protein to DNA by formaldehyde alone. Following protein-protein cross-link, formaldehyde is used as the second cross-linker. The DNA that is bound by the protein will be enriched and is recovered, followed by a PCR amplification step. The IP and input samples are then differentially labelled and finally hybridised to microarray slides. The data is then extracted by software and analysed later (all the teaching and training on data analysis was conducted by Dr. Patrick Van Eijk) using the R programming environment using the Sandcastle R-package (Bennett et al., 2015). Protein chromatin occupancy is read out as the ratio between IP and input. Previously, genome-wide maps of HDACs were generated in yeast cells using ChIP-on-chip experiments (Kurdistani et al, 2002). Several studies have employed GWA in yeast to determine the effects of acetylation and deacetylation. This was done via localising HATs and HDACs and mapping of histone modifications (Lieb et al, 2001, Robyr et al, 2002, Kurdistani et al, 2002; Robert et al, 2004). These studies provided substantial associations between histone modifiers and gene repression. Studies have found roles for HDACs at active genes in yeast (Pokholok et al., 2005). For example, Rpd3 is recruited during stress conditions, to genes that control the stress response to osmosis as well as heat shock genes. As a result, the acetylation of histone H4 is reduced (Alejandro-Osorio et al., 2009). Furthermore, the activation of these genes is defective in the absence of Rpd3, demonstrating the HDAC activity is recruited for their activation.

Moreover, more than 250 transcripts are down regulated as a result of the *RPD3* deletion (which is higher than the up regulated genes). While some of these changes are indirect, other studies have confirmed a direct Rpd3 involvement in gene activation (Sertil, 2007).

UV-induced histone H3 hyper-acetylation was observed at certain sites and throughout the yeast genome (Yu et al., 2005; Yu et al, 2016). HATs control this acetylation and it has been revealed to have connection in NER (Brand et al., 2001, Guo et al., 2010, Martinez et al., 2001, Yu et al., 2005; Yu et al, 2016). As determined by using a combination of chromatin immunoprecipitation, MNase digestion and NER assays, Reed lab has found that chromatin remodeling is taking place following damage induced histone H3 acetylation at the *MFA2* gene, and that Rad7/Rad16 GG-NER complex is responsible for these changes in the chromatin (Yu et al., 2011, Yu et al., 2005). The genome-wide analysis of UV-induced H3 hyper acetylation revealed that increased levels of histone H3 acetylation at lysines 9 and 14 and the subsequent chromatin remodeling play a vital role in the efficient repair process. Previously, Reed's lab found that this UV-induced increased levels of H3 acetylation is present more abundantly at promoter regions than around the coding region (K. Evans, PhD thesis 2011). This damage-induced level of H3 hyper-acetylation decreases gradually with time as repair finishes.

In this chapter the relationship between GG-NER and the HDACs Rpd3 and Hda1 was investigated using ChIP and microarray to understand the final stage of the ARR model after repair of UV-induced DNA damage. The genome-wide binding of Rpd3 and Hda1 was investigated prior UV exposure and at 1 h and 3 h following UV irradiation to examine any changes the chromatin occupancy of these two HDACs and their relation to efficient GG-NER. In addition, the relation of each of the Rad7/Rad16 GG-NER complex binding, histone H3 acetylation at K9/K14 and CPD repair to HDAC binding peaks will also be investigated to understand how the repair process is organised in relation to the HDAC (Rpd3 or Hda1) occupancy.

5.2 Materials and methods

For detail see chapter 2 (sections 2.15 on page 72)

Microarrays: In this study Yeast Microarrays 4x44k (G4493A) were used which have an average 60-mer oligonucleotides printed uniformly on them (Agilent 60-mer Sureprint technology). The features represent the genome, with an average spatial resolution of a probe every ~290 base pairs. This offers a high resolution approach to analysing the entire yeast genome. Chromatin was prepared for ChIP-on-chip analysis as described previously (Chapter 2 materials and methods). This protocol consists of three main stages before the DNA is ready to be applied to the arrays. Firstly, the UV-induced CPDs repaired from the IP and input samples via using PreCR repair kit (for explanation see chapter 2 section 2.15 on page 72); second, the DNA is blunt-ended followed by ligation of the linker hybrid adapter; third, amplification of DNA fragments via ligation mediated PCR. Finally, differential labeling of the amplified input and IP DNA fragments by Cy5 and Cy3 dyes respectively is performed before the DNA is hybridised to the microarray slide.

Chromatin Immunoprecipitation and DNA microarray

In brief, cells are treated with DMA to crosslink protein to protein in addition to using formaldehyde to crosslinks proteins to DNA. Then, the cells are lysed in lysis buffer and the chromatin is fragmented by sonication (Bioruptor Sonicator (Diagenode)). Specific antibodies, anti-myc antibody, are used to pull down the protein of interest (myc tagged proteins), which bound the sonicated chromatin. Then, the protein-DNA crosslinks are reversed before being purified and then amplification of both IP and IN (input samples were prepared directly after chromatin preparation without adding antibody but it also subjected to overnight incubation with pronase at 65ºC and purification) done by PCR. Following amplification the samples are differentially labelled with different fluorescent dyes (input and IP DNA fragments by Cy5 and Cy3 dyes respectively) and hybridised to the microarray slides (Shivaswamy and Iyer, 2007) [see Figure 5.1]. The aspects of the ChIP-on-chip method are illustrated below. For the detailed protocol see page 72 in chapter 2 (section 2.15).

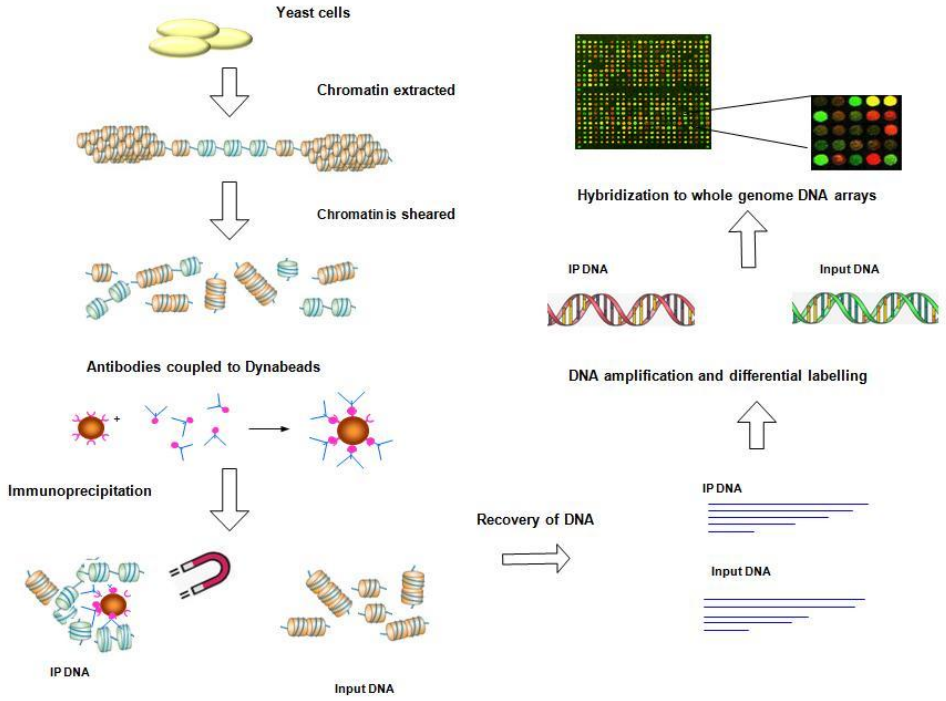

Figure 5.1: Diagram summarising the various stages of the ChIP-chip protocol. Chromatin was extracted from yeast cells and sonicated to fragment the DNA. Antibodies against the protein of interest were used in conjunction with Dynabeads to immunoprecipitate the DNA fragment where the protein of interest had bound (IP). A control genomic DNA sample (input), where no antibody was used, was also obtained. Both the IP and input samples were purified, amplified and differentially labelled with either Cy3 or Cy5 dyes. The differentially labelled IP and input samples were combined and hybridised to the microarray. Following hybridisation, the microarrays were washed and scanned and the relative fluorescent values for each probe on the microarray extracted and these values were used in all further analyses. ref

5.3 Results

To map chromatin occupancy of Rpd3–Myc and Hda1–Myc throughout the genome, ChIP-on-chip experiment was performed targeting both factors. Using an anti-Myc antibody, both HDACs were immunoprecipitated individually from chromatin of UV-treated and untreated cells. The experiments for Rpd3 were repeated twice, while the data for only one experiment is available for Hda1. To validate the Rpd3 data the normalisation assumption function in Sandcastle was used. The results showed that the two replicate data sets of all three time points of Rpd3 and one replicate data set of Hda1 (un-irradiated samples) are correlated and can be normalised this way (see appendix-V, page 195-199). However, in the case of the Hda1 datasets only the untreated samples showed sufficient correlation, while the one hour and two hour sample of the second dataset were not correlated and could therefore not be used in the analysis. (See appendix-V, page 195-199)

5.3.1 Describing Genome-wide Occupancy of the HDACs Rpd3 and Hda1 and their change in chromatin binding in response to UV irradiation

5.3.1.1 Investigating the Rpd3 and Hda1 binding peaks before UV exposure

The antagonising function of Gcn5 HAT and HDACs is an important feature of histone acetylation since these two classes of modifiers impede each other for recruitment to the same promoter. For example, the Hda1-Tup1 complex can occupy promoters that are also targeted by Gcn5 by physically blocking the promoter binding site. This cross-talk can be eliminated by *GCN5* deletion (Islam et al., 2011). Based on the properties of HATs and HDACs (Bernstein, et al, 2000; Kurdistani et al, 2002; Robyr et al 2002; Ekwall, 2005; Sabet et al, 2004, Sertil et al, 2007) and the previous work that has been done by my colleagues either at *MFA2* and other locations or globally (Yu et al, 2016), together with the data presented in chapter 4 on Rpd3 and Hda1, suggests a possible role for these HDACs in restoring UV-induced histone H3 hyperacetylation levels to pre UV levels following repair of DNA damage.

Several studies have employed genome-wide studies in yeast to determine the effects of acetylation and deacetylation. In 2002 Kurdistani and his colleagues have reported that the majority of Rpd3 is targeted to promoters, while the coding regions are relatively depleted (Kurdistani, 2002). Genome-wide deacetylation maps by Robyr et al. In 2002 and the binding map for HDAC binding shed considerable light on HDAC

function. Like Rpd3, studies on Hda1 demonstrated the deacetylation activity at both a single locus as well as genome-wide (Robyr et al., 2002). Hda1 activity has also been described at subtelomeric domains of chromosomes (10–25 kb away from the telomeres). Although there is some degree of redundancy between Rpd3 and Hda1 globally, they carry out the majority of the deacetylations at promoters (Robyr et al, 2002).

In order to study the involvement of HDACs in restoration of chromatin in the context of GG-NER, at first the genome-wide occupancy of Rpd3 was established and the detected peaks is comparable to that described in the literature. More than 1,500 Rpd3 peaks can be detected around promoters and over 300 Rpd3 peaks are inside the coding area (intragenic regions) (Kurdistani et al, 2002). The number of peaks I detected was much lower (1700 peaks less) than previously published data (Kurdistani et al., 2002) but we are using different software for peak detection. It is possible that different software packages apply different cut-off or threshold values, explaining the difference in peak detected. Rpd3 preferentially binds upstream of genes and around the promoter region of several genes and drives transcriptional activity (Kurdistani et al., 2002). It has been described that Rpd3 favorably associates with promoters that direct high transcriptional activity and that it is excluded from large sub-telomeric domains. In addition to its main recruitment protein (Ume6) Rpd3 is also recruited to numerous promoters by other factors (Kurdistani et al., 2002).

To investigate the chromatin occupancy of Rpd3 and Hda1, composite plots was generated around gene structure using Sandcastle. These plots show the average occupancy of Rpd3 along all of the genes. My results show that Rpd3 binding is enriched around the promoter regions and at the beginning of the coding regions (see Figure 5.2). The composite plot for Hda1 reveals that Hda1 is preferentially bound to the chromatin at intergenic regions both at the promoter and downstream regions of genes but to a lesser extends at the coding areas (Figure 5.3).

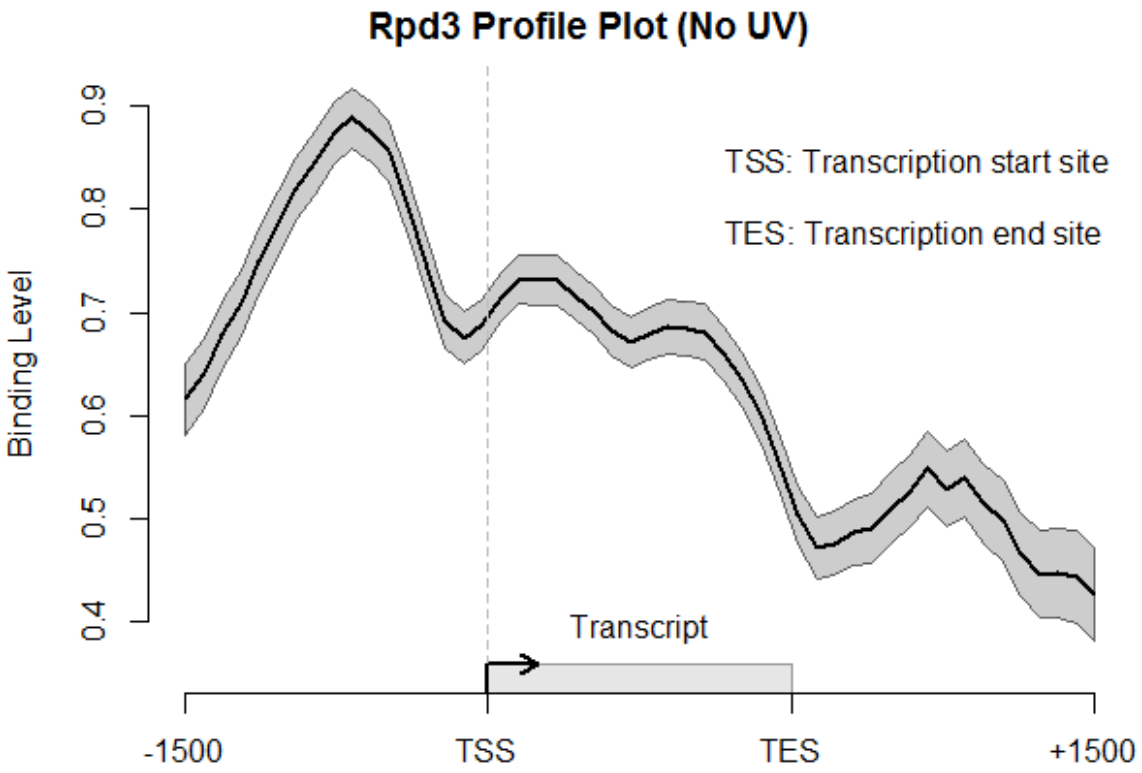

Figure 5.2 Rpd3 binding profile before UV irradiation in wild type strain: this plot shows the occupancy of Rpd3 around promoter, transcript and downstream of the genes in the wild type strain at all genes (2800 genes). The trend line represent the average Rpd3 level at thousands of genes. This is the average of two datasets of untreated WT-Rpd3-Myc.

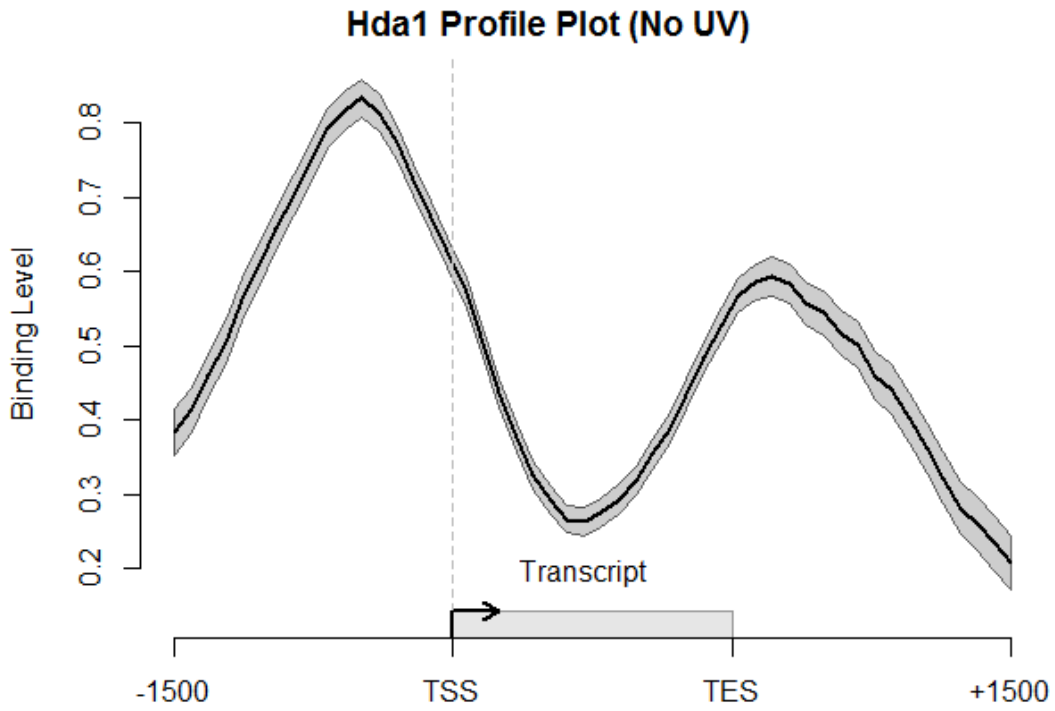

Figure 5.3 Hda1 binding profile before UV irradiation in wild type strain: this plot shows the occupancy of Hda1 around promoter, transcript and downstream of the genes in the wild type strain at all genes (2800 genes). The trend line represent the average Hda1 level at thousands of genes. This is the average of two datasets of untreated WT-Hda1-Myc.

To study the distribution of Rpd3 and Hda1 binding sites peak detection was also employed throughout the entire genome (Bennett et al., 2015). This method scans through the data on a stable and fixed window size (average 400 bp) to detect peaks from the genome (corresponding to the size of the sonicated chromatin). In the absence of UV irradiation, 854 and 508 Rpd3 and Hda1 peaks can be detected, respectively. The locations of the peaks are specified using sandcastle software and are listed in Table 5.1 and 5.2, respectively. From the total number of identified binding sites of Rpd3, 53% localise to intergenic areas, while the remaining 47% peaks are located in the intragenic sections (Table 5.1). On the other hand, from the 508 Hda1 binding peaks 77.4% are located at intergenic areas and only 22.6% of the peaks are in the coding areas (Table 5.2).

To identify the exact position of the peaks in wild type cells (before UV irradiation) position plot function was utilised, as can be seen in figure 5.5 that the majority of the peaks are settled around promoter region and some are situated inside the coding area while very few of them are present at the downstream regions. For Hda1, most of the peaks are positioned at the promoter and downstream with very little inside the transcript areas figure 5.6

Table 5.1 Rpd3 binding peaks locations before UV irradiation

Rpd3 peak position	**Number of peaks**	**% of peaks**
Intragenic	403	47
Intergenic	451	53
- Promoter	304	35.6
- Downstream	147	17
Total	854	100

Table 5.2 Hda1 binding peaks locations before UV irradiation

Hda1 peak position	Number of peaks	% of peaks
Intragenic	115	22.6
Intergenic	393	77.4
- Promoter	270	53
- Downstream	123	24
Total	478	100

5.3.1.2 UV-induced alterations in HDAC (Rpd3 and/or Hda1) occupancy around ORFs

In the previous chapter (chapter 4, page 105-112), I have determined that in response to UV, there is an immediate loss of occupancy of both Rpd3 and Hda1 at the *MFA2*, *HML* and *RAD23* loci. Here, I extended the study to investigate the effect of UV on the occupancy and the localisation of the binding peaks of both Rpd3 and Hda1 after UV irradiation throughout the entire genome. Using the profile plot function, I plotted my genome-wide Rpd3 and Hda1 binding data one-hour and three-hours following UV irradiation in comparison with the untreated samples. Figure 5.4A shows that 1 h after UV irradiation (5.4A red line) there is a minor loss of occupancy at the promoter region. However, three-hours after UV irradiation (5.4A green line) the occupancy of Rpd3 increases to levels exceeding those before DNA damage induction. However, in the coding area the loss of Rpd3 occupancy is more prominent at both repair times (see Figure 5.4A). On the other hand, there is a major loss of Hda1 occupancy downstream of genes in response to UV exposure (Figure 5.4B red line), while only minor changes are observed around the promoter regions. Subsequently, three hours following repair the loss of Hda1 occupancy was restored at the downstream regions (Figure 5.4B, green line). Similarly, the minor loss of Hda1 at promoters is restored after 3 h as well.

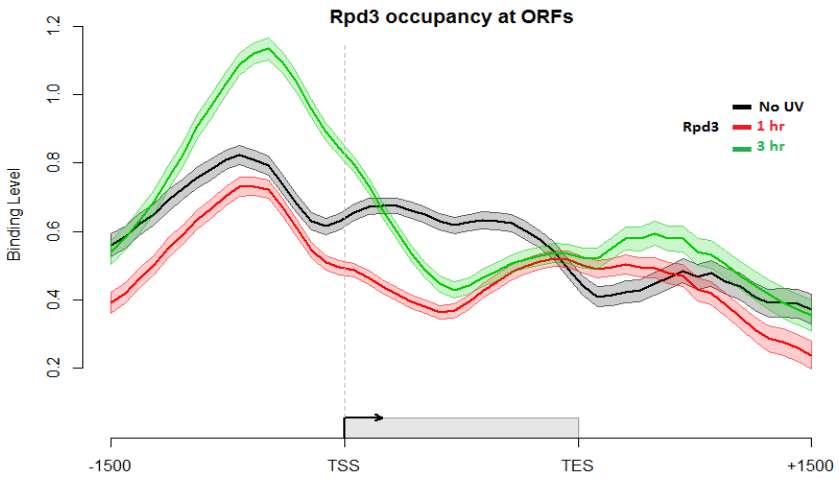

Figure 5.4A Composite plot of Rpd3 binding around gene structure in wild type cells: this plot shows the occupancy of Rpd3 around promoter, transcript and downstream of the genes in the wild type strain at all genes before and one-hour and three-hours after UV. All of the trend lines represent the average Rpd3 level at thousands of genes. This is the average of two datasets of untreated WT-Rpd3-Myc. Black line represents untreated sample, red line and green lines represent one hour and three hour after UV, respectively.

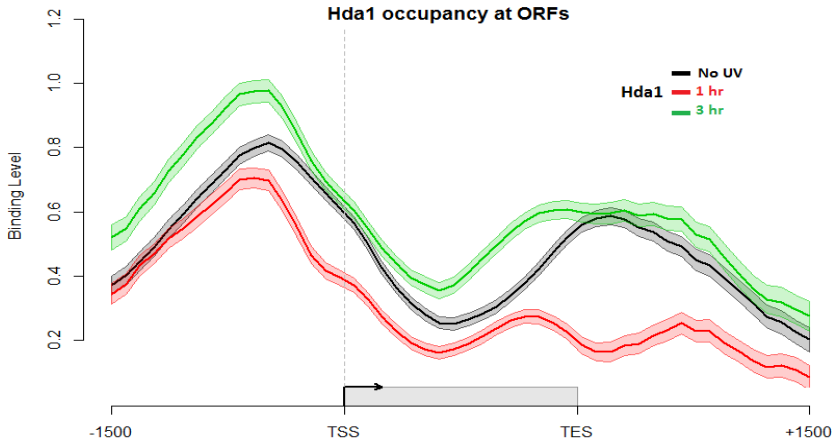

Figure 5.4B: Composite plot of Hda1 binding around gene structure in wild type cells: this plot shows the occupancy of Hda1 around promoter, transcript and downstream of the genes in the wild type strain at all genes before and one-hour and three-hours after UV. Both of the trend lines represent the average Rpd3 level at thousands of genes. This is the average of two datasets of untreated WT-Hda1-Myc. Black line represents untreated sample, red line and green lines represent one hour and three hour after UV, respectively.

5.3.1.3 UV-induced dynamic changes to HDAC occupancy on the chromatin

To examine the changes of the positions of Rpd3 and Hda1 on the chromatin in response to UV irradiation, peak detection (explained in this chapter, section 5.3.1.1.see table 5.1 and 5.2), scatter plot and Venn diagram analysis of the ChIP-chip data of UV irradiated wild type cells were performed. One experiment was conducted

for Hda1 and two biological repeats for Rpd3 were performed and the data showed that 854, 580 and 1103 binding peaks of Rpd3 were found for untreated, one-hour and three-hours samples, respectively (figure 5.7A Rpd3 total peaks before, and 1 & 2 h after UV). I also found the following binding peaks for Hda1 binding; 508 binding peaks before UV irradiation, 326 following one hour of repair and 572 three hours after repair (figure 5.8 A Hda1 total peaks before, and 1 & 2 h after UV). To illustrate the distribution of all the above peaks in relation to gene locations, the scatter plot (position plot) was utilised. In this plot the position and peak height of each peak detected is displayed in relation to gene structure. The results show that the vast majority of the Rpd3 occupancy was found at or around the promoter regions at all the time points tested (Figure 5.5). There are also some peaks in the coding area and at the downstream regions as well. One hour following UV irradiation the majority of binding sites are lost from the open reading frames, but this loss was recovered 3 h after repair (Figure 5.5, bottom panel). A similar analysis was performed using the Hda1 datasets. With Hda1 data 508 binding peaks for un-irradiated, 326 for one hour after UV and 572 binding peaks 3 h following UV (figure 5.8 A Hda1 total peaks before, and 1 & 2 h after UV) were found. At all three time points, the bulk of the peaks were localised at and adjacent to the intergenic and downstream regions (Figure 5.6). This analysis demonstrates that Rpd3 and Hda1 binding changes in response to UV irradiation. After 1 h of UV irradiation the number of peaks decreased by about 32% (from 854 to 580 Rpd3 peaks) for Rpd3 (see table 5.3A and 5.3B) and by 36% (from 508 to 326 Hda1 peaks) for Hda1 (see table 5.4A and 5.4B), respectively, compared to the un-irradiated datasets (Table 5.1 and 5.2). This indicates that following 1 h of UV exposure the occupancy of Rpd3 or Hda1 is either decreased or decreased and re-localised to different regions of the genome from the positions observed in the un-irradiated datasets. Interestingly, 3 h after UV irradiation this 32% and 36% loss in peaks detected, is mostly regained. However, the increased number of peaks at this time point did not not occur at all genes and at the exact same locations, as new peaks can be detected at the 3 h time point (figure 5.4A and 5.4B).

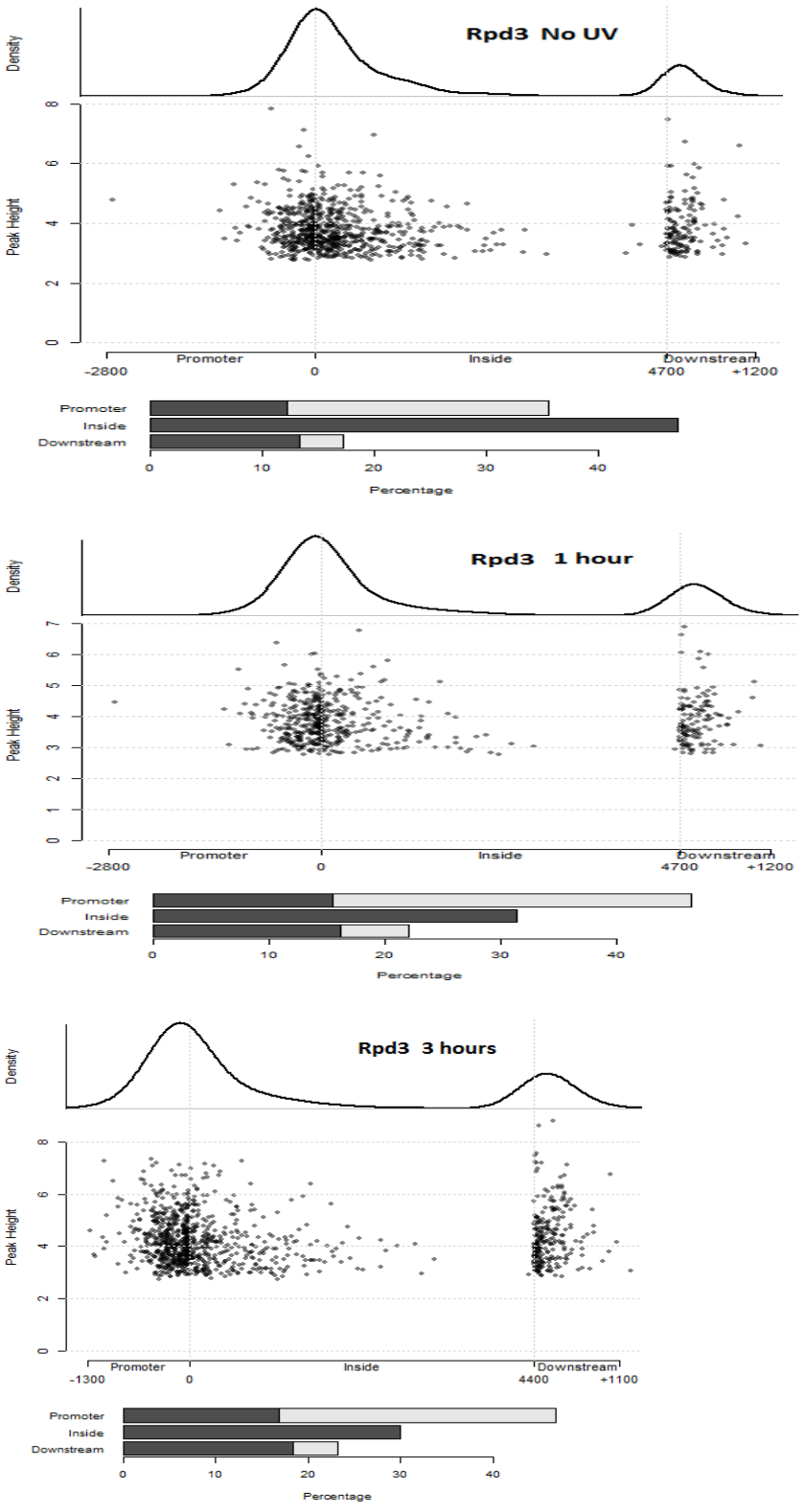

Figure 5.5 Position plot of Rpd3 binding peaks of un-irradiated, 1-h and 3-h following UV. It revealed the Rpd3 peak locations on the each gene genome-wide. The percentage of the peak distribution of the various regions is represented by the bar chart. Grey bars are the percentages of divergent promoter areas and convergent downstream regions.

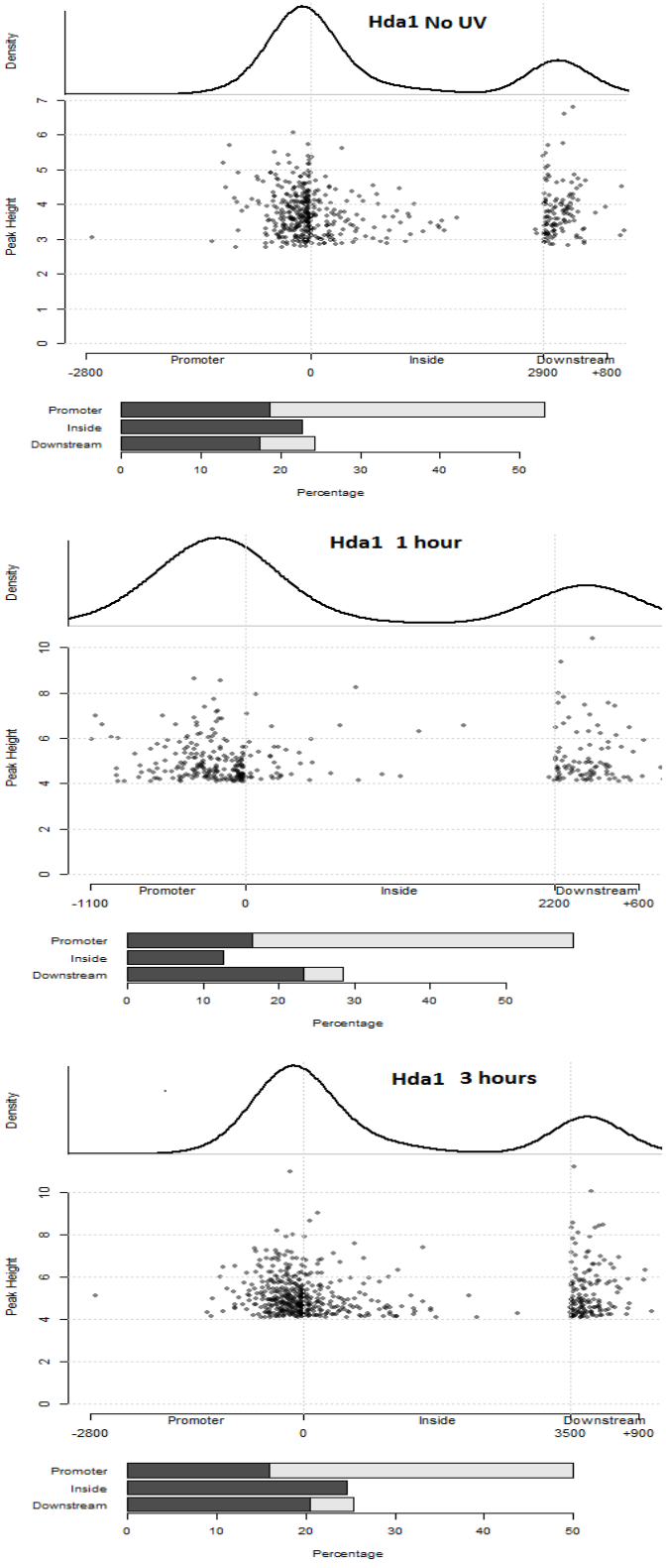

Figure 5.6 Position plot of Hda1 binding peaks for un-exposed samples to UV, or 1-h and 3-h after UV irradiation. It revealed the Hda1 peak locations on the each gene genome-wide. The percentage of the peak distribution of the various regions is represented by the bar chart. Grey bars are the percentages of divergent promoter areas and convergent downstream regions.

Table 5.3A Rpd3 binding peaks locations 1 h after UV irradiation

Rpd3 peak position	Number of peaks	% of peaks
Intragenic	182	31.4
Intergenic	398	68.6
- Promoter	270	46.5
- Downstream	128	22
Total	580	100

Table 5.3B Rpd3 binding peaks locations 3 h after UV irradiation

Rpd3 peak position	Number of peaks	% of peaks
Intragenic	330	30
Intergenic	773	70
- Promoter	517	47
- Downstream	256	23
Total	1103	100

Table 5.4A Hda1 binding peaks locations 1 h after UV irradiation

Rpd3 peak position	Number of peaks	% of peaks
Intragenic	41	12.57
Intergenic	285	87.43
- Promoter	192	58.9
- Downstream	93	28.5
Total	326	100

Table 5.4B Hda1 binding peaks locations 3 h after UV irradiation

Rpd3 peak position	Number of peaks	% of peaks
Intragenic	141	24.65
Intergenic	431	75.35
- Promoter	286	50
- Downstream	145	30.72
Total	572	100

It is clear that UV irradiation and the response of the cells to DNA damage have a great effect on the genome-wide distribution of both Rpd3 and Hda1. In the intergenic region, one hour after UV, the number of Rpd3 peaks dropped from 451 (table5.1) to 398 (table 5.3A). However, 3 h following UV irradiation the number of the Rpd3 peaks (773) (table 5.3B) and the percentage of Rpd3 binding (70%) increased (table 5.3A and 5.3B). Similar changes can be discerned for Hda1 but to a lesser extend. To investigate the number of peaks that are unique or shared between the un-irradiated and two repair samples, I generated Venn diagrams for both Rpd3 and Hda1 peaks. In addition, I also compared Rpd3 and Hda1 occupancy at different regions throughout the genome. Figure 5.7 shows that there are 410 Rpd3 binding peaks that are shared among all three conditions, which is about 48% of un-irradiated, 48% of 1 h and 37% of 3 h of their total Rpd3 binding peaks. Moreover, 454 peaks are shared between untreated and one-hour repair point, 505 are between one-hour and three-hour and 607 Rpd3 binding peaks are common between un-irradiated and 3 h period. On the other hand there are some unique binding peaks that are specific to each condition. For instance, 203, 31 and 401 binding sites are unique to untreated, 1 h and 3 h samples respectively.

A similar approach was followed for Hda1 binding peaks; there are 172 peaks that remain unchanged among all three conditions which accounts for 34%, 52% and 30% of the untreated, 1 h and 3 h samples, respectively. Hda1 binding peaks also has unique bindings at each state, the untreated sample has 206 distinctive peaks which is 40.5% of its total peaks, following UV only 17 peaks are exclusive to 1 h which represent 5% of all one hour peaks (326) and 165 are restricted to a 3 h period which represent 29% of total 3 h peaks (572) (see Figure 5.8).

When I investigate the features of these binding sites and extend it to promoters, the coding area and downstream region of genes, some unique peaks were found and that they are only exist at a specific position with specific condition (Un-treated, 1 h or 3 h) see Figure 5.7B-D for Rpd3 and Figure 5.8B-D for Hda1.

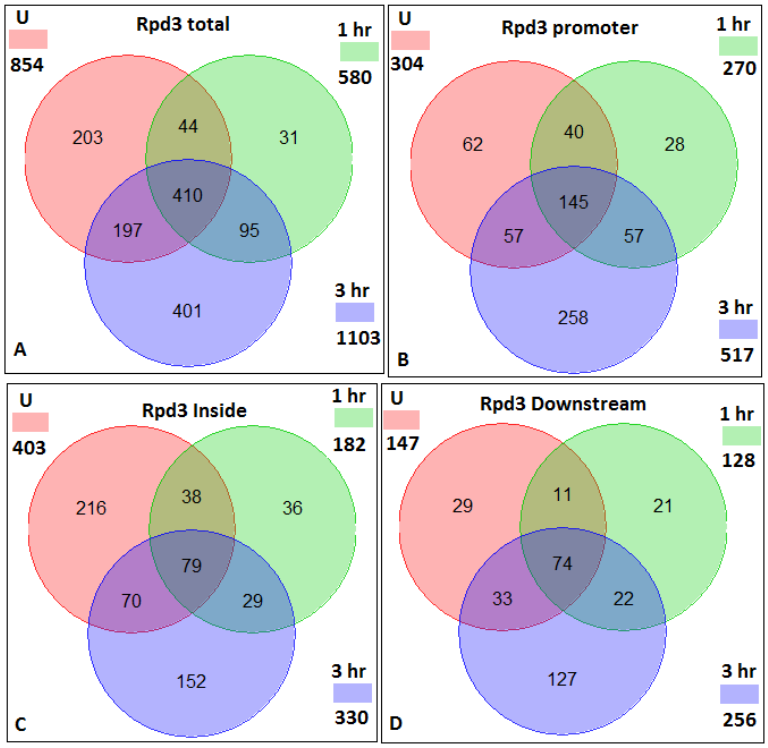

Figure 5.7 Venn diagrams of Rpd3peak overlaps: no UV, 1 h and 3 h following UV. These Venn diagrams show the result of comparing the Rpd3 peaks detected without UV, 1 h and 3 h after UV. The diagram shows total peak overlap and the overlap in different regions.

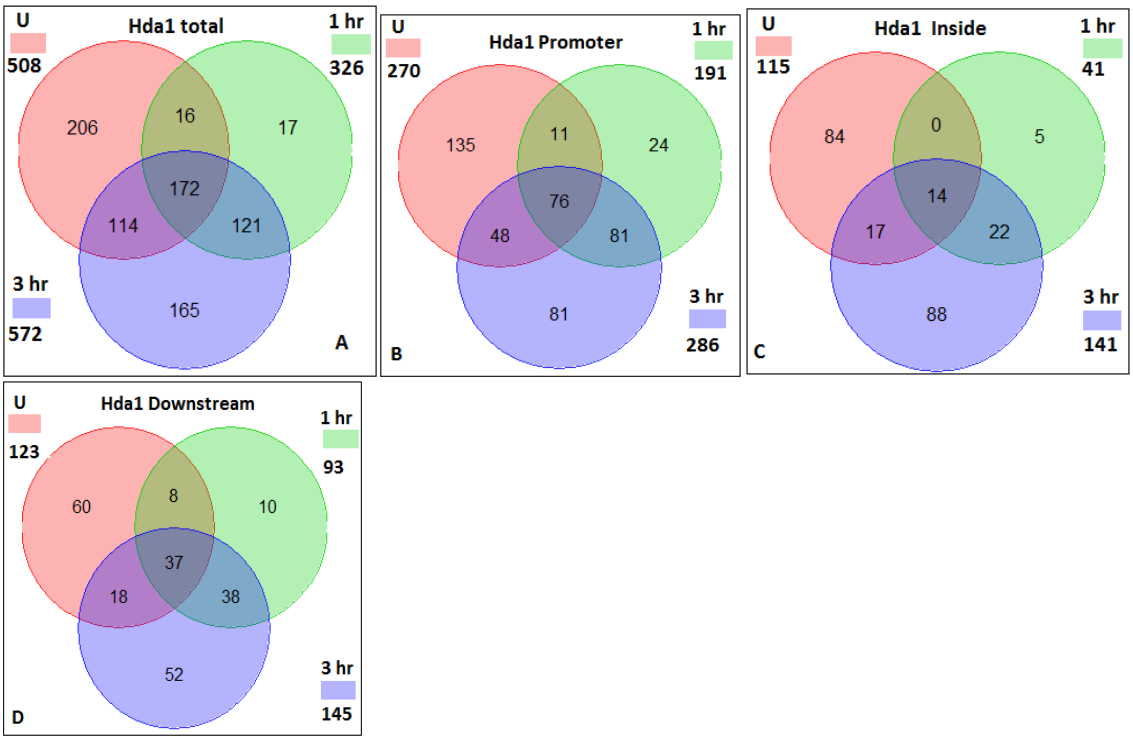

Figure 5.8 Venn diagrams of Hda1 peak overlaps: no UV, 1-h and 3-=h following UV. These Venn diagrams show the result of comparing the Hda1 peaks detected without UV, 1-h and 3-h after UV. The diagram shows total peak overlap and the overlap in different regions at various time points.

In addition to the presence of shared binding peaks among different time points of the same factors, Rpd3 and Hda1 also share several binding peaks for a number of locations at all conditions investigated in this study. For instance, Prior to UV, 329 peaks (38.5% of Rpd3 peaks and 65% of Hda1 peaks) overlap between them, while 224 (38.6 of Rpd3 and 69% of Hda1) and 450 binding peaks (41% of Rpd3 and 78.6% of Hda1) were shared 1 h and 3 h respectively following repair (Figure 5.9A-C). the main conclusion for peak detection is there are unique peaks that are exclusive to each time point and they can be analysed further. These unique peaks It can be plotted against GG-NER factors, Gcn5, H3 acetylation CPD repairs CPD trepair rates and finde that the particular gene has an effect on chromatin and/or repair.

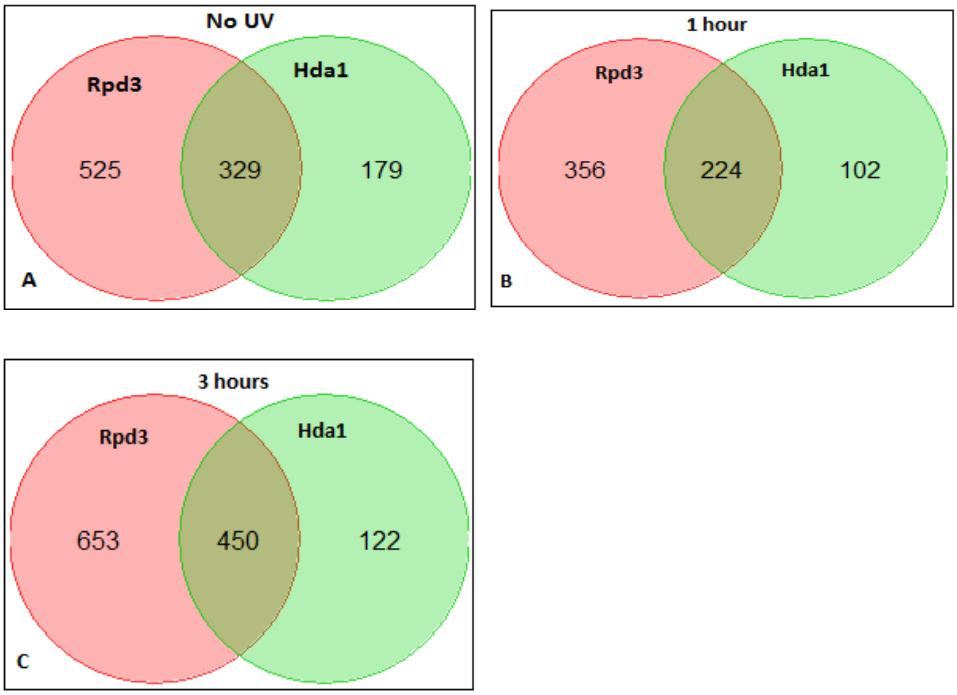

Figure 5.9 Venn diagrams of Rpd3 and Hda1 peak overlaps: no UV, 1-h and 3-h after UV. It shows the shared and non shared peaks between Rpd3 and Hda1 without UV, 1-h and 3-h post UV. The diagram shows total peak overlap at various time points.

5.3.2. HDAC chromatin occupancy in relation to GG-NER

5.3.2.1. HDAC occupancy enriched at Abf1 binding sites

My results on the role of HDACs is in line with the model of GG-NER that our lab has contributed that describes how the chromatin is set up for the repair to take place efficiently (Yu et al. 2016). In context of the ARR model, Yu and her colleagues have reported that Abf1 binding sites are positions from which GG-NER is organised. The GG-NER complex redistributes from these positions to start the first step of ARR in response to UV damage and promote efficient genomic DNA repair (Yu et al. 2009; Yu et al 2016). Researchers in the Reed's lab established that the Rad7/Rad16 GG-NER components form a complex with the Abf1 factor at ABS (Reed et al, 1999), promoting efficient GG-NER and UV-induced lesion removal both *in vitro* and *in vivo* (Yu et al. 2009). These data confirmed that the Rad7/Rad16 GG-NER complex colocalises with Abf1 at intergenic positions, predominantly at promoter regions. We also found that in response to UV, while Abf1 stays bound to the ABS, the GG-NER Rad7/Rad16 complex dissociate from Abf1 complex and distribute away from the ABS (Yu et al 2009; 2016) to exercise their role in efficient GG-NER.

My previous ChIP qPCR data showed that Rpd3 and Hda1 have a role in efficient GG-NER at some genomic locations (*MFA2*, *HMLI* and RAD23) see chapter 4 (section 4.3.6, 4.3.7 and 4.3.8, page 105-112). To examine the role of these HDACs in association with GG-NER at a genome-wide scale, HDAC data of this study was analysed in relation to Abf1 binding sites, GG-NER factors binding, Gcn5 H3 acetylation and CPD repair rates.

Firstly, a possible colocalisation of Rpd3 and/or Hda1 at Abf1 binding sites was investigated. Both Rpd3 and Hda1 data was plotted at Abf1 binding sites genome-wide as a composite plot. As shown in Figure 5.10 A and B, HDAC enrichment can be observed for both Rpd3 and Hda1 at Abf1 binding sites. In addition, the figure also shows that there is an alteration to the occupancy of HDAC at Abf1 binding sites in response to UV.

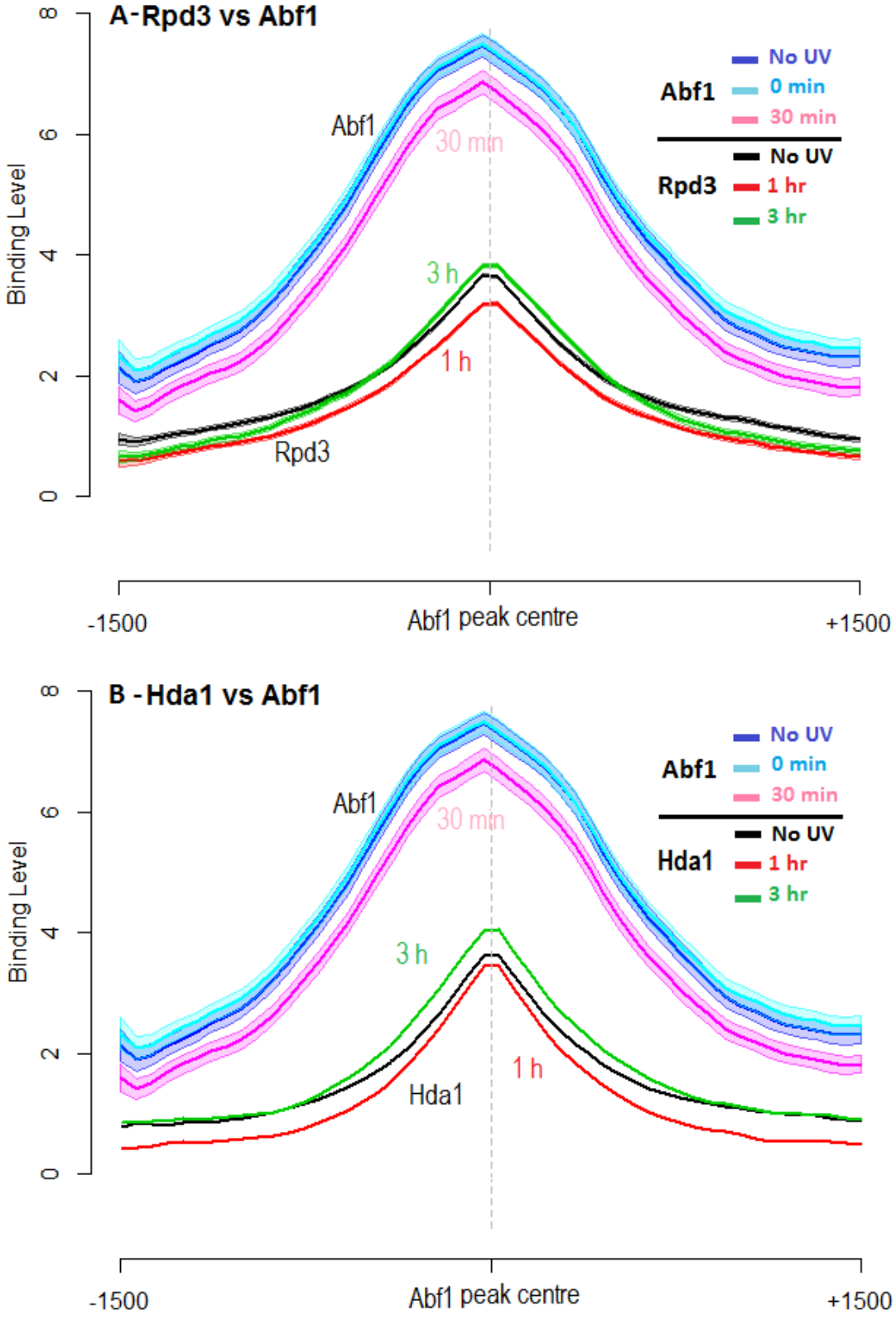

Figure 5.10 Co-localisation of the HDACs with Abf1 on chromatin at the Abf1 binding sites before and following UV irradiation. Abf1 and Rpd3 colocalisation at the Abf1 BS. (B) Abf1 and Hda1 colocalisation at the Abf1 BS .

5.3.2.2. Rad7 GG-NER and HDAC factor colocalised on chromatin around Abf1 binding sites before UV irradiation.

Previously our lab has established that in response to UV irradiation, histone H3 acetylation increases both locally and genome wide (Yu et al., 2016). This UV-induced histone H3 hyper acetylation depends on Gcn5 and the Rad7/Rad16 GG-NER complex, which is necessary for chromatin remodeling and efficient DNA damage removal and repair (Yu et al 2005, Yu et al 2011, Yu et al, 2016). The Gcn5 HAT is actively recruited to the chromatin by the GG-NER complex.

Yu and his colleagues have reported that H3K9/K14 remains hyper-acetylated at the *MFA2* gene in repair deficient *RAD4* and *RAD14* deleted cells (Yu et al, 2005). This indicates that completion of the repair reaction is required to revert the hyperacetylated state of the chromatin. To investigate the relationship between the GG-NER proteins (Rad7) and the HDACS (Rpd3 and Hda1), ChIP-on-chip data of this study was analysed before and after UV irradiation in wild type cells. The profile plots was utilised to represent the chromatin occupancy data of GG-NER and both HDACS at Abf1 peak centers. Similarly, the Rpd3 or Hda1 peak centres were also used as a frame of reference to detect GG-NER complex enrichments at positions of HDAC binding. Before UV irradiation, Rpd3 and Rad7 colocalise at Abf1 binding sites (Figure 5.11A, blue lines). However, in response to UV irradiation, Rad7 binding at the Abf1 BS was completely lost as described previously (Figure 5.11A, cyan line 15 min post UV), while only a minor loss of occupancy of Rpd3 can be observed (Figure 5.11A, red line 1 h post UV). A similar pattern can be observed for Hda1 (Figure 5.11B). In summary, HDAC occupancy colocalises with the GG-NER complex at Abf1 binding sites before UV irradiation.

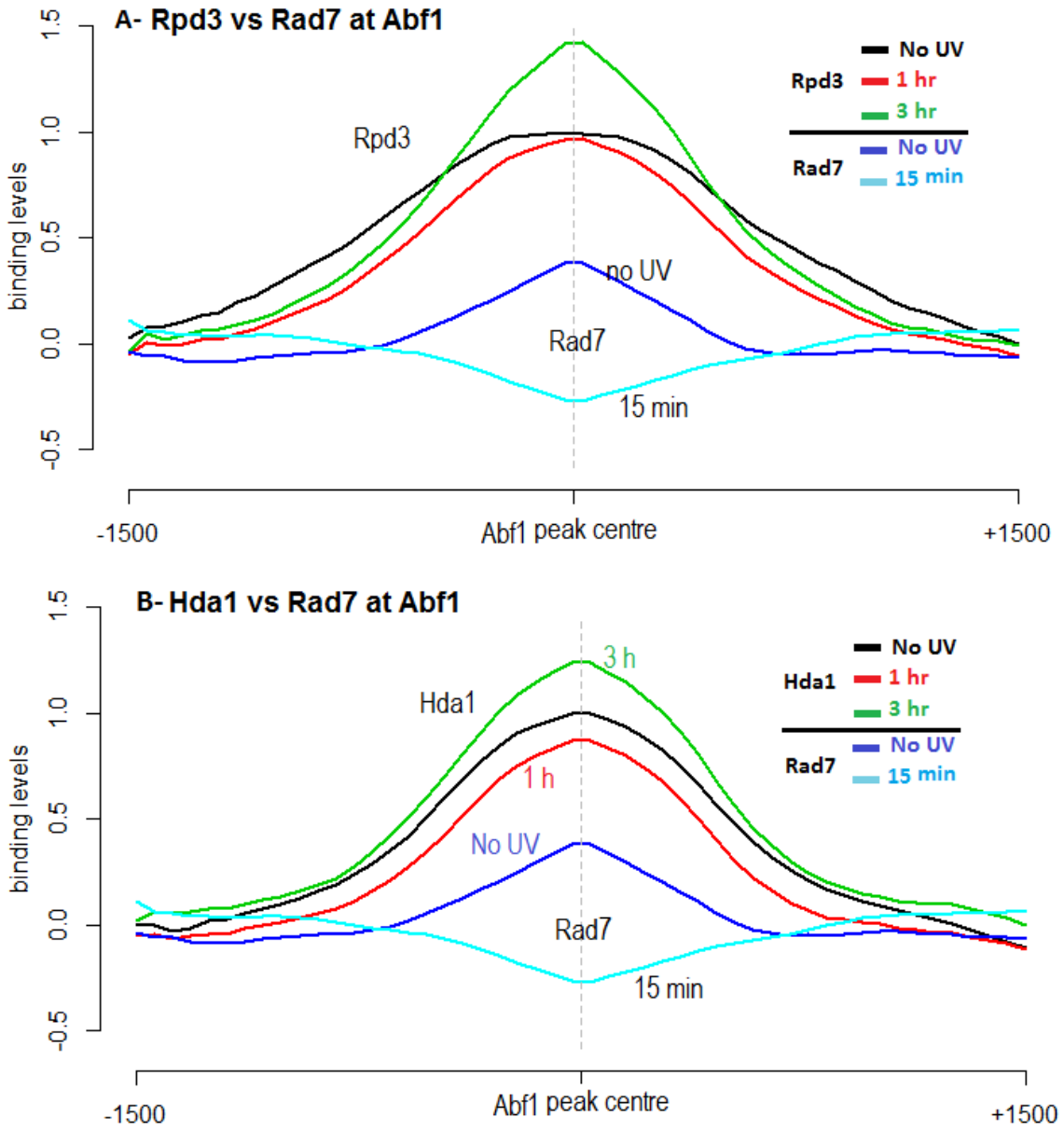

Figure 5.11 The co-localisation of HDAC and GG-NER (Rad7) on the chromatin at the Abf1 binding sites and their redistribution following UV irradiation. (A) RPd3 binding peaks in relation to Rad7 at and around Abf1 binding sites for Rpd3 (un-irradiated = black line, and post UV which are 1 h = red line ,and 3 h = green line) and for Rad7 (un-irradiated = blue line and 15 min = cyan line post UV). (B) Same as (A) but instead Rpd3 it is Hda1

To examine the relation between HDAC and GG-NER complex occupancy at and around the transcript, the profile plot was used to determine the change in chromatin position and occupancy at promoter, transcript and TES regions before and after UV irradiation. Figure 5.12 shows that before UV exposure, HDAC occupancy and Rad7 binding colocalise at the promoter and downstream regions. The binding levels prior to UV irradiation at around the coding area shows an inverse relationship between Rpd3

and Rad7 occupancy. At the coding region Rad7 binding is low while the Rpd3 levels are enriched. However, in response to UV, Rad7 redistributes from the promoter region into the coding area, while the binding levels of Rpd3 are reduced over the transcript. On the other hand, Hda1 occupancy change is most severely affected at downstream regions where Rad7 binding is lost. Taken together, the UV-induced redistribution of the GG-NER complex is mirrored by a reciprocal change to HDACs occupancy on chromatin especially for Rpd3.

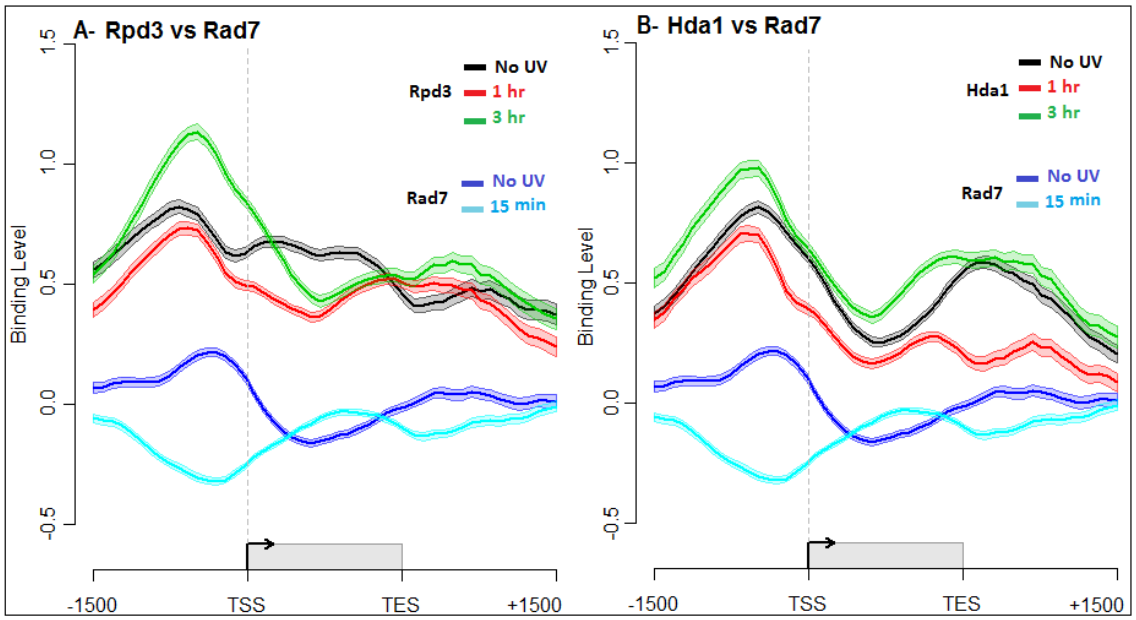

Figure 5.12 Gene profile plot of the HDACs and the GG-NER factor Rad7 in wild type cells before and following UV exposure. (A) Rpd3 chromatin distribution at and around coding areas in association with Rad7 at different repair points is shown here. Chromatin occupancy of Rpd3 before UV (black line) and post UV are shown in red 1 h and green 3 h. Rad7 occupancy on the chromatin prior to UV irradiation is represented by (blue line) and 15 min following UV (cyan). (B) Same observation was seen in case of Hda1 in relation to Rad7 as represented in (A).

5.3.2.3. Examining HDAC chromatin occupancy in relation to Gcn5

Previously, our lab established that Gcn5 is required for histone H3 acetylation and modification of the chromatin necessary for efficient repair at the *MFA2* locus during GG-NER (Yu et al. 2005). Reed's lab found that Gcn5 localises around Abf1 binding sites before UV irradiation (Yu et al, 2016). After UV irradiation, the occupancy of Gcn5 on the chromatin increases rapidly at the proximity of these sites, and then decreases gradually during repair (Yu et al. 2011, 2016). The GG-NER complex contributes to this regulation throughout the genome. The redistribution of Gcn5 and H3 acetylation occurs from promoter proximal domains to the inside of genes in response to UV exposure during repair (Yu et al, 2016).

In chapter 4, I determined that Gcn5 is responsible for the continuous hyper-acetylation in *RAD14* deleted cells due to its prolonged residence on the chromatin after UV exposure. Here I study the possible relation between HDACs and Gcn5 occupancy in wild type cells and the effect UV irradiation on their chromatin occupancy. First I examined their co-localisation at the Abf1 binding sites. As displayed in Figure 5.13 A and B HDAC and Gcn5 chromatin occupancy is enriched at the Abf1 peak centres, indicating that these factors can occupy similar regions of the genome simultaneously.

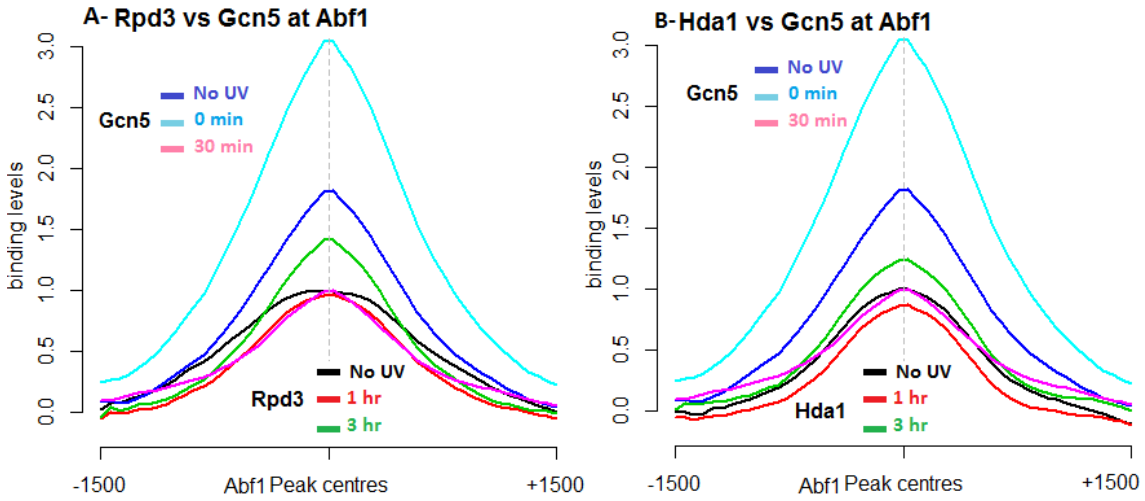

Figure 5.13 The co-localisation of HDAC and Gcn5 on the chromatin at the Abf1 binding sites and their redistribution following UV irradiation. (A) Rpd3 chromatin occupancy in relation to Gcn5 at and around Abf1 binding sites. Rpd3 is represented by un-irradiated, black line, and are 1 h post UV, red line and 3 h post UV, green line) and for Gcn5 and both 0 min (cyan) and 30 min (pink) following UV. (B) Same observation was seen in case of Hda1 in relation to Rad7 as was seen in (A).

To gain insight into the distribution of HDAC in relation to Gcn5 around gene structure, Gcn5 binding data was also plotted against HDACs chromatin occupancy at and around the coding regions Before UV irradiation, Gcn5 and both HDACs take up a very similar genomic distribution. Occupancy of these factors is enriched at the intergenic regions upstream and downstream of genes.

Immediately following UV irradiation, there is an immediate increase of Gcn5 occupancy at all the regions (promoter, transcript and downstream), maintaining a similar pattern of distribution as to that observed in un-irradiated cells (Figure 5.14, blue and cyan line). Importantly, the binding levels of both Rpd3 and Hda1 decrease but in a less pronounced way as Gcn5. The major loss of Rpd3 occupancy was in the coding

area 1 h after UV and the greatest loss of Hda1 occupancy was at downstream regions of the genes (Figure 5.14, black and red line). These data demonstrate that an increase in Gcn5 occupancy is accompanied by a reciprocal loss of Rpd3 and Hda1 binding in response to UV irradiation. After three hours of repair time Rpd3 and Hda1 occupancy is restored to pre-damage levels, while after 30 to 60 minute of repair Gcn5 occupancy decreases significantly. This indicates that after repair has taken place, Gcn5 occupancy is lost while HDAC factors take up their original distribution on the chromatin.

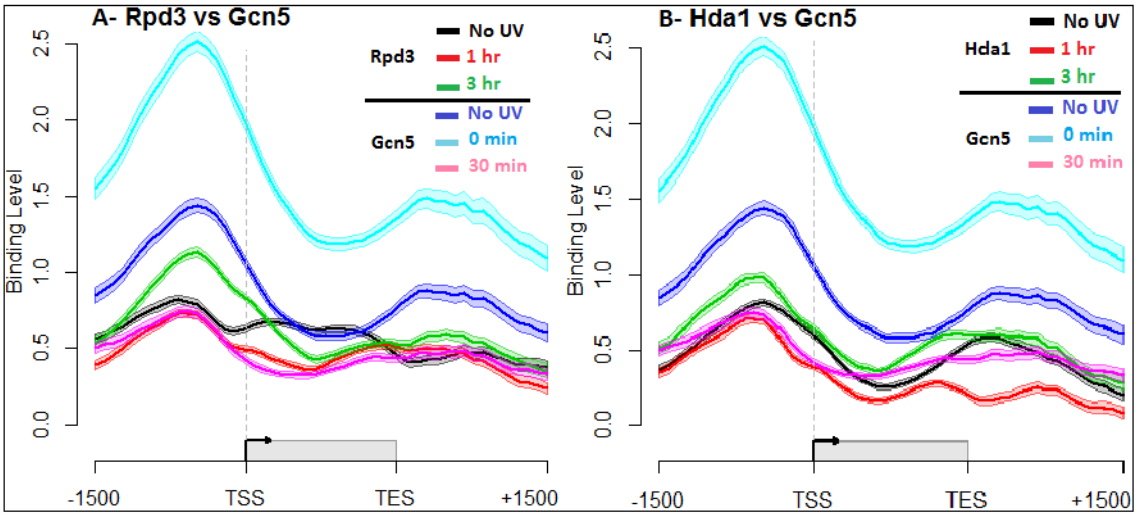

Figure 5.14 gene profile plot of the HDACs and the Gcn5 in wild type cells before and following UV exposure. (A) Rpd3 chromatin distribution at and around coding areas in association with Gcn5 at different repair points. Chromatin occupancy in Rpd3 before UV (black line) and post UV (red 1 h and green 3 h). Gcn5 occupancy on the chromatin prior to UV irradiation is represented by (blue line) and both 0 min (cyan) and 30 min (pink) following UV. (B) Same observation was seen in case of Hda1 in relation to Rad7 as was seen in (A).

5.3.2.4 Investigating histone H3 K9/14 acetylation at HDAC peaks

Here, the relationship between HDACs and H3K9/K14 acetylation was investigated throughout the genome in response to UV irradiation in wild type cells. As displayed in Figure 5.15 there is a mutually exclusive relationship between H3 K9/K14 acetylation levels and both HDACs (Rpd3 and Hda1) at the Abf1 binding site. It is known that Abf1 binds to nucleosome free regions. Therefore, low levels of histone H3 acetylation at Abf1 binding sites are a direct result of the lack of any nucleosomes at these positions. However, at positions up- and downstream of these sites, histone H3 acetylation can be detected and reaches a local maximum around 500 bp either side of the Abf1 peak centre (Yu et al. 2016). Before UV irradiation there is a basal level of HDAC occupancy and H3K9/K14 around the Abf1 binding sites. However, one hour after UV irradiation, while the levels of H3K9/K14 increase, the HDAC levels decrease. Three hours

following UV irradiation the levels of Rpd3 and Hda1 increase again and exceed their pre-UV levels (Figure 5.15 green lines). In chapter 4, I demonstrated that histone H3 acetylation is reduced at the 3 h time point at *MFA2*; this is in line with the data presented here demonstrating that HDACs are recruited to chromatin at time points after repair is finished.

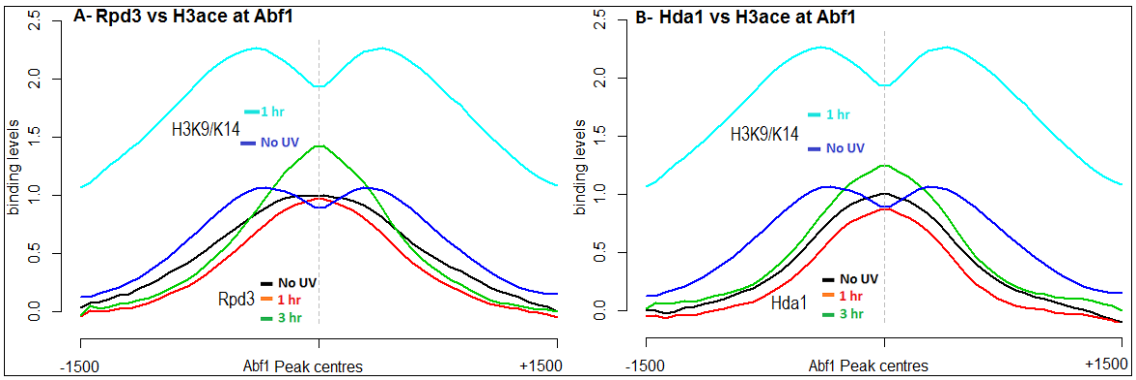

Figure 5.15 ChIP-chip data of HDAC occupancy and histone H3 acetylation at the Abf1 binding sites both before and after UV irradiation. (A) Rpd3 binding peaks in relation to H3K9/K14 at and around Abf1 binding sites for Rpd3 represented as black line, un-irradiated, red line, 1 h post UV, and green line, 3 h post UV. Histone H3K9/K14 acetylation is shown prior to UV irradiation (blue line) and 1 h after UV irradiation (cyan line). (B) Same as (A) but here Hda1 ChIP-chip is shown in relation to histone H3K9/K14 acetylation data.

To understand how UV-induced changes to Rpd3 and Hda1 chromatin occupancy correspond to histone H3 acetylation around genes, the data was plotted in relation to transcript before and after UV irradiation. As can seen in Figure 5.16 before UV irradiation there is a basal level of histone H3 H3K9/K14 acetylation that is enriched at the promoter region and start of genes. Rpd3 and Hda1 chromatin occupancy, on the other hand, is much lower around the start of genes and is enriched at positions upstream of the promoter regions (Figure 5.16). One h following UV irradiation histone H3 is hyperacetylated at al genomic positions upstream and downstream of genes, maintaining a clear enrichment of acetylation at the 5'-end of genes (Evans PhD thesis 2011, Yu et al 2016). The Rpd3 occupancy decreases significantly at the coding regions (Figure 5.16A, red line), whereas only a small drop in Hda1 occupancy at the promoter and coding regions can be detected (Figure 5.16B, red line). The predominant loss of Hda1 occupancy occurs downstream of genes as shown in Figure 5.16B. These reciprocal changes between HDACs on one hand and histone H3K9/K14 acetylation are in line with the inverse relationship between HAT and HDAC chromatin occupancy in response to UV irradiation.

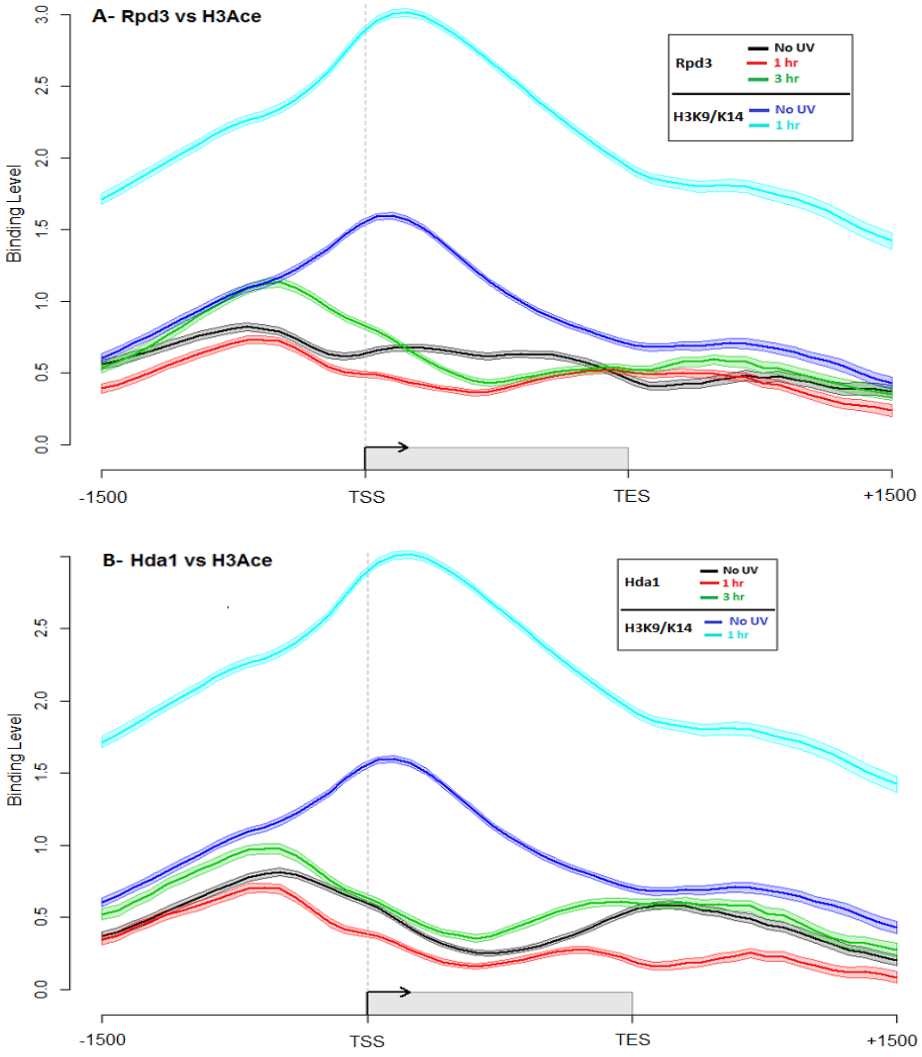

Figure 5.16 : Gene profile plot display HDACs contribution in the UV-induced H3 K9K14 hyper acetylation. (A) Rpd3 occupancy in relation to H3 K9K14 acetylation before and after UV in wild type cells. For Rpd3 (un-irradiated = black line, and post UV (1 h = red line and 3 h = green line)) and for Rad7 (un-irradiated = blue line and 1 h = cyan line post UV). (B) Same as (A) but instead Rpd3 it is Hda1

5.3.2.5. Investigating HDAC roles in relation with the rate of CPD repair

In Chapter 4, I presented ChIP-qPCR data that revealed that chromatin occupancy of Rpd3 and Hda1 changes in response to UV irradiation and requires active NER to re-establish their chromatin occupancy during restoration. This implies that chromatin occupancy of HDACs is linked to the repair mechanism. To inspect the relationship between GG-NER activity and HDACs occupancy throughout the genome, I compared my HDAC data with previously generated CPD repair data using the profile plot function in Sandcastle (Bennett et al., 2015). Previously, our lab has showed a direct link between repair efficiency and histone H3 acetylation (Teng et al., 2008, Yu et al., 2016). Acetylation mapping following UV irradiation showed that histone H3K9/14 acetylation is controlled by the redistribution of Gcn5 by the Rad7-Rad16 complex.

Interestingly, measuring CPD removal in *GCN5* deleted cells revealed that the distribution of repair rates was severely altered while these cells are not extremely UV sensitive (Yu et al., 2016). Based on these findings and the antagonistic function of HDACs and HATs, together with my and other previous data, we hypothesised that HDACs might play a role in removing CPDs genome-wide via its role during access and restoration of the chromatin. The HDAC data was mapped in relation to CPD repair rates to investigate how changes in HDACs binding may correspond to the organisation of repair rates around gene structure. As can be seen from Figure 5.17A, UV-induced loss of Rpd3 occupancy at coding regions corresponds with higher repair rates of CPDs (and the UV-induced increased levels of H3K9/K14 acetylation). For Hda1, UV-induced loss of occupancy downstream of coding area does not correspond with any significant features of the DNA repair pattern (Figure 5.17B). However, the faster repair rates at the coding regions are accompanied by a minor loss of Hda1 occupancy (Figure 5.17 B). In summary, loss of HDAC occupancy from chromatin around genes structure occurs at sites of efficient repair. This implies a potential role for HDAC eviction and concomitant HAT recruitment as a dual mechanism for UV-induced chromatin remodelling to facilitate DNA repair.

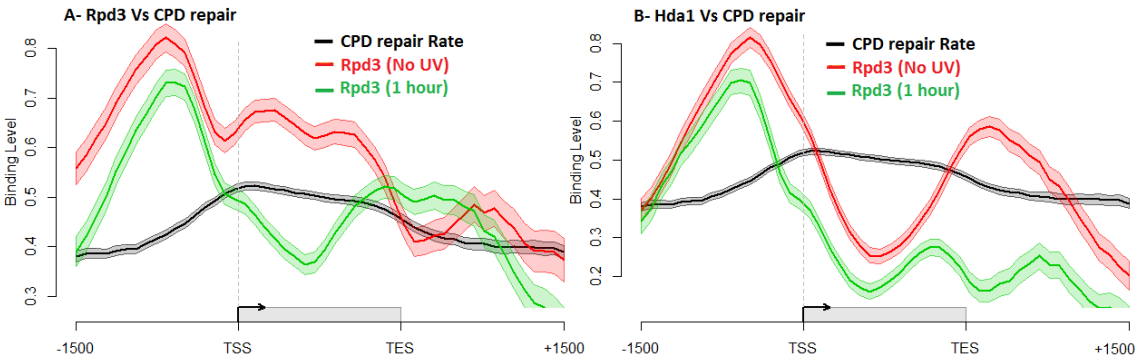

Figure 5.17: Profile plot showing HDAC distribution in connection with the CPD repair rates. (A) Rpd3 occupancy in relation to repair rate after UV in wild type cells. CPD repair rates is represented by black line (which is a subtraction of the CPD removal in 2 h following UV from zero repair time immediately after UV exposure), Rpd3 un-irradiated = red line and 1 h post UV = green line. (B) Same as (A) but instead Rpd3 it is Hda1

5.4 Discussion

To acquire a thorough understanding of the genome-wide chromatin occupancy of HDACs in response to UV irradiation, the microarray technology was utilised to examine the Rpd3 and Hda1 occupancy throughout the yeast genome in wild type cells. In addition, I compared my data to those produced in my lab previously, to evaluate the mechanism of chromatin remodelling during GG-NER.

Before doing any analysis of the data generated here, I validated them using the Sandcastle R-package (Bennett et al., 2015). Using the normalisation assumption function I was able to establish a 80 and 74% Pearson's correlation between biological repeats. In addition, the ChIP-qPCR data from chapter 4 (page 105-1123) was used to validate the results described in this chapter. Taken together the datasets are suitable for normalisation and analysis.

The first level of analysis was based on peak detection. I have detected around 854, 580 and 1103 binding sites of Rpd3 binding in the absence of DNA damage, one-hour and three hour after UV irradiation, respectively and 508, 326 and 572 Hda1 peaks in the absence of UV irradiation, one-hour and three hour after UV irradiation, respectively. Analysis of the Venn-diagrams presented here, revealed that HDAC occupancy at a subset of genomic positions does not change in response to UV irradiation. These could be sites of reduced repair efficiency or HDAC binding sites that are not involved in repair. The occupancy of both Rpd3 and Hda1 has been previously studied with ChIP-on-chip and chromatin occupancy was mainly found at promoter regions. It is known that HDACs participate in a number of cellular processes and have numerous functions in processes such as transcription and the regulation of the cell cycle (Kurdistani et al., 2002; Robert et al., 2004; Robyr et al., 2002). However, genome-wide HDAC occupancy in response to UV irradiation had not been studied before. My ChIP-on-chip datasets illustrate HDAC distribution after UV irradiation. Comparing the occupancy of HDACs around gene structure revealed that their binding patterns are very similar to those of the Rad7/Rad16 GG-NER repair factors. Since HDACs are involved in transcription, we suggest that they might also participate in DNA repair. In order to confirm their direct role in repair, it is worth to measure genome-wide CPD repair in HDAC deficient cells and compare that data with our previous wild type repair rate data. Based on our finding in Gcn5 deficient cells, I predict that the absence of HDAC activity could alter the distribution of repair rates since the genomic regions most affected by loss of GG-NER matched to the regions

most affected by UV-induced, GG-NER-dependent histone H3 acetylation (Yu, et al, 2016).

Given the antagonistic activity of HATs and HDACs, we suggested that HDACs might get evicted from the chromatin during repair to allow hyperacetylation to take place in response to UV-induced DNA damage. UV-induced histone H3 acetylation levels increase to make the necessary changes for setting the chromatin up for repair. Our results indeed show that there was a general UV-induced loss of Rpd3 and Hda1 chromatin occupancy in response to UV, both based on composite plots and peak detection. This demonstrates that UV-induced hyperacetylation is catalysed by a dual *recruitment* of HATs and *eviction* of HDACs from the chromatin.

During the restoration phase of the ARR model we suggest that HDAC proteins are recruited on to the chromatin to revert the hyperacetylated status of the genome. This phenomenon of Rpd3 or Hda1 recruitment by binding factors is not uncommon and has been described for gene repression and activation. Our results confirm that 3 h following repair, HDACs are recruited to the chromatin as shown by an increased occupancy of both HDACs, especially in the promoter region and downstream of genes. This UV-induced recruitment of HDACs during restoration can be confirmed by examining the chromatin occupancy of the factors that are known to assemble the HDAC complex to the chromatin. These targets are Ume6 for Rpd3 (Kurdistani and Grunstein, 2003) and Tup1 for Hda1 (Wu et al., 2001). Changes to the chromatin occupancy of Ume6 and Tup1 in response to UV irradiation, could be indicative of active HDAC recruitment to chromatin by these factors.

In chapter 4, I have reported that in repair deficient cells like *RAD14*, Rpd3 and Hda1 occupancy does not increase up to three hours following UV exposure as in wild type cells at a single genetic locus. ChIP-on-chip analysis of HDAC localisation in *RAD14* deleted cells would allow these findings to be confirmed. Based on the results in chapter 4 I predict that HDACs might not reoccupy chromatin again after repair. These future experiments and the UV-induced changes to HDAC occupancy described here would help to describe how HDACs contribute to efficient DNA repair.

I have also shown that chromatin responds to UV irradiation in a dynamic way to HDAC chromatin occupancy at different repair times. The presence of Rpd3 or Hda1 at certain genomic positions does not change in response to UV irradiation. The presence of these unique binding sites has important biological meaning which needs further investigation and analysis.

Using our previously generated datasets (Yu et al, 2016), the relationship between HDAC occupancy and each of the factors involved in GG-NER (Gcn5 and Rad7/Rad16 complex) was investigated. Interestingly, significant levels of Rpd3 and Hda1 was detected at Abf1 binding sites from where repair is organised. These sites are predominantly located upstream of genes and are sites from where GG-NER is organised. The presence of HDACs at these positions in the genome prior to DNA damage induction and repair might indicate that in addition to the involvement of HATs in the access phase of the ARR model, HDACs may also participate in this stage as well or it may just serve as a reservoir place for these factors..

Following UV irradiation, chromatin occupancy of Rpd3 is reduced at promoter and coding area and the occupancy of Hda1 decreases at promoter and downstream regions as measured by the total number of peaks detected. Interestingly, when plotting each of the Rpd3 and Hda1 data together with the GG-NER Rad7 occupancy data at the Abf1 binding sites colocalisation prior to UV can be observed. However, immediately after UV irradiation this colocalisation was completely lost and protein occupancy reveals antagonistic relationship between HDACs and Rad7. We know from our previous study that Rad7 dissociates from Abf1 binding sites and recruits the HAT Gcn5 on to the chromatin, leading to increased histone H3 acetylation. This indicates that during the time that Rad7 recruits Gcn5 to the chromatin, HDACs are removed from the chromatin. Significantly, plotting ChIP-on-chip data for both HDAC and Rad7 around gene structure confirms the antagonistic relationship at all three positions around ORF structure (promoter, transcript and downstream) throughout the genome. To confirm that HDAC eviction and recruitment is dependent on the GG-NER factors, HDAC chromatin occupancy was investigated in *RAD7* or *RAD16* deleted cells. This experiment would reveal whether or not the GG-NER complex is responsible for eviction and/or recruitment of Rpd3 and Hda1 in response to UV exposure.

Comparing the HDAC data with chromatin occupancy of Gcn5 and histone H3 acetylation, largely confirmed our previous findings. HAT and HDAC occupancy is enriched at intergenic regions both upstream and downstream of genes prior to DNA damage induction. Following UV iradiation, Gcn5 occupancy increases immediately, while HDACs binding decreases. Within 30 to 60 min Gcn5 occupancy is reduced while HDAC occupancy remains low. This UV-induced increase of Gcn5 occupancy and the mirrored decrease of HDAC occupancy apears to be a general feature of the response to UV irradiation. When we plotted the data around ORF structure this behaviour was reproduced. Further analysis of my data in relation to histone H3 K9/K14 acetylation data revealed and confirmed the opposite relationship between these two factors.

Finally, the connection between CPD repair rates and HDAC occupancy was analysed. Plotting the CPD repair rate and HDAC binding in response to UV around gene structure, revealed that in the coding regions when repair rates are high, Rpd3 occupancy was low. Conversely, when repair rates are low, the Rpd3 occupancy was high. However, for Hda1 this is not the case. To find a direct link between HDACs and CPD repair, the present wild type data can be investigated and compared with the repair rates in HDAC mutants. I predict that in *RPD3* mutant cells the effect on repair will be greatest at the coding area, while for Hda1 deficient cells, it will be the downstream area that is affected the most. Nevertheless, downstream and the promoter will be predicted to be affected if both Rpd3 and Hda1 were both deficient (double mutant).

In all the data sets examined; GG-NER factors, HDACs, H3 acetylation and others, the time points compared following UV irradiation do always not matched for various reasons. GG-NER complex redistribution and Gcn5 recruitment change immediately after DNA damage inducation, while other process occur at a later time points. Taken together, it would be worthwhile to obtain histone H3 acetylation data at two and three hours after UV irradiation to determine whether histone H3 K9/K14 deacetylation take place and how this process is organised throughout the genome. Comparing these data with the HDAC occupancy at three hours will reveal the overlap and specific contribution of Rpd3 and Hda1 to the deactylation of chromatin after DNA repair.

The genome-wide investigation presented here added to our previous results, and revealed that HATs and HDACs act in concert to remodel chromatin in the GG-NER context. The results obtained are all in line with our previous achievements in our lab. My results on Rpd3 and Hda1 also confirmed the previous results obtained in chapter 4 at the different genomic locations and are also applicable throughout the genome in wild type cells. I have shown that in response to UV, HDAC occupancy is lost throughout the genome accompanied by histone H3 hyperacetylation. This dual mechanism subsequently alters the chromatin and facilitates efficient GG-NER. However, how this event is controlled by the GG-NER complex and how this remodelles chromatin at the level of individual nucleosomes is a topic for future study.

In summary the results described in this chapter build on the observations made in Chapter 4 at individual loci, by examining events on a genome wide scale:

1- Following UV irradiation in wild type cells, there is a general loss of HDAC occupancy throughout the genome. This results in increased histone H3 acetylation levels

2- The colocalisation of HDACs at Abf1 binding site with other GG-NER factors before UV irradiation suggests their possible involvement in the repair process..

3- In response to UV irradiation, HDAC chromatin occupancy is lost at the time where Rad7/Rad16 GGNER complex recruits Gcn5 HAT on to the chromatin. As a result of this dual action histone H3 acetylation levels increase and subsequently the chromatin is altered to a more open conformation.

4- Following repair, HDACs re-occupy the chromatin and the levels of acetylation are reduced to normal pre-damaged levels. This promotes the restoration of chromatin structure following repair.

5- This study showed that there is an inverse relationship between HDAC binding levels and the rate of CPD repair. The repair is more efficient when the HDAC binding is low. This study has contributed to understanding of the mechanism of chromatin restoration following repair of UV-induced DNA damage and how events are organised in relation to Abf1 and GG-NER complex occupancy in the genome.

Chapter Six

General discussion:

All Eukaryotic organisms contained genomic DNA in their nucleus that is organised into chromatin. On this template DNA transactions take place, among which is repair (Luger, 2006; Luger et al., 2012). The chromatin is made up of nucleosome, DNA, histone and non histone proteins. Nucleosome is the basic fundamental subunit of chromatin to it 6 million bases of DNA are compacted. Approximately 147bp of DNA is folded around a dimer of an octamer core histones (two copies of each H2A, H2B, H3 and H4 histones) (Kornberg, 1977) and a fifth histone (H1) which serves as linker protein connects the DNA (linker DNA) between the adjacent nucleosomes which create a “beads on a string” structure. Further chromatin compaction stabilization (to 30nm fiber) to a higher order structure (heterochromatin) is achieved via the linker protein (Hargreaves and Crabtree, 2011). Thus chromatin is further classified into heterochromatin "30 to 300nm fiber" and euchromatin (10nm fiber). Chromatin is considered to be in an active state when it is in euchromatin configuration and it is in inactive condition when in heterochromatin situation. Hence, at compacted structure, chromatin presents resistant to normal cellular processes including DNA repair.

Therefore, in order to facilitate efficient DNA repair and other cellular metabolism, disruption of histone DNA contacts is essential. ATP dependent chromatin remodelling enzymes and covalent, post-translational modification of histone tails by histone modifying enzymes are two of the most frequently observed mechanisms to efficiently regulate these cellular processes. Nevertheless, following removal of the lesion and successful DNA repair, these processes must be reversed (Zhu and Wani, 2010). The Access-Repair-Restore (ARR) model has been proposed decades ago to study various mechanisms of chromatin remodelling during DNA repair. According to this model; in response to DNA damage, local chromatin is disassembled allowing the repair factors to gain access to the DNA damaged sites. However, to maintain genomic integrity chromatin restoration to its normal structural and functional state is takes place after efficient completion of repair. This indicates that chromatin must behave in a dynamic way throughout this process (Green and Almouzni, 2002; Polo and Almouzni, 2015; Smerdon, 1991).

Different cellular strategies can be carried out by living cells to reassemble chromatin to its normal pre-damaged compact position, such as histone post-translational modification (Kouzarides, 2007) and nucleosome or histone eviction (Adam et al., 2014; Polo and Almouzni, 2006, 2015; Polo et al., 2006). Regulation of chromatin

structure is adapted by modifying histones through HATs and HDACs (Kurdistani and Grunstein, 2003). These two histone modifiers present in an equilibrium state and can fine tune the structure of chromatin in a dynamic way. since changing the charge of that lysine on the histone tails attract other remodellers and factors to condense/de-condense the chromatin structure. There is a good understanding on the first two phases of the ARR model during NER. Extensive work has been done on how chromatin is set up after DNA damage to facilitate access of the repair machinery to the damage and the remodelling that takes place during the repair phase itself. The restoration phase on the other hand, is the phase that is studied less extensively and our current knowledge is in its infancy. We know that histone H3 acetylation at lysine 9 and 14 is induced in response to UV irradiation and facilitates efficient NER (Yu et al., 2005, Yu et al 2016). Similarly, it has been described that the damage-induced histone H3 hyperacetylation is restored to its pre-damaged conditions following repair in wild type cells. However, this restoration does not take place in repair defective strains such as *RAD14* deleted cells, resulting in the constitutive hyperacetylation of histone H3.

A number of mechanisms are available that might be active during the restoration phase including; direct involvement of HDACs, nucleosome eviction or exchange or a combination of both. Here , two possible mechanisms that may participate in returning chromatin structure to its pre-damaged state was investigated. Since HDACs are involved in many cellular processes such as gene repression, cell cycle regulation, cell growth and many more, it is feasible that they may also participate in reversing UV-induced histone H3 acetylation. My study intended to investigate possible mechanisms used in reversing DNA damage induced histone H3 hyper acetylation following efficient DNA repair in yeast.

Therefore, first genetic and ChIP-qPCR experiments was performed using different HDAC mutants (Rpd3, Hda1, Hos1 and Hos2) to find out whether HDACs are involved in the response to UV damage. In chapter three these HDAC mutants were used to study their effect on UV survival and DNA repair and found that these HDACs in isolation (single mutant) do not contribute to the UV survival or DNA repair process. Lastly, histone H3 acetylation levels at the *MFA2* gene was measured using standard ChIP-qPCR. These experiments revealed that there is no difference in the gradual loss of UV-induced histone H3 hyperacetylation levels between wild type and HDAC mutants. Overall, we obtained similar results with three different experimental techniques, confirming that all the approaches were consistent with each other and that the HDACs tested here in isolation, have no effect on UV survival, CPD removal or histone H3 deacetylation. Nevertheless, HDACs involvement in the repair mechanism

cannot be ruled out since there exists considerable redundancy between HDACs in other mechanisms such as gene expression regulation and other processes such as the DDR and DSB repair. Therefore, deleting only one HDAC gene might not affect a specific pathway and could be masked by the activity of the other HDACs due to the redundancy. Thus deactelyation activity is never completely lost and its effect on DNA metabolism, repair in this case, can not be discerned. Deleting more than one HDAC at the same time could resolve this problem, but double and triple HDAC mutant have severe growth defects in yeast (unpublished data, this lab). Alternatively, HDAC inhibitors can be introduced to maintain elevated levels of histone H3 acetylation in response to UV irradiation and measure how this affects the organisation of GG-NER.

Due to the fact that HDACs display high levels of redundancy *in vivo*, the chromatin occupancy of the two main HDACs (Rpd3 and Hda1) was investigated in relation to the occupancy of the HAT Gcn5 and the GG-NER repair factors (Rad7 and Rad16) both before and after UV irradiation. We know that, to facilitate chromatin remodelling for efficient repair, Gcn5 and the Rad7-Rad16 (GG-NER) factors are needed to control increased levels of UV-induced histone H3 acetylation at *MFA2* (Yu et al., Yu et al.,2016). Yu and her colleagues have found that Gcn5 plays an important role in repair events at a genome-wide scale as well (Yu et al., 2016). Importantly, the UV-induced histone H3 hyperacetylation can be reversed by an as yet unknown mechanism in wild type cells (Yu et al., 2005). Nevertheless, deactelyation is not detected when repair is defective as is the case in *rad4* and *rad14* cells. Instead, the hyperacetylation persists for several hours after DNA damage induction. So examining the factors that control these events will give a clear indication of whether or not these factors mediate histone H3 hyperacetylation. My results revealed that, consistent with the previous findings, chromatin retention of the GG-NER complex and Gcn5 drives histone H3 hyperacetylation in repair defective cells (Yu et al., 2005). As a result, the process that mediates deacetylation might be not adequate enough to oppose the sustained Gcn5 activity due to Rad7-Rad16 retention on the chromatin. Although I have shown that sustained high acetylation levels of histone H3 are due to the persistent chromatin occupancy of Gcn5 and Rad7-Rad16 complex at a single locus (*MFA2*) the same might not hold true genome-wide or at other locations throughout the genome. Therefore, investigating these factors on a genome-wide level in *RAD14* deleted strains will provide a better understanding of whether or not the phenomena (of constitutive histone H3 hyperacetylation) that have been seen on *MFA2* are also applicable throughout the entire genome. Genome-wide investigatiion of Gcn5 chromatin occupancy and histone H3 acetylation in wild type cells at 2 and 3 h after repair will

confirm my prediction that there will be a decrease in Gcn5 occupancy and histone H3 acetylation because at the point where repair is finished, the HDAC occupancy is elevated. HDACs and HATs work in an antagonistic way as we saw at 1 h time point, but this time their patterns is predicted that it will be exactly opposite at 3 h with high levels of HDACs and low levels of HATs on the chromatin.

A possible mechanism that could explain the constitutive hyperacetylation in repair deficient cells is the failure to recruit any deactelyation activity. Therefore the UV-induced changes to chromatin occupancy of the HDACs Rpd3 and Hda1 was investigated directly via ChIP-qPCR at some genomic regions to overcome the caveats of redundancy we initially encountered when genetic approaches were applied. Prior to exposure to UV irradiation, both Rpd3 and Hda1 occupy the chromatin at a basal level as was the case for Gcn5. This state of equilibrium between HDACs and HATs I describe here for the first time in the context of DNA repair. This balance controls the levels of acetylation of histones on the chromatin and maintains a steady state. HDAC and HAT colocalisation on chromatin in the absence of DNA damage might imply that HDACs play an active role in the access phase of the ARR model by preparing the chromatin for repair factors after UV exposure. Immediately after UV, HDAC occupancy is lost in both wild type and *RAD14* deleted cells. This was concomitant with the reduction of GG-NER factor binding, Gcn5 occupancy and histone H3 hyperacetylation on the chromatin. This indicates that, HDAC occupancy and its loss following UV irradiation is independent of the initial stages of the DNA repair pathway. However, HDAC occupancy does not recover 3 h after DNA damage induction in the *RAD14* deleted strains. Instead, the HDAC occupancy remains low while the occupancy of the other factors described here remains high in the *RAD14* deleted cells. This indicates that, recovery of HDAC chromatin occupancy depends on active repair. Hence, chromatin restoration depends on both the loss Gcn5 and concomittent recruitment of Rpd3 and Hda1 to the chromatin after repair at a single genetic locus. To examine whether chromatin occupancy of the HDACs is regulated by GG-NER factors, it is important to investigate their chromatin occupancy in the GG-NER deleted strains (*RAD7* or *RAD16* mutant).

All the above studies have been carried out at the level of single loci, which although revealing the UV-induced recruitment of these factors to chromatin and how they affect the acetylation levels on chromatin conformation at different stages during the repair process *in vivo,* it fails to translate to the entire genome. To capture an overall picture of what might happen to these factors and to assess the role for any of the above mentioned repair factors, it is worth to explore their roles individually and in relation to

each other on a genome-wide scale to find out whether chromatin remodelling is coordinated during GG-NER. Therefore, I first analysed genome-wide HDAC occupancy in relation to GG-NER complex binding using ChIP-on-chip both before and after UV irradiation in wild type cells. In addition, I compared my data to previously generated datasets from our lab to find connections between the chromatin occupancy of these factors.

In budding yeast DNA microarray studies have shown that HDACs are required for many cellular processes such as transcriptional activation and repression (Kurdistani and Grunstein, 2003). I showed that HDACs are recruited to chromatin after repair at several regions of the yeast genome and I aimed to expand that over the entire genome via the use of ChIP-chip. As predicted, there is a general loss of HDAC occupancy in response to UV irradiation throughout the genome (see chapter 5, section **5.3.1.2 page 128-129**). These changes are mirrored by the increased levels of histone H3 acetylation. This indicates that, in addition to the redistribution of Rad7/Rad16 GG-NER and recruitment of Gcn5, reciprocal HDAC loss of occupancy in response to UV irradiation helps to induce histone H3 hyperacetylation and the subsequent chromatin remodelling to allow efficient repair. However, as soon as repair is finished I observed recruitment of HDACs on to the chromatin concomitant with the reduction of histone H3 acetylation level to a pre-damaged state. This indicates that HDACs might play an active role in deacteylating histone H3 tails following repair to facilitate subsequent chromatin restoration. Measuring histone H3 acetylation in a *rpd3* or *hda1* mutant on a genome-wide scale could shed light on the redundancy and highlight different regions of the genome that rely on specific HDACs for deactelyation during restoration. To confirm that active repair is required for the recruitment of HDACs during restoration, it is highly recommended to perform the same experiment using repair defective cells like a *RAD14* deleted strain. Based on the results at a single genetic locus examining both histone H3 acetylation (Yu et al., 2005) and my previous results on HDACs (see chapter 4, page 102-112), I predict, that following UV irradiation there will be a general loss of HDACs occupancy genome-wide as we observed in wild type cells. However, three h after UV irradiation, the chromatin occupancy of HDACs will remain low because repair is defective. This follows from the fact that DNA damage detection does not appear to be required for the initial loss of HDAC occupancy to take place. Measuring HDAC chromatin occupancy in a *RAD4* or *RAD7/RAD16* mutant could anwser that question.

Analysing my data in the context of GG-NER showed that HDACs are enriched at the Abf1 binding sites before UV irradiation. Additionally, when I plot my data at these sites

together with other repair factors such as the GG-NER complex Rad7-Rad16 and Gcn5, I noticed the presence of an antagonistic relationship between HDACs and both of the GG-NER and Gcn5 factors. This relationship has been described for other cellular process as well such as transcription but not for GG-NER. Nevertheless, this reciprocal change in chromatin occupancy of HATs and HDACs during repair has not been shown before. These observations are very important because Abf1 serves as a binding site from which the repair reaction is primed as soon as the cells are hit with UV irradiation. However, more studies need to be undertaken to understand how these factors regulate HDAC eviction and recruitment to the chromatin. In order to find this out it is important to investigate HDAC occupancy in *RAD7*, *RAD16* or *GCN5* deleted cells. It is possible that the GG-NER complex is required for tethering HDACs to the chromatin in the absence of DNA damage as it does for Gcn5. If this is the case the genomic distribution of HDACs would be severely disrupted in these mutants. However, if chromatin occupancy of HDACs is independent of the GG-NER complex no change will occur and the chromatin occupancy of HDACs will remain un-altered. Even though these factors regulate histone H3 acetylation in response to UV irradiation, minor Rad16-independent acetylation can be detected in response to DNA damage (Yu et al., 2016). This indicates that in these mutants other factors might regulate the HAT to HDAC balance in an attempt to remodel chromatin for repair. Measuring UV-induced HDAC occupancy in these mutants will reveal whether or not the GG-NER complex is involved in recruiting the deacetylation activity onto the chromatin after repair. If the UV-induced loss of HDACs occupancy depends on the GG-NER complex, I predict that there will be no change in response to UV irradiation in GG-NER defective cells. In wild type cells, it is possible that at the 3 h mark, the GG-NER factors take up their pre-damage chromatin occupancy enabling them to recruit HDACs to regions of the genome that are hyperacetylated after DNA repair. This process will be disrupted in GG-NER deficient cells. These future studies might help identify the factors required for HDAC eviction from the chromatin during repair and the process that recruits them back to facilitate restoration after the repair reaction is completed.

Finally, I wanted to know if there is any relationship between CPD repair rates and HDACs. To study this I plotted the CPD repair rate data and HDACs occupancy in response to UV irradiation around gene structure. The interesting feature is that repair rate data is inversely related to Rpd3 occupancy. In gene bodies, where the repair rate is high, Rpd3 occupancy is at its lowest level. Conversely, locations of slow repair, at

the promoter- and downstream regions of genes, are sites of higher Rpd3 occupancy. Importantly, this is not the case for Hda1 and could therefore be a specific feature of Rpd3. UV-induced changes to Hda1 occupancy are most prominent downstream of genes. It remains be determined what the significance is of this behaviour. To find a direct link between genome-wide HDAC occupancy and the distribution of CPD repair, repair rates in HDAC mutants can be investigated and compared with the present wild type data. If there is a direct link between HDAC occupancy and repair rates, it is possible that repair at the coding regions is affected in the absence of Rpd3, while the downstream regions are affected in the absence of Hda1. If the HDACs are essential in setting up a chromatin landscape that is important during the access phase, DNA repair initiation will be affected. On the other hand, if it turns out that the GG-NER factors and active repair only attracts HDACs for restoration, recovery of chromatin structure after DNA repair might be more severely affected without impacting the repair reaction directly.

It has been discovered that the genome is organised in such a way that DNA lesions are removed at the right time in the right place by the NER pathway. This mechanism revolves around the Abf1 binding sites that serve as sites from which GG-NER is organised and repair is primed to repair DNA damage efficiently. My study has contributed to the understanding of the mechanism involved in restoration of chromatin following repair of UV-induced DNA damage and how the events are organised in relation to the GG-NER. There is a clear inverse relationship between HATs and HDACs in the context of GG-NER. These findings are all consistent with previous findings. My results indicate that Rpd3 and Hda1 are evicted and later recruited to chromatin in response to UV irradiation and may have a role in setting up chromatin at the access phase as well as the restoration phase. My results have expanded our understanding on how the last phase of ARR model might be working. When the chromatin occupancy of Gcn5 and histone H3 acetylation levels diminish, HDAC restoration takes place. This confirms that HDACs are involved in the restoration phase of the ARR model by deacetylating histone H3 after the repair reaction is completed. This will eventually lead to compaction and remodelling of the chromatin. How the chromatin is remodelled at the level of the nucleosome during this process is a topic for future study.

It is possible that the deacetylation occurs indirectly by eviction of the acetylated histones from the chromatin. The nucleosome itself or part of the nucleosome including histone H3 may be evicted from chromatin and then replaced by a new unmodified histone. Such a mechanism is catalysed by chromatin assembly factor CAF-1 (Polo et

al., 2006; Adam and Polo, 2012) and HIRA (Bergink et al., 2006; Polo and Almouzni, 2015). New histones are deposited at the site of DNA damage by CAF-1 (Polo et al., 2006). One way to test this is by examining histone H3 lysine 56 acetylation status. Acetylation of lysine 56 on histone H3 is indicative of newly incorporated histones in chromatin (Masumoto et al., 2005; Simoneau et al., 2015)). The result can be confirmed by applying an independent method such as a classical pulse chase experiment or SNAP-tag-based pulse chase imaging (Adam and Polo, 2012) which both rely on differential labelling old versus newly synthesised histones.

The organisation of repair and the effect chromatin remodellers and chromatin structure has on it, has important implication for mutagenesis and cancer. HDAC inhibitors can induce DNA damage via changes in transcription-replication collisions and result in the formation of DNA:RNA structure referred to as R-loops, which can induced DSBs and ultimately lead to the cancer and neurologic diseases.

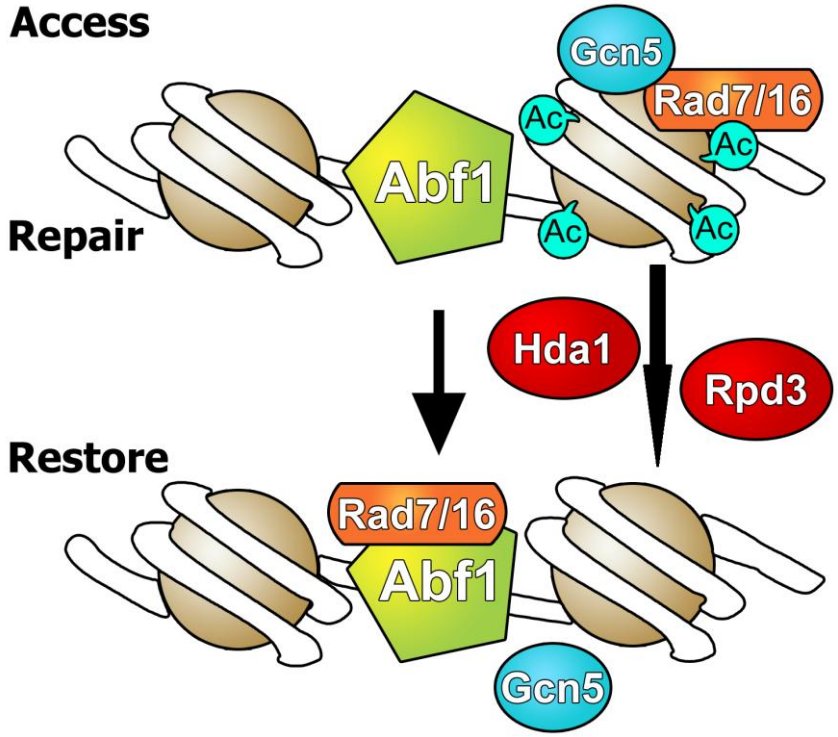

Figure 6.1, the role of Rpd3 and Hda1 deacetylases in restoration of UV-induced DNA damage. During the access phase Rad7/Rad16 introduce necessary chromatin changes and recruit the HAT Gcn5 on to the chromatin. Then histone H3 acetylation is up regulated and as a result chromatin becomes more accessible for specific DNA repair factors (Upper panel: access phase). Next, repair enzymes, recognise, confirm

and remove the lesion (repair phase). Finally, the chromatin is restored to its normal pre-damaged structural configuration which is achieved by the HDACs.

Appendix I

Appendix I - Liquid and solid media

1. Growth media

YPD (400 ml)

4 g Bacto Yeast Extract

8 g Bacto Peptone

8 g Glucose

Made up to 400 ml with H_2O

YPD plates were obtained by supplementing above medium with 8 g Bacto Agar

MM (400 ml)

2.68 g Yeast Nitrogen Base w/o Amino Acids

8 g Glucose

Made up to 400 ml with H_2O

For plates supplement with 2% Bacto Agar

Dosage of Amino Acids added:

Adenine	40 µg/ml	Tryptophan	40 µg/ml
Leucine	60 µg/ml	Lysine	40 µg/ml
Uracil	20 µg/ml	Histidine	40 µg/ml

2. Stock Solutions

0.5 M EDTA (pH 8.0)

EDTA . Na2. $2H_2O$	186.1 g
H_2O	800 ml

Stir on a magnetic stirrer. Adjust the pH to 8.0 with NaOH (~22 g of NaOH pellets).

Add H_2O to make 1 L and sterilise by autoclaving.

1 M Tris

Tris base	121.1 g
H_2O	800 ml

Adjust the pH to the desired value by adding concentrated HCl. Add H_2O to make 1 L.

pH	HCl
7.6	~60 ml
8.0	~42 ml

10 x TE Buffer (400 ml)

40 ml 1 M Tris-HCl, pH 7.5

8 ml 0.5 M EDTA, pH 8.0

352 ml of H_2O

3 M Sodium acetate (pH 5.2) (400 ml)

Sodium acetate 3H2O	163.24 g
H2O	300 ml

Adjust the pH to 5.2 with acetic acid. Adjust the volume to 400 ml with H2O. Filter to sterilise.

5 M NaCL (400 ml)

Dissolve 116.9 g of NaCl in 350 ml of H2O. Adjust the volume to 400 ml with H2O. Sterilise by autoclaving.

10% SDS (Sodium dodecyl sulfate) (1 L)

Dissolve 100g of SDS in 800 ml of distilled H2O. Add distilled H2O to make a total volume of 1 L.

20% SDS (Sodium dodecyl sulfate) (500 ml)

Dissolve 100 g of SDS in 350 ml of distilled H2O. Add dissolved H2O to make a total volume of 500 ml.

PBS (1 L)

NaCL		8.00 g
KCl		0.20 g
Na2HPO4	1.44 g or Na2HPO4.2H H2O	1.80 g
KH2PO4		0.24 g
H2O		800.00 ml

Adjust the pH to 7.4. Add H2O to 1 L. Sterilise by autoclaving.

Sorbitol TE (1L) (Kept in cold room)

Sorbitol	165 g
Tris . HCl (pH8.0)	100 ml
EDTA	200 ml

Add 500 ml H2O to dissolve the sorbitol. Adjust the final volume to 1L.

DNA Lysis Buffer (1 L)

Urea	240.00 g
NaCl	11.69 g
CDTA	5.00 g
SDS	5.00 g
1 M Tris-HCl (pH 8.0)	100.00 ml

Add 700 ml of H2O to dissolve the chemicals, and then adjust the final volume to 1L.

1 M DTT (Dithiothreitol)

DTT	3.09 g

Dissolved in 20 ml of 0.01 M sodium acetate (pH 5.2)

Sterilise by filtration. Do not autoclave and solutions containing DTT.

3. Solutions for electrophoresis

50 x TAE (Tris-acetate) (1 L)

Tris base	242 g

Sodium Acetate . 3 H2O	136 g
0.5 M EDTA	200 ml

Adjust to pH 7.2 with acetic acid. Add H2O to make 1 L.

10 x TBE (1 L)

Tris base	108 g
Boric acid	~55 g
EDTA	8.3 g

Add H2O to 1 L.

Non-denaturing loading buffer 10 ml

Ficoll	10%	1 g
SDS	0.5%	0.5 ml of 10% solution
Bromophenol Blue	0.06%	6 mg

Made up in 1 x TAE

4. Solutions for ChIP

FA/SDS Buffer

HEPES KOH pH 7.5	50mM
NaCl	150mM
EDTA	1mM
Triton X 100	1%
Deoxycholate Na	0.1%
SDS	0.1%
PMSF *	1Mm

*Add just before use as the activity decreases in H2O solution

The NaCl concentration can be adjusted to 500mM.

5 x Pronase Buffer (100 ml)

1 M Tris pH7.5	12.5 ml
0.5 M EDTA	5 ml
10% SDS	25 ml

Add H2O to mak100 ml.

LiCl Buffer (500 ml)

1 M Tris pH 8.0	5 ml
5 M LiCl	25 ml
0.5 M EDTA	1 ml
NP40	2.5 ml
Deoxycholate Na	25 ml
Add H2O to make 500 ml	

Appendix II

Appendix-167167 **primers used in this study qPCR-Chip primers (for acetylation, Gcn5, Rad7, Rad16, Rpd3 and Hda1 binding)**

Primer names	Sequence
MFA2	Forward 5’ – AAAGCAGCATGTTTTCATTTGAAACA – 3’ Reverse: 5’ – TATGGGCGTCCTATGCATGCAC – 3’
HML	Forward: 5'-CTCTAATGCCAGCTGAGTAAC-3' Reverse: 5'-CACCCAACAAAGCACAATAAGCATC-3'
RAD23	Forward: 5’ – TAGCAAGCTTGTCTGCGAAC – 3’ Reverse: 5’ - AGGC A AG AAAT AGCG AC AGC – 3’
POL30	Forward: 5’ - AACACACCGGATTCCATCAT – 3’ Reverse: 5’ – TTGTTCGTGACTTGTCCCAA – 3’
NAT4	Forward: 5’ – TATATGAGGCGCTTGGGTTC – 3’ Reverse: 5’ – GTCGGAGTCAAGGATTCGAG – 3’
IRC5	Forward: 5’ - AGTCGGGGCAGATACAGTTG Reverse: 5’ – GGCCGCTCTGGTCAATATAA

Transformation and checking primers

Rad14 deleted primers

Deletion of *rad14* in wild-type (Gcn5Myc, Rad7Myc, Rad16Myc, Rpd3Myc & Hda1Myc) strains. Using PRS313 plasmid that contain histidine.

Rad 14 sequence + 750bp on top of start codon and +750bp at the end of stop codon

GTTGAAGACCCATTCTTCTTTGACGTACCTGTTGATGTATTCGTCCCCGTAATGAGAGGCA
AGTGCGTCTCTGACATCCTGTAACAGGTCTTCAGTGGATAAACCTTCTGCTGCGTTGTGTT
TGCTAATCACCGAGTTACATATTTCGTTCAAAGTTTTTGGATCGAACATGTAATTGGTTGGC
AACCAGGTAGTGAACAATACGTTCATAATGTAGCCTACAACACCAATCAACAAAAGGAGTG

GGAAAAACTTCATGGCTATAATGGTCTGGGCTAGTCTTAGTTTGATTGAGCGACAAGAGAG
ATCTGAACCCAGTGTCAAACGTTACCGCTTCTTTCTCTTATATACCATGGCGCTGCAGATCT
ATCCAAATTCTTCCATACTGAAAATCATCCAAACGAGAACGATAGCACCGGTAGTTTTCCTT
GCGGCTTATACGAGGGCCGTGGTTCGATTCTGCCCTGGAGCGTAAGGGCAGGAATGTGC
ATTGCATAAGATCATAATGGGATACTTCGTTGATAATAAGCAGAATCAACATAGCAGACTGC
TAGTGGCATACTCCACAACCCTTGTTTTTTTTTTTTTTTTTGTTTGAATAACTGTACTTCTATA
GAAGCTCTATCTACAGCATGTTTGACGTTTGCTAAGTTGTAGGGAGAAAAGAGGAAAGTGA
AAAGAAGGTAAGGAATTTATCGGAACTAGAAAAAGAGTTTGGATCTTCGTAGTGAAGGTAT
CGAACGTAACGCTATGACTCCCGAACAAAAGGCCAAACTAGTATGTGTGAAAATGATTCTG
TGTTTGTATTTTAACCGTGGGTTTCTTTTTACTAACAATTTAACGATGAGATGAGCTGTGCA
GGAGGCTAACAGGAAATTAGCAATAGAACGGTTAAGAAAAAGGGGAATACTGAGTAGCGA
CCAATTGAATCGAATAGAAAGTAGGAATGAACCTTTAAAAACCCGGCCTCTCGCAGTTACT
AGTGGCAGCAATCGGGATGATAATGCAGCAGCCGCAGTACATGTGCCAAATCATAATGGA
CAACCGTCTGCGCTTGCTAACACTAACACTAACACTACTTCACTTTATGGTAGCGGAGTAG
TTGATGGAAGTAAAAGGGATGCGTCGGTACTCGACAAAAGGCCAACGGATAGAATCAGAC
CTAGCATAAGGAAACAAGATTACATTGAGTACGATTTTGCCACCATGCAGAACTTGAATGGT
GGTTATATCAACCCTAAGGACAAGCTTCCAAATTCTGACTTTACCGATGACCAAGAATTTGA
ATCTGAGTTTGGATCTAAAAAGCAGAAGACACTACAGGACTGGAAAAAGGAACAACTTGAA
CGGAAAATGCTGTACGAAAATGCACCTCCTCCAGAGCATATTTCAAAGGCGCCGAAATGTA
TTGAATGTCATATTAATATTGAGATGGATCCTGTGCTACATGATGTGTTCAAGTTACAAGTTT
GTAAACAGTGTTCTAAGGAGCATCCAGAAAAGTATGCACTACTGACGAAAACAGAATGTAA
GGAAGATTACTTTTTAACAGACCCCGAATTGAATGATGAGGATCTCTTTCATAGACTAGAAA
AGCCGAACCCTCATTCGGGGACATTTGCAAGAATGCAACTATTTGTTAGATGTGAAGTGGA
AGCCTTTGCGTTCAAGAAATGGGGTGGAGAAGAAGGTTTAGATGAGGAATGGCAACGTCG
TGAAGAAGGAAAGGCTCACAGAAGGGAGAAAAAATACGAAAAGAAAATCAAGGAAATGCG
ACTGAAAACAAGAGCTCAAGAATATACTAATAGATTAAGAGAAAAGAAGCATGGGAAAGCC
CATATTCATCATTTTAGTGATCCAGTTGATGGAGGTATTGATGAAGACGGTTATCAAATTCA
AAGAAGAAGATGTACAGACTGCGGGCTAGAAACTGAAGAAATTGACATTTAAATGTTGGTT
ATGTATATAAGAATATAACAAGAAAGTCATAATAAGGTGTTTTGATTGTGTTCATTGATTGAT
ATCCCATTTGTCACTCGTACATAATTAACTATCTCGGAAAAACTGGTTTGAAAATCTTTTATT
CATCCACCTTATTTAATAATATGATTACAATCAATTCCTTGGGTGCATAAAATTACACCTATT
CTTGCTTCTCTTTCTCGCCTGATAAAGTTGTTTTGCCTTATATGTTTATAGTTTTTAATATTTA
TTTGAAGGCCACATGGGGCCTCTTTCCCCCATTGGTTGAATAAGTATCCCTGTAGTGCGCC
TAAAATGCTAAAAATAATAATGAACCTACACCTAGCATACCCGCAGAAATATACCAAATGGC
ATTGGAGGTTAAAAATGAGGTATTTTGTCTTTTAATGGCATTCGTCTTGTGTCTGTTTTCCAG
GCTCCTCCTCACTAAACTTCTCAGTGATCTTTTCTTATTAGAGGATGGGTCGTCAG
TGCTGGTCGCTGACGATGTTGGGTTCAAAGTTTCTGTTGGAAGCATCATTGGTGG
TCTATAAGCCAAATATAGTGGTTGCATTGGAGTACCATCATATTGGTACAATTGCA
GGGTGTAAATACCATGGTAAGGATCTATACCTACGGCATATTCCTTGAAAGTTTCT
GTTTGGTTATATCTAGAATAAGTCGAAACTCCGTCATCATTGCATGGGTCGCTGAA
TAGTTGTCTACCGTCAACTTCAA

Histidine sequence:

TAGGAGTCACTGCCAGGTATCGTTTGAACACGGCATTAGTCAG
GGAAGTCATAACACAGTCCTTTCCCGCAATTTTCTTTTTCTATT
ACTCTTGGCCTCCTCTAGTACACTCTATATTTTTTTATGCCTCG
GTAA TGAT TTTCAT TT TTTTTTTTCCACCTAGCGGATGACTCT
TTTTTTTTCTTAG CGATTGGCATTATCACATAATGAATTATACA
TTATATAAAGTAATGTGATTTCTTCGAAGAATATACTAAAAAAT
GAGCAGGCAAGATAAA CGAAGGCAAAGATGACAGAGCAGA A
AGCCC TAGTAAAGCGT AT TACAAATGAAACCAAGATTCAGAT
TGCGATCTCTTTAAAGGGTGGTCCCCTAGCGATAGA GCACTCG
ATCTTC CCAGAAAAAG AGGCAGAAGCAGTAGCAGAACAGGCC
ACACAATCGCAAGTGATTAACGTCCACACAGGTATAGGGTTTC
TGGACCATATGATACATGCTCTGGCCA AGC ATTCCGGCTGGT
CGCTAATCGTTGAGTGCATTGGTGACTTACACATAGACGACC A
TCACACCACTGA AGACTGCGGGATTGCTCTCGGTCAAG CTTTT

A A A G A G G C C C T A C T G G C G C G T G G A G T A A A A A G G T T T G G A T C A G G A T T T G C G C C T T T G G A T G A G G C A C T T T C C A G A G C G G T G G T A G A T C T T T C G A A C A G G C C G T A C G C A G T T G T C G A A C T T G G T T T G C A A A G G G A G A A A A G T A G G A G A T C T C T C T T G C G A G A T G A T C C C G C A T T T T C T T G A A A G C T T T G C A G A G G C T A G C A G A A T T A C C C T C C A C G T T G A T T G T C T G C G A G G C A A G A A T G A T C A T C A C C G T A G T G A G A G T G C G T T C A A G G C T C T T G C G G T T G C C A T A A G A G A A G C C A C C T C G C C C A A T G G T A C C A A C G A T G T T C C C T C C A C C A A A G G T G T T C T T A T G T A G T G A C A C C G A T T A T T T A A A G C T G C A G C A T A C G A T A T A T A T A C A T G T G T A T A T A T G T A T A C C T A T G A A T G T C A G T A A G T A T G T A T A C G A A C A G T A T G A T A C T G A A G A T G A C A A G G T A A T G C A T C A T T C T A T A C G T G T C A T T C T G A A C G A G G C G C G C T T T C C T T T T C T T T T T G C T

Histidine sequence with the flanking region of *RAD14* gene after PCR amplification

G G C A A C C A G G T A G T G A A C A A T A C G T T C A T A A T G T A G C C T A C A A C A C C A A T C A A C A A A A G G A G T G G G A A A A A C T T C A T G G C T A T A A T G G T C T G G G C T A G T C T T A G T T T G A T T G A G C G A C **T A G G A G T C A C T G C C A G G T A T C G T T T G A** A C A C G G C A T T A G T C A G G G A A G T C A T A A C A C A G T C C T T T C C C G C A A T T T T C T T T T T C T A T T A C T C T T G G C C T C C T C T A G T A C A C T C T A T A T T T T T T T A T G C C T C G G T A A T G A T T T T C A T T T T T T T T T T C C A C C T A G C G G A T G A C T C T T T T T T T T T C T T A G C G A T T G G C A T T A T C A C A T A A T G A A T T A T A C A T T A T A T A A A G T A A T G T G A T T T C T T C G A A G A A T A T A C T A A A A A A T G A G C A G G C A A G A T A A A C G A A G G C A A A G A T G A C A G A G C A G A A A G C C C T A G T A A A G C G T A T T A C A A A T G A A A C C A A G A T T C A G A T T G C G A T C T C T T T A A A G G G T G G T C C C C T A G C G A T A G A G C A C T C G A T C T T C C C A G A A A A A G A G G C A G A A G C A G T A G C A G A A C A G G C C A C A C A A T C G C A A G T G A T T A A C G T C C A C A C A G G T A T A G G G T T T C T G G A C C A T A T G A T A C A T G C T C T G G C C A A G C A T T C C G G C T G G T C G C T A A T C G T T G A G T G C A T T G G T G A C T T A C A C A T A G A C G A C C A T C A C A C C A C T G A A G A C T G C G G G A T T G C T C T C G G T C A A G C T T T T A A A G A G G C C C T A C T G G C G C G T G G A G T A A A A A G G T T T G G A T C A G G A T T T G C G C C T T T G G A T G A G G C A C T T T C C A G A G C G G T G G T A G A T C T T T C G A A C A G G C C G T A C G C A G T T G T C G A A C T T G G T T T G C A A A G G G A G A A A G T A G G A G A T C T C T C T T G C G A G A T G A T C C C G C A T T T T C T T G A A A G C T T T G C A G A G G C T A G C A G A A T T A C C C T C C A C G T T G A T T G T C T G C G A G G C A A G A A T G A T C A T C A C C G T A G T G A G A G T G C G T T C A A G G C T C T T G C G G T T G C C A T A A G A G A A G C C A C C T C G C C C A A T G G T A C C A A C G A T G T T C C C T C C A C C A A A G G T G T T C T T A T G T A G T G A C A C C G A T T A T T T A A A G C T G C A G C A T A C G A T A T A T A C A T G T G T A T A T A T G T A T A C C T A T G A A T G T C A G T A A G T A T G T

A T A C G A A C A G T A T G A T A C T G A A G A T G A C A A G G T A A T G C A T C A T T C T A T A C G T G T C A T T C T G A A C G A G G **C G C G C T T T C C T T T T T T C T T T T T G C T** T T A T T C C A C A A A A C T A A C A C A A G T A A C T A A C T A T A G G G T A A A C A G T G A G C A T G T A T T A A T T G A T A G A G C C T T T T T G A C C A A A C T T T T A G A A A A T A A G T A G G T G G A A T A A A T T A T T A T A C T A A T G T T A G T T A A G G A A C C C A C G T A T

The plasmid size is **1122**

Correctly transformed cells amplicon size will be **1385** bp

WT control and untransformed cells will be **1953** bp

1). For RAD14 knockout:

Rad14-His3-F:

5'-AAACTTCATGGCTATAATGGTCTGGGCTAGTCTTAGTTTGATTGAGCGACTAGGAGTCACTGCCAGGTATCGTTTGA-3'

Rad14-His3-R:

5'-CGAGTGACAAATGGGATATCAATCAATGAACACAATCAAAACACCTTATTAGCAAAAAGAAAAAAGGAAAGCGCG-3'

2). For checking:

Rad14-Check-F: 5'-GGCAACCAGGTAGTGAACA-3'

Rad14-Check-R: 5'-TATGCACCCAAGGAATTGAT-3'

For checking any Rad14 knock out (Gcn5-myc, Rad-myc, Rad16-myc, Rpd3-myc and Hda1-myc)

Myc tagging primers

Transforming BY4742 wild-type strains to BY4742 Rpd3Myc tagged

F- 5′ – GTTCGCAATATGCGAGGGACCTACATGTTGAGCATGACAATGAATTCTAT

TCCGGTTCTGCTGCTAG –3′

R- 5′ – TTTTGTTTCACATTATTTATATTCGTATATACTTCCAACTCTTTTTT

CCTCGAGGCCAGAAGAC –3′

Checking the transformation by colony PCR

RPD3- checkF1 5`- ACA TGG TGC TTT GAA ACA GGT CT-3`

RPD3-checkR1 5`- GGA TAG CGT CTT AAG TGC CT-3`

RPD3- check-F2 5`- GATGCCGAAGATTTGGGTGAT-3`

RPD3- check-F2 5`-CTAGCAGCAGAACCGGAAT-3` (Complimentary

of the end portion of Rpd3-C-myc-F1 primer)

Transforming BY4742 wild-type strains to BY4742 Hda1Myc tagged

F- 5′ – GGCTACAGACTTTATACTGGATTCGTTTGAAGAATGGAGTGATGAAGAA

TCCGGTTCTGCTGCTAG –3′

R- 5′ – TTCATAAGGCATGAAGGTTGCCGAAAAAAAATTATTAATGGCCAGTTTTT

CCCCTCGAGGCCAGAAGAC –3′

Checking the transformation by colony PCR

HDA1-check F1 5`-CGT ACA TCT GCT TGG TCA CA-3`

HDA1-check R1 5`- AGC ATC CAC TTT AAT GTA TAC G-3`

HDA1- check-F2 5` - CAAGAAAAAAATTCGGTAGAGT-3`

HDA1- check-R2 5`-CTAGCAGCAGAACCGGATT-3` (Complimentary

of the end portion of Hda1-C-myc-F1 primer)

Appendix- III

Appendix- III Raw data and supplementary figure for chapter 3

UV dose (J/M^2)	Dilution	**Wild-type** Number of colonies			Mean Survival (%)	Standard deviation (%)
		Exp.1	Exp.2	Exp.3		
0	10^-4	120/135/98	99/123/110	80/72/114	100	0
30	10^-4	33/36/32	42/43/53	49/49/51	42.06	13.7
50	10^-3	107/113/133	198/216/212	84/72/76	12.525	5.52
80	10^-3	18/16/17	13/23/2	39/03/14	1.74	0.33
100	10^-2	27/27/24	9/2/17	22/28/09	0.193	0.047

UV dose (J/M^2)	Dilution	***hda1Δα***			Mean Survival	Standard deviation
		Exp.1	Exp.2	Exp.3		
0	10^-4	142/139/131	141/112/136	148/134/158	100	0
30	10^-4	52/45/38	58/65/67	65/60/70	42.5	7.4
50	10^-3	116/103/139	169/215/188	139/156/131	11.16	3.1
80	10^-3	17/19/23	11/19/21	16/12/15	1.26	0.26
100	10^-2	22/39/30	16/35/15	18/17/18	0.17	0.55

UV dose (J/M^2)	Dilution	***hos1Δα*** Number of colonies			Mean Survival (%)	Standard deviation (%)
		Exp.1	Exp.2	Exp.3		
0	10^-4	110/144/145	111/103/102	93/78/114	100	0
30	10^-4	85/91/103	60/44/49	41/41/43	54	13.9
50	10^-3	39/51/33	141/128/116	159/113/123	9.7	5.7
80	10^-3	9/12/9	22/20/28	25/38/70	2.55	1.9
100	10^-2	15/86/-	22/26/34	16/72/16	0.33	0.065

UV dose (J/M^2)	Dilution	***hos2Δα*** Number of colonies			Mean Survival (%)	Standard deviation (%)
		Exp.1	Exp.2	Exp.3		
0	10^-4	160/110/120	175/153/182	87/117/78	100	0
30	10^-4	32/43/24	66/65/50	42/52/43	36.6	11.6
50	10^-3	93/79/86	164/173/154	126/132/126	9.95	3.5
80	10^-2	71/26/50	13/18/21	47/42/23	2.9	1.65

100	10^-2	----	25/24/21	13/36/19	0.19	0.07

Irradiation time (s)	Dilution	***rpd3Δa*** Number of colonies			Mean Survival (%)	Standard deviation (%)
		Exp.1	Exp.2	Exp.3		
0	10^-4	87/87/89	110/103/116	89/95/88	100	0
30	10^-4	36/36/37	36/37/43	43/34/35	39.3	3.5
50	10^-3	102/95/136	77/63/70	139/127/122	11.1	4.1
80	10^-3	12/15/13	10/---/9	12/13/08	1.2	0.32
100	10^-2	30/18/41	12/---/12	36/39/28	0.27	0.14

UV dose (J/M^2)	Dilution	***rpd3Δα*** Number of colonies			Mean Survival (%)	Standard deviation (%)
		Exp.1	Exp.2	Exp.3		
0	10^-4	93/110/116	110/89/88	102/106/108	100	0
30	10^-4	48/61/37	48/61/37	38/57/49	46.88	3.5
50	10^-3	248/122/217	185/165/156	217/206/187	18.44	0.837
80	10^-3	29/35/33	---/46/84	36/28/27	4.23	2.2
100	10^-2	53/80/49	80/55/64	57/61/81	0.63	0.061

CPD raw data in WT and some HDAC mutants

WT	Percentage of CPD remain							Average and standard devia	
Time	Exp1	Exp2	Exp3	Exp4	Exp5	Exp6	Exp7	Aver	SD
No repair	100	100	100	100	100	100	100	100	0
1h	70.8	55.056	81.384	76.194	77.326	73.516	77.937	73.1	8.6
2h	53.8	46.16	49.904	34.267	52.754	51.327	57.506	49.38	7.5
3h			23.663	30.575	33.924	44.15	38.4	34.1	7.7

Hda1Δ	Percentage of CPD remain							Average and standard devia	
Time	Exp1	Exp2	Exp3	Exp4	Exp5	Exp6	Exp7	Av	SD
No repair	100	100	100					100	0
1h	79.642	86.456	80.430					82	3.7
2h	59.463	49.833	65.661					58	7.9
3h	47.152	41.151	38.691					42	4.3

hos1Δ	Percentage of CPD remain							Average & standard devia	
Time	Exp1	Exp2	Exp3	Exp4	Exp5	Exp6	Exp7	Ave	SD
No repair	100	100						100	0
1h	79.160	85.048						82	4.1
2h	56.484	65.643						61	6.4
3h	47.967	38.054						43	7

ChiP-qPCR data (H3K9/K14 levels at *MFA2*) in wild-type and HDAC delete

H3K9/K14 at *MFA2* in *wild-type strains*							
		SQ Mean					
WT	**Time**	**Input**	**IP**	**IP/Input**	**Fold**	**Average**	**St Dev**
Exp1	No UV	0.001138	0.0026	0.2868021	1.0000	1.000	0
	1 h	0.000845	0.000654	0.7742082	2.6994504	2138	0.547
	2 h	0.000765	0.000659	0.8616919	3.0044821	2.562	0.769
	3 h	0.000920	0.000581	0.6321022	2.203966	1.748	0.655
Exp2	No UV	0.00087	0.00099	1.26531	1.0000		
	1 h	0.0007	0.00186	2.67081	2.1108		
	2 h	0.00044	0.00167	3.80608	3.00802		
	3 h	0.00056	0.00145	2.58583	2.04363		
Exp3	No UV	0.087	0.0459	0.527586	1.0000		
	1 h	0.0649	0.055	0.847458	1.606292		
	2 h	0.0786	0.0694	0.882952	1.673568		
	3 h	0.0593	0.0312	0.526138	0.997256		

H3K9/K14 at *MFA2* in *hda1Δ*							
hda1Δ		SQ Mean					
Exp1	**Time**	**Input**	**IP**	**IP/Input**	**Fold**	**Average**	**St Dev**
	No	0.001030	0.001912	1.8562728	6.4723115	4.938468	1.333879
	1 h	0.001052	0.001589	1.5096897	5.2638718	3.18527	1.814294
	2 h	0.000956	0.003766	3.9375222	13.729054	8.04385	5.21695
	3 h	0.001246	0.002044	1.6403927	5.7195969	4.270552	1.622934
Exp2	No	0.00063	0.002356	3.739683	4.049006		
	1 h	0.000834	0.001827	2.190647	2.371845		
	2 h	0.000803	0.002579	3.211706	3.477359		
	3 h	0.000726	0.001689	2.326446	2.518876		
Exp3	No	0.0521	0.118	2.264875	4.292901		
	1 h	0.0861	0.0872	1.012776	1.91964		
	2 h	0.0613	0.224	3.65416	6.926185		
	3 h	0.0841	0.203	2.413793	4.575163		

hos1Δ		**SQ Mean**					
	Time	**Input**	**IP**	**IP/Input**	**Fold**	**Average**	**St Dev**
Exp1	No	0.1131	0.0953	0.842617	1	1	0
	1 h	0.091935	0.09035	0.98276	1.166318	1.511511	0.777668
	2 h	0.0826	0.13121	1.588499	1.885196	2.407594	0.931196
	3 h	0.0943	0.1269	1.345705	1.597054	1.924446	0.43346
Exp2	No	0.00087	0.00099	1.137931	1		
	1 h	0.0006	0.00164	2.733333	2.40202		
	2 h	0.00065	0.002576	3.963077	3.482704		
	3 h	0.00067	0.001842	2.749254	2.416011		
Exp3	No	0.0899335	0.077984	0.867125	1		
	1 h	0.0707736	0.059295	0.837812	0.966195		
	2 h	0.0677899	0.109034	1.608415	1.854882		
	3 h	0.0689851	0.105297	1.526377	1.760273		

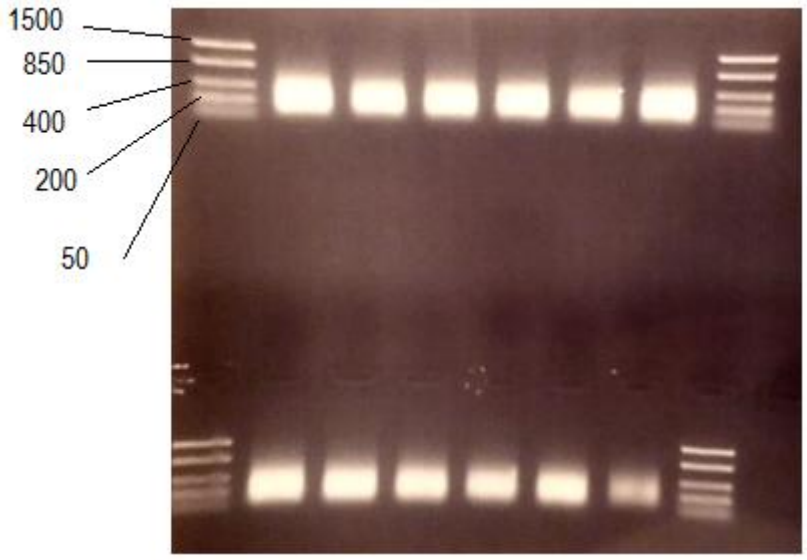

Figure 1: Typical agarose gel electrophoresis studies demonstrating DNA samples fragment length following sonication. 1.2% agarose gel used

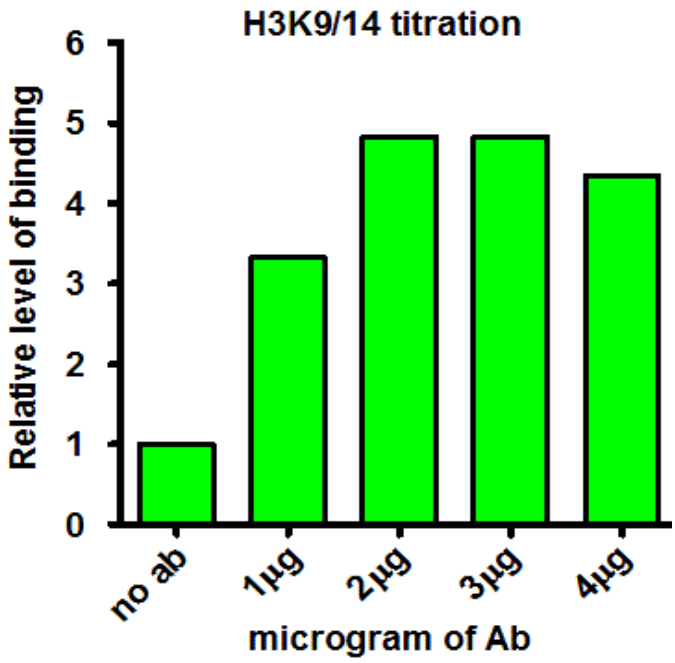

Figure 2: titration for anti H3K9/K14 antibody using 0 to 4 µg .

Appendix- IV

Raw data and supplementary figures for chapter 4

H3 acetylation appendix in GCN5 Myc strains (WT, *rad14Δ* and *rad7Δ*)

		SQ Mean					
H3K9/K14 acetyl in WT-Gcn5 myc	Time Point	Input	IP	IP/Input	Fold change	Average	St Dev
Exp1	No UV	0.00104	0.00126	1.211538	1	1	0
	zero	0.000938	0.00109	1.162047	0.959	1.24	0.28
	1h	0.000949	0.00261	2.750263	2.27	2.19	0.167
	2h	0.000875	0.001929	2.204571	1.819	1.64	0.279
	3h	0.000985	0.00156	1.583756	1.307	1.39	0.122
Exp2	No UV	0.00113	0.00247	2.185841	1		
	zero	0.00108	0.003594	3.327407	1.522		
	1h	0.000983	0.004302	4.376501	2.002		
	2h	0.001071	0.00418	3.902894	1.786		
	3h	0.000876	0.002835	3.236301	1.48		
Exp3	No UV	0.000952	0.00207	2.17437	1		
	zero	0.00101	0.002747	2.719802	1.25		
	1h	0.00103	0.005182	5.031068	2.31		
	2h	0.000898	0.00259	2.884187	1.32		
	3h						

		SQ Mean					
H3K9/K14 rad14Δ-Gcn5-myc	Time Point	Input	IP	IP/Input	Fold change	Average	St Dev
Exp1	No UV	0.00115	0.021629	18.807947	1	1	0
	Zero	0.00123	0.017192	13.977053	0.74	1.08	0.464
	1h	0.00103	0.046366	45.015994	2.39	2.610	0.471
	2h	0.000985	0.053734	54.552187	2.90	2.311	0.621
	3h	0.00097	0.049292	50.816966	2.70	2.437	0.374
Exp2	No UV	0.00107	0.001999	1.8686132	1		
	Zero	0.00112	0.001463	1.3062746	0.699		
	1h	0.00118	0.006564	5.5627454	2.977		
	2h	0.00124	0.004172	3.3642922	1.8		
	3h	0.00101	0.0041	4.059270	2.17		

Exp3	No UV	0.00983	0.00318	0.3234995	1		
	zero	0.00101	0.000553	0.5474808	1.69		
	1h	0.00898	0.005952	0.6627948	2.05		
	2h	0.00994	0.005628	0.5661946	1.75		
Exp4	No UV	0.082	0.0411	0.5012195	1		
	zero	0.0539	0.032397	0.6010534	1.2		
	1h	0.0694	0.105115	1.5146312	3.02		
	2h	0.0903	0.126491	1.4007913	2.79		

		SQ Mean					
H3K9/K14 acetyl in rad7Δ-Gcn5-myc	Time Point	Input	IP	IP/Input	Fold change	Average	St Dev
Exp1	No UV	0.00867	0.0389	4.486736	1	2.26	3.145
	zero	0.01061	0.052612476	4.958763	1.1	2.505	3.47
	1h	0.00963	0.044564235	4.627646	1.03	2.34	3.24
	2h	0.0103	0.0416005	4.038883	0.9	2.04	2.8
	3h	0.00795	0.030078385	3.783445	0.84	1.9	
Exp2	No UV	0.0127	0.063758307	5.020339	1		
	zero	0.011	0.071951494	6.541045	1.303		
	1h	0.0134	0.099705914	7.44074	1.482		
	2h	0.00939	0.060604778	6.454183	1.285		
	3h						

Gcn5 binding at *MFA2* in wild-type							
		SQ Mean					
WT	**Time**	**Input**	**IP**	**IP/Input**	**Fold**	**Average**	**St**
Exp1	No UV	0.000962	0.000577	0.599792	1	1	0
	zero					0.97	0.22
	1h	0.000815	0.000689	0.845399	1.409486	2.27	1.06
	2h	0.000981	0.000317	0.32314	0.538753	1.59	0.81
	3h	0.000685	0.000366	0.534307	0.89082	1.18	0.41
Exp2	No UV	0.00103	0.000475	0.461165	1		
	zero	0.000977	0.000336	0.34391	0.745742		
	1h	0.00104	0.000847	0.814423	1.766012		
	2h	0.00114	0.000531	0.465789	1.010028		

Exp3	No UV	0.00102	0.000222	0.217647	1		
	zero	0.000756	0.000196	0.259259	1.191191		
	1h	0.000922	0.000725	0.786334	3.612886		
	2h	0.000757	0.000396	0.523118	2.403513		
E xp4	U	0.00147	0.00133	0.904762	1		
	zero						
	1h	0.000734	0.00117	1.594005	1.761795		
	2h	0.00105	0.000786	0.748571	0.827368		
	No UV	0.00104	0.00126	1.211538	1		
	zero	0.000914	0.00108	1.181619	0.975305		
	1h	0.000948	0.00277	2.921941	2.411761		
	2h	0.000875	0.00214	2.445714	2.018685		
	3h	0.000979	0.00175	1.787538	1.475428		
	No UV	0.000454	0.00117	0.388034	1		
	zero						
	1h	0.00125	0.000844	1.481043	3.816784		
	2h	0.000373	0.000362	1.030387	2.655402		
	No UV	0.00106	0.000564	0.532075	1		
	zero						
	1h	0.000951	0.000565	0.594111	1.116592		
	2h	0.000771	0.000692	0.897536	1.686858		

Gcn5 binding at MFA2 in *rad7Δ*							
rad7Δ		**SQ Mean**					
	Time	**Input**	**IP**	**IP/Input**	**Fold**	**Average**	**St**
Exp1	No	0.00115	0.000538	0.467826	1	1	0
	Zero	0.000828	0.000624	0.753623	1.610905	1.345	0.376
	1h	0.00108	0.000625	0.578704	1.237006	1.36	0.124
	2h	0.0007	0.000397	0.567143	1.212294	1.24	0.117
Exp2	No	0.00107	0.000918	0.857944	1		
	zero	0.000515	0.000476	0.924271845	1.07876		
	1h	0.000459	0.000536	1.167756	1.36111		
	2h	0.000584	0.00057	0.976027	1.137635		
Exp3	No	0.001	0.000791	0.791	1		
	zero						
	1h	0.000627	0.000736	1.173844	1.484		
	2h	0.000634	0.000686	1.082019	1.367913		

Gcn5 binding at MFA2 in *rad14Δ*							
		SQ Mean					
rad14Δ	**Time**	**Input**	**IP**	**IP/Input**	**Fold**	**Average**	**St**
Exp1	No UV	0.0012	0.000944	0.786667	1	1	0
	zero	0.000857	0.000408	0.476079		1.38	0.30
	1h	0.00101	0.00243	2.405941	3.058399	2.02	0.64
	2h	0.000918	0.0016	1.742919	2.215575	2.15	0.32
	3h	0.00104	0.00264	2.538462	3.226858	2.64	0.51
Exp2	No UV	0.00108	0.000343	0.317593	1		
	zero	0.00101	0.000539	0.533366	1.679404		
	1h	0.00106	0.000574	0.541509	1.705044		
	2h	0.000867	0.000598	0.689735	2.171759		
	3h						
Exp3	No UV	0.00105	0.000234	0.222857	1		
	Zero	0.000782	0.000188	0.240409	1.078759		
	1h	0.000793	0.000321	0.404792	1.816374		
	2h	0.000996	0.00049	0.491968	2.207548		
	3h	0.000791	0.000398	0.503161	2.257772		
Exp4	No UV	0.000876	0.000375	0.428082	1		
	zero						
	1h	0.00064	0.00044	0.6875	1.606		
	2h	0.00079	0.000537	0.679747	1.587889		
	3h	0.000781	0.000815	1.043534	2.437695		
Exp5	No UV	0.00129	0.000461	0.357364	1		
	zero	0.00106	0.000529	0.499057	1.396492		
	1h	0.00118	0.000584	0.494915	1.384904		
	2h	0.0011	0.00083	0.754545	2.111418		
	3h						
	No UV	0.000882	0.000424	0.480726	1		
	zero						
	1h	0.000501	0.000617	1.231537	2.561829		
	2h	0.000487	0.000609	1.250513	2.601304		
	3h						

Rad7 and Rad16 bindings at MFA2

Rad7 binding at MFA2 in wild-type							
		SQ Mean					
	Time	**IP**	**INput**	**IP/Input**	**Fold**	**Average**	**St Dev**
Exp1		IP	IN	IP/IN	Ratio		
	U	0.0000742	0.0000545	1.361468	1	1	0
	Zero	0.000141	0.0000462	3.051948	2.24166	1.97	0.36
	15 m	0.000116	0.0000691	1.678726	1.233027	1.24	0.156
	30 m	0.000108	0.0000769	1.404421	1.031549	1.19	0.26
Exp2	No UV	0.00838	0.000895	9.363128	1		
	Zero	0.00472	0.000198	23.83838	2.545985		
	15 m	0.00883	0.00066	13.37879	1.42888		
	30 m	0.0097	0.00072	13.47222	1.438859		
Exp3	No UV	0.000264	0.000871	0.3031	1		
	Zero	0.000338	0.000649	0.520801	1.71825		
	30 m	0.000311	0.00098	0.317347	1.047004		
E xp4	No UV	26900	84200	0.319477	1		
	Zero	31000	55000	0.563636	1.764245		
	15 m						
	30 m	66000	150000	0.44	1.377249		
E xp5	No UV	0.0237	0.0803	0.295143	1		
	Zero	0.0295	0.0632	0.466772	1.581511		
	15 m	0.052	0.142	0.366197	1.240744		
	30 m						
E xp5	No UV	0.00116	0.000102	0.087931	1		
	Zero	0.00101	0.000173	0.171287	1.947971		
	15 m						
	30 m	0.000671	5.36E-05	0.079881	0.908448		

Rad7 binding at MFA2 in *rad14Δ*							
		SQ Mean					
rad14Δ	**Time**	**INput**	**IP**	**IP/Input**	**Fold**	**Average**	**St**
Exp1	No UV	0.000369	0.00356	9.647696	1	1	0
	Zero	0.000312	0.00498	15.96154	1.65	1.69	0.26
	15 m					1.48	0.22
	30 m	0.000679	0.00835	12.2975	1.27	1.92	0.54
Exp2	No UV	0.0000792	U	0.000078	1		
	Zero	0.000133	Zero	0.000083	1.565		
	15 m	0.000127	15 m	0.000085	1.46		
	30 m	0.000135	30 m	0.00006	2.215		
Exp3	No UV	0.000091	0.000101	1.10989	1		
	Zero	0.0000558	0.000132	2.365591	2.131374		
	15 m	0.0000648	0.000123	1.898148	1.710213		
	30 m	0.0000492	0.000143	2.906504	2.618731		
E xp4	No UV	0.00107	0.000246	0.229907	1		
	Zero	0.000875	0.000331	0.378286	1.6453890		
	15 m						
	30 m	0.00109	0.00038	0.348624	1.5163720		
	No UV				1		
	Zero				1.457014		
	15 m				1.270885		
	30 m				2.003102		

Rad16 binding at *MFA2* in wild-type & *rad14Δ*							
Rad16		**SQ Mean**					
	Time	**Input**	**IP**	**IP/Input**	**Fold**	**Average**	**St Dev**
WT						1	0
	No UV	0.107	0.00899	0.084019	1	3.09	0.89
	Zero	0.106	0.019	0.179245	2.133398	1.70	0.09
	15m	0.104	0.0149	0.143269	1.705207	2.44	0.42
	30m	0.0843	0.0139	0.164887	1.962507	1.64	0.37
	60m	0.107	0.0112	0.104673	1.245829		
	No UV	0.0979	0.00479	0.048927	1		
	Zero	0.0838	0.0159	0.189737	3.877933		
	15m	0.0938	0.00825	0.087953	1.797622		
	30m	0.095	0.0121	0.127368	2.603208		
	60m	0.0891	0.0086	0.096521	1.972731		
	No UV	0.11	0.00253	0.023	1		
	Zero	0.0958	0.00724	0.075574	3.285831		
	15m	0.1	0.00371	0.0371	1.613043		
	30m	0.0912	0.00579	0.063487	2.760297		
	60m	0.121	0.00479	0.039587	1.721164		
rad14Δ						**Average**	**St Dev**
	No UV	0.118	0.00837	0.070932	1	1	0
	Zero	0.131	0.0191	0.145802	2.055505	1.87	0.31
	15m	0.106	0.0143	0.134906	1.901896	1.83	0.53
	30m	0.101	0.0163	0.161386	2.275217	2.13	0.34
	60m	0.0969	0.0141	0.145511	2.051407	2.34	0.32
	No UV	0.106	0.00431	0.04066	1		
	Zero	0.101	0.00843	0.083465	2.052744		
	15m	0.102	0.00965	0.094608	2.326782		
	30m	0.095	0.00919	0.096737	2.379143		
	60m	0.0895	0.00981	0.109609	2.695719		
	No UV	0.108	0.00288	0.026667	1		
	Zero	0.0898	0.00363	0.040423	1.515869		
	15m	0.104	0.00349	0.033558	1.258413		
	30m	0.107	0.00496	0.046355	1.738318		
	60m	0.0728	0.00445	0.061126	2.292239		

Rpd3 and Hda1 binding at different loci

Rpd3 binding at *MFA2* in wild-type & *rad14Δ*							
		SQ Mean					
Rpd3	**Time**	**INput**	**IP**	**IP/Input**	**Fold**	**Average**	**St Dev**
WT						1	0
	No UV	0.11825752	0.0718	0.607	1	0.457	0.16
	1h	0.16718669	0.0397	0.2375	0.391	0.819	0.26
	3h	0.08706877	0.0477	0.5487	0.90		
	No UV	0.0646	0.0371	0.574303	1		
	1h	0.106	0.0444	0.418868	0.72935		
	3h	0.0229	0.0163	0.71179	1.239398		
	No UV	0.0512	0.0973	1.9003906	1		
	1h	0.104	0.0809	0.7778846	0.409329		
	3h	0.0312	0.0399	1.2788461	0.672939		
	No UV	0.133	1.67	12.556391	1		
	1h	0.368	1.35	3.6684782	0.29216		
	3h	0.0923	0.66	7.1505958	0.569479		
	No UV	0.0967	0.0483	0.499483	1		
	1h	0.134	0.0311	0.23209	0.46466		
	3h	0.0516	0.0184	0.356589	0.713917		
rad14Δ						**Averag**	**St Dev**
	No UV	0.0471	0.1	0.471	1	1	0
	1h	0.0164	0.0691	0.237337	0.503901	0.4850	0.20
	3h	0.0212	0.111	0.190991	0.405501	0.3556	0.11
	No UV	0.0268	0.0953	0.281217	1		
	1h	0.0111	0.0606	0.183168	0.651341		
	3h	0.0142	0.106	0.133962	0.476366		
	No UV	0.0435	0.103	0.42233	1		
	1h	0.0239	0.0952	0.25105	0.594441		
	3h	0.011	0.0803	0.136986	0.324358		
	No UV	0.0714	0.0533	0.746499	1		
	1h	0.116	0.0165	0.142241	0.190545		
	3h	0.0793	0.0128	0.161412	0.216226		

Hda1 binding at *MFA2* in wild-type & *rad14Δ*							
		SQ Mean					
Hda1	**Time**	**INput**	**IP**	**IP/Input**	**Fold**	**Average**	**St**
WT						1	0
	No	0.11825752	0.07186154	0.60766997	1	0.512	0.15
	1h	0.16718669	0.03971822	0.23756805	0.390949	0.985	0.25
	3h	0.10465445	0.04777955	0.45654581	0.751306		
	No	0.103	0.0581	0.564078	1		
	1h	0.129	0.0532	0.412403	0.73111		
	3h	0.0335	0.0254	0.758209	1.344157		
	No	0.0458	0.0808	1.76419214	1		
	1h	0.0882	0.0744	0.84353741	0.478144		
	3h	0.0386	0.0633	1.63989637	0.929545		
	No	0.117	1.25	10.6837607	1		
	1h	0.329	1.58	4.80243161	0.449508		
	3h	0.0863	0.845	9.79142526	0.916477		
rad14Δ						**Average**	**St**
	No	0.129	0.165	1.27907	1	1	0
	1h	0.106	0.0793	0.748113	0.584889	0.476	0.21
	3h	0.102	0.0321	0.314706	0.246043	0.357	0.17
	No	0.0671	0.133	0.504511	1		
	1h	0.0192	0.0623	0.308186	0.610861		
	3h	0.0262	0.0932	0.281116	0.557204		
	No	0.0353	0.0699	0.505007	1		
	1h	0.0127	0.108	0.117593	0.232853		
	3h	0.0119	0.0876	0.135845	0.268996		

Rpd3 binding at *HML* in wild-type & *rad14Δ*							
		SQ Mean					
	Time	**INput**	**IP**	**IP/Input**	**Fold**	**Average**	**St Dev**
WT							
Exp1	No UV	0.127773	0.04179043	0.327069	1	1	0
	1h	0.127129	0.02118544	0.166646	0.509512	0.55	0.192
	3h	0.064484	0.03423951	0.530978	1.623445	1.428	0.476
Exp2	No UV	0.0605	0.0173	0.28595	1		
	1h	0.111	0.0264	0.237838	0.831745		
	3h	0.0187	0.0104	0.55615	1.944917		
Exp3	No UV	0.291	1.03	3.539519	1		
	1h	0.0967	0.133	1.375388	0.38858		
	3h	0.117	0.54	4.615385	1.303958		
Exp4	No UV	0.0542	0.0648	1.195572	1		
	1h	0.0973	0.057	0.585817	0.489989		
	3h	0.0266	0.0267	1.003759	0.839564		
rad14Δ						**Average**	**ST Dev**
Exp1	No UV	0.0734	0.0368	0.501362	1	1	0
	1h	0.0984	0.0114	0.115854	0.231078	0.3280	0.137
	3h	0.113	0.0118	0.104425	0.208282	0.2878	0.112
Exp2	No UV	0.283	1.55	5.477032	1		
	1h	0.125	0.291	2.328	0.425048		
	3h	0.249	0.501	2.012048	0.367361		

Hda1 binding at *HML* in wild-type & *rad14Δ*							
		SQ Mean					
	Time	**INput**	**IP**	**IP/Input**	**Fold**	**Average**	**St Dev**
WT	No UV	0.214	1.49	6.962617	1	1	0
Exp1	1h	0.664	1.92	2.891566	0.415299	0.56	0.180
	3h	0.134	1.05	7.835821	1.125413	1.11	0.400
Exp2	No UV	0.0777	0.0286	0.368082	1		
	1h	0.11	0.0364	0.330909	0.899008		
	3h	0.028	0.0183	0.653571	1.775612		
Exp3	No UV	0.0446	0.0495	1.109865	1		
	1h	0.0809	0.0488	0.603214	0.543502		
	3h	0.0378	0.0453	1.198413	1.079782		
Exp4	No UV	0.251	0.957	3.812749	1		
	1h	0.696	1.51	2.16954	0569023		
	3h	0.212	0.851	4.014151	1.05		
Exp5	No UV	0.0989	0.145	1.466127	1		
	1h	0.0978	0.0577	0.58998	0.402407		
	3h	0.0654	0.0493	0.753823	0.514159		
rad14Δ						**Average**	**ST Dev**
	No UV	0.147	0.138	0.938776	1	1	0
	1h	0.114	0.0594	0.521053	0.555034	0.476	0.112
	3h	0.116	0.0365	0.314655	0.335176	0.348	0.019
	No UV	0.308	2.091	6.788961	1		
	1h	0.618	1.669	2.700647	0.3978		
	3h	0.757	1.863	2.46103	0.362505		

Rpd3 binding at *Rad23* in wild-type and rad14Δ

		SQ Mean					
	Time	**INput**	**IP**	**IP/Input**	**Fold**	**Average**	**St Dev**
WT						1	0
Exp1	No UV	0.0835	0.0496	1.683468	1	0.39	0.0556
	1h	0.0606	0.11	0.550909	0.327247	0.62858	0.0517
	3h	0.0334	0.0338	0.988166	0.586982		
Exp2	No UV	1.89	0.285	6.631579	1		
	1h	0.591	1.69	2.85956	0.431204		
	3h	0.739	0.182	4.06044	0.612289		
Expe3	No UV	0.0991	0.0424	0.427851	1		
	1h	0.121	0.0214	0.1768	0.414		
	3h	0.0572	0.0168	0.2937	0.686469		
rad14Δ	No UV	0.0849	0.0445	0.524146	1	1	0
Exp1	1h	0.116	0.0172	0.148276	0.28289	0.4184	0.192
	3h	0.0876	0.0117	0.133562	0.254818	0.3428	0.1245
Exp2	No UV	1	1	1	1		
	1h	0.553936	0.553936	0.553936	0.553936		
	3h	0.430886	0.430886	0.430886	0.430886		

Hda1 binding at *Rad23* in wild-type and rad14Δ

		SQ Mean					
WT	**Time**	**IP**	**INput**	**IP/Input**	**Fold**	**Average**	**St**
	No UV	0.037395	0.0783245	0.477434	1	1	0
	1h	0.014886	0.0711500	0.209223	0.438223	0.41	0.028
	3h	0.031087	0.0417884	0.74391	1.558141	1.2	0.318
	No UV	0.0713	0.0436	1.635321	1		
	1h	0.0519	0.0747	0.694779	0.424858		
	3h	0.0536	0.0347	1.544669	0.944566		
	No UV	0.201	6.567164	71.73913	1		
	1h	0.679	2.518409	27.51089	0.383485		
	3h	0.156	7.24359	79.12834	1.103001		
rad14Δ	No UV	0.06062	0.1197	0.506433	1	1	0
	1h	0.02542	0.08704	0.29205	0.57668	0.502	0.104
	3h	0.01706	0.07049	0.24202	0.477892	0.439	0.054
	No UV	0.103	0.05145	0.499515	1		
	1h	0.097	0.0208	0.214433	0.4292828		
	3h	0.0893	0.0179	0.200448	0.4012855		

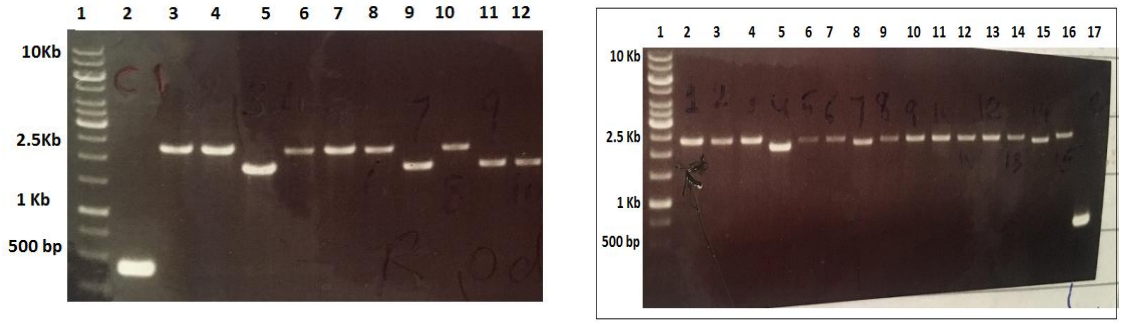

A-Rpd3-Myc B- Hda1-Myc

Figure 1: colony PCR for (A) WT-Rpd3-Myc and (B) WT-Hda1-Myc. Primers were designed for Tagging 18 copies of Myc epitope. A. Tagging of MYc genes is confirmed in lane 3, 4, 6, 7, 8 and 10 for Rpd3, lane 1 is WT untagged sample with the same set of primers used to tag Rpd3. B. Tagging of Hda1 with 18 copies of Myc was observed in all lanes except lane 5 (less than 18 copies). Lane 17 is untagged control using same primers as were used for Hda1.

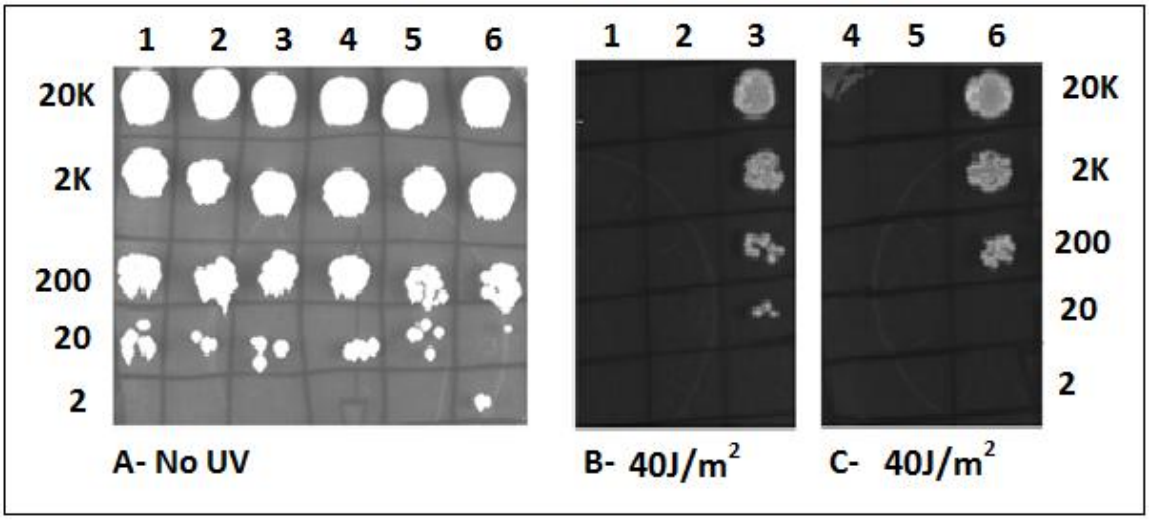

Figurer 2. UV sensitivity assay (drop test) of the both wild type Rpd3 and Hda1 Myc tagged strains with their isogenic *Rad14* deleted strains: (A) WT-Rpd3-Myc lane 3, WT-Hda1-Myc lane 6, rad14Δ-Rpd3-Myc lane 1 and 2 and rad14Δ-Hda1-Myc lane 4 and 5. The strains were grown to exponential phase and diluted with serial dilution (starting from 20000 cells/µL to 2 cells/µL). (A) No UV in which none of the strains were exposed to UV. (B) and (C) strains were exposed to 40J/M2. (B) WT-Rpd3-Myc lane 3 and rad14Δ-Rpd3-Myc lane 1 and 2. (c) shows WT-Hda1-Myc lane 6 and rad14Δ-Hda1-Myc lane 4 and 5.

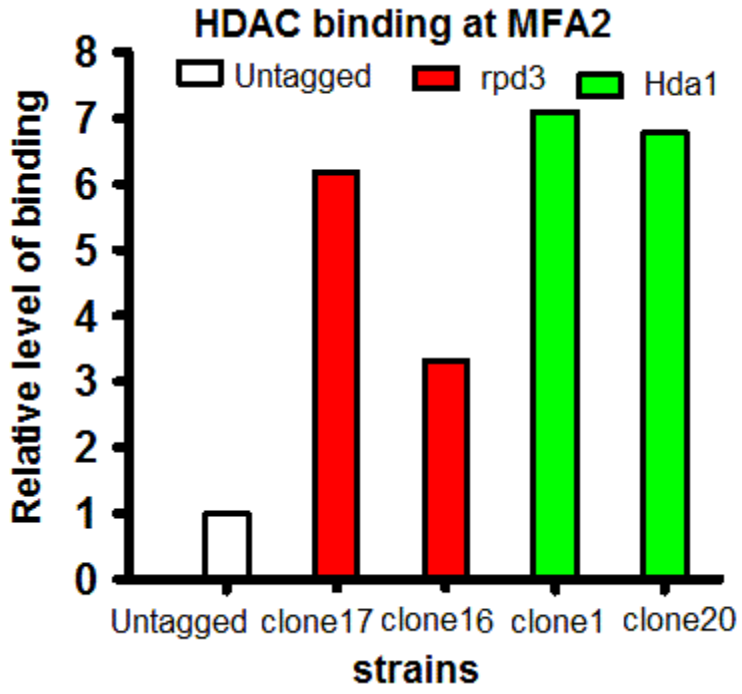

Figure 3: selecting transformed clones.

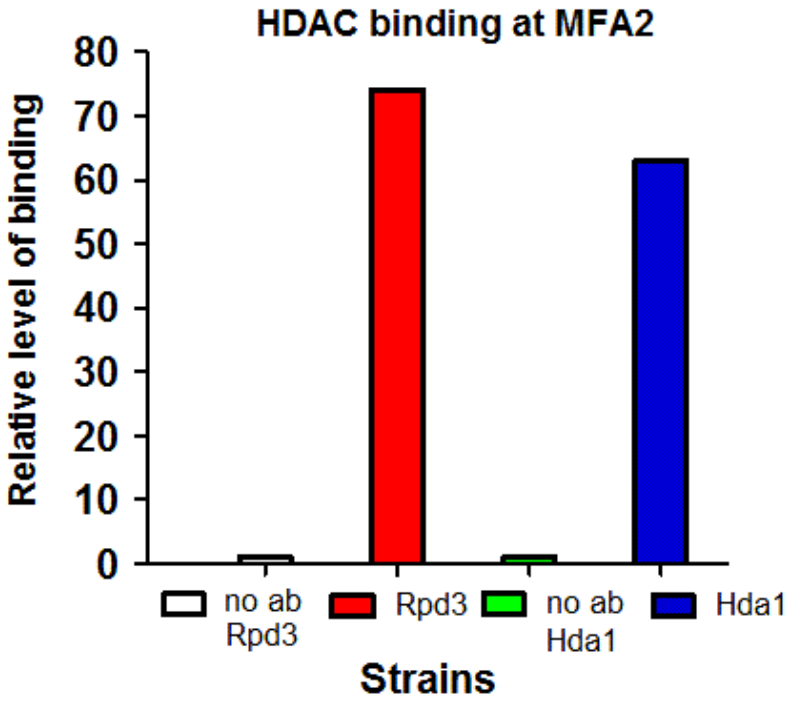

Figure 4:No antibody (no coloured for Rpd3 and green coloured for Hda1) or 2µg of anti-myc antibody used in (red coloured for Rpd3 and blue coloured for Hda1).

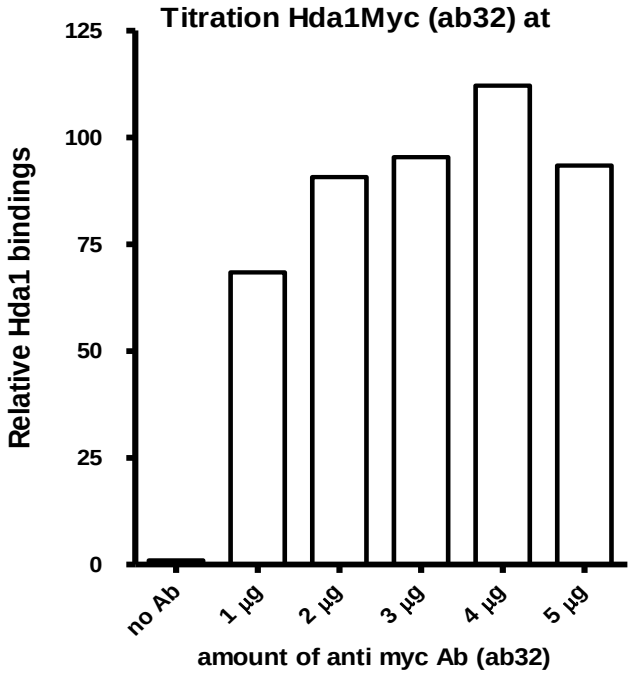

Figure 5:Titration of anti myc antibody.

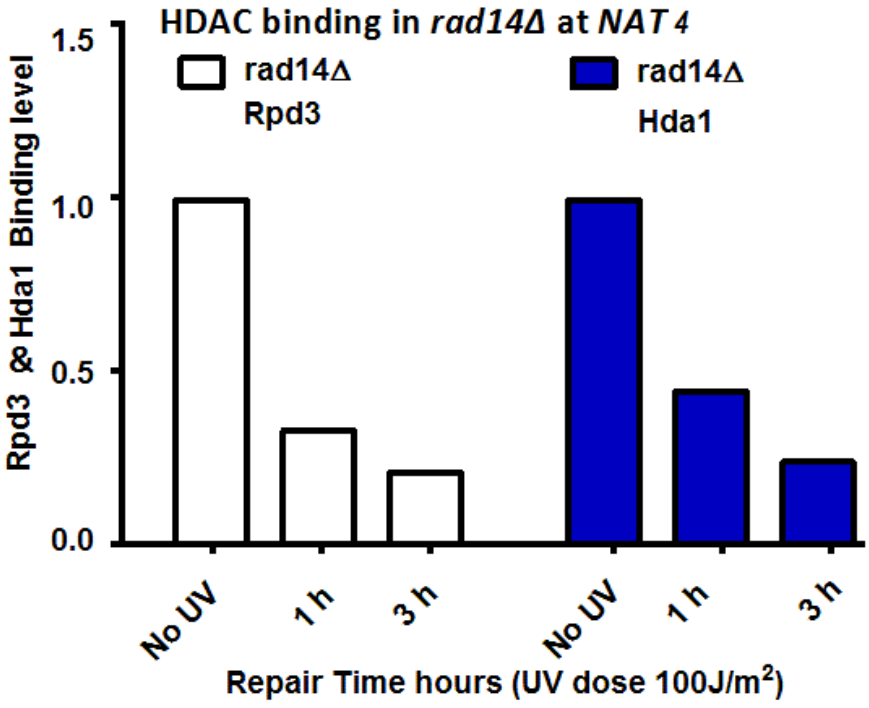

Figure 6: HDAC occupancy (Rpd3 or Hda1) at *NAT4* loci in *rad14Δ*

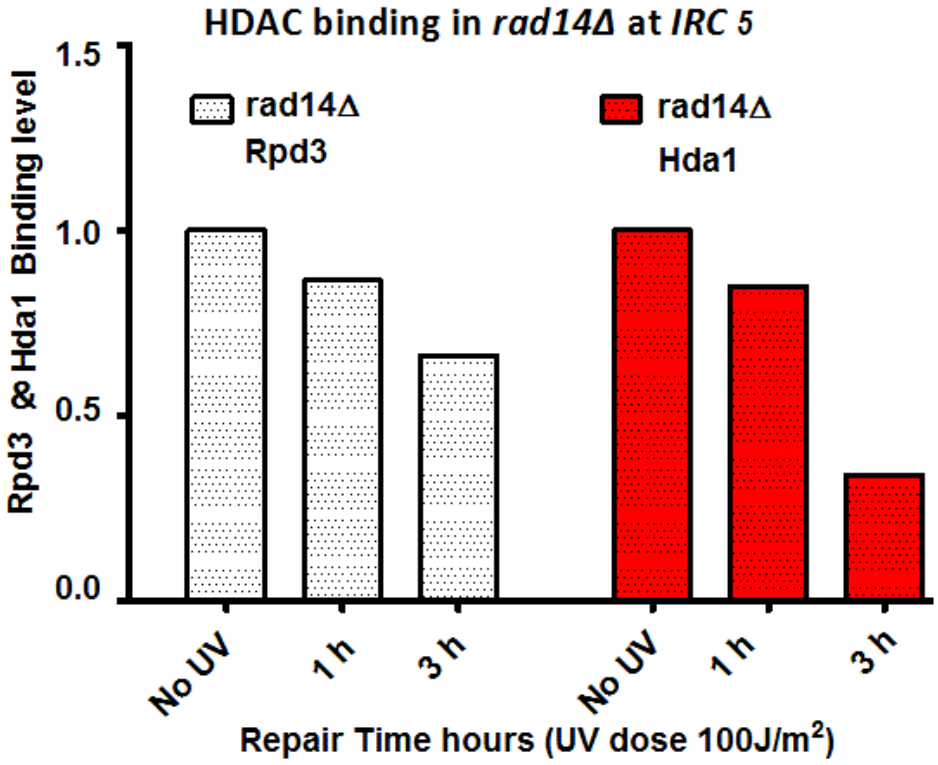

Figure 7: HDAC occupancy (Rpd3 or Hda1) at *IRC5* loci in *rad14Δ*

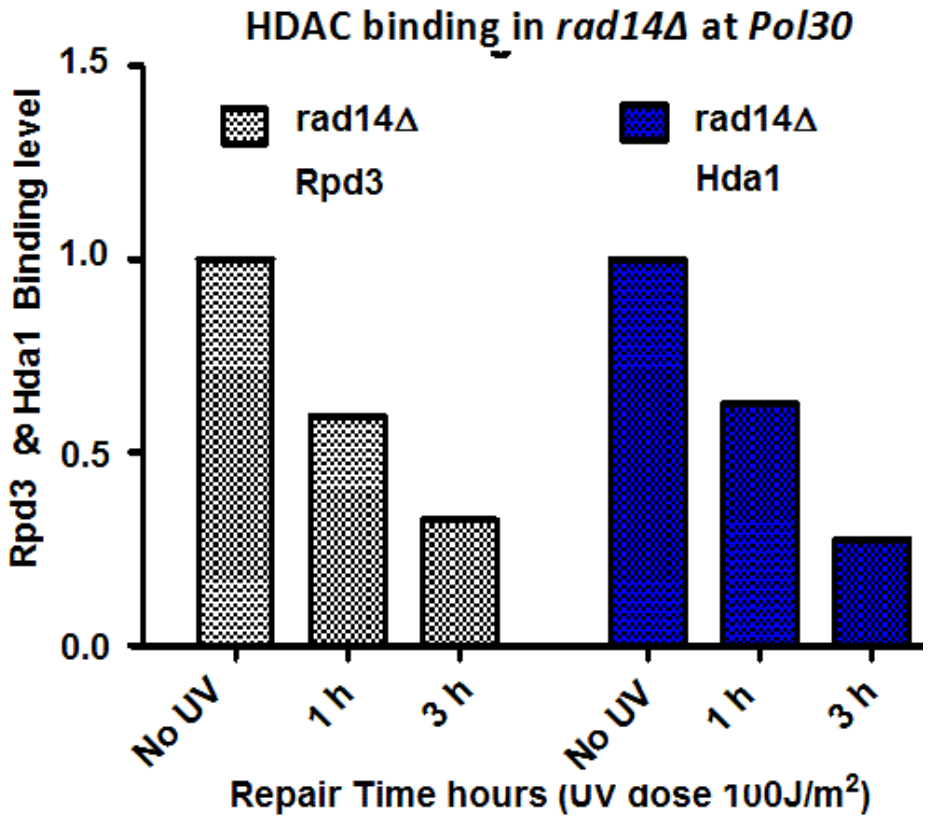

Figure 8: HDAC occupancy (Rpd3 or Hda1) at *POL30* loci in *rad14Δ*

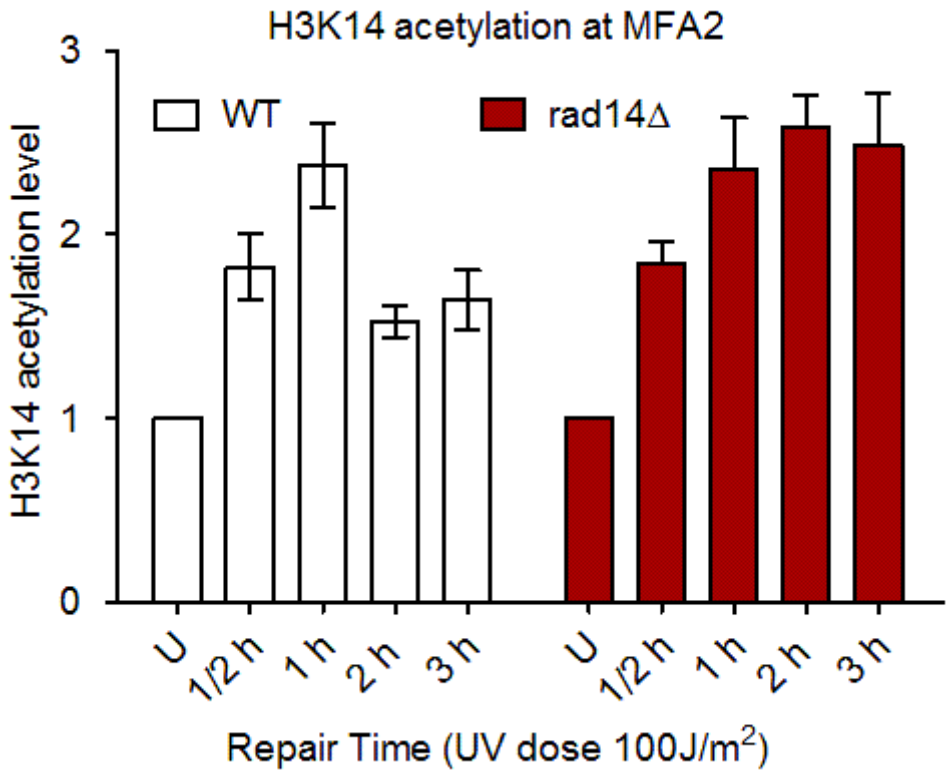

Figure 9. Rad16 binding (GG-NER factor) at MFA2 in WT and *rad14Δ* befor UV irradiation and at different repair points (3 independent biological experiments)

Appendix- V

Appendix- 195 **Raw data and supplementary figures for chapter 5**

Normalisation assumptions for **Rpd3** before UV exposure

(First dataset and second dataset are - (Rpd3) before UV irradiate)

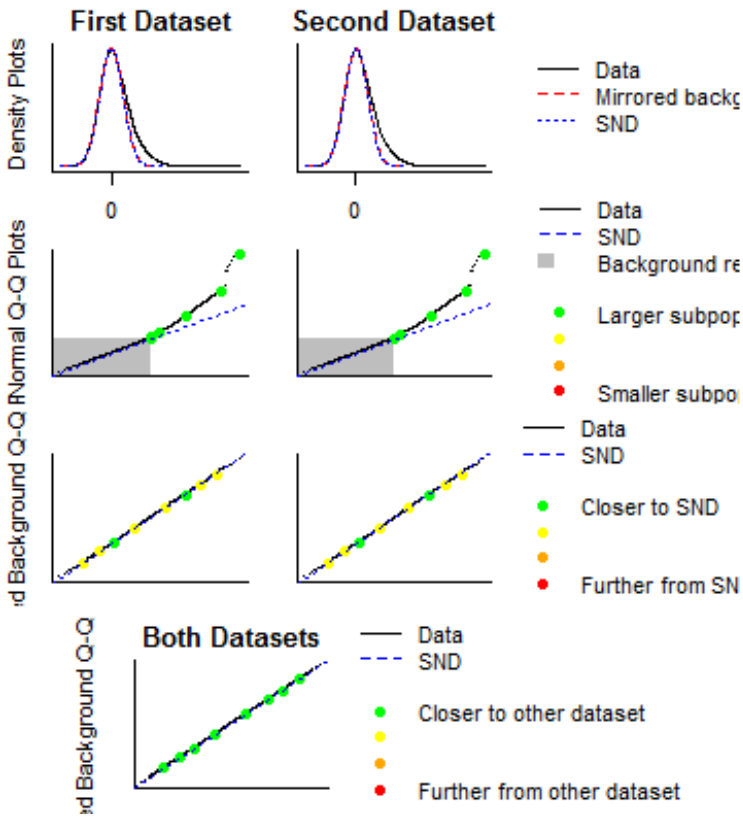

Normalisation assumptions for **Rpd3** before UV exposure

(First dataset and second dataset are Rpd3 before UV irradiate)

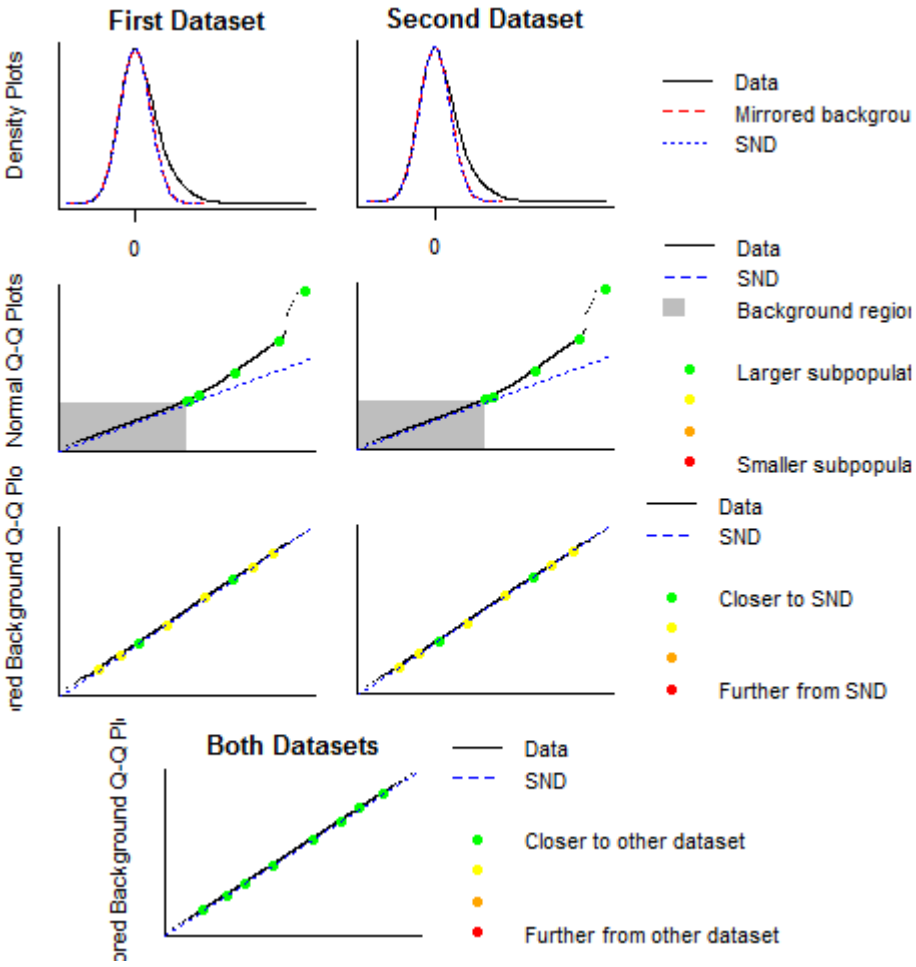


```
Pearson's product-moment correlation of Un-irradiated Rpd3

data: Rpd3.n$ratios[, 1] and Rpd3.n$ratios[, 2]
t = 278.47, df = 41446, p-value < 2.2e-16
alternative hypothesis: true correlation is not equal to 0
95 percent confidence interval:
 0.8038941 0.8106010
sample estimates:
      cor
0.8072736
```

Normalisation assumptions for **Rpd3** one h after UV exposure

(First dataset and second dataset are Rpd3 one h following UV irradiation)

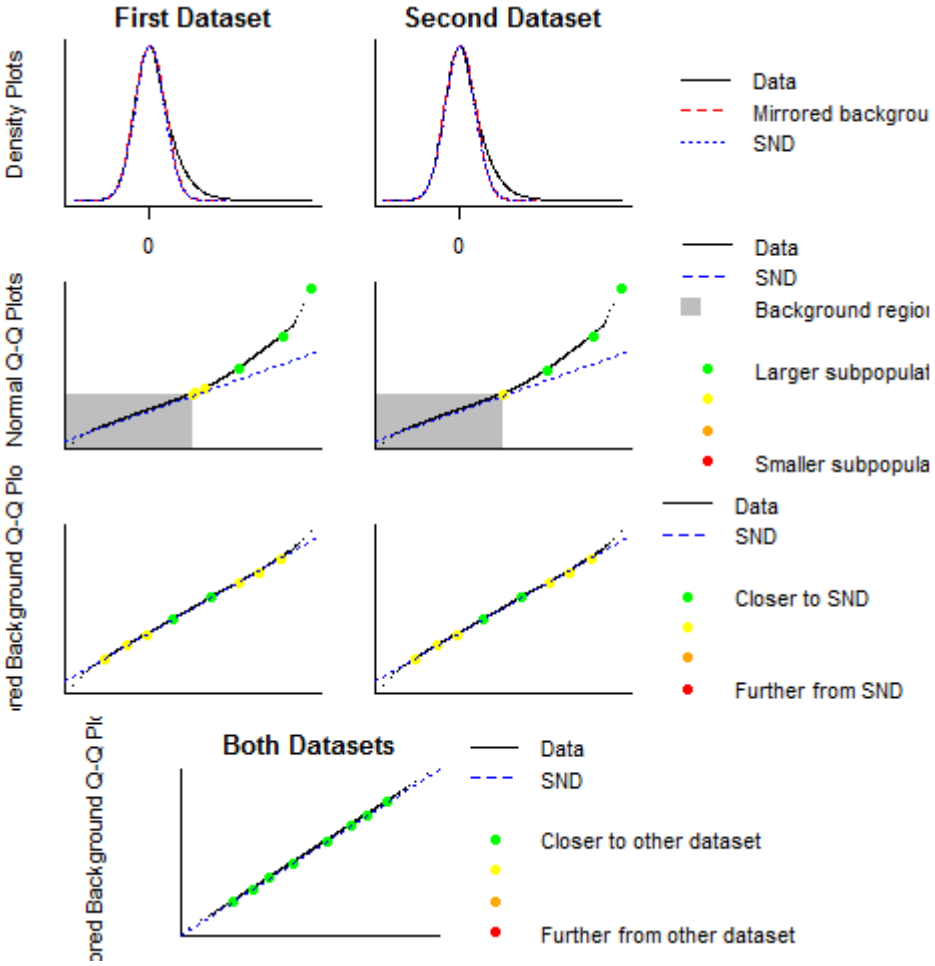

Pearson's product-moment correlation of Rpd3 1 h following UV irradiation

```
data: Rpd3.n$ratios[, 3] and Rpd3.n$ratios[, 4]
t = 131.9, df = 41446, p-value < 2.2e-16
alternative hypothesis: true correlation is not equal to 0
95 percent confidence interval:
 0.5369191 0.5504813
sample estimates:
      cor
0.5437357
```

Normalisation assumptions for Rpd3 three hours following UV exposure

First dataset and second dataset are Rpd3 three h after UV irradiation)

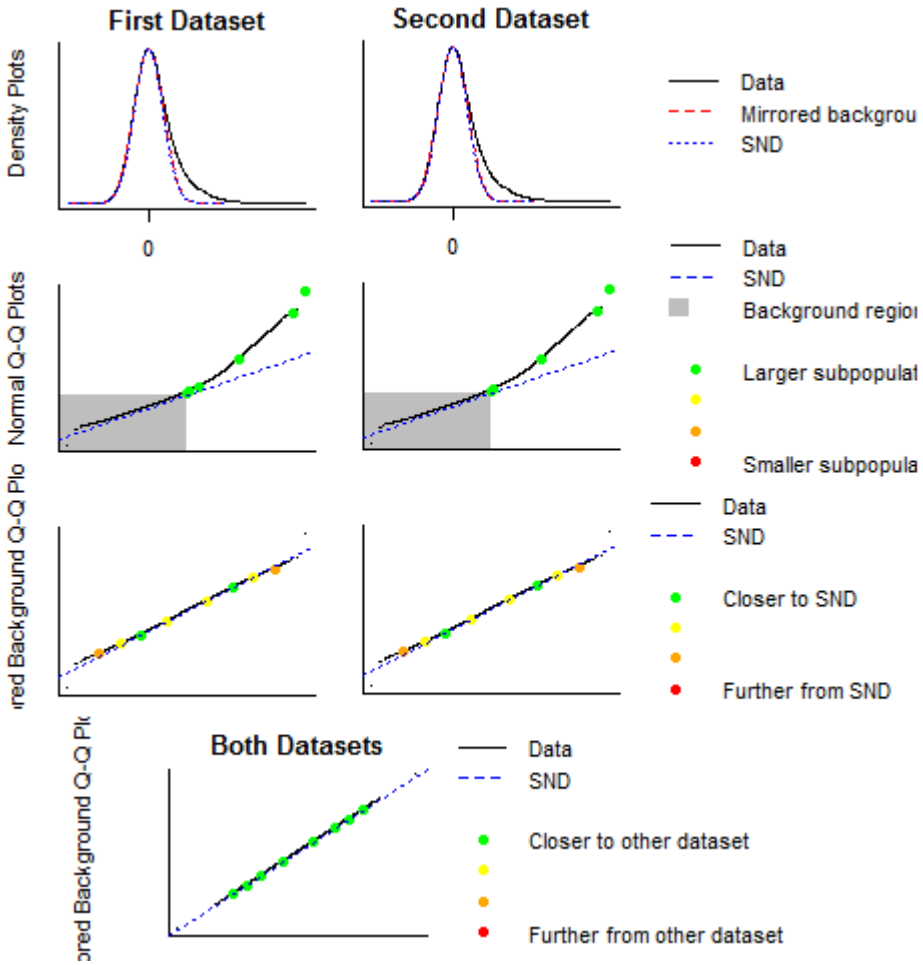

Pearson's product-moment correlation **Rpd3 3 h following UV irradiation**

```
data:  Rpd3.n$ratios[, 5] and Rpd3.n$ratios[, 6]
t = 224.57, df = 41446, p-value < 2.2e-16
alternative hypothesis: true correlation is not equal to 0
95 percent confidence interval:
 0.7365014 0.7451875
sample estimates:
      cor
0.7408754
```

Normalisation assumptions for Hda1 before UV exposure

(First dataset and second dataset are HDA1 Before UV irradiate)

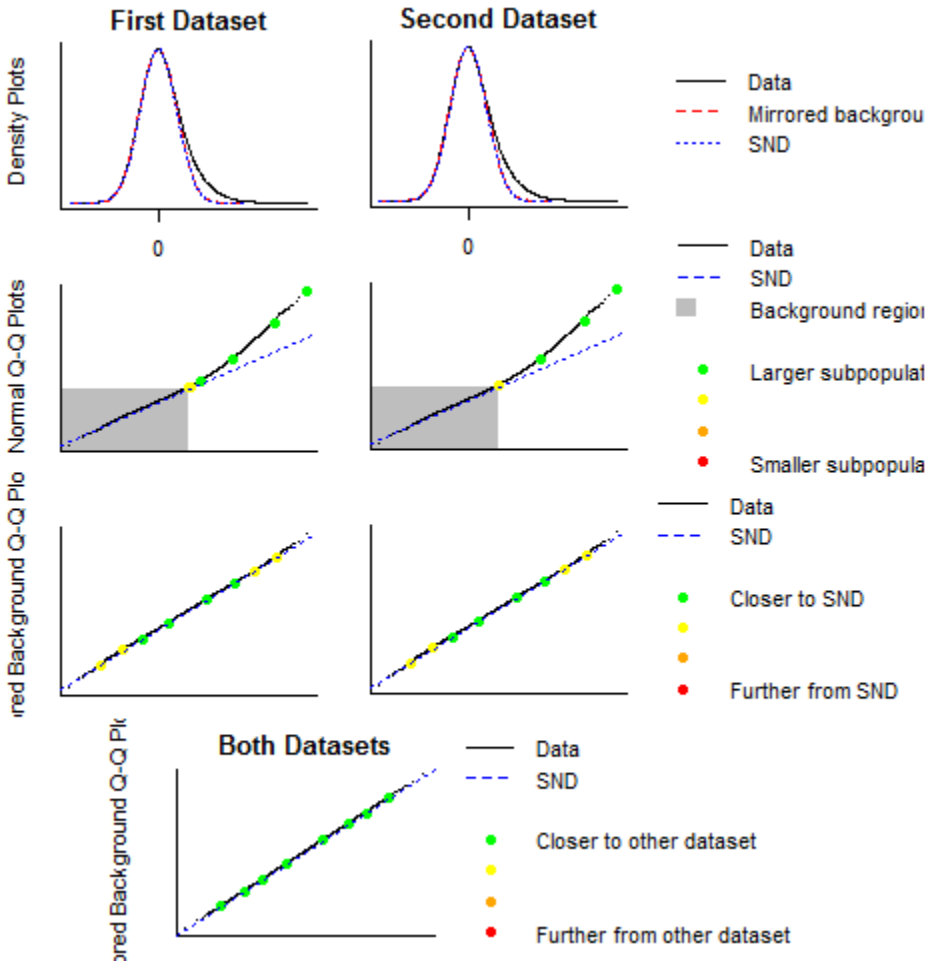

Pearson's product-moment correlation of Un-irradiated Hda1

```
data:  Hda1.n$ratios[, 1] and Hda1.n$ratios[, 2]
t = 146.44, df = 41447, p-value < 2.2e-16
alternative hypothesis: true correlation is not equal to 0
95 percent confidence interval:
 0.5775607 0.5902498
sample estimates:
      cor
0.5839409
```

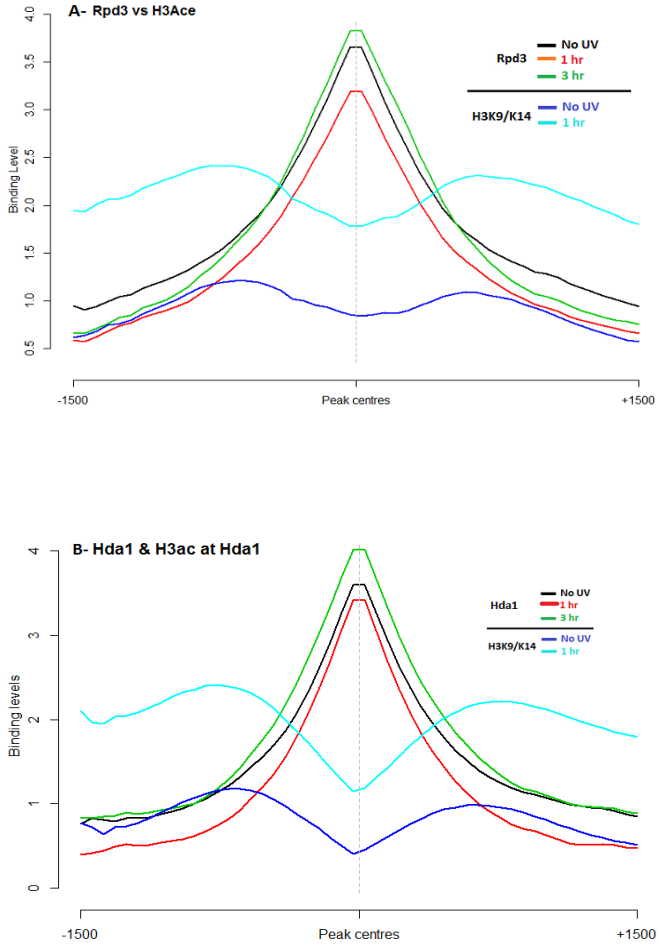

Figure :ChIP-chip data of HDAC occupancy and histone H3K9/K14 acetylation at the HDACs peak center both before and after UV irradiation. Data presented here is simlar to that shown in figure 5.14, the only difference here is that the data was plotted against Rpd3 (A) and Hda1 (B) peak centres.

References

Aaronson, J. S., B. Eckman, R. A. Blevins, J. A. Borkowski, J. Myerson, S. Imran, and K. O. Elliston, 1996, Toward the development of a gene index to the human genome: an assessment of the nature of high-throughput EST sequence data: Genome Res, v. 6, p. 829-45.

Abraham, R. T., 2001, Cell cycle checkpoint signaling through the ATM and ATR kinases: Genes Dev, v. 15, p. 2177-96.

Adam, S., and S. E. Polo, 2012, Chromatin dynamics during nucleotide excision repair: histones on the move: Int J Mol Sci, v. 13, p. 11895-911.

Adam, S., S. E. Polo, and G. Almouzni, 2014, How to restore chromatin structure and function in response to DNA damage--let the chaperones play: delivered on 9 July 2013 at the 38th FEBS Congress in St Petersburg, Russia: Febs j, v. 281, p. 2315-23.

Alarcon-Vargas, D., and Z. Ronai, 2002, p53-Mdm2--the affair that never ends: Carcinogenesis, v. 23, p. 541-7.

Alberts, B., A. Johnson, J. Lewis, M. Raff, K. Roberts, and P. Walter, 2002, Molecular Biology of the Cell.

Alejandro-Osorio, A. L., D. J. Huebert, D. T. Porcaro, M. E. Sonntag, S. Nillasithanukroh, J. L. Will, and A. P. Gasch, 2009, The histone deacetylase Rpd3p is required for transient changes in genomic expression in response to stress: Genome Biol, v. 10, p. R57.

Allfrey, V. G., R. Faulkner, and A. E. Mirsky, 1964, ACETYLATION AND METHYLATION OF HISTONES AND THEIR POSSIBLE ROLE IN THE REGULATION OF RNA SYNTHESIS: Proc Natl Acad Sci U S A, v. 51, p. 786-94.

Andrews, C. A., A. C. Vas, B. Meier, J. F. Giménez-Abián, L. A. Díaz-Martínez, J. Green, S. L. Erickson, K. E. VanderWaal, W. S. Hsu, and D. J. Clarke, 2006, A mitotic topoisomerase II checkpoint in budding yeast is required for genome stability but acts independently of Pds1/securin: Genes Dev, v. 20, p. 1162-74.

Anna, B., Z. Blazej, G. Jacqueline, C. J. Andrew, R. Jeffrey, and S. Andrzej, 2007, Mechanism of UV-related carcinogenesis and its contribution to nevi/melanoma: Expert Rev Dermatol, v. 2, p. 451-69.

Ataian, Y., and J. E. Krebs, 2006, Five repair pathways in one context: chromatin modification during DNA repair: Biochem Cell Biol, v. 84, p. 490-504.

Auffray, C., and F. Rougeon, 1980, Nucleotide sequence of a cloned cDNA corresponding to secreted mu chain of mouse immunoglobulin: Gene, v. 12, p. 77-86.

Avery, O. T., C. M. MacLeod, and M. McCarty, 1944, STUDIES ON THE CHEMICAL NATURE OF THE SUBSTANCE INDUCING TRANSFORMATION OF PNEUMOCOCCAL TYPES : INDUCTION OF TRANSFORMATION BY A DESOXYRIBONUCLEIC ACID FRACTION ISOLATED FROM PNEUMOCOCCUS TYPE III: J Exp Med, v. 79, p. 137-58.

Bakkenist, C. J., and M. B. Kastan, 2003, DNA damage activates ATM through intermolecular autophosphorylation and dimer dissociation: Nature, v. 421, p. 499-506.

Bannister, A. J., and T. Kouzarides, 2011, Regulation of chromatin by histone modifications: Cell Res, v. 21, p. 381-95.

Barnhart, B. J., 1989, The Department of Energy (DOE) Human Genome Initiative: Genomics, v. 5, p. 657-60.

Bartsch, H., and R. Montesano, 1984, Relevance of nitrosamines to human cancer: Carcinogenesis, v. 5, p. 1381-93.

Batista, L. F., B. Kaina, R. Meneghini, and C. F. Menck, 2009, How DNA lesions are turned into powerful killing structures: insights from UV-induced apoptosis: Mutat Res, v. 681, p. 197-208.

Batista, L. F., V. Chigancas, G. Brumatti, G. P. Amarante-Mendes, and C. F. Menck, 2006, Involvement of DNA replication in ultraviolet-induced apoptosis of mammalian cells: Apoptosis, v. 11, p. 1139-48.

Beckouët, F., B. Hu, M. B. Roig, T. Sutani, M. Komata, P. Uluocak, V. L. Katis, K. Shirahige, and K. Nasmyth, 2010, An Smc3 Acetylation Cycle Is Essential for Establishment of Sister Chromatid Cohesion: Mol Cell, v. 39, p. 689-99.

Beckouët, F., M. Srinivasan, M. Roig, K. L. Chan, J. Scheinost, P. Batty, B. Hu, N. Petela, T. Gligoris, A. Smith, L. Strmecki, B. Rowland, and K. Nasmyth, 2016, Releasing Activity Disengages Cohesin's Smc3/Scc1 Interface in a Process Blocked by Acetylation, Mol Cell, v. 61, p. 563-74.

Bennett, M., K. E. Evans, S. Yu, Y. Teng, R. M. Webster, J. Powell, R. Waters, and S. H. Reed, 2015, Sandcastle: software for revealing latent information in multiple experimental ChIP-chip datasets via a novel normalisation procedure: Sci Rep, v. 5, p. 13395.

Bergink, S., F. A. Salomons, D. Hoogstraten, T. A. Groothuis, H. de Waard, J. Wu, L. Yuan, E. Citterio, A. B. Houtsmuller, J. Neefjes, J. H. Hoeijmakers, W. Vermeulen, and N. P. Dantuma, 2006, DNA damage triggers nucleotide excision repair-dependent monoubiquitylation of histone H2A: Genes Dev, v. 20, p. 1343-52.

Bi, X., 2015, Mechanism of DNA damage tolerance: World J Biol Chem, v. 6, p. 48-56.

Bjelland, S., and E. Seeberg, 2003, Mutagenicity, toxicity and repair of DNA base damage induced by oxidation: Mutat Res, v. 531, p. 37-80.

Bjerling, P., R. A. Silverstein, G. Thon, A. Caudy, S. Grewal, and K. Ekwall, 2002, Functional divergence between histone deacetylases in fission yeast by distinct cellular localization and in vivo specificity: Mol Cell Biol, v. 22, p. 2170-81.

Bohgaki, T., M. Bohgaki, and R. Hakem, 2010, DNA double-strand break signaling and human disorders: Genome Integr, v. 1, p. 15

Bonaldo, M. F., G. Lennon, and M. B. Soares, 1996, Normalization and subtraction: two approaches to facilitate gene discovery: Genome Res, v. 6, p. 791-806.

Bonilla, C. Y., J. A. Melo, and D. P. Toczyski, 2008, Colocalization of sensors is sufficient to activate the DNA damage checkpoint in the absence of damage: Mol Cell, v. 30, p. 267-76.

Botstein, D., and G. R. Fink, 2011, Yeast: An Experimental Organism for 21st Century Biology, Genetics, v. 189, p. 695-704.

Boulton, S. J., and S. P. Jackson, 1998, Components of the Ku-dependent non-homologous end-joining pathway are involved in telomeric length maintenance and telomeric silencing: Embo j, v. 17, p. 1819-28.

Bouwman, P., and J. Jonkers, 2012, The effects of deregulated DNA damage signalling on cancer chemotherapy response and resistance: Nat Rev Cancer, v. 12, p. 587-98.

Branco, M. R., G. Ficz, and W. Reik, 2011, Uncovering the role of 5-hydroxymethylcytosine in the epigenome: Nat Rev Genet, v. 13, p. 7-13.

Branzei, D., and M. Foiani, 2008, Regulation of DNA repair throughout the cell cycle: Nat Rev Mol Cell Biol, v. 9, p. 297-308.

Brash, D. E., W. A. Franklin, G. B. Sancar, A. Sancar, and W. A. Haseltine, 1985, Escherichia coli DNA photolyase reverses cyclobutane pyrimidine dimers but not pyrimidine-pyrimidone (6-4) photoproducts: J Biol Chem, v. 260, p. 11438-41.

Brown, T. A., 2002, *in* nd, ed., Genomes: Oxford, Wiley-LissGarland Science.

Butnariu, M., 2012, The Oxygen Paradox: Journal of Pharmacogenomics & Pharmacoproteomics, v. 3.

Butnariu, M., 2012, The Oxygen Paradox: Journal of Pharmacogenomics & Pharmacoproteomics, v. 3.

Cairns, B. R., Y. Lorch, Y. Li, M. Zhang, L. Lacomis, H. Erdjument-Bromage, P. Tempst, J. Du, B. Laurent, and R. D. Kornberg, 1996, RSC, an essential, abundant chromatin-remodeling complex: Cell, v. 87, p. 1249-60.

Callegari, A. J., and T. J. Kelly, 2006, UV irradiation induces a postreplication DNA damage checkpoint, Proc Natl Acad Sci U S A, v. 103, p. 15877-82.

Carey, M., B. Li, and J. L. Workman, 2006, RSC exploits histone acetylation to abrogate the nucleosomal block to RNA polymerase II elongation: Mol Cell, v. 24, p. 481-7.

Carr, M. I., and S. N. Jones, 2016, Regulation of the Mdm2-p53 signaling axis in the DNA damage response and tumorigenesis: Transl Cancer Res, v. 5, p. 707-24.

Carrozza, M. J., L. Florens, S. K. Swanson, W. J. Shia, S. Anderson, J. Yates, M. P. Washburn, and J. L. Workman, 2005, Stable incorporation of sequence specific repressors Ash1 and Ume6 into the Rpd3L complex: Biochim Biophys Acta, v. 1731, p. 77-87; discussion 75-6.

Cecchini, S., C. Masson, C. La Madeleine, M. A. Huels, L. Sanche, J. R. Wagner, and D. J. Hunting, 2005, Interstrand cross-link induction by UV radiation in bromodeoxyuridine-substituted DNA: dependence on DNA conformation: Biochemistry, v. 44, p. 16957-66.

Chen, C. C., J. J. Carson, J. Feser, B. Tamburini, S. Zabaronick, J. Linger, and J. K. Tyler, 2008, Acetylated lysine 56 on histone H3 drives chromatin assembly after repair, signaling for the completion of repair: Cell, v. 134, p. 231-43.

Chen, X. F., B. Kuryan, T. Kitada, N. Tran, J. Y. Li, S. Kurdistani, M. Grunstein, B. Li, and M. Carey, 2012, The Rpd3 core complex is a chromatin stabilization module: Curr Biol, v. 22, p. 56-63.

Chinnaiyan, A. M., C. G. Tepper, M. F. Seldin, K. O'Rourke, F. C. Kischkel, S. Hellbardt, P. H. Krammer, M. E. Peter, and V. M. Dixit, 1996, FADD/MORT1 is a common mediator of CD95 (Fas/APO-1) and tumor necrosis factor receptor-induced apoptosis: J Biol Chem, v. 271, p. 4961-5.

Christmann, M., M. T. Tomicic, W. P. Roos, and B. Kaina, 2003, Mechanisms of human DNA repair: an update: Toxicology, v. 193, p. 3-34.

Christmann, M., M. T. Tomicic, D. Aasland, and B. Kaina, 2007, A role for UV-light-induced c-Fos: Stimulation of nucleotide excision repair and protection against sustained JNK activation and apoptosis: Carcinogenesis, v. 28, p. 183-90.

Ciccia, A., and S. J. Elledge, 2010, The DNA damage response: making it safe to play with knives: Mol Cell, v. 40, p. 179-204.

Cleveland, D. W., Y. Mao, and K. F. Sullivan, 2003, Centromeres and kinetochores: from epigenetics to mitotic checkpoint signaling: Cell, v. 112, p. 407-21.

Colina, A. R., and D. Young, 2005, Raf60, a novel component of the Rpd3 histone deacetylase complex required for Rpd3 activity in Saccharomyces cerevisiae: J Biol Chem, v. 280, p. 42552-6.

Craig, A. G., D. Nizetic, J. D. Hoheisel, G. Zehetner, and H. Lehrach, 1990, Ordering of cosmid clones covering the herpes simplex virus type I (HSV-I) genome: a test case for fingerprinting by hybridisation: Nucleic Acids Res, v. 18, p. 2653-60.

Crampton, J., S. Humphries, D. Woods, and R. Williamson, 1980, The isolation of cloned cDNA sequences which are differentially expressed in human lymphocytes and fibroblasts: Nucleic Acids Res, v. 8, p. 6007-17.

Dahmann, C., J. F. Diffley, and K. A. Nasmyth, 1995, S-phase-promoting cyclin-dependent kinases prevent re-replication by inhibiting the transition of replication origins to a pre-replicative state: Curr Biol, v. 5, p. 1257-69.

Davies, K. J., 2016, The Oxygen Paradox, oxidative stress, and ageing: Arch Biochem Biophys, v. 595, p. 28-32.

De Gruijl, F. R., H. J. van Kranen, and L. H. Mullenders, 2001, UV-induced DNA damage, repair, mutations and oncogenic pathways in skin cancer: J Photochem Photobiol B, v. 63, p. 19-27.

Delacroix, S., J. M. Wagner, M. Kobayashi, K. Yamamoto, and L. M. Karnitz, 2007, The Rad9–Hus1–Rad1 (9–1–1) clamp activates checkpoint signaling via TopBP1: Genes Dev, v. 21, p. 1472-7.

DeMarini, D. M., 2004, Genotoxicity of tobacco smoke and tobacco smoke condensate: a review: Mutat Res, v. 567, p. 447-74.

Dias Neto, E., R. G. Correa, S. Verjovski-Almeida, M. R. Briones, M. A. Nagai, W. da Silva, Jr., M. A. Zago, S. Bordin, F. F. Costa, G. H. Goldman, A. F. Carvalho, A. Matsukuma, G. S. Baia, D. H. Simpson, A. Brunstein, P. S. de Oliveira, P. Bucher, C. V. Jongeneel, M. J. O'Hare, F. Soares, R. R. Brentani, L. F. Reis, S. J. de Souza, and A. J. Simpson, 2000, Shotgun sequencing of the human transcriptome with ORF expressed sequence tags: Proc Natl Acad Sci U S A, v. 97, p. 3491-6.

Diffley, J. F., and B. Stillman, 1989, Similarity between the transcriptional silencer binding proteins ABF1 and RAP1: Science, v. 246, p. 1034-8.

DiGiovanna, J. J., and K. H. Kraemer, 2012, SHINING A LIGHT ON XERODERMA PIGMENTOSUM: J Invest Dermatol, v. 132, p. 785-96

Dinant, C., J. Bartek, and S. Bekker-Jensen, 2012, Histone Displacement during Nucleotide Excision Repair, Int J Mol Sci, v. 13, p. 13322-37.

Donehower, L. A., 2014, Phosphatases reverse p53-mediated cell cycle checkpoints, Proc Natl Acad Sci U S A, v. 111, p. 7172-3.

Doll, R., and R. Peto, 1981, The causes of cancer: quantitative estimates of avoidable risks of cancer in the United States today: J Natl Cancer Inst, v. 66, p. 1191-308.

Douki, T., 2013, The variety of UV-induced pyrimidine dimeric photoproducts in DNA as shown by chromatographic quantification methods: Photochem Photobiol Sci, v. 12, p. 1286-302.

Duan, M. R., and M. J. Smerdon, 2010, UV damage in DNA promotes nucleosome unwrapping: J Biol Chem, v. 285, p. 26295-303.

Duan, M. R., and M. J. Smerdon, 2014, Histone H3 lysine 14 (H3K14) acetylation facilitates DNA repair in a positioned nucleosome by stabilizing the binding of the chromatin Remodeler RSC (Remodels Structure of Chromatin): J Biol Chem, v. 289, p. 8353-63.

Dzantiev, L., N. Constantin, J. Genschel, R. R. Iyer, P. M. Burgers, and P. Modrich, 2004, A defined human system that supports bidirectional mismatch-provoked excision: Mol Cell, v. 15, p. 31-41

Ekwall, K., 2005, Genome-wide analysis of HDAC function: Trends Genet, v. 21, p. 608-15.

Eliopoulos, A. G., S. Havaki, and V. G. Gorgoulis, 2016, DNA Damage Response and Autophagy: A Meaningful Partnership: Front Genet, v. 7.

Farber, J. L., 1994, Mechanisms of cell injury by activated oxygen species: Environ Health Perspect, v. 102 Suppl 10, p. 17-24.

Farrell, A. W., G. M. Halliday, and J. G. Lyons, 2011, Chromatin structure following UV-induced DNA damage-repair or death?: Int J Mol Sci, v. 12, p. 8063-85.

Felsenfeld, G., and M. Groudine, 2003, Controlling the double helix: Nature, v. 421, p. 448-53.

Foiani, M., A. Pellicioli, M. Lopes, C. Lucca, M. Ferrari, G. Liberi, M. Muzi Falconi, and P. Plevani, 2000, DNA damage checkpoints and DNA replication controls in Saccharomyces cerevisiae: Mutat Res, v. 451, p. 187-96.

Fortini, P., and E. Dogliotti, 2007, Base damage and single-strand break repair: mechanisms and functional significance of short- and long-patch repair subpathways: DNA Repair (Amst), v. 6, p. 398-409.

Friedberg, E. C., 2001, How nucleotide excision repair protects against cancer: Nat Rev Cancer, v. 1, p. 22-33.

Friedberg, E. C., 2005, DNA Repair and Mutagenesis by Friedberg, Errol C.: ASM Press 9781555813192 - TextbookRush.

Fukui, K., M. Nishida, N. Nakagawa, R. Masui, and S. Kuramitsu, 2008, Bound nucleotide controls the endonuclease activity of mismatch repair enzyme MutL: J Biol Chem, v. 283, p. 12136-45.

Gale, J. M., K. A. Nissen, and M. J. Smerdon, 1987, UV-induced formation of pyrimidine dimers in nucleosome core DNA is strongly modulated with a period of 10.3 bases: Proc Natl Acad Sci U S A, v. 84, p. 6644-8.

Gaur, U., and B. B. Aggarwal, 2003, Regulation of proliferation, survival and apoptosis by members of the TNF superfamily: Biochem Pharmacol, v. 66, p. 1403-8.

Genschel, J., L. R. Bazemore, and P. Modrich, 2002, Human exonuclease I is required for 5' and 3' mismatch repair: J Biol Chem, v. 277, p. 13302-11.

Gergen, J. P., R. H. Stern, and P. C. Wensink, 1979, Filter replicas and permanent collections of recombinant DNA plasmids: Nucleic Acids Res, v. 7, p. 2115-36.

Giannattasio, M., F. Lazzaro, M. P. Longhese, P. Plevani, and M. Muzi-Falconi, 2004, Physical and functional interactions between nucleotide excision repair and DNA damage checkpoint, EMBO J, v. 23, p. 429-38.

Gietz, R. D., and R. A. Woods, 2002, Transformation of yeast by lithium acetate/single-stranded carrier DNA/polyethylene glycol method: Methods Enzymol, v. 350, p. 87-96.

Gietz, R. D., and R. H. Schiestl, 1991, Applications of high efficiency lithium acetate transformation of intact yeast cells using single-stranded nucleic acids as carrier: Yeast, v. 7, p. 253-63.

Gietz, R. D., and R. H. Schiestl, 2007, High-efficiency yeast transformation using the LiAc/SS carrier DNA/PEG method: Nat Protoc, v. 2, p. 31-4.

Gillet, L. C., and O. D. Scharer, 2006, Molecular mechanisms of mammalian global genome nucleotide excision repair: Chem Rev, v. 106, p. 253-76.

Gillette, T. G., S. Yu, Z. Zhou, R. Waters, S. A. Johnston, and S. H. Reed, 2006, Distinct functions of the ubiquitin-proteasome pathway influence nucleotide excision repair: Embo j, v. 25, p. 2529-38.

Glassner, B. J., G. Weeda, J. M. Allan, J. L. Broekhof, N. H. Carls, I. Donker, B. P. Engelward, R. J. Hampson, R. Hersmus, M. J. Hickman, R. B. Roth, H. B. Warren, M. M. Wu, J. H. Hoeijmakers, and L. D. Samson, 1999, DNA repair methyltransferase (Mgmt) knockout mice are sensitive to the lethal effects of chemotherapeutic alkylating agents: Mutagenesis, v. 14, p. 339-47.

Gong, F., Y. Kwon, and M. J. Smerdon, 2005, Nucleotide excision repair in chromatin and the right of entry: DNA Repair (Amst), v. 4, p. 884-96.

Green, C. M., and G. Almouzni, 2002, When repair meets chromatin: First in series on chromatin dynamics, EMBO Rep, v. 3, p. 28-33.

Gregoretti, I. V., Y. M. Lee, and H. V. Goodson, 2004, Molecular evolution of the histone deacetylase family: functional implications of phylogenetic analysis: J Mol Biol, v. 338, p. 17-31.

Groth, A., W. Rocha, A. Verreault, and G. Almouzni, 2007, Chromatin challenges during DNA replication and repair: Cell, v. 128, p. 721-33.

Grunstein, M., and D. S. Hogness, 1975, Colony hybridization: a method for the isolation of cloned DNAs that contain a specific gene: Proc Natl Acad Sci U S A, v. 72, p. 3961-5.

Guainazzi, A., A. J. Campbell, T. Angelov, C. Simmerling, and O. D. Scharer, 2010, Synthesis and molecular modeling of a nitrogen mustard DNA interstrand crosslink: Chemistry, v. 16, p. 12100-3.

Guzder, S. N., P. Sung, L. Prakash, and S. Prakash, 1997, Yeast Rad7-Rad16 complex, specific for the nucleotide excision repair of the nontranscribed DNA strand, is an ATP-dependent DNA damage sensor: J Biol Chem, v. 272, p. 21665-8.

Guzder, S. N., P. Sung, L. Prakash, and S. Prakash, 1998, The DNA-dependent ATPase activity of yeast nucleotide excision repair factor 4 and its role in DNA damage recognition: J Biol Chem, v. 273, p. 6292-6.

Haber, L. T., and G. C. Walker, 1991, Altering the conserved nucleotide binding motif in the Salmonella typhimurium MutS mismatch repair protein affects both its ATPase and mismatch binding activities: EMBO J, v. 10, p. 2707-15.

Halazonetis, T. D., V. G. Gorgoulis, and J. Bartek, 2008, An oncogene-induced DNA damage model for cancer development: Science, v. 319, p. 1352-5.

Hanawalt, P. C., 2002, Subpathways of nucleotide excision repair and their regulation: Oncogene, v. 21, p. 8949-56.

Hanawalt, P. C., and G. Spivak, 2008, Transcription-coupled DNA repair: two decades of progress and surprises: Nat Rev Mol Cell Biol, v. 9, p. 958-70.

Hargreaves, D. C., and G. R. Crabtree, 2011, ATP-dependent chromatin remodeling: genetics, genomics and mechanisms: Cell Res, v. 21, p. 396-420.

Harper, J. W., and S. J. Elledge, 2007, The DNA damage response: ten years after: Mol Cell, v. 28, p. 739-45..

Harrison, J. C., E. S. Bardes, Y. Ohya, and D. J. Lew, 2001, A role for the Pkc1p/Mpk1p kinase cascade in the morphogenesis checkpoint: Nat Cell Biol, v. 3, p. 417-20.

Hartwell, L. H., 1991, Twenty-five years of cell cycle genetics: Genetics, v. 129, p. 975-80.

Hartwell, L. H., and T. A. Weinert, 1989, Checkpoints: controls that ensure the order of cell cycle events: Science, v. 246, p. 629-34.

Havas, K., A. Flaus, M. Phelan, R. Kingston, P. A. Wade, D. M. Lilley, and T. Owen-Hughes, 2000, Generation of superhelical torsion by ATP-dependent chromatin remodeling activities: Cell, v. 103, p. 1133-42.

Hinz, J. M., 2010, Role of homologous recombination in DNA interstrand crosslink repair: Environ Mol Mutagen, v. 51, p. 582-603.

Hoege, C., B. Pfander, G. L. Moldovan, G. Pyrowolakis, and S. Jentsch, 2002, RAD6-dependent DNA repair is linked to modification of PCNA by ubiquitin and SUMO: Nature, v. 419, p. 135-41.

House, N. C. M., M. R. Koch, and C. H. Freudenreich, 2014, Chromatin modifications and DNA repair: beyond double-strand breaks: Front Genet, v. 5.

Howlett, S. K., and W. Reik, 1991, Methylation levels of maternal and paternal genomes during preimplantation development.

Huang, J. C., D. L. Svoboda, J. T. Reardon, and A. Sancar, 1992, Human nucleotide excision nuclease removes thymine dimers from DNA by incising the 22nd phosphodiester bond 5' and the 6th phosphodiester bond 3' to the photodimer: Proc Natl Acad Sci U S A, v. 89, p. 3664-8.

Huang, J., and W. S. Dynan, 2002, Reconstitution of the mammalian DNA double-strand break end-joining reaction reveals a requirement for an Mre11/Rad50/NBS1-containing fraction: Nucleic Acids Res, v. 30, p. 667-74.

Huen, M. S., and J. Chen, 2008, The DNA damage response pathways: at the crossroad of protein modifications: Cell Res, v. 18, p. 8-16.

Huen, M. S., and J. Chen, 2010, Assembly of checkpoint and repair machineries at DNA damage sites: Trends Biochem Sci, v. 35, p. 101-8.

Huen, M. S., and J. Chen, 2010, Assembly of checkpoint and repair machineries at DNA damage sites: Trends Biochem Sci, v. 35, p. 101-8.Hydbring, P., M. Malumbres, and P. Sicinski, 2016, Non-canonical functions of cell cycle cyclins and cyclin-dependent kinases: Nat Rev Mol Cell Biol, v. 17, p. 280-92.

Humphries, P., M. Cochet, A. Krust, P. Gerlinger, P. Kourilsky, and P. Chambon, 1977, Molecular cloning of extensive sequences of the in vitro synthesized chicken ovalbumin structural gene: Nucleic Acids Res, v. 4, p. 2389-406.

Hunt, C. R., D. Ramnarain, N. Horikoshi, P. Iyengar, R. K. Pandita, J. W. Shay, and T. K. Pandita, 2013, Histone Modifications and DNA Double-Strand Break Repair after Exposure to Ionizing Radiations: Radiat Res, v. 179, p. 383-92.

Hydbring, P., M. Malumbres, and P. Sicinski, 2016, Non-canonical functions of cell cycle cyclins and cyclin-dependent kinases: Nat Rev Mol Cell Biol, v. 17, p. 280-92.

Ichihashi, M., M. Ueda, A. Budiyanto, T. Bito, M. Oka, M. Fukunaga, K. Tsuru, and T. Horikawa, 2003, UV-induced skin damage: Toxicology, v. 189, p. 21-39.

Irizar, A., Y. Yu, S. H. Reed, E. J. Louis, and R. Waters, 2010, Silenced yeast chromatin is maintained by Sir2 in preference to permitting histone acetylations for efficient NER: Nucleic Acids Res, v. 38, p. 4675-86.

Islam, A., E. L. Turner, J. Menzel, M. E. Malo, and T. A. Harkness, 2011, Antagonistic Gcn5-Hda1 interactions revealed by mutations to the Anaphase Promoting Complex in yeast, Cell Div, v. 6, p. 13.

Ito, H., Y. Fukuda, K. Murata, and A. Kimura, 1983, Transformation of intact yeast cells treated with alkali cations: J Bacteriol, v. 153, p. 163-8.

Jackson, S. P., and J. Bartek, 2009, The DNA-damage response in human biology and disease: Nature, v. 461, p. 1071-8.

Jagerstad, M., and K. Skog, 2005, Genotoxicity of heat-processed foods: Mutat Res, v. 574, p. 156-72.

Jamieson, E. R., and S. J. Lippard, 1999, Structure, Recognition, and Processing of Cisplatin-DNA Adducts: Chem Rev, v. 99, p. 2467-98.

Jazayeri, A., A. D. McAinsh, and S. P. Jackson, 2004, Saccharomyces cerevisiae Sin3p facilitates DNA double-strand break repair, Proc Natl Acad Sci U S A, v. 101, p. 1644-9.

Jen, J., D. L. Mitchell, R. P. Cunningham, C. A. Smith, J. S. Taylor, and J. E. Cleaver, 1997, Ultraviolet irradiation produces novel endonuclease III-sensitive cytosine photoproducts at dipyrimidine sites: Photochem Photobiol, v. 65, p. 323-9.

Jones, D. P., and R. Radi, 2014, Redox pioneer: professor Helmut Sies: Antioxid Redox Signal, v. 21, p. 2459-68.

Kadosh, D., and K. Struhl, 1997, Repression by Ume6 involves recruitment of a complex containing Sin3 corepressor and Rpd3 histone deacetylase to target promoters: Cell, v. 89, p. 365-71.

Kastan, M. B., and J. Bartek, 2004, Cell-cycle checkpoints and cancer: Nature, v. 432, p. 316-23.

Keogh, M. C., S. K. Kurdistani, S. A. Morris, S. H. Ahn, V. Podolny, S. R. Collins, M. Schuldiner, K. Chin, T. Punna, N. J. Thompson, C. Boone, A. Emili, J. S. Weissman, T. R. Hughes, B. D. Strahl, M. Grunstein, J. F. Greenblatt, S. Buratowski, and N. J. Krogan, 2005, Cotranscriptional set2 methylation of histone H3 lysine 36 recruits a repressive Rpd3 complex: Cell, v. 123, p. 593-605.

Kim, S. T., D. S. Lim, C. E. Canman, and M. B. Kastan, 1999, Substrate specificities and identification of putative substrates of ATM kinase family members: J Biol Chem, v. 274, p. 37538-43.

Kim, S. T., P. F. Heelis, T. Okamura, Y. Hirata, N. Mataga, and A. Sancar, 1991, Determination of rates and yields of interchromophore (folate----flavin) energy transfer and intermolecular (flavin----DNA) electron transfer in Escherichia coli photolyase by time-resolved fluorescence and absorption spectroscopy: Biochemistry, v. 30, p. 11262-70.

Kornberg, R. D., 1977, Structure of chromatin: Annu Rev Biochem, v. 46, p. 931-54.

Korolev, V. G., 2011, [Chromatin and DNA damage repair]: Genetika, v. 47, p. 449-59.

Kouzarides, T., 2000, NEW EMBO MEMBER'S REVIEW: Acetylation: a regulatory modification to rival phosphorylation?, EMBO J, v. 19, p. 1176-9.

Kouzarides, T., 2007, Chromatin modifications and their function: Cell, v. 128, p. 693-705.

Kraemer, K. H., N. J. Patronas, R. Schiffmann, B. P. Brooks, D. Tamura, and J. J. DiGiovanna, 2007, Xeroderma pigmentosum, trichothiodystrophy and Cockayne syndrome: a complex genotype-phenotype relationship: Neuroscience, v. 145, p. 1388-96.

Krasikova, Y. S., N. I. Rechkunova, E. A. Maltseva, P. E. Pestryakov, I. O. Petruseva, K. Sugasawa, X. Chen, J. H. Min, and O. I. Lavrik, 2013, Comparative Analysis of Interaction of Human and Yeast DNA Damage Recognition Complexes with Damaged DNA in Nucleotide Excision Repair*, J Biol Chem, v. 288, p. 10936-47.

Krejci, L., V. Altmannova, M. Spirek, and X. Zhao, 2012, Homologous recombination and its regulation: Nucleic Acids Res, v. 40, p. 5795-818.

Krokan, H. E., R. Standal, and G. Slupphaug, 1997, DNA glycosylases in the base excision repair of DNA: Biochem J, v. 325 (Pt 1), p. 1-16.

Kuksal, N., J. Chalker, and R. J. Mailloux, 2017, Review. Progress in understanding the molecular oxygen paradox - function of mitochondrial reactive oxygen species in cell signaling: Biol Chem.

Kunkel, T. A., and K. Bebenek, 2000, DNA replication fidelity: Annu Rev Biochem, v. 69, p. 497-529.

Kunkel, T. A., and D. A. Erie, 2005, DNA mismatch repair: Annu Rev Biochem, v. 74, p. 681-710.

Pai, C. C., and S. E. Kearsey, 2017, A Critical Balance: dNTPs and the Maintenance of Genome Stability, Genes (Basel), v. 8.

Kurdistani, S. K., and M. Grunstein, 2003, Histone acetylation and deacetylation in yeast: Nat Rev Mol Cell Biol, v. 4, p. 276-84.

Kurdistani, S. K., D. Robyr, S. Tavazoie, and M. Grunstein, 2002, Genome-wide binding map of the histone deacetylase Rpd3 in yeast: Nat Genet, v. 31, p. 248-54.

Kurdistani, S. K., S. Tavazoie, and M. Grunstein, 2004, Mapping global histone acetylation patterns to gene expression: Cell, v. 117, p. 721-33.

Landry, J., A. Sutton, S. T. Tafrov, R. C. Heller, J. Stebbins, L. Pillus, and R. Sternglanz, 2000, The silencing protein SIR2 and its homologs are NAD-dependent protein deacetylases: Proc Natl Acad Sci U S A, v. 97, p. 5807-11.

Lane, N., W. Dean, S. Erhardt, P. Hajkova, A. Surani, J. Walter, and W. Reik, 2003, Resistance of IAPs to methylation reprogramming may provide a mechanism for epigenetic inheritance in the mouse: Genesis, v. 35, p. 88-93.

Lashkari, D. A., J. L. DeRisi, J. H. McCusker, A. F. Namath, C. Gentile, S. Y. Hwang, P. O. Brown, and R. W. Davis, 1997, Yeast microarrays for genome wide parallel genetic and gene expression analysis: Proc Natl Acad Sci U S A, v. 94, p. 13057-62.

Lazzaro, F., M. Giannattasio, F. Puddu, M. Granata, A. Pellicioli, P. Plevani, and M. Muzi-Falconi, 2009, Checkpoint mechanisms at the intersection between DNA damage and repair: DNA Repair (Amst), v. 8, p. 1055-67.

Lawley, P. D., and D. H. Phillips, 1996, DNA adducts from chemotherapeutic agents: Mutat Res, v. 355, p. 13-40.

Le May, N., J. M. Egly, and F. Coin, 2010, True Lies: The Double Life of the Nucleotide Excision Repair Factors in Transcription and DNA Repair: J Nucleic Acids, v. 2010.

Lee, J. H., K. Maskos, and R. Huber, 2009, Structural and functional studies of the yeast class II Hda1 histone deacetylase complex: J Mol Biol, v. 391, p. 744-57.

Lee, K. K., and J. L. Workman, 2007, Histone acetyltransferase complexes: one size doesn't fit all: Nat Rev Mol Cell Biol, v. 8, p. 284-95.

Lempiäinen, H., and T. D. Halazonetis, 2009, Emerging common themes in regulation of PIKKs and PI3Ks, EMBO J, v. 28, p. 3067-73.

Lennon, G. G., and H. Lehrach, 1991, Hybridization analyses of arrayed cDNA libraries: Trends Genet, v. 7, p. 314-7.

Lennon, G., C. Auffray, M. Polymeropoulos, and M. B. Soares, 1996, The I.M.A.G.E. Consortium: an integrated molecular analysis of genomes and their expression: Genomics, v. 33, p. 151-2.

Leyns, L., and L. Gonzalez, 2012, Genomic Integrity of Mouse Embryonic Stem Cells | IntechOpen.

Li, J., and D. F. Stern, 2005, Regulation of CHK2 by DNA-dependent protein kinase: J Biol Chem, v. 280, p. 12041-50.

Li, J., T. Uchida, T. Todo, and T. Kitagawa, 2006, Similarities and differences between cyclobutane pyrimidine dimer photolyase and (6-4) photolyase as revealed by resonance Raman spectroscopy: Electron transfer from the FAD cofactor to ultraviolet-damaged DNA: J Biol Chem, v. 281, p. 25551-9.

Lieber, M. R., 2010, The mechanism of double-strand DNA break repair by the nonhomologous DNA end-joining pathway: Annu Rev Biochem, v. 79, p. 181-211.

Lin, S. J., C. P. Wardlaw, T. Morishita, I. Miyabe, C. Chahwan, T. Caspari, U. Schmidt, A. M. Carr, and V. Garcia, 2012, The Rad4TopBP1 ATR-Activation Domain Functions in G1/S Phase in a Chromatin-Dependent Manner, PLoS Genet, v. 8.

Lindahl, T., 1974, An N-glycosidase from Escherichia coli that releases free uracil from DNA containing deaminated cytosine residues: Proc Natl Acad Sci U S A, v. 71, p. 3649-53.

Lindahl, T., 1993, Instability and decay of the primary structure of DNA: Nature, v. 362, p. 709-15.

Linger, J. G., and J. K. Tyler, 2007, Chromatin Disassembly and Reassembly During DNA Repair: Mutat Res, v. 618, p. 52-64.

Liu, G., C. Lanham, J. R. Buchan, and M. E. Kaplan, 2017, High-throughput transformation of Saccharomyces cerevisiae using liquid handling robots: PLoS One, v. 12, p. e0174128.

Liu, Y., I. Stuparevic, B. Xie, E. Becker, M. J. Law, and M. Primig, 2015, The conserved histone deacetylase Rpd3 and the DNA binding regulator Ume6 repress BOI1's meiotic transcript isoform during vegetative growth in Saccharomyces cerevisiae: Mol Microbiol, v. 96, p. 861-74.

Ljungman, M., and F. Zhang, 1996, Blockage of RNA polymerase as a possible trigger for u.v. light-induced apoptosis: Oncogene, v. 13, p. 823-31.

Lobachev, K. S., A. Rattray, and V. Narayanan, 2007, Hairpin- and cruciform-mediated chromosome breakage: causes and consequences in eukaryotic cells: Front Biosci, v. 12, p. 4208-20.

Lodish, B., Matsudaira, Kaiser, Krieger, Scott, Zipursky and Darnell, 2004, {Molecular Cell Biology By Lodish, Berk, etc. (5th, Fifth Edition)}, WHFreeman.

Lucas, R. M., and A. L. Ponsonby, 2006, Considering the potential benefits as well as adverse effects of sun exposure: can all the potential benefits be provided by oral vitamin D supplementation?: Prog Biophys Mol Biol, v. 92, p. 140-9.

Luger, K., 2006, Dynamic nucleosomes: Chromosome Res, v. 14, p. 5-16.

Luger, K., A. W. Mader, R. K. Richmond, D. F. Sargent, and T. J. Richmond, 1997, Crystal structure of the nucleosome core particle at 2.8 A resolution: Nature, v. 389, p. 251-60.

Luger, K., M. L. Dechassa, and D. J. Tremethick, 2012, New insights into nucleosome and chromatin structure: an ordered state or a disordered affair?: Nat Rev Mol Cell Biol, v. 13, p. 436-47.

Malumbres, M., 2014, Cyclin-dependent kinases, Genome Biol, v. 15, p. 122.

Manfredi, J. J., 2003, p53 and apoptosis: it's not just in the nucleus anymore: Mol Cell, v. 11, p. 552-4.

Maréchal, A., and L. Zou, 2013, DNA Damage Sensing by the ATM and ATR Kinases, Cold Spring Harb Perspect Biol, v. 5.

Marteijn, J. A., H. Lans, W. Vermeulen, and J. H. Hoeijmakers, 2014, Understanding nucleotide excision repair and its roles in cancer and ageing: Nat Rev Mol Cell Biol, v. 15, p. 465-81.

Marteijn, J. A., J. H. Hoeijmakers, and W. Vermeulen, 2015, Check, Check ...Triple Check: Multi-Step DNA Lesion Identification by Nucleotide Excision Repair: Mol Cell, v. 59, p. 885-6.

Masumoto, H., D. Hawke, R. Kobayashi, and A. Verreault, 2005, A role for cell-cycle-regulated histone H3 lysine 56 acetylation in the DNA damage response: Nature, v. 436, p. 294-8.

Matsuoka, S., B. A. Ballif, A. Smogorzewska, E. R. McDonald, 3rd, K. E. Hurov, J. Luo, C. E. Bakalarski, Z. Zhao, N. Solimini, Y. Lerenthal, Y. Shiloh, S. P. Gygi, and S. J. Elledge, 2007, ATM and ATR substrate analysis reveals extensive protein networks responsive to DNA damage: Science, v. 316, p. 1160-6.

Matsuoka, S., G. Rotman, A. Ogawa, Y. Shiloh, K. Tamai, and S. J. Elledge, 2000, Ataxia telangiectasia-mutated phosphorylates Chk2 in vivo and in vitro: Proc Natl Acad Sci U S A, v. 97, p. 10389-94.

Maynard, S., S. H. Schurman, C. Harboe, N. C. de Souza-Pinto, and V. A. Bohr, 2009, Base excision repair of oxidative DNA damage and association with cancer and aging: Carcinogenesis, v. 30, p. 2-10.

Maynard, S., S. H. Schurman, C. Harboe, N. C. de Souza-Pinto, and V. A. Bohr, 2009, Base excision repair of oxidative DNA damage and association with cancer and aging: Carcinogenesis, v. 30, p. 2-10.

McHugh, P. J., W. R. Sones, and J. A. Hartley, 2000, Repair of intermediate structures produced at DNA interstrand cross-links in Saccharomyces cerevisiae: Mol Cell Biol, v. 20, p. 3425-33.

McPherson, J. P., B. Lemmers, R. Chahwan, A. Pamidi, E. Migon, E. Matysiak-Zablocki, M. E. Moynahan, J. Essers, K. Hanada, A. Poonepalli, O. Sanchez-Sweatman, R. Khokha, R. Kanaar, M. Jasin, M. P. Hande, and R. Hakem, 2004, Involvement of mammalian Mus81 in genome integrity and tumor suppression: Science, v. 304, p. 1822-6

Melis, J. P., S. W. Wijnhoven, R. B. Beems, M. Roodbergen, J. van den Berg, H. Moon, E. Friedberg, G. T. van der Horst, J. H. Hoeijmakers, J. Vijg, and H. van Steeg, 2008, Mouse models for xeroderma pigmentosum group A and group C show divergent cancer phenotypes: Cancer Res, v. 68, p. 1347-53.

Memisoglu, A., and L. Samson, 2000, Base excision repair in yeast and mammals: Mutat Res, v. 451, p. 39-51.

Menck, C. F., and V. Munford, 2014, DNA repair diseases: What do they tell us about cancer and aging?, Genet Mol Biol, v. 37, p. 220-33.

Miller, D. L., and M. A. Weinstock, 1994, Nonmelanoma skin cancer in the United States: incidence: J Am Acad Dermatol, v. 30, p. 774-8.

Miller, J. K., and W. M. Barnes, 1986, Colony probing as an alternative to standard sequencing as a means of direct analysis of chromosomal DNA to determine the spectrum of single-base changes in regions of known sequence: Proc Natl Acad Sci U S A, v. 83, p. 1026-30.

Miller, K. M., J. V. Tjeertes, J. Coates, G. Legube, S. E. Polo, S. Britton, and S. P. Jackson, 2010, Human HDAC1 and HDAC2 function in the DNA-damage response to promote DNA nonhomologous end-joining: Nat Struct Mol Biol, v. 17, p. 1144-51.

Mimitou, E. P., and L. S. Symington, 2009, Nucleases and helicases take center stage in homologous recombination: Trends Biochem Sci, v. 34, p. 264-72.

Modrich, P., 1991, Mechanisms and biological effects of mismatch repair: Annu Rev Genet, v. 25, p. 229-53.

Modrich, P., 1994, Mismatch repair, genetic stability, and cancer: Science, v. 266, p. 1959-60.

Modrich, P., 2006, MECHANISMS IN EUKARYOTIC MISMATCH REPAIR*: J Biol Chem, v. 281, p. 30305-9.

Monk, M., M. Boubelik, and S. Lehnert, 1987, Temporal and regional changes in DNA methylation in the embryonic, extraembryonic and germ cell lineages during mouse embryo development.

Mordes, D. A., E. A. Nam, and D. Cortez, 2008, Dpb11 activates the Mec1-Ddc2 complex: Proc Natl Acad Sci U S A, v. 105, p. 18730-4.Masumoto, H., D. Hawke, R. Kobayashi, and A. Verreault, 2005, A role for cell-cycle-regulated histone H3 lysine 56 acetylation in the DNA damage response: Nature, v. 436, p. 294-8.

Morgan, 2007, Cell Cycle: Principles of Control: Yale J Biol Med, v. 80, p. 141-2.

Mouret, S., C. Philippe, J. Gracia-Chantegrel, A. Banyasz, S. Karpati, D. Markovitsi, and T. Douki, 2010, UVA-induced cyclobutane pyrimidine dimers in DNA: a direct photochemical mechanism?: Org Biomol Chem, v. 8, p. 1706-11.

Müller, B., J. Blackburn, C. Feijoo, X. Zhao, and C. Smythe, 2007, DNA-activated protein kinase functions in a newly observed S phase checkpoint that links histone mRNA abundance with DNA replication, J Cell Biol, v. 179, p. 1385-98.

Munoz, M. J., N. Nieto Moreno, L. E. Giono, A. E. Cambindo Botto, G. Dujardin, G. Bastianello, S. Lavore, A. Torres-Mendez, C. F. M. Menck, B. J. Blencowe, M. Irimia, M. Foiani, and A. R. Kornblihtt, 2017, Major Roles for Pyrimidine Dimers, Nucleotide Excision Repair, and ATR in the Alternative Splicing Response to UV Irradiation: Cell Rep, v. 18, p. 2868-2879.

Nakamura, T. M., B. A. Moser, and P. Russell, 2002, Telomere binding of checkpoint sensor and DNA repair proteins contributes to maintenance of functional fission yeast telomeres: Genetics, v. 161, p. 1437-52.

Narayanan, D. L., R. N. Saladi, and J. L. Fox, 2010, Ultraviolet radiation and skin cancer: Int J Dermatol, v. 49, p. 978-86.

Natarajan, C., and K. Takeda, 2017, Regulation of various DNA repair pathways by E3 ubiquitin ligases: J Cancer Res Ther, v. 13, p. 157-169.

Navadgi-Patil, V. M., and P. M. Burgers, 2008, Yeast DNA Replication Protein Dpb11 Activates the Mec1/ATR Checkpoint Kinase*, J Biol Chem, v. 283, p. 35853-9.

Niida, H., and M. Nakanishi, 2006, DNA damage checkpoints in mammals: Mutagenesis, v. 21, p. 3-9.

Norbury, C. J., and B. Zhivotovsky, 2004, DNA damage-induced apoptosis: Oncogene, v. 23, p. 2797-808.

Novarina, D., F. Amara, F. Lazzaro, P. Plevani, and M. Muzi-Falconi, 2011, Mind the gap: keeping UV lesions in check: DNA Repair (Amst), v. 10, p. 751-9.

Nurse, P., 2000, A long twentieth century of the cell cycle and beyond: Cell, v. 100, p. 71-8.

Nusinzon, I., and C. M. Horvath, 2005, Histone deacetylases as transcriptional activators? Role reversal in inducible gene regulation: Sci STKE, v. 2005, p. re11.

Nyberg, K. A., R. J. Michelson, C. W. Putnam, and T. A. Weinert, 2002, Toward maintaining the genome: DNA damage and replication checkpoints: Annu Rev Genet, v. 36, p. 617-56.

Ochs, K., and B. Kaina, 2000, Apoptosis induced by DNA damage O6-methylguanine is Bcl-2 and caspase-9/3 regulated and Fas/caspase-8 independent: Cancer Res, v. 60, p. 5815-24.

Oda, M., A. Yamagiwa, S. Yamamoto, T. Nakayama, A. Tsumura, H. Sasaki, K. Nakao, E. Li, and M. Okano, 2006, DNA methylation regulates long-range gene silencing of an X-linked homeobox gene cluster in a lineage-specific manner.

Oh, K. S., M. Bustin, S. J. Mazur, E. Appella, and K. H. Kraemer, 2011, UV-induced histone H2AX phosphorylation and DNA damage related proteins accumulate and persist in nucleotide excision repair-deficient XP-B cells: DNA Repair (Amst), v. 10, p. 5-15

Okano, M., D. W. Bell, D. A. Haber, and E. Li, 1999, DNA methyltransferases Dnmt3a and Dnmt3b are essential for de novo methylation and mammalian development: Cell, v. 99, p. 247-57.

Osborn, A. J., S. J. Elledge, and L. Zou, 2002, Checking on the fork: the DNA-replication stress-response pathway: Trends Cell Biol, v. 12, p. 509-16.

Pepponi, R., G. Marra, M. P. Fuggetta, S. Falcinelli, E. Pagani, E. Bonmassar, J. Jiricny, and S. D'Atri, 2003, The effect of O6-alkylguanine-DNA alkyltransferase and mismatch repair activities on the sensitivity of human melanoma cells to temozolomide, 1,3-

bis(2-chloroethyl)1-nitrosourea, and cisplatin: J Pharmacol Exp Ther, v. 304, p. 661-8.

Peterson, C. L., and G. Almouzni, 2013, Nucleosome dynamics as modular systems that integrate DNA damage and repair: Cold Spring Harb Perspect Biol, v. 5.

Pokholok, D. K., C. T. Harbison, S. Levine, M. Cole, N. M. Hannett, T. I. Lee, G. W. Bell, K. Walker, P. A. Rolfe, E. Herbolsheimer, J. Zeitlinger, F. Lewitter, D. K. Gifford, and R. A. Young, 2005, Genome-wide map of nucleosome acetylation and methylation in yeast: Cell, v. 122, p. 517-27.

Polo, S. E., 2015, Reshaping chromatin after DNA damage: the choreography of histone proteins: J Mol Biol, v. 427, p. 626-36.

Polo, S. E., and G. Almouzni, 2006, Chromatin assembly: a basic recipe with various flavours: Curr Opin Genet Dev, v. 16, p. 104-11.

Polo, S. E., and G. Almouzni, 2015, Chromatin dynamics after DNA damage: the legacy of the Access-Repair-Restore model: DNA Repair (Amst), v. 36, p. 114-21.

Polo, S. E., D. Roche, and G. Almouzni, 2006, New histone incorporation marks sites of UV repair in human cells: Cell, v. 127, p. 481-93.

Prakash, S., and L. Prakash, 2000, Nucleotide excision repair in yeast: Mutat Res, v. 451, p. 13-24.

Pray, A. L., 2008, Discovery of DNA Double Helix: Watson and Crick.

Puddu, F., M. Granata, L. Di Nola, A. Balestrini, G. Piergiovanni, F. Lazzaro, M. Giannattasio, P. Plevani, and M. Muzi-Falconi, 2008, Phosphorylation of the budding yeast 9-1-1 complex is required for Dpb11 function in the full activation of the UV-induced DNA damage checkpoint: Mol Cell Biol, v. 28, p. 4782-93.

Ramanathan, B., and M. J. Smerdon, 1986, Changes in nuclear protein acetylation in u.v.-damaged human cells: Carcinogenesis, v. 7, p. 1087-94.

Ramanathan, B., and M. J. Smerdon, 1989, Enhanced DNA repair synthesis in hyperacetylated nucleosomes: J Biol Chem, v. 264, p. 11026-34.

Ramsey, K. L., J. J. Smith, A. Dasgupta, N. Maqani, P. Grant, and D. T. Auble, 2004, The NEF4 Complex Regulates Rad4 Levels and Utilizes Snf2/Swi2-Related ATPase Activity for Nucleotide Excision Repair, Mol Cell Biol, v. 24, p. 6362-78.

Ravanat, J. L., T. Douki, and J. Cadet, 2001, Direct and indirect effects of UV radiation on DNA and its components: J Photochem Photobiol B, v. 63, p. 88-102.

Ray, A., K. Milum, A. Battu, G. Wani, and A. A. Wani, 2013, NER initiation factors, DDB2 and XPC, regulate UV radiation response by recruiting ATR and ATM kinases to DNA damage sites: DNA Repair (Amst), v. 12, p. 273-83.

Reed, S. H., 2005, Nucleotide excision repair in chromatin: the shape of things to come: DNA Repair (Amst), v. 4, p. 909-18.

Reed, S. H., 2011, Nucleotide excision repair in chromatin: damage removal at the drop of a HAT: DNA Repair (Amst), v. 10, p. 734-42.

Reed, S. H., M. Akiyama, B. Stillman, and E. C. Friedberg, 1999, Yeast autonomously replicating sequence binding factor is involved in nucleotide excision repair: Genes Dev, v. 13, p. 3052-8.

Reed, S. H., Z. You, and E. C. Friedberg, 1998, The yeast RAD7 and RAD16 genes are required for postincision events during nucleotide excision repair. In vitro and in vivo studies with rad7 and rad16 mutants and purification of a Rad7/Rad16-containing protein complex: J Biol Chem, v. 273, p. 29481-8.

Renehan, A. G., C. Booth, and C. S. Potten, 2001, What is apoptosis, and why is it important?: BMJ, v. 322, p. 1536-8.

Ribar, B., L. Prakash, and S. Prakash, 2006, Requirement of ELC1 for RNA Polymerase II Polyubiquitylation and Degradation in Response to DNA Damage in Saccharomyces cerevisiae, Mol Cell Biol, v. 26, p. 3999-4005.

Ribezzo, F., Y. Shiloh, and B. Schumacher, 2016, Systemic DNA damage responses in aging and diseases: Semin Cancer Biol, v. 37-38, p. 26-35.

Richmond, C. S., J. D. Glasner, R. Mau, H. Jin, and F. R. Blattner, 1999, Genome-wide expression profiling in Escherichia coli K-12: Nucleic Acids Res, v. 27, p. 3821-35.

Rizki, R. M., and T. M. Rizki, 1969, Somatic cell lesions induced by the base analog 5-bromodeoxyuridine: Cancer Res, v. 29, p. 201-8

Robert, F., D. K. Pokholok, N. M. Hannett, N. J. Rinaldi, M. Chandy, A. Rolfe, J. L. Workman, D. K. Gifford, and R. A. Young, 2004, Global position and recruitment of HATs and HDACs in the yeast genome: Mol Cell, v. 16, p. 199-209.

Robertson, A. B., A. Klungland, T. Rognes, and I. Leiros, 2009, DNA repair in mammalian cells: Base excision repair: the long and short of it: Cell Mol Life Sci, v. 66, p. 981-93.

Robyr, D., Y. Suka, I. Xenarios, S. K. Kurdistani, A. Wang, N. Suka, and M. Grunstein, 2002, Microarray deacetylation maps determine genome-wide functions for yeast histone deacetylases: Cell, v. 109, p. 437-46.

Roos, W. P., A. D. Thomas, and B. Kaina, 2016, DNA damage and the balance between survival and death in cancer biology: Nat Rev Cancer, v. 16, p. 20-33.

Roos, W. P., and B. Kaina, 2006, DNA damage-induced cell death by apoptosis: Trends Mol Med, v. 12, p. 440-50.

Roos, W. P., and B. Kaina, 2013, DNA damage-induced cell death: from specific DNA lesions to the DNA damage response and apoptosis: Cancer Lett, v. 332, p. 237-48.

Roth, D. B., J. P. Menetski, P. B. Nakajima, M. J. Bosma, and M. Gellert, 1992, V(D)J recombination: broken DNA molecules with covalently sealed (hairpin) coding ends in scid mouse thymocytes: Cell, v. 70, p. 983-91.

Rougier, N., D. Bourc'his, D. M. Gomes, A. Niveleau, M. Plachot, A. Pàldi, and E. Viegas-Péquignot, 1998, Chromosome methylation patterns during mammalian preimplantation development.

Rundlett, S. E., A. A. Carmen, R. Kobayashi, S. Bavykin, B. M. Turner, and M. Grunstein, 1996, HDA1 and RPD3 are members of distinct yeast histone deacetylase complexes that regulate silencing and transcription: Proc Natl Acad Sci U S A, v. 93, p. 14503-8.

Saitou, M., S. Kagiwada, and K. Kurimoto, 2012, Epigenetic reprogramming in mouse pre-implantation development and primordial germ cells: Development, v. 139, p. 15-31.

Sakumi, K., and M. Sekiguchi, 1990, Structures and functions of DNA glycosylases: Mutat Res, v. 236, p. 161-72.

Sancar, A., and C. S. Rupert, 1978, Cloning of the phr gene and amplification of photolyase in Escherichia coli: Gene, v. 4, p. 295-308.

Sancar, A., L. A. Lindsey-Boltz, K. Unsal-Kacmaz, and S. Linn, 2004, Molecular mechanisms of mammalian DNA repair and the DNA damage checkpoints: Annu Rev Biochem, v. 73, p. 39-85.

Sanchez, Y., J. Bachant, H. Wang, F. Hu, D. Liu, M. Tetzlaff, and S. J. Elledge, 1999, Control of the DNA damage checkpoint by chk1 and rad53 protein kinases through distinct mechanisms: Science, v. 286, p. 1166-71.

San Filippo, J., P. Sung, and H. Klein, 2008, Mechanism of eukaryotic homologous recombination: Annu Rev Biochem, v. 77, p. 229-57.

Scharer, O. D., 2005, DNA interstrand crosslinks: natural and drug-induced DNA adducts that induce unique cellular responses: Chembiochem, v. 6, p. 27-32.

Schärer, O. D., 2013, Nucleotide Excision Repair in Eukaryotes, Cold Spring Harb Perspect Biol, v. 5.

Seeberg, E., L. Eide, and M. Bjoras, 1995, The base excision repair pathway: Trends Biochem Sci, v. 20, p. 391-7.

Setlow, R. B., and W. L. Carrier, 1964, THE DISAPPEARANCE OF THYMINE DIMERS FROM DNA: AN ERROR-CORRECTING MECHANISM: Proc Natl Acad Sci U S A, v. 51, p. 226-31.

Sharma, V. M., R. S. Tomar, A. E. Dempsey, and J. C. Reese, 2007, Histone deacetylases RPD3 and HOS2 regulate the transcriptional activation of DNA damage-inducible genes: Mol Cell Biol, v. 27, p. 3199-210.

Sherr, C. J., 2004, Principles of tumor suppression: Cell, v. 116, p. 235-46.

Shiloh, Y., 2003, ATM and related protein kinases: safeguarding genome integrity: Nat Rev Cancer, v. 3, p. 155-68.

Shiloh, Y., and M. B. Kastan, 2001, ATM: genome stability, neuronal development, and cancer cross paths: Adv Cancer Res, v. 83, p. 209-54.

Siddik, Z. H., T. U. o. T. M. D. A. C. C. H. T. USA, and Z. H. Siddik, 2005a, Mechanisms of Action of Cancer Chemotherapeutic Agents: DNA-Interactive Alkylating Agents and Antitumour Platinum-Based Drugs: The Cancer Handbook. John Wiley & Sons, Ltd

Simoneau, A., N. Delgoshaie, I. Celic, J. Dai, N. Abshiru, S. Costantino, P. Thibault, J. D. Boeke, A. Verreault, and H. Wurtele, 2015, Interplay between histone H3 lysine 56 deacetylation and chromatin modifiers in response to DNA damage: Genetics, v. 200, p. 185-205.

Slominski, A., and J. Pawelek, 1998, Animals under the sun: effects of ultraviolet radiation on mammalian skin: Clin Dermatol, v. 16, p. 503-15.

Smerdon, M. J., 1991, DNA repair and the role of chromatin structure: Curr Opin Cell Biol, v. 3, p. 422-8.

Smerdon, M. J., and F. Thoma, 1990, Site-specific DNA repair at the nucleosome level in a yeast minichromosome: Cell, v. 61, p. 675-84.

Smerdon, M. J., and M. W. Lieberman, 1978, Nucleosome rearrangement in human chromatin during UV-induced DNA- reapir synthesis: Proc Natl Acad Sci U S A, v. 75, p. 4238-41.

Sorensen, C. S., L. T. Hansen, J. Dziegielewski, R. G. Syljuasen, C. Lundin, J. Bartek, and T. Helleday, 2005, The cell-cycle checkpoint kinase Chk1 is required for mammalian homologous

Spellman, P. T., G. Sherlock, M. Q. Zhang, V. R. Iyer, K. Anders, M. B. Eisen, P. O. Brown, D. Botstein, and B. Futcher, 1998, Comprehensive identification of cell cycle-regulated genes of the yeast Saccharomyces cerevisiae by microarray hybridization: Mol Biol Cell, v. 9, p. 3273-97.

Stadler, J., and H. Richly, 2017, Regulation of DNA Repair Mechanisms: How the Chromatin Environment Regulates the DNA Damage Response, Int J Mol Sci, v. 18.

Stern, R. S., 2007, Psoralen and ultraviolet a light therapy for psoriasis: N Engl J Med, v. 357, p. 682-90.

Sugasawa, K., 2010, Regulation of damage recognition in mammalian global genomic nucleotide excision repair: Mutat Res, v. 685, p. 29-37.

Sugasawa, K., 2016, Molecular mechanisms of DNA damage recognition for mammalian nucleotide excision repair: DNA Repair (Amst), v. 44, p. 110-117.

Suka, N., Y. Suka, A. A. Carmen, J. Wu, and M. Grunstein, 2001, Highly specific antibodies determine histone acetylation site usage in yeast heterochromatin and euchromatin: Mol Cell, v. 8, p. 473-9.

Sun, Z., D. S. Fay, F. Marini, M. Foiani, and D. F. Stern, 1996, Spk1/Rad53 is regulated by Mec1-dependent protein phosphorylation in DNA replication and damage checkpoint pathways: Genes Dev, v. 10, p. 395-406.

Sung, J. S., and B. Demple, 2006, Roles of base excision repair subpathways in correcting oxidized abasic sites in DNA: Febs j, v. 273, p. 1620-9.

Szumiel, I., 2008, Intrinsic radiation sensitivity: cellular signaling is the key, Radiat Res, v. 169: United States, p. 249-58.

Tao, R., H. Xue, J. Zhang, J. Liu, H. Deng, and Y. G. Chen, 2013, Deacetylase Rpd3 facilitates checkpoint adaptation by preventing Rad53 overactivation: Mol Cell Biol, v. 33, p. 4212-24.

Tatum,D. and Li,S. (2011) Nucleotide excision repair in S. cerevisiae . In: Storici,F (ed). DNA Repair––On the Pathways to Fixing DNA Damage and Errors. InTech Open Access Publisher, Rijeka, Croatia, pp. 97–122

Taunton, J., C. A. Hassig, and S. L. Schreiber, 1996, A mammalian histone deacetylase related to the yeast transcriptional regulator Rpd3p: Science, v. 272, p. 408-11.

Teng, Y., H. Liu, H. W. Gill, Y. Yu, R. Waters, and S. H. Reed, 2008, Saccharomyces cerevisiae Rad16 mediates ultraviolet-dependent histone H3 acetylation required for efficient global genome nucleotide-excision repair: EMBO Rep, v. 9, p. 97-102.

Teng, Y., M. Bennett, K. E. Evans, H. Zhuang-Jackson, A. Higgs, S. H. Reed, and R. Waters, 2011, A novel method for the genome-wide high resolution analysis of DNA damage: Nucleic Acids Res, v. 39, p. e10.

Teng, Y., Y. Yu, and R. Waters, 2002, The Saccharomyces cerevisiae histone acetyltransferase Gcn5 has a role in the photoreactivation and nucleotide excision repair of UV-induced cyclobutane pyrimidine dimers in the MFA2 gene: J Mol Biol, v. 316, p. 489-99.

Thoma, F., 1999, Light and dark in chromatin repair: repair of UV-induced DNA lesions by photolyase and nucleotide excision repair.

Todo, T., H. Ryo, K. Yamamoto, H. Toh, T. Inui, H. Ayaki, T. Nomura, and M. Ikenaga, 1996, Similarity among the Drosophila (6-4)photolyase, a human photolyase homolog, and the DNA photolyase-blue-light photoreceptor family: Science, v. 272, p. 109-12.

Todo, T., S. T. Kim, K. Hitomi, E. Otoshi, T. Inui, H. Morioka, H. Kobayashi, E. Ohtsuka, H. Toh, and M. Ikenaga, 1997, Flavin adenine dinucleotide as a chromophore of the Xenopus (6-4)photolyase: Nucleic Acids Res, v. 25, p. 764-8.

Tomasz, M., R. Lipman, D. Chowdary, J. Pawlak, G. L. Verdine, and K. Nakanishi, 1987, Isolation and structure of a covalent cross-link adduct between mitomycin C and DNA: Science, v. 235, p. 1204-8.

Tournier, C., P. Hess, D. D. Yang, J. Xu, T. K. Turner, A. Nimnual, D. Bar-Sagi, S. N. Jones, R. A. Flavell, and R. J. Davis, 2000, Requirement of JNK for stress-induced activation of the cytochrome c-mediated death pathway: Science, v. 288, p. 870-4.

Tuorkey, M. J., 2015, Solar ultraviolet radiation from cancer induction to cancer prevention: solar ultraviolet radiation and cell biology: Eur J Cancer Prev, v. 24, p. 430-8.

Tyson, J. J., and B. Novak, 2008, Temporal organization of the cell cycle: Curr Biol, v. 18, p. R759-r768.

van Gent, D. C., and M. van der Burg, 2007, Non-homologous end-joining, a sticky affair: Oncogene, v. 26, p. 7731-40.

van Steeg, H., and K. H. Kraemer, 1999, Xeroderma pigmentosum and the role of UV-induced DNA damage in skin cancer: Mol Med Today, v. 5, p. 86-94.

Venters, B. J., S. Wachi, T. N. Mavrich, B. E. Andersen, P. Jena, A. J. Sinnamon, P. Jain, N. S. Rolleri, C. Jiang, C. Hemeryck-Walsh, and B. F. Pugh, 2011, A Comprehensive Genomic Binding Map of Gene and Chromatin Regulatory Proteins in Saccharomyces: Mol Cell, v. 41, p. 480-92.

Verdin, E., F. Dequiedt, and H. G. Kasler, 2003, Class II histone deacetylases: versatile regulators: Trends Genet, v. 19, p. 286-93.

Verhage, R. A., A. J. van Gool, N. de Groot, J. H. Hoeijmakers, P. van de Putte, and J. Brouwer, 1996, Double mutants of Saccharomyces cerevisiae with alterations in global genome and transcription-coupled repair: Mol Cell Biol, v. 16, p. 496-502.

Verhage, R., A. M. Zeeman, N. de Groot, F. Gleig, D. D. Bang, P. van de Putte, and J. Brouwer, 1994, The RAD7 and RAD16 genes, which are essential for pyrimidine dimer removal from the silent mating type loci, are also required for repair of the

nontranscribed strand of an active gene in Saccharomyces cerevisiae: Mol Cell Biol, v. 14, p. 6135-42.

Vogelauer, M., J. Wu, N. Suka, and M. Grunstein, 2000, Global histone acetylation and deacetylation in yeast: Nature, v. 408, p. 495-8.

Wakasugi, M., M. Shimizu, H. Morioka, S. Linn, O. Nikaido, and T. Matsunaga, 2001, Damaged DNA-binding protein DDB stimulates the excision of cyclobutane pyrimidine dimers in vitro in concert with XPA and replication protein A: J Biol Chem, v. 276, p. 15434-40..

Waldman, T., K. W. Kinzler, and B. Vogelstein, 1995, p21 is necessary for the p53-mediated G1 arrest in human cancer cells: Cancer Res, v. 55, p. 5187-90.

Wallace, S. S., 2014, Base excision repair: a critical player in many games: DNA Repair (Amst), v. 19, p. 14-26.

Wang, A., S. K. Kurdistani, and M. Grunstein, 2002, Requirement of Hos2 histone deacetylase for gene activity in yeast: Science, v. 298, p. 1412-4.

Wang, Z., C. Zang, K. Cui, D. E. Schones, A. Barski, W. Peng, and K. Zhao, 2009, Genome-wide mapping of HATs and HDACs reveals distinct functions in active and inactive genes: Cell, v. 138, p. 1019-31.

Wang, Z., S. Wei, S. H. Reed, X. Wu, J. Q. Svejstrup, W. J. Feaver, R. D. Kornberg, and E. C. Friedberg, 1997, The RAD7, RAD16, and RAD23 genes of Saccharomyces cerevisiae: requirement for transcription-independent nucleotide excision repair in vitro and interactions between the gene products: Mol Cell Biol, v. 17, p. 635-43.

Waters, R., K. Evans, M. Bennett, S. Yu, and S. Reed, 2012, Nucleotide excision repair in cellular chromatin: studies with yeast from nucleotide to gene to genome: Int J Mol Sci, v. 13, p. 11141-64.

Watson, J. D., and E. Jordan, 1989, The Human Genome Program at the National Institutes of Health: Genomics, v. 5, p. 654-6.

Watt, D. L., R. J. Buckland, S. A. Lujan, T. A. Kunkel, and A. Chabes, 2016, Genome-wide analysis of the specificity and mechanisms of replication infidelity driven by imbalanced dNTP pools: Nucleic Acids Res, v. 44, p. 1669-80.

Weinert, T. A., and L. H. Hartwell, 1988, The RAD9 gene controls the cell cycle response to DNA damage in Saccharomyces cerevisiae: Science, v. 241, p. 317-22.

Wellinger, R. E., and F. Thoma, 1997, Nucleosome structure and positioning modulate nucleotide eFxcision repair in the non-transcribed strand of an active gene: EMBO J, v. 16, p. 5046-56.

Weterings, E., and D. C. van Gent, 2004, The mechanism of non-homologous end-joining: a synopsis of synapsis: DNA Repair (Amst), v. 3, p. 1425-35.

Willis, N., and N. Rhind, 2009, Regulation of DNA replication by the S-phase DNA damage checkpoint: Cell Div, v. 4, p. 13.

Wilner Martínez-López, L. M.-A., Verónica Bervejillo,Jonatan Valencia-Payan and Dayana Moreno-Ortega, 2013, Chromatin Remodeling in Nucleotide Excision Repair in Mammalian Cells.

Wood, R. D., 2010, Mammalian nucleotide excision repair proteins and interstrand crosslink repair: Environ Mol Mutagen, v. 51, p. 520-6.

Wu, J., N. Suka, M. Carlson, and M. Grunstein, 2001, TUP1 utilizes histone H3/H2B-specific HDA1 deacetylase to repress gene activity in yeast: Mol Cell, v. 7, p. 117-26.

Xiaofei, E., and T. F. Kowalik, 2014, The DNA damage response induced by infection with human cytomegalovirus and other viruses: Viruses, v. 6, p. 2155-85.

Yamanaka, K., I. G. Minko, K. Takata, A. Kolbanovskiy, I. D. Kozekov, R. D. Wood, C. J. Rizzo, and R. S. Lloyd, 2010, Novel enzymatic function of DNA polymerase nu in translesion DNA synthesis past major groove DNA-peptide and DNA-DNA cross-links: Chem Res Toxicol, v. 23, p. 689-95.

Yang, X. J., and E. Seto, 2008, The Rpd3/Hda1 family of lysine deacetylases: from bacteria and yeast to mice and men: Nat Rev Mol Cell Biol, v. 9, p. 206-18.

Yankulov, K., 2015, Book review: Epigenetics (second edition, eds. Allis, Caparros, Jenuwein, Reinberg): Front Genet, v. 6.

Yeheskely-Hayon, D., A. Kotler, M. Stark, T. Hashimshony, S. Sagee, and Y. Kassir, 2013, The Roles of the Catalytic and Noncatalytic Activities of Rpd3L and Rpd3S in the Regulation of Gene Transcription in Yeast, PLoS One, v. 8.

Yoshioka, K., Y. Yoshioka, and P. Hsieh, 2006, ATR Kinase Activation Mediated by MutSα and MutLα in Response to Cytotoxic O6-Methylguanine Adducts: Mol Cell, v. 22, p. 501-10

Yu, S., J. B. Smirnova, E. C. Friedberg, B. Stillman, M. Akiyama, T. Owen-Hughes, R. Waters, and S. H. Reed, 2009, ABF1-binding sites promote efficient global genome nucleotide excision repair: J Biol Chem, v. 284, p. 966-73.

Yu, S., K. Evans, P. van Eijk, M. Bennett, R. M. Webster, M. Leadbitter, Y. Teng, R. Waters, S. P. Jackson, and S. H. Reed, 2016, Global genome nucleotide excision repair is organized into domains that promote efficient DNA repair in chromatin: Genome Res, v. 26, p. 1376-1387.

Yu, S., T. Owen-Hughes, E. C. Friedberg, R. Waters, and S. H. Reed, 2004, The yeast Rad7/Rad16/Abf1 complex generates superhelical torsion in DNA that is required for nucleotide excision repair: DNA Repair (Amst), v. 3, p. 277-87.

Yu, S., Y. Teng, R. Waters, and S. H. Reed, 2011, How chromatin is remodelled during DNA repair of UV-induced DNA damage in Saccharomyces cerevisiae: PLoS Genet, v. 7, p. e1002124.

Yu, Y., Y. Teng, H. Liu, S. H. Reed, and R. Waters, 2005, UV irradiation stimulates histone acetylation and chromatin remodeling at a repressed yeast locus: Proc Natl Acad Sci U S A, v. 102, p. 8650-5.

Yudkovsky, N., C. Logie, S. Hahn, and C. L. Peterson, 1999, Recruitment of the SWI/SNF chromatin remodeling complex by transcriptional activators: Genes Dev, v. 13, p. 2369-74.

Zavala, A. G., R. T. Morris, J. J. Wyrick, and M. J. Smerdon, 2014, High-resolution characterization of CPD hotspot formation in human fibroblasts, Nucleic Acids Res, v. 42, p. 893-905.

Zeman, M. K., and K. A. Cimprich, 2014, Causes and Consequences of Replication Stress: Nat Cell Biol, v. 16, p. 2-9.

Zhang, D., H. B. Wang, K. L. Brinkman, S. X. Han, and B. Xu, 2012, Strategies for targeting the DNA damage response for cancer therapeutics, Chin J Cancer, v. 31: England, p. 359-63.

Zhao, X., J. Liu, D. S. Hsu, S. Zhao, J.-S. Taylor, and A. Sancar, 1997, Reaction Mechanism of (6-4) Photolyase.

Zhou, B. B., and S. J. Elledge, 2000, The DNA damage response: putting checkpoints in perspective: Nature, v. 408, p. 433-9.

Zhou, J., B. O. Zhou, B. A. Lenzmeier, and J. Q. Zhou, 2009, Histone deacetylase Rpd3 antagonizes Sir2-dependent silent chromatin propagation: Nucleic Acids Res, v. 37, p. 3699-713.

Zhu, Q., and A. A. Wani, 2010, Histone Modifications: Crucial Elements for Damage Response and Chromatin Restoration: J Cell Physiol, v. 223, p. 283-8.